Final Report: Analysis of Lidar Remote Sensing Concepts

Contract No. NAS 8-97095 Task No. H-28503D

Prepared by

Gary D. Spiers

Center for Applied Optics

University of Alabama in Huntsville

Huntsville

AL 35803

(256) 890 6030

Report Period 8/10/97 – 8/10/98

Contents

1.0 Introduction

An orbiting coherent Doppler lidar for measuring winds is required to provide two basic pieces of data to the user community. The first is the line of sight wind velocity and the second is knowledge of the position at which the measurement was made. In order to obtain this data for targets of interest to the atmospheric community the instrument must also have a level of backscatter sensitivity sufficient to achieve the goal.

Sensitivity analyses for the line of sight velocity and position requirements for two lidar instruments, one with a nadir angle of 30 deg. in a 300 km altitude, 58 deg. inclination orbit and the second for a 45 deg. nadir angle instrument in a 833 km altitude , 89 deg. inclination orbit are performed. The issues relating to the backscatter sensitivity of a coherent lidar have been well documented previously [1] and are not discussed here other than to identify a space-specific issue that does not typically need to be considered for ground and aircraft based coherent lidars. Section 2 and appendices A1 and A2 document these sensitivity analyses.

This contract was intended to develop requirements for a space shuttle (STS) based coherent lidar however, shortly after the award of this contract NASA MSFC won the SPARCLE program to put a coherent Doppler lidar on STS. Consequently much of the work conducted under this contract has been documented within the development of the SPARCLE project documentation. The relevant portions of the SPARCLE documentation are identified in section 3.0 and included in appendices A3 and A4.

Section 4.0 briefly outlines miscellaneous other activities that occurred under this contract.

2.0 Sensitivity analysis

2.1 Line of sight velocity accuracy

A lidar instrument measures wind velocity by measuring the frequency difference between the transmitted laser beam and the return signal. This frequency difference is due to the transmitted frequency being Doppler shifted by the line of sight velocity seen by the instrument. There are two aspects to determining the line of sight velocity. The first is due to the geometry of the problem and the second is due to the design of the instrument.

2.1.1 Geometry issues

The line of sight velocity is comprised of velocity components due to the satellite velocity, the earth's rotational velocity and the velocity of the target. Figure (1) shows the velocities that contribute to the line of sight velocity in the horizontal plane and figure (2) shows the geometry in the vertical plane.

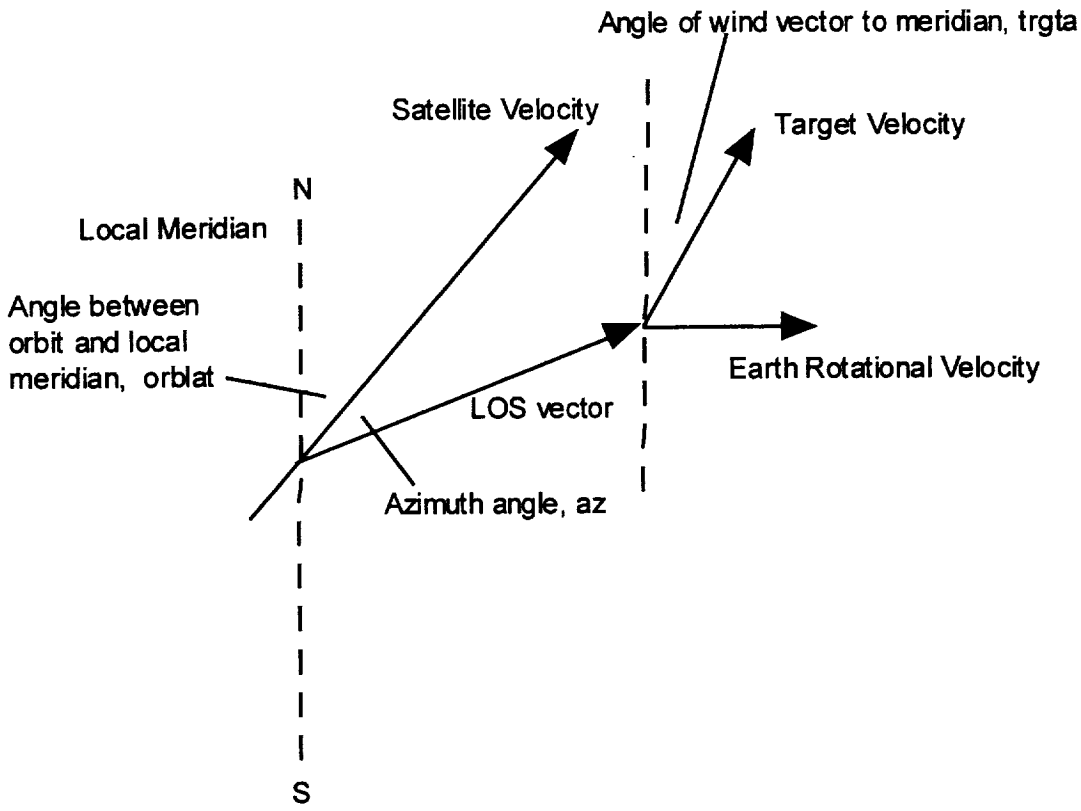

Figure 1) The velocities contributing to the line of sight velocity in the horizontal plane.

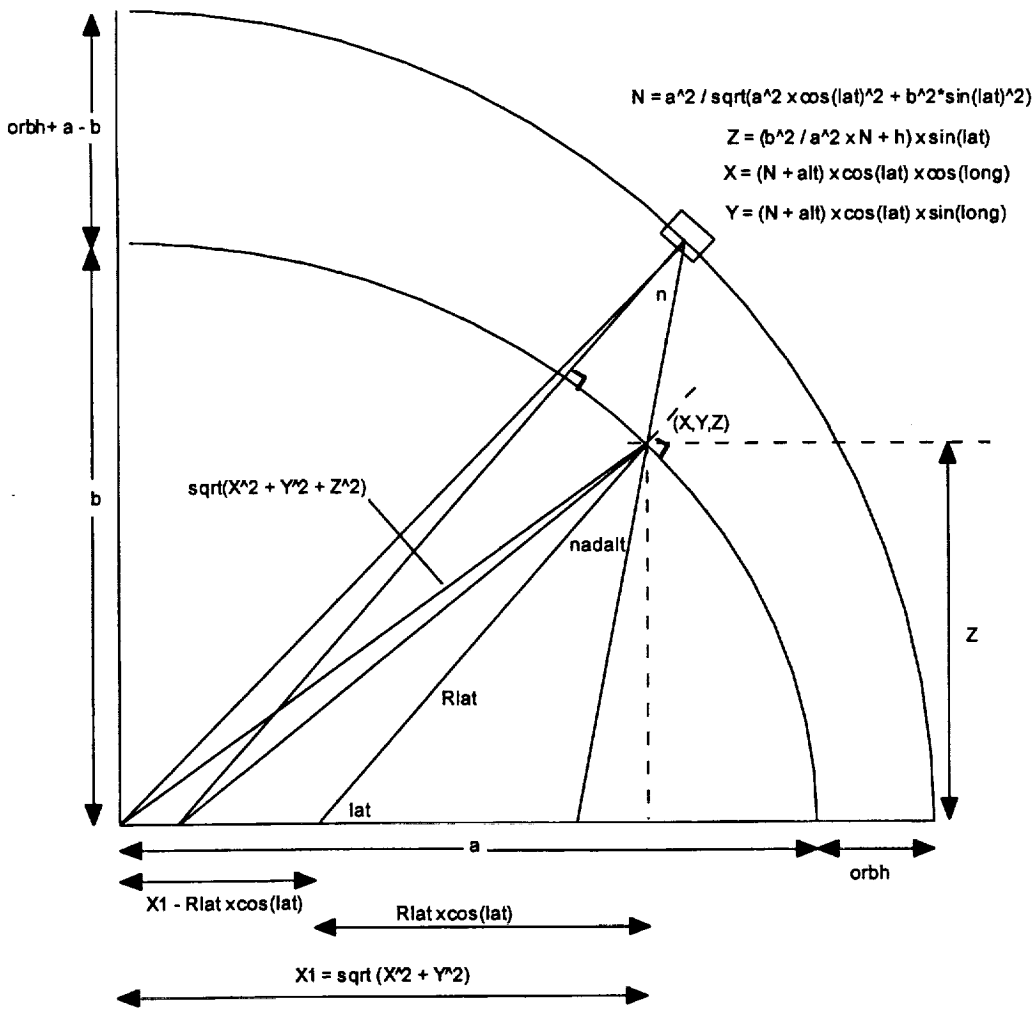

Figure 2) The measurement geometry in the 'vertical' plane

The combined line of sight velocity is given by:

$$los\_vel := htrgtv\ \cos(-az - \text{orblat}(lat, inc) + trgta)\ \sin(\text{nadalt}(orbh, n, alt, lat))$$
$$+ vtrgtv\ \cos(\text{nadalt}(orbh, n, alt, lat)) + hsatv\ \cos(az)\ \sin(n) + vsatv\ \cos(n)$$
$$+ \text{Vlat}(lat)\ \sin(\text{orblat}(lat, inc) + az)\ \sin(\text{nadalt}(orbh, n, alt, lat)) \qquad \text{EQ(1)}$$

where the first and second terms are the line of sight components of the target velocity with respect to the local WGS84 [2,3] earth ellipsoid surface. The third and fourth terms are the line of sight components of the spacecraft horizontal and vertical velocities. The final term is the component of the earth's rotational velocity along the line of sight. Table (1) lists the 11 base parameters listed in this equation while table (2) identifies the functions called out in equation (1):

Symbol	Parameter
htrgtv	target horizontal velocity
vtrgtv	target vertical velocity
trgta	angle of the target velocity with respect to the local meridian
az	azimuth angle with respect to the spacecraft velocity vector
lat	latitude of the spacecraft
inc	orbit inclination angle
orbh	orbit height
n	instrument nadir angle
alt	altitude of the target with respect to the local WGS84 ellipsoid surface
hsatv	horizontal component of the spacecraft velocity
vsatv	vertical component of the spacecraft velocity

Table 1) Fundamental parameters.

Function	Purpose
orblat(lat,inc)	The angle of the satellite velocity vector to the local meridian
nadalt(orbh,n,alt,lat)	The nadir angle the line of sight makes with the target with respect to the local WGS84 ellipsoid surface
vlat(lat)	The earth's rotational velocity at a latitude, lat

Table 2) Functions referred to in equation (1).

For the purpose of assessing the line of sight performance of the instrument we look at the velocity returns from the earth ground return ie the first two terms of equation (1) are zero. We can look at the sensitivity of the line of sight velocity as a function of the parameters listed in table (1). The analyses shown here also include the dependencies of the functions listed in table (2) on the parameters listed in table (1) as well as any dependencies on the WGS84 ellipsoid model[2,3]. Unless otherwise stated these analyses used the baseline parameter values listed in table (3).

		300 km orbit	833 km orbit
Horizontal target velocity	htrgtv, (m/s)	0	0
Vertical target velocity	vtrgtv, (m/s)	0	0
Angle of target velocity wrt local meridian	trgta, (m/s)	0	0
Scanner azimuth angle wrt velocity vector	az, (deg)	varies	varies
Latitude	lat, (deg)	45	45

Orbit inclination	inc, (deg)	52	89
Orbit height at the equator	orbh, (km)	300	833
Nadir angle	n, (deg)	30	45
Target altitude	alt, (m)	0	0
Satellite horizontal velocity	hsatv, (m/s)	Sqrt(Me x G / (orbh+a))	sqrt(Me x G / (orbh+a))
Satellite vertical velocity	vsatv	0	0

Table 3) Baseline parameter values used for analyses.

For the purpose of the analyses the spacecraft horizontal velocity was calculated using the equation given in table (3), where Me is the earth's mass, G is the gravitational constant and a is the WGS84 semimajor ellipsoid axis. The sensitivity of the line of sight velocity to each of the parameters is summarized in table (4) for a 300 km orbit altitude and table (5) for a 833 km orbit altitude. These two altitudes represent the orbit heights for an STS based instrument and an instrument flying on the NPOESS platform respectively.

Parameter	Maximum Error Rate	Error required to give 1 m/s los error
Azimuth angle	68 (m/s)/deg	256 microradians
Nadir angle	118 (m/s)/deg	125 microradians
Orbit height	0.31 (m/s)/km	3.22 km
Latitude	24 (m/s)/deg *	725 microradians
Orbit inclination	3.7 (m/s)/deg	4.7 milliradians
Target altitude	0.02 (m/s)/km	50 km
Satellite horiz. velocity	0.5 (m/s)/(m/s)	2 (m/s)
Satellite vert. velocity	0.87 (m/s)/(m/s)	1.15 (m/s)

* This is the error rate at a latitude 0.5 deg. below the maximum latitude.

Table 4) LOS velocity sensitivities for a lidar with a 30 deg. nadir angle, in a 300 km, 58 deg inclination orbit.

Parameter	Maximum Error Rate	Error required to give 1 m/s los error
Azimuth angle	93 (m/s)/deg	187 microradians
Nadir angle	93 (m/s)/deg	187 microradians
Orbit height	0.36 (m/s)/km	2.77 km
Latitude	19 (m/s)/deg *	919 microradians
Orbit inclination	6.5 (m/s)/deg	2.68 milliradians
Target altitude	0.03 (m/s)/km	33 km
Satellite horiz. Velocity	0.7 (m/s)/(m/s)	1.4 (m/s)
Satellite vert. Velocity	0.7 (m/s)/(m/s)	1.4 (m/s)

* This is the error rate at a latitude 0.5 deg. below the maximum latitude.

Table 5) LOS velocity sensitivities for a lidar with a 45 deg. nadir angle in a 833 km, 89 deg. inclination orbit

Note that the error due to each of the parameters is generally a complex function of other parameters (typically azimuth and/or latitude) and the values in tables (4) & (5) represent the worst case analysis except where noted. Appendices (1) & (2) contain plots of the variation of the line of sight velocity with each of these parameters and with combinations of each of these parameters.

It should be noted in passing that the sensitivities above are valid for any instrument, regardless of measurement technique, that is intended to measure wind velocities on a single shot basis.

2.1.2 Instrument measurement technique

In addition to the sensitivities listed above there will be line of sight velocity sensitivities associated with the measurement technique itself. For a coherent Doppler lidar, the technique under consideration, a single frequency stable laser pulse is transmitted out into the atmosphere and the Doppler shifted return signal is detected by heterodyning with a second local oscillator laser whose frequency is known with respect to the outgoing laser pulse. At the 2 micron wavelength currently envisioned for a space based coherent Doppler lidar the large Doppler shifts due to the spacecraft velocity result in frequency shifts greater than the bandwidth of available detectors. This detector bandwidth limitation can be overcome by tuning either the local oscillator or the transmitted outgoing pulse to reduce the bandwidth requirement on the detector [4].

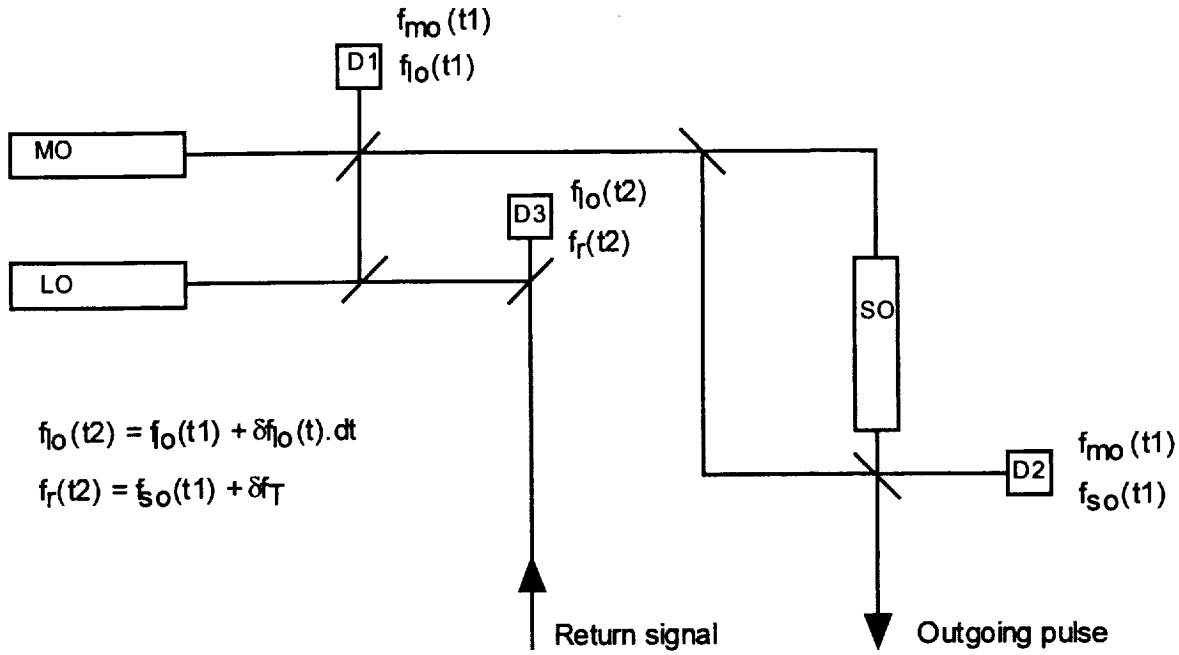

Figure 3) A schematic representation of a coherent lidar

Figure (3) shows a schematic representation of a coherent lidar that differs from that presented in reference [4] in that there is no absolute frequency stabilisation. The figure shows the various optical frequencies, f_x at each of the detectors where the subscript x is either mo, lo or so which represent the master oscillator, local oscillator and slave oscillator laser respectively. The frequency is also potentially a function of time and $f_x(t1)$ represents the time of the outgoing (transmitted) pulse and $f_x(t2)$ represents the returning signal pulse a few milliseconds later. The object to be measured, the Doppler shift induced on the signal due to the spacecraft velocity, earth's rotational velocity and the atmospheric wind velocity is δf_T. The heterodyne beat frequencies fD1(t1), fD2(t1) and fD3(t2) on each of the detectors D1, D2 and D3 respectively are given by:

$$fD1(t1) = f_{lo}(t1) - f_{mo}(t1) \qquad \text{EQ(2)}$$

$$fD2(t1) = f_{so}(t1) - f_{mo}(t1) \quad \text{and} \qquad \text{EQ(3)}$$

$$fD3(t2) = f_{so}(t1) + \delta f_T - f_{lo}(t2) \qquad \text{EQ(4)}$$

where

$$f_{lo}(t2) = f_{lo}(t1) + df_{lo}.dt \qquad \text{EQ(5)}$$

df_{lo} is the local oscillator frequency drift rate and dt is the round trip time of flight. Combining these we obtain:

$$df_T = fD3(t2) + fD1(t1) - fD2(t1) - \delta f_{lo}.dt \qquad \text{EQ(6)}$$

which expresses the Doppler shift frequency in terms of the measured heterodyne frequencies and the local oscillator frequency stability during the round trip time. This technique reduces the bandwidth required on the atmospheric signal detector, D3 by transferring the full Doppler shifted bandwidth to the MO/LO detector, D1. The high signal to noise ratio present on this detector permits the falloff in sensitivity associated with exceeding the detector bandwidth to be tolerated. For the frequency measurement on each detector there will be a component due to the electronics used to capture the signal and a component due to the algorithm used to determine the frequency of the measured signal. The contribution due to the algorithm will vary depending on the signal to noise ratio, time duration of the sample used to measure the frequency, the frequency bandwidth of the return signal and the velocity algorithm used[5]. In order to separate out the errors due to the instrument from those due to the target the line of sight velocity accuracy due to the instrument is usually specified in terms of a high signal to noise ratio and assuming a quiescent atmosphere [6]. The frequency bandwidth of the return signal can then be assumed to be that of the outgoing laser pulse.

2.1.2.1 Tuning algorithm

In a practical lidar the tuning algorithm will have to accomplish a number of tasks. It must:

- Reduce the bandwidth on the atmospheric return signal detector. For a target velocity of 0 m/s we would like the return signal frequency to be independent of both the lidar azimuth angle and the position on orbit. This means that the tuning algorithm must compensate for both the line of sight component of the spacecraft velocity (effectively Figures A1.34 and A2.34) and the line of sight component of the earth's rotational velocity (Figures A1.58 and A2.58).
- Permit the MO/LO offset frequency to be accurately determined. This typically means that it is desired that the MO/LO frequency remain above some minimum frequency to permit adequate frequency measurement.
- Allow for any frequency offsets introduced by the slave oscillator.

Appendices A1 and A2 outline an algorithm to achieve these requirements. For the purposes of this analysis it needs to be noted that the algorithm for tuning the master oscillator introduces a Doppler offset error (Figures A1.71 and A2.71) that must either be accounted for in post-processing or included as an element in the line of sight velocity error budget.

2.2 Position accuracy

Knowledge of the instrument position is required in order to be able to correctly assign a position to the velocity measurement.

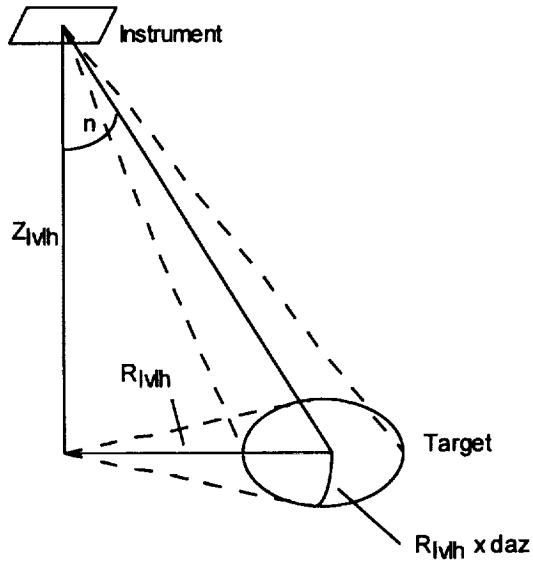

Figure 4) The geometry for determining the position of the measurement with respect to the instrument position.

From Figure (4) we can conceptually see that errors in the azimuth or nadir angle cause the line of sight to describe a cone about the 'true' or 'ideal' value. The position of the measurement relative to the instrument is simply:

$$Z_{lvlh} := \frac{1}{2} c\, t_{rtrp} \cos(n) \qquad \text{EQ(7)}$$

in the vertical and

$$R_{lvlh} := \frac{1}{2} c\, t_{rtrp} \sin(n) \qquad \text{EQ(8)}$$

is the radial distance from the sub-instrument point to the target location, c and t_{rtrp} are the velocity of light and the round trip time of flight respectively. Finally we must constrain the azimuthal direction such that the circumferential distance from the 'true position' can be determined. This distance is simply (R_{lvlh} x daz) where daz is the error in azimuth angle. This provides the target position in a local coordinate frame which can then be transformed to obtain the target position with respect to WGS84.

Tables (6) and (7) show the sensitivity of the vertical and horizontal position knowledge for a lidar with a 30 deg nadir angle in a 300 km, 58 deg orbit while tables (8) and (9) show the sensitivities for a lidar with a 45 deg nadir angle in a 833 km, 89 deg orbit.

Parameter	Error Rate	Error required to give 1m error
Instrument vertical position	1 m /m	1 m
Nadir angle	44 m / 200 μrad	4.55 μrad
Round trip time	40 m / 300 ns	7.5 ns

Table 6) Vertical position assignment sensitivity for a lidar with a 30 deg. nadir angle in a 300 km, 58 deg. orbit.

Parameter	Error Rate	Error required to give 1m error
Instrument horizontal position	1 m /m	1 m
Nadir angle	40 m / 100 μrad	2.5 μrad
Round trip time	24 m / 300 ns	12.5 ns
Azimuth angle	24 m/ 100 μrad	4.17 μrad

Table 7) Horizontal position assignment sensitivity for a lidar with a 30 deg. nadir angle in a 300 km, 58 deg. orbit.

Instrument vertical position	1 m /m	1 m
Nadir angle	180 m / 200 μrad	0.9 μrad
Round trip time	32 m / 300 ns	9.4 ns

Table 8) Vertical position assignment sensitivity for a lidar with a 45 deg. nadir angle in a 833 km, 89 deg. orbit.

Parameter	Error Rate	Error required to give 1m error
Instrument horizontal position	1 m /m	1 m
Nadir angle	180 m / 100 μrad	0.9 μrad
Round trip time	32 m / 300 ns	9.4 ns
Azimuth angle	91 m/ 100 μrad	1.1 μrad

Table 9) Horizontal position assignment sensitivity for a lidar with a 45 deg. nadir angle in a 833 km, 89 deg. orbit.

2.3 Backscatter sensitivity

The signal to noise ratio dependence on backscatter sensitivity has been comprehensively documented in the literature [1] and will not be discussed extensively here. The main difference between ground and

aircraft based coherent lidar and space based coherent lidar relates to the extended time of flight of the photons from the lidar to the target and back again. The round trip time of flight to a typical target distance of 20 km for a ground or aircraft based lidar system is < 150 μs. This is not the case for a space based coherent lidar where the round trip time of flight varies from ~2 ms at 300 km orbit heights to ~9 ms at 833 km (figures A1.31 and A2.31).

2.3.1 Round trip pointing alignment

The round trip pointing alignment is a critical consideration for a space based coherent lidar. It directly affects the sensitivity of the lidar instrument. The coherent lidar heterodyne and system efficiencies are given by the overlap integral [6]:

$$\eta_h = \frac{(\lambda \cdot r)^2 \cdot T_L}{A_R} \cdot \frac{\int I_T(s) \cdot I_L(s) d^2 s}{T_T \cdot T_L \cdot P_T \cdot P_R} \qquad \text{EQ(9)}$$

and

$$\eta_s = T_T \cdot \frac{A_R}{A_T} \cdot \eta_h \qquad \text{EQ(10)}$$

where λ is the wavelength, r is the distance to the far field, P_T and P_R are the transmit and backpropagated local oscillator (BPLO) powers before truncation, $I_T(s)$ and $I_L(s)$ are the intensity distributions of the transmit and BPLO beams in the far field, T_L and T_T are the power truncation ratios at the lidar pupil, A_R and A_T are the area of the receiver and transmit lidar pupils respectively. Typically a coherent lidar system uses a monostatic configuration in which $A_R = A_T$.

The overlap integral in equation (9) results in a reduction in efficiency when the return signal and local oscillator beams are misaligned. Figure (5), normalised to the efficiency for no misalignment, shows how the heterodyne efficiency falls off for a 2 micron lidar as a function of misalignment for telescope diameters of 0.25, 0.5 and 1 m. In a typical ground or aircraft based lidar the only contribution to this misalignment comes from misalignments within the instrument itself and these are typically removed during the lidar alignment process.

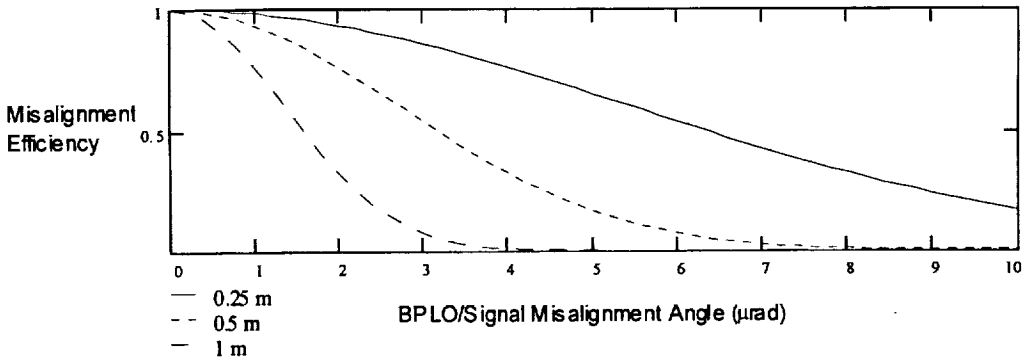

Figure 5) The lidar system efficiency dependence on jitter during the signal round trip time.

During the round trip time a number of things occur or can occur that are typically not an issue for ground or aircraft based coherent lidars:

- the nadir angle tips due to rotation of the orbiting platform about the earth. From figures A1.32-1.33 and A2.32-2.33 we see that this varies from ~3 μrad. for a 30 deg. nadir angle instrument in a 300 km orbit to ~9 μrad. for a 45 deg. nadir angle instrument in a 833 km orbit. As this effect is predictable it can in principle be compensated for. For small aperture coherent lidars this effect can either be taken as a direct loss in SNR (low orbits only) or can be compensated for with a static misalignment built into the system. For large aperture systems with tight alignment budgets a dynamic alignment system may be required to compensate for nadir tipping angle variations as a function of orbit altitude and platform attitude changes (on time scales greater than the round trip time).
- the platform attitude changes during the round trip drift time. Figures (6 and 7) show the change for round trip times of 2 ms and 9 ms respectively.

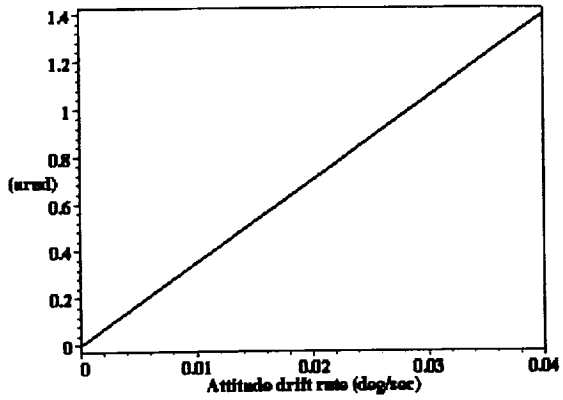

Figure 6) Misalignment due to attitude drift for a 2ms round trip time

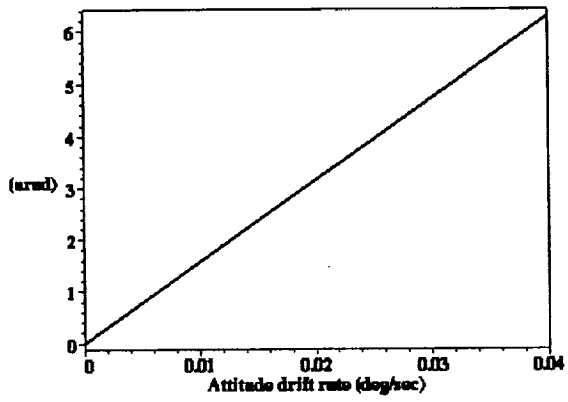

Figure 7) Misalignment due to attitude drift for a 9ms round trip time

Although a more difficult problem than the nadir tipping issue this effect can in principle be dynamically compensated for provided that adequate knowledge of the attitude drift rate is available. It should be noted that platform drift rates generally change over long time scales relative to the lidar round trip time. The small magnitude of the alignment changes required to maintain high heterodyne efficiency for large optical diameters initially appears to be the major issue however a significant benefit can be obtained by placing the compensating element in the small beam portion of the lidar before the expanding telescope. This increases the magnitude of the change required from the compensating element by the magnification of the telescope.

- A vibration source on the platform or in the instrument causes a change in the optical alignment. Due to the 'random' nature of vibration this is potentially the most difficult issue to deal with especially at the higher orbit altitudes where a greater range of frequencies can impact the alignment. The solution of this issue will be very platform dependent.

2.4 Conclusion

The development of an error budget from these sensitivity analyses will be highly dependent on the platform and instrument configuration flown. The SPARCLE instrument [5] represents one possible combination of these errors [7] to meet a desired set of requirements.

3.0 SPARCLE activities

Many of the activities under this contract were intended to prepare for a coherent lidar mission on the NASA space shuttle (STS). Shortly after the award of this contract, NASA MSFC won a New Millenium Program mission to build and fly a coherent lidar, called SPARCLE on the STS. At the time of the conclusion of the period of performance of this contract the SPARCLE program was about to enter Preliminary Design Review. The work conducted under this contract including performance analysis for a shuttle lidar and the discussions with the atmospheric science community concerning modes of operation referred to in the statement of work for this contract were directly relevant to and used by the SPARCLE program.

Consequently appendices A3 and A4 are draft copies of the SPARCLE Preliminary Design Review (PDR) Performance Report and the SPARCLE Appendix E: NASA Hitchhiker Program Customer Payload Requirements (CPR) documentation provided to the Hitchhiker office for manifesting SPARCLE. The Performance Report is a direct result of the work conducted under this contract. The SPARCLE PDR was due to be held in September 1998 and the CPR was also due for submission after the completion of the period of performance of this contract. As a consequence of their draft status there are some inconsistencies in these documents. The PDR performance report contains some duplication of the work presented earlier and the Appendices referred to in the PDR performance report are not included here as they are a subset of the work presented in Appendices A1 and A2 of this report.

The sections in the CPR relating to Principle of Instrument Operation, Modes of Operation, Table of Instrument Functional Modes (Table 1), Operations Scenario Description (2.4.1), Operational Scenario (4.1) including Pointing Knowledge Initialization (OSM6) Details, Experiment Commanding (4.4), Orbiter Pointing (4.7), Field of View (4.8), Operational Science Modes (Appendix 1) were either substantially written by this author or had considerable contribution from this author in consultation with the SPARCLE science and engineering teams. Note that this draft CPR contains some blank pages (pages A4.4, A4.8, A4.9, A4.14, A4.18) which have not been included here – this results in some apparent missing pages when the page numbering is checked.

4.0 Other activities

Part of this contract was intended to commence assembly of a ground based lidar using a 100mJ lidar transceiver, prototype telescope and a structure to be supplied by MSFC. Activities on this were extremely curtailed mostly due to the award of the SPARCLE program to MSFC however the following factors also contributed:

The laboratory in which the 100mJ laser transceiver was housed and in which the ground based lidar was to be developed was converted by MSFC to a conference room. MSFC moved the transceiver into a storage area.

Drawings, developed by UAH under another contract, for a preliminary structure to mount the lidar transceiver to a prototype telescope and scanner were submitted to the MSFC machine shops but withdrawn when the SPARCLE program commenced.

The NASA MSFC coherent lidar database was translated from the prior Borland Paradox format to Microsoft Access and several hundred references with abstracts were added. Table (10) outlines the current number of entries in the lidar database.

Type of Entry	No. of entries
Journal paper	1900
Reports	536
Memos	48
Books	27
Proposals	24
Theses	10

Table 10) Coherent lidar database statistics

5.0 References

[1] See for example R.G. Frehlich and M.J. Kavaya, "Coherent laser radar performance for general atmospheric refractive turbulence", Appl. Opt., 30, 5325 – 5352, 1991.

[2] MIL-STD-240, "Department of Defence World Geodetic System (WGS)", 11 January 1994.

[3] DMATR 8350.2, "Department of Defence World Geodetic System 1984, Its Definition and Relationships with Local Geodetic Systems", Second Edition 1 September 1991.

[4] Gary D. Spiers, "Analyses of Coherent Lidar Wind Measurement Missions", Final Report on Contract No. NAS8-38609, Delivery Order No. 128, Report Date 8/28/96.

[5] See for example "Space Read Coherent Lidar Experiment (SPARCLE) Mission and Science Requirements Document", MSFC-RQMT-2828, NASA Marshall Space Flight Center, 1998.

[6] This form of the overlap integral is described in B.J. Rye and R.G. Frehlich, "Optimal truncation and optical efficiency of an apertured coherent lidar focused on an incoherent backscatter target", Appl. Opt. , 31, 2891 – 2899, 1992.

[7] Gary D. Spiers, "MSFC Space Readiness Coherent Lidar Experiment (SPARCLE) Preliminary Design Review System Performance Analysis Report", NASA MSFC, September 1998 enclsoed here in draft form as Appendix A3 and subsequent reports.

Appendix A1: Satellite Lidar Sensitivity Analyses

300 km, 58 deg inclination orbit, 30 deg nadir instrument

The equations in this document are in MAPLE, a symbolics mathematics package format. Define some constants:

$$r2d := 180\,\frac{1}{\pi}$$

$$d2r := \frac{1}{180}\,\pi$$

$$v\_c := .2997924590\ 10^{9}$$

$$G := .6672590000\ 10^{-10}$$

$$Me := .5979000000\ 10^{25}$$

where r2d and d2r are constants for converting between degrees and radians, v_c is the velocity of light in m/s , G is the Gravitational constant in N m^2/kg^2 and Me is the mass of the earth in kg. Now define the WGS84 ellipsoid parameters:

$$a := .63781370\ 10^{7}$$

$$b := .63567523142\ 10^{7}$$

$$We := .00007292115$$

$$ee := .0818191908426$$

$$ee2 := .00669437999013$$

where a and b are the semimajor (equatorial) and semiminor (polar) radii respectively, We is the angular velocity of the earth, ee and ee2 are the first eccentricity and its square respectively.
Finally define the parameters for this analysis:

$$maxlat := 58$$

$$orbit1 := 300000$$

$$nadir1 := 30$$

where maxlat is the highest latitude that the orbit passes over, orbit1 is the orbit height with respect to the equatorial earth radius, a and nadir1 is the instrument nadir at the spacecraft. We now define a procedure to calculate the radius of the oblate earth with respect to the geodetic latitude. Note that the expression for calculating the geodetic latitude breaks down at the poles and so a check must be made for a latitude of Pi/2 radians.

```
Rlat := proc(lat)
global a, b;
    if lat = 1 / 2*π or lat = - 1 / 2*π then b else 1 / (sqrt(1 / a^2 + tan(lat)^2 / b^2)*cos(lat)) fi
end
```

This next procedure calculates the differential of the earths radius as a function of latitude.

```
dRlat := proc(lat)
global a, b;
    sin(lat) / (cos(lat)^2*sqrt(1 / a^2 + tan(lat)^2 / b^2))
    - 2*tan(lat)*(1 + tan(lat)^2) / (cos(lat)*(1 / a^2 + tan(lat)^2 / b^2)^3*b^2)
end
```

This procedure calculates the earth's rotational velocity at a latitude, lat :

```
Vlat := proc(lat) global We, a, ee2; We*a*cos(lat) / sqrt((1 - ee2)*sin(lat)^2 + cos(lat)^2) end
```

Consider a satellite at some latitude, lat in an orbit of inclination, inc then the angle the satellite orbit makes to a meridian line at latitude, lat is:

```
orblat := proc(lat, inc) arcsin(cos(inc) / cos(lat)) end
```

Plot the angle between orbit and meridian as a function of latitude for the parameters above.

Figure A1.1: Angle between orbit and meridian

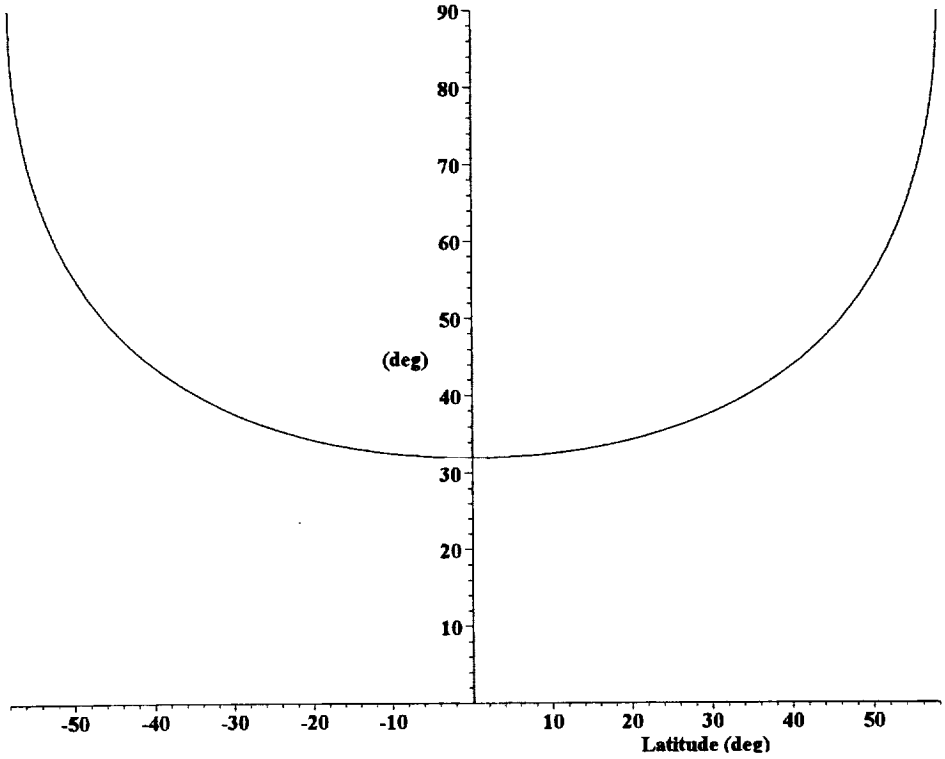

We can also plot the rate of change of the angle between the orbit and meridian as a function of latitude.

Figure A1.2: Rate of change of angle to local meridian

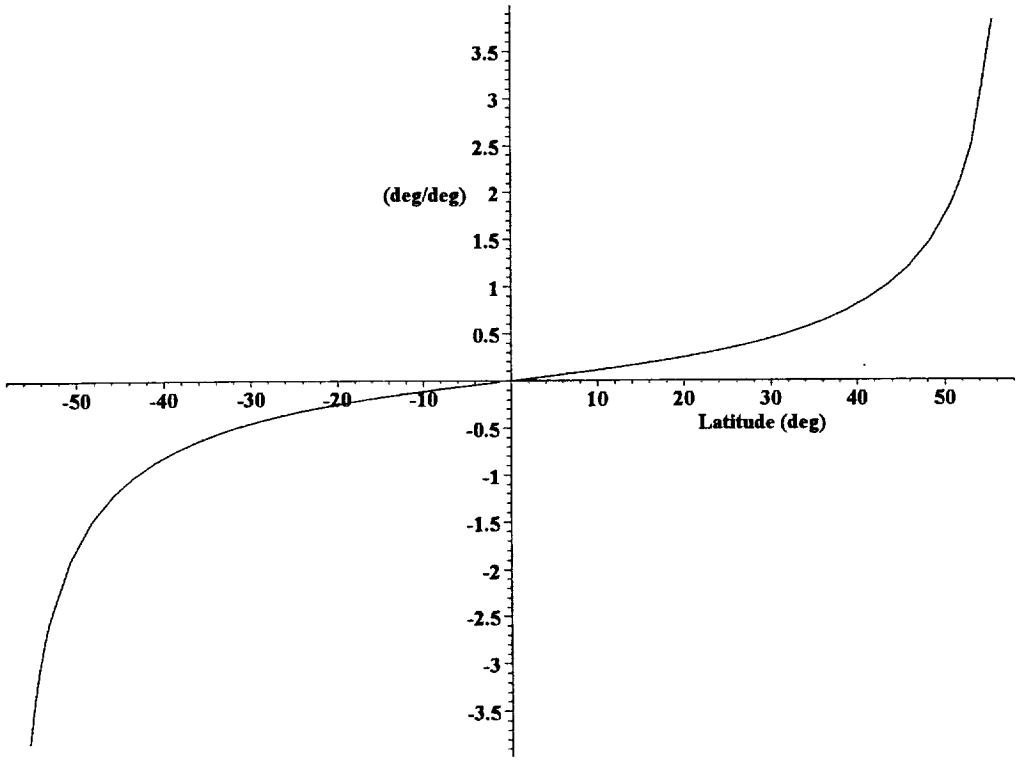

Plot the change in WGS84 earth radius with respect to the equatorial radius as a function of latitude.

Figure A1.3: Variation in the earth's radius as a function of latitude

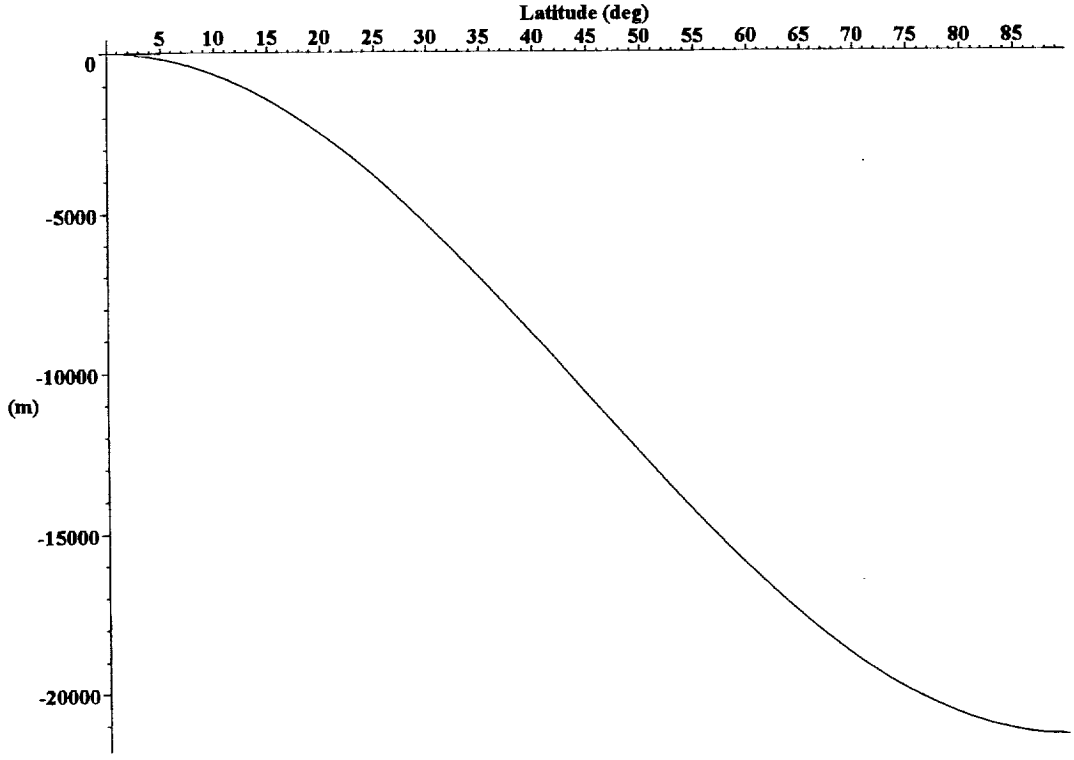

This clearly shows the 20 km difference between the two radii. Plot the distance moved along the surface for one degree

change in latitude.

Figure A1.4: Latitude surface distance

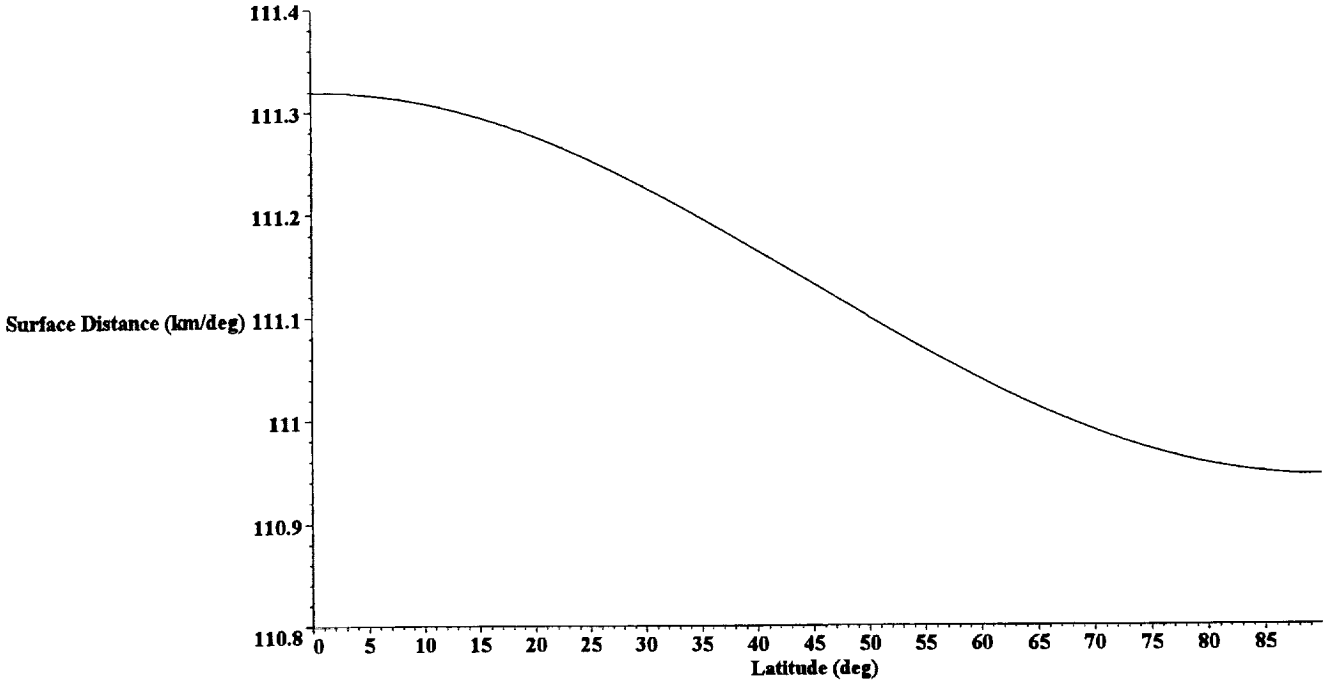

We can replot this as a delta change from the value at the equator.

Figure A1.5: Delta change in Latitude surface distance

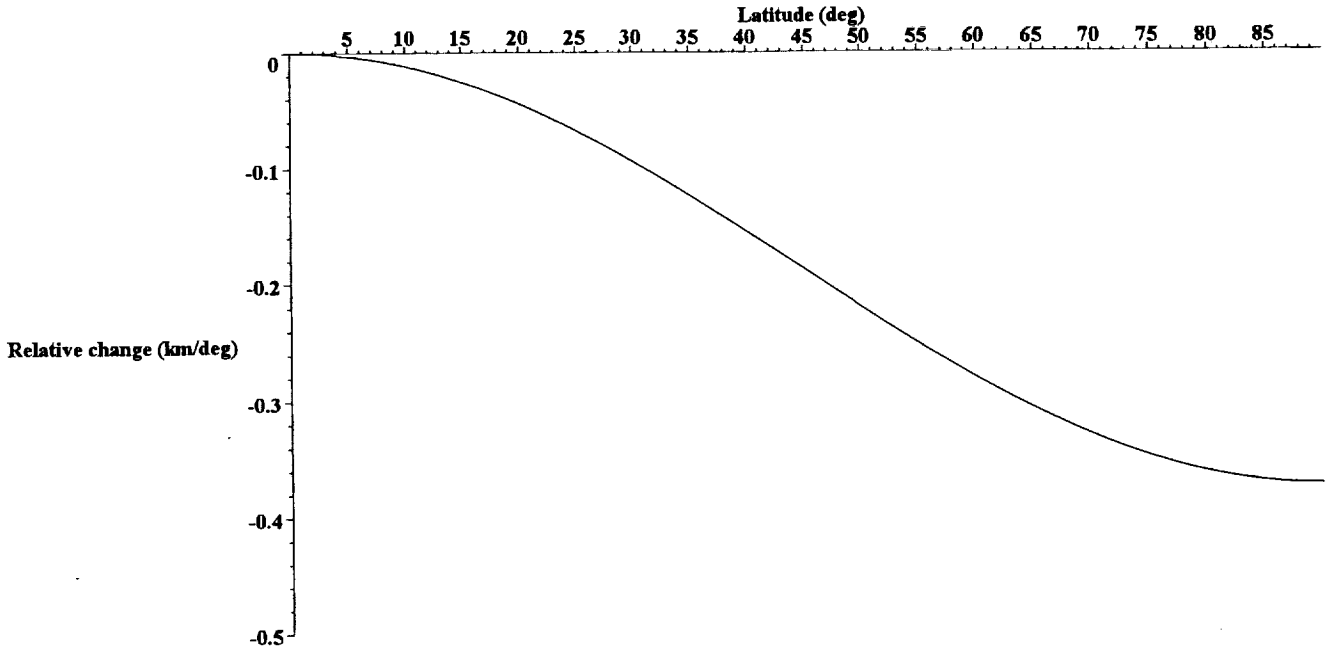

The rate of change of the WGS84 ellipsoid radius is given by:

```
dRlat := proc(lat)
global a, b;
    sin(lat) / (cos(lat)^2*sqrt(1 / a^2 + 1 / (cos(lat)^2*b^2) - 1 / b^2))
    - sin(lat) / (cos(lat)^4*(1 / a^2 + 1 / (cos(lat)^2*b^2) - 1 / b^2)^(3 / 2)*b^2)
end
```

and we can also plot it:

Figure A1.6: Rate of change of the WGS84 ellipsoid radius

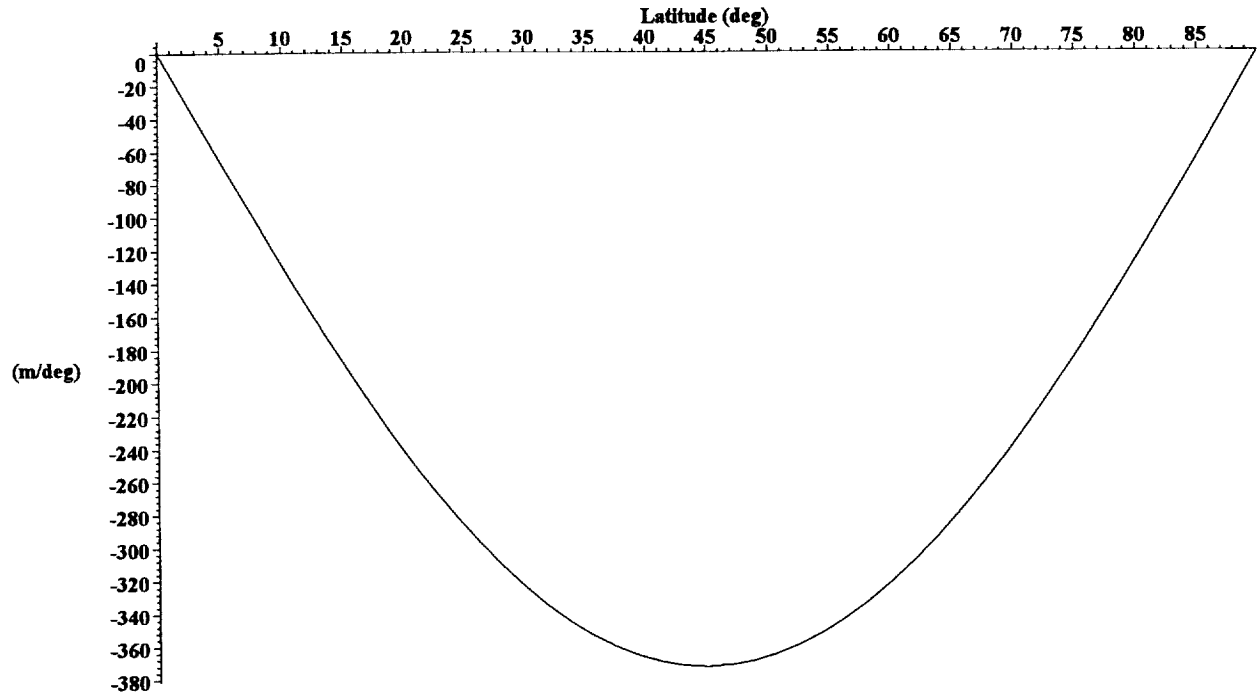

If we plot the integral of the rate of change of the WGS84 ellipsoid with latitude we should get back to the initial plot.

Figure A1.7: Integral of dWGS84/dlat as a fn of lat (sanity check)

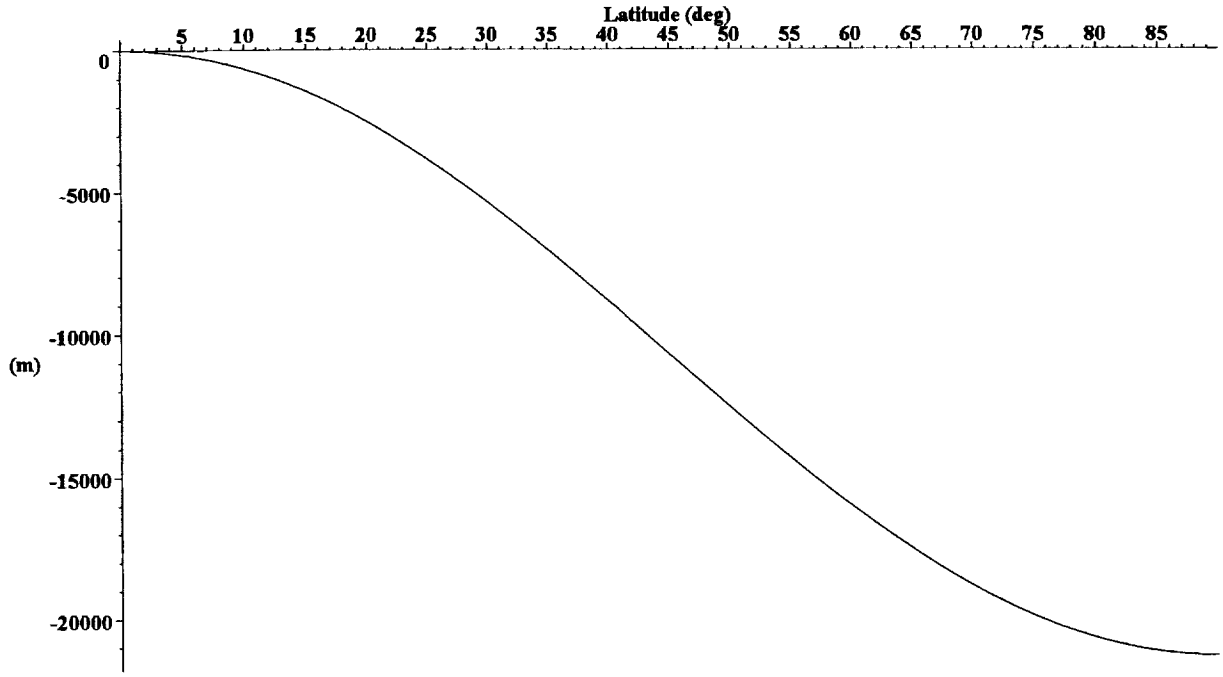

A satellite in a circular orbit around the earth with an orbit radius of (orbh + a), where orbh is the height of the orbit above the equator, has a velocity given by:

vsat := **proc**(*orbh*) **global** *a*, *b*, *G*, *Me*; sqrt(*G***Me* / (*orbh* + *a*)) **end**

The following plot shows the variation in velocity over the orbit heights within 50 km of the nominal orbit height.

Figure A1.8: Satellite Velocity

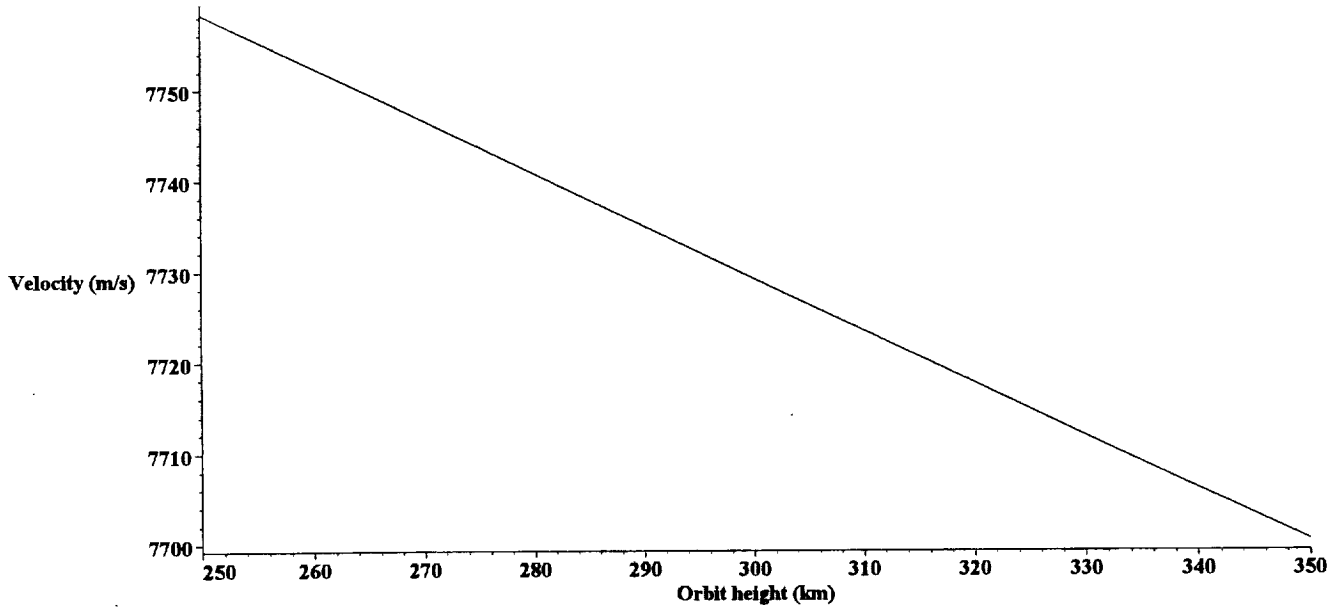

We can replot this as a change in satellite velocity relative to the nominal orbit height.

Figure A1.9: Change in Satellite Velocity

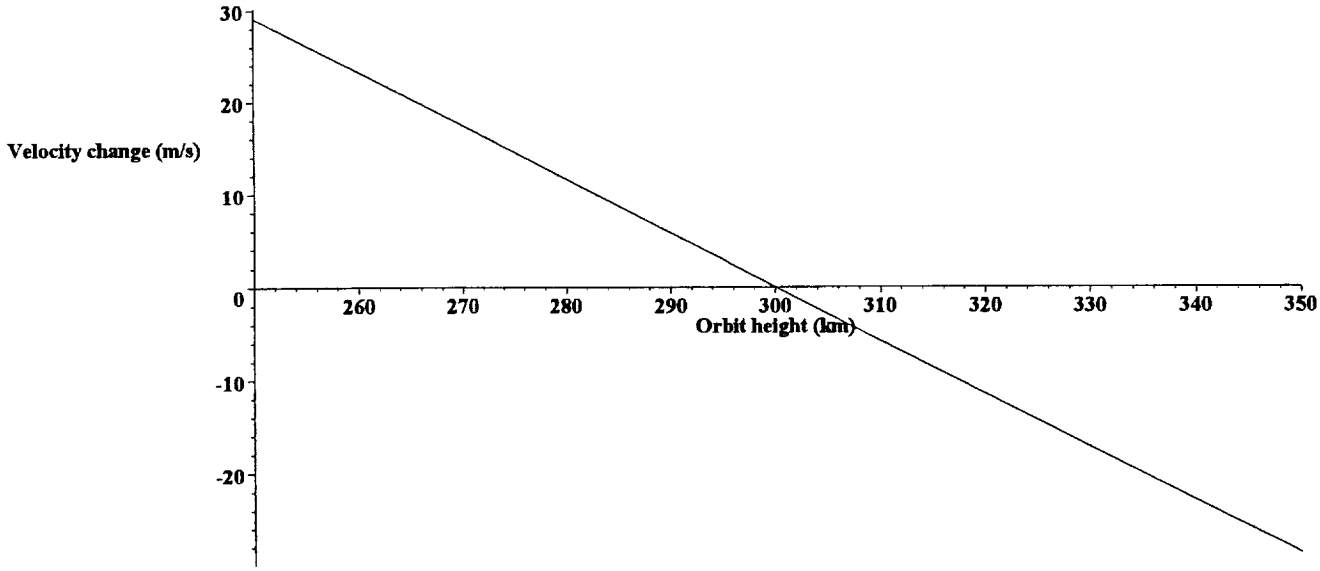

The sensitivity of the satellite velocity to changes in orbit height can be determined by plotting the differential wrt the orbit height:

Figure A1.10: Rate of change in satellite velocity vs. orbit height

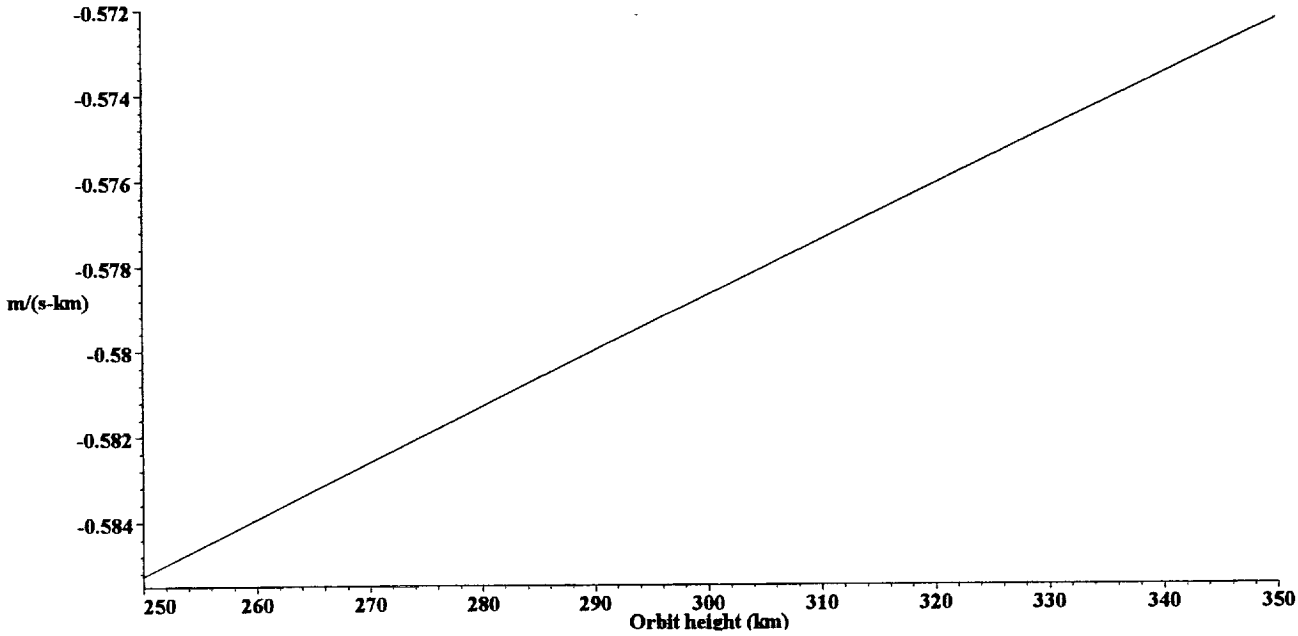

The time for one orbit is simply given by:

torbit := **proc**(*orbh*) **global** *a*, *b*; 2*π*(*orbh* + *a*) / vsat(*orbh*) **end**

and the variation in orbit period over the orbit heights of interest is shown in the following plot:

Figure A1.11: Orbit Period

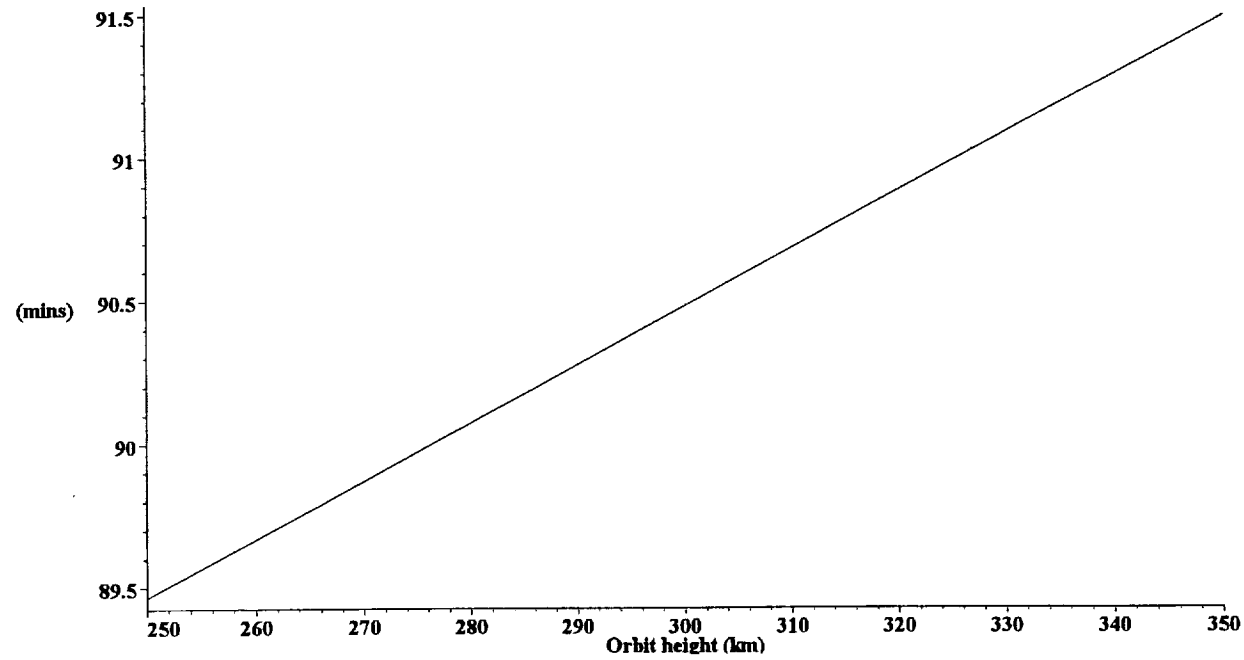

We can modify this to show a delta change wrt the lowest orbit height:

Figure A1.12: Change in orbit period with orbit height

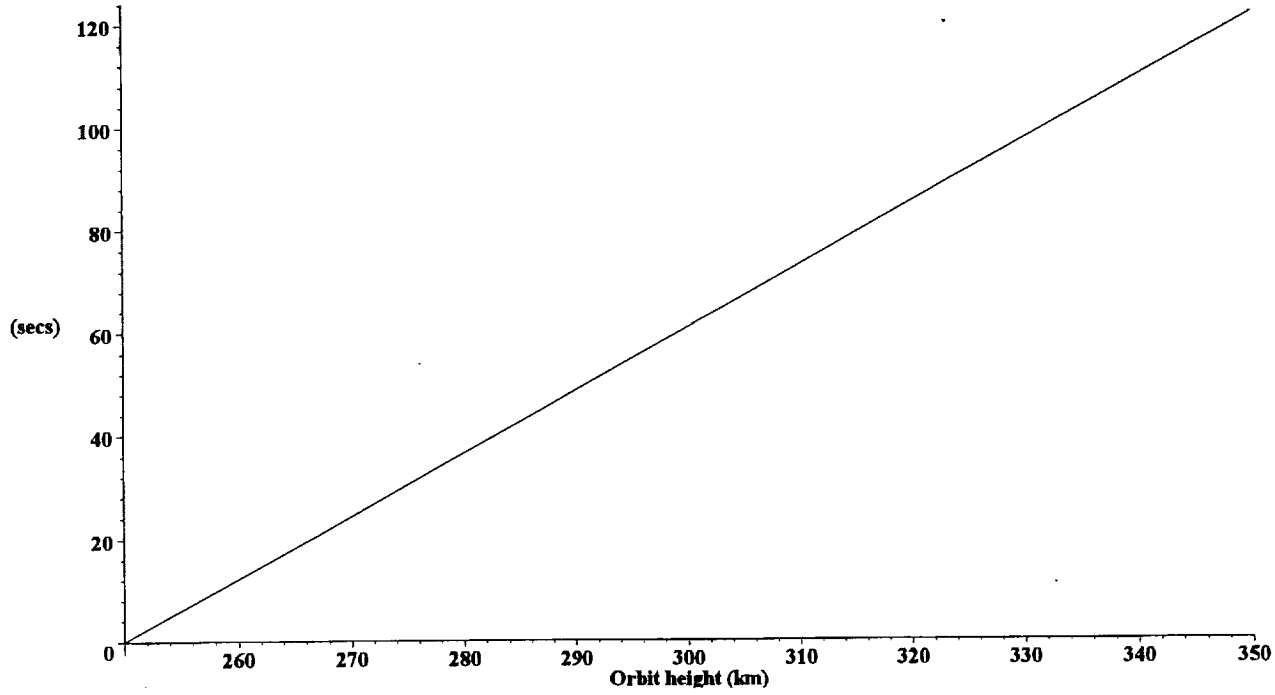

For the orbit conditions specified at the beginning of this document the component of the satellite velocity parallel to the local line of meridian at a given latitude is:

vlat := **proc**(*lat*, *orbh*, *inc*) **global** *a*, *b*; vsat(*orbh*)*cos(orblat(*lat*, *inc*)) **end**

Figure A1.13: Satellite velocity parallel to lines of meridian

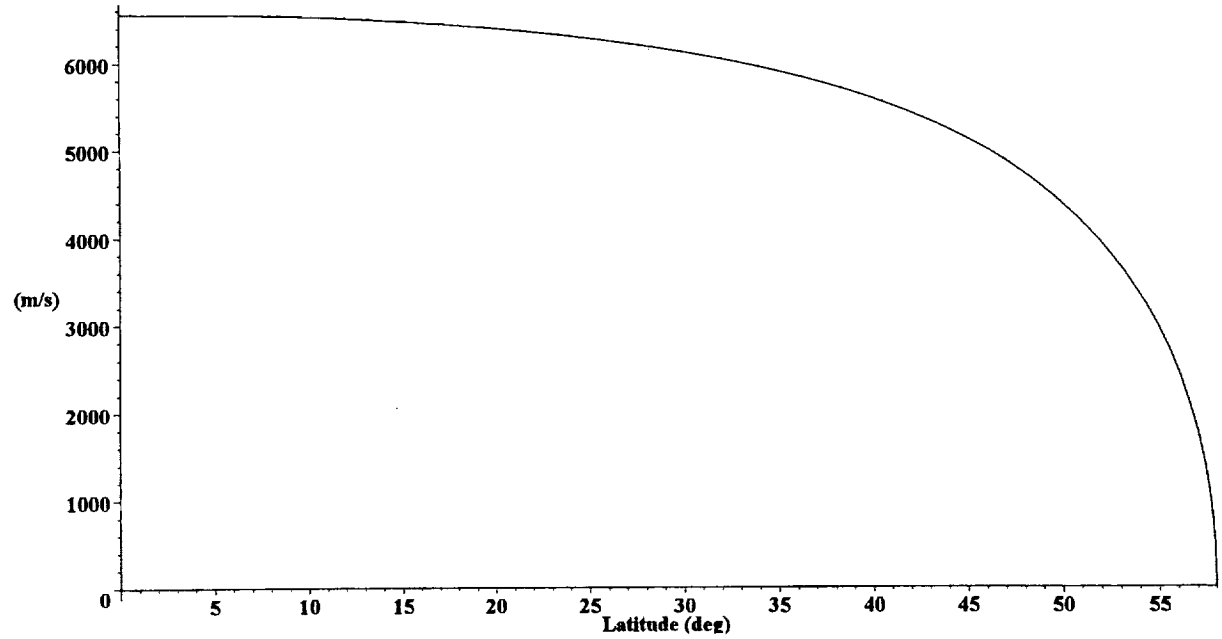

Similarly the component of the satellite velocity parallel to the lines of longitude at a given latitude is:

vlong := **proc**(*lat*, *orbh*, *inc*) **global** *a*, *b*; vsat(*orbh*)*sin(orblat(*lat*, *inc*)) **end**

Figure A1.14: Satellite velocity parallel to lines of longitude

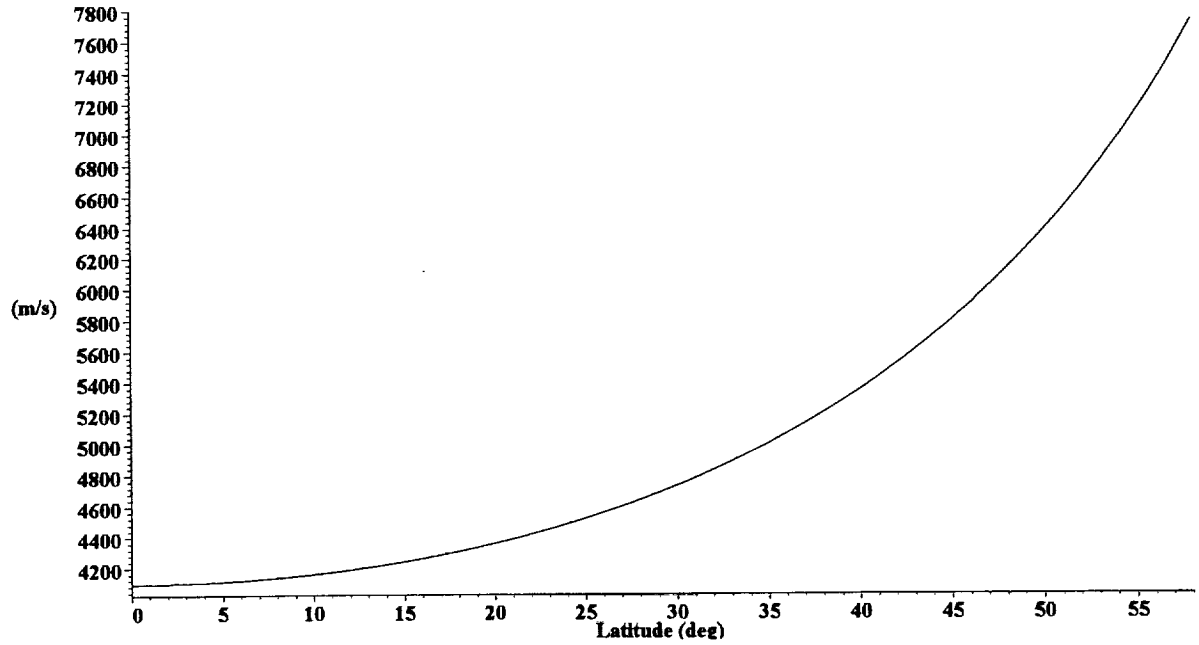

Recombining these we should get a constant satellite velocity independent of latitude:

Figure A1.15: Sqrt(Vlong^2+Vlat^2) (sanity/numerics check)

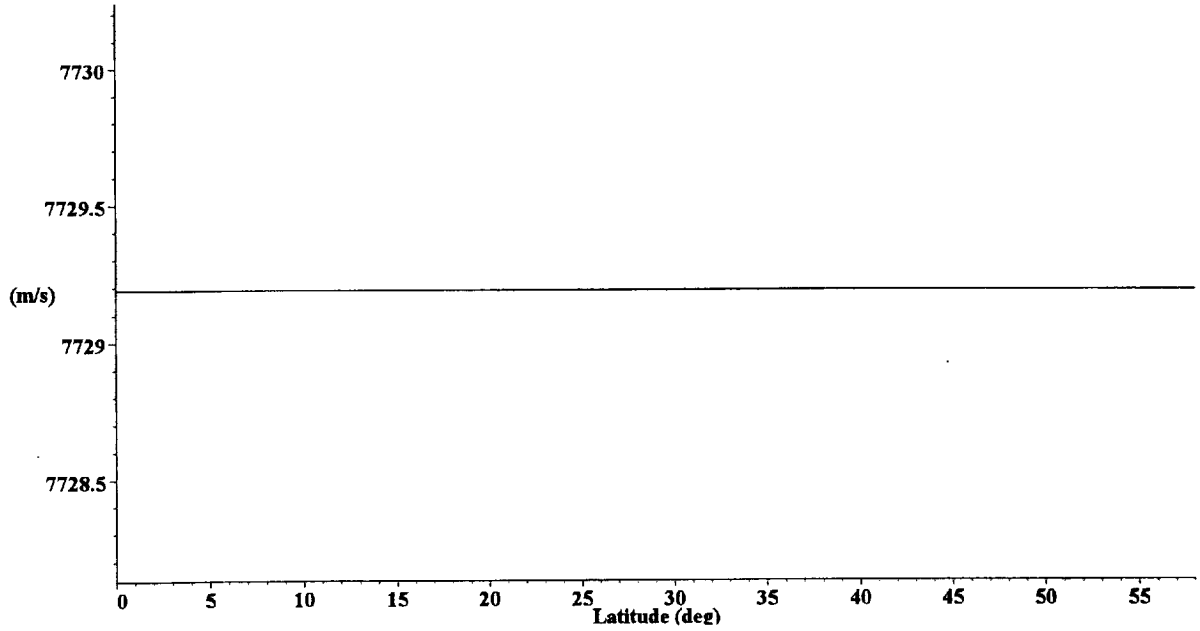

Once we know the component of the velocity along the lines of latitude we can determine the rate of change of latitude as a function of latitude for any given orbit.

$$dlatdt := \textbf{proc}(lat, orbh, inc)\ \textbf{global}\ a, b;\ \text{vlat}(lat, orbh, inc) * r2d / (orbh + a)\ \textbf{end}$$

For the orbit under consideration this gives:

Figure A1.16: Rate of change of latitude

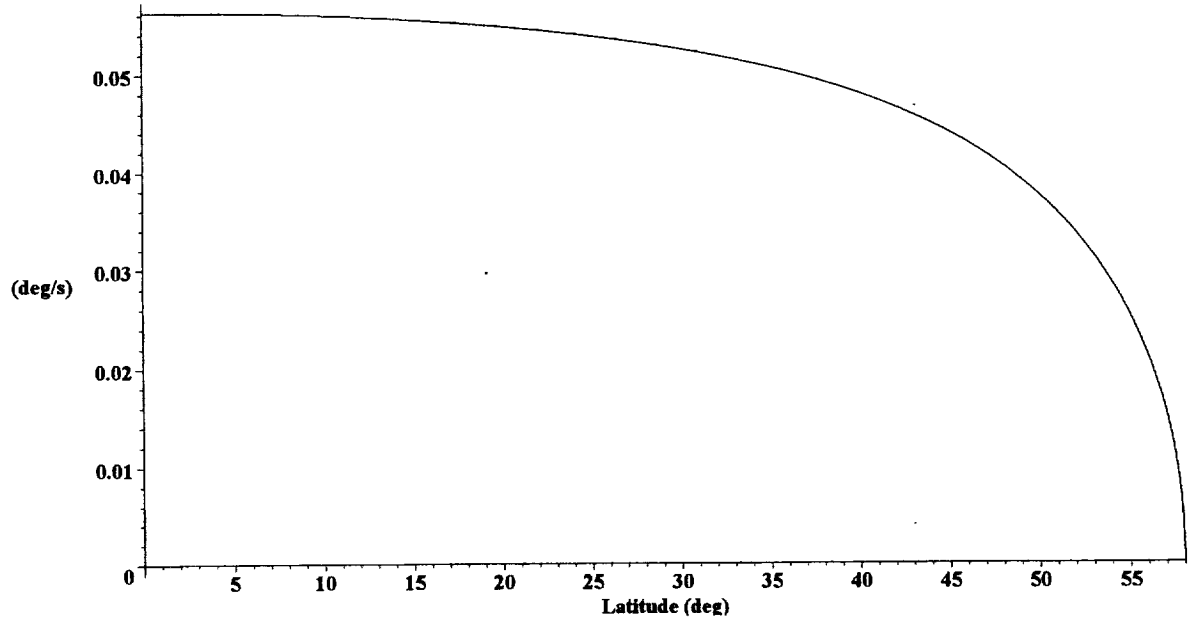

We can then combine this with the WGS84 ellipsoid radius to get the time rate of change of the Earth's radius as a function of latitude for this orbit configuration.

dRlatdt := **proc**(*lat*, *orbh*, *inc*) **global** *a*, *b*; dlatdt(*lat*, *orbh*, *inc*)*dRlat(*lat*)**d2r* **end**

Figure A1.17: Rate of change of the Earth's radius

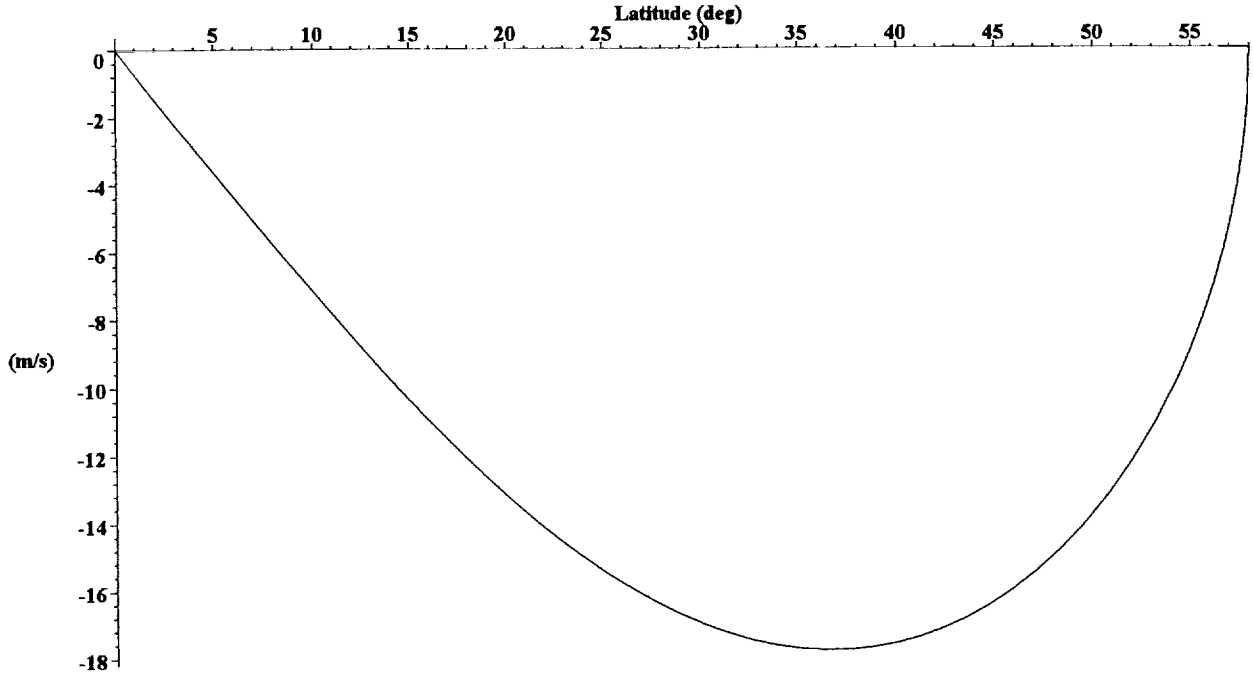

We can look at the earth's rotational velocity as a function of latitude:

Figure A1.18: Earth's rotational velocity at the WGS84 ellipsoid radius

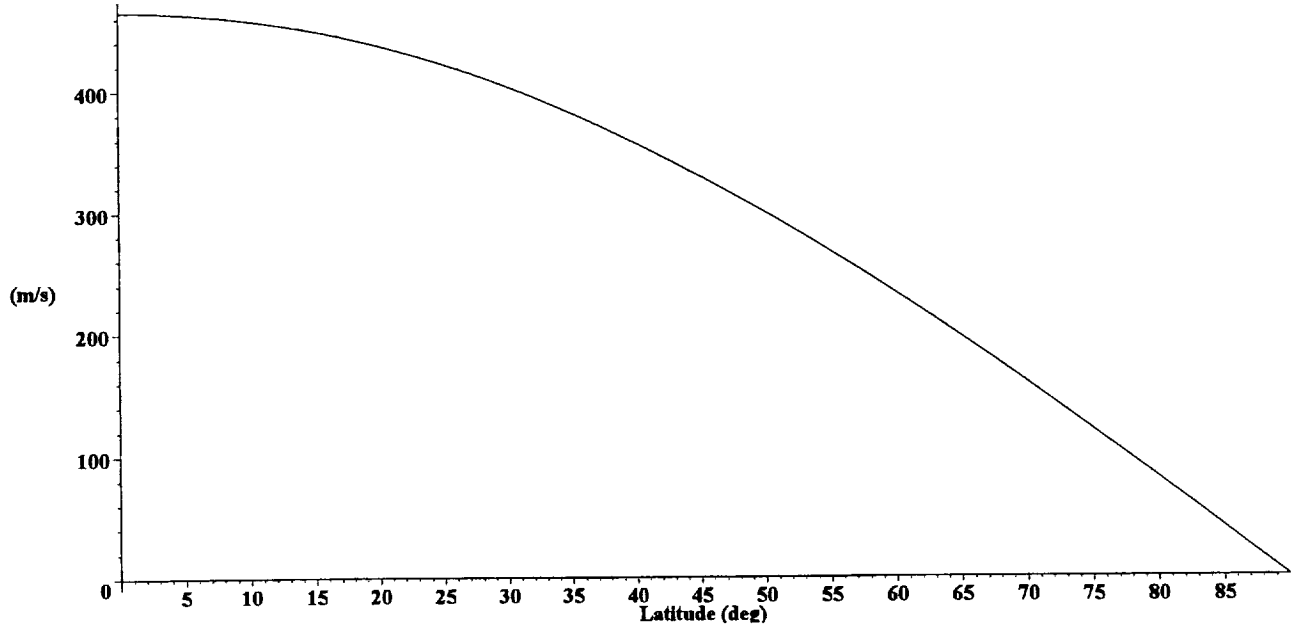

and the rate of change of the earth's rotational velocity with latitude:

Figure A1.19: Rate of change of Earth's rotational velocity with latitude

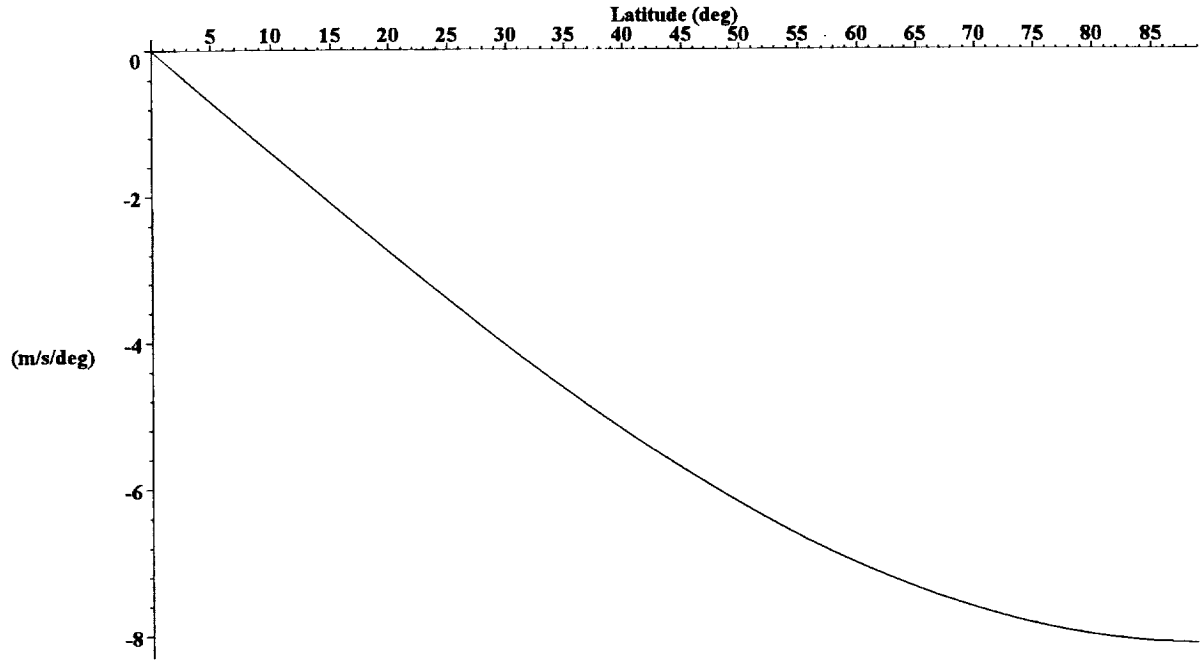

The nadir angle at a target height, alt above the ground is given by:

nadalt := **proc**(*orbh*, *nadir*, *alt*, *lat*) **global** *a*; arcsin(((*orbh* + *a*)*sin(*nadir*)) / (Rlat(*lat*) + *alt*)) **end**

where nadir is the nadir angle at the spacecraft. We can then plot the change in nadir angle at the earth's surface, for the current orbit height and nadir angle as a function of latitude.

Figure A1.20: Nadir angle at the earth's surface

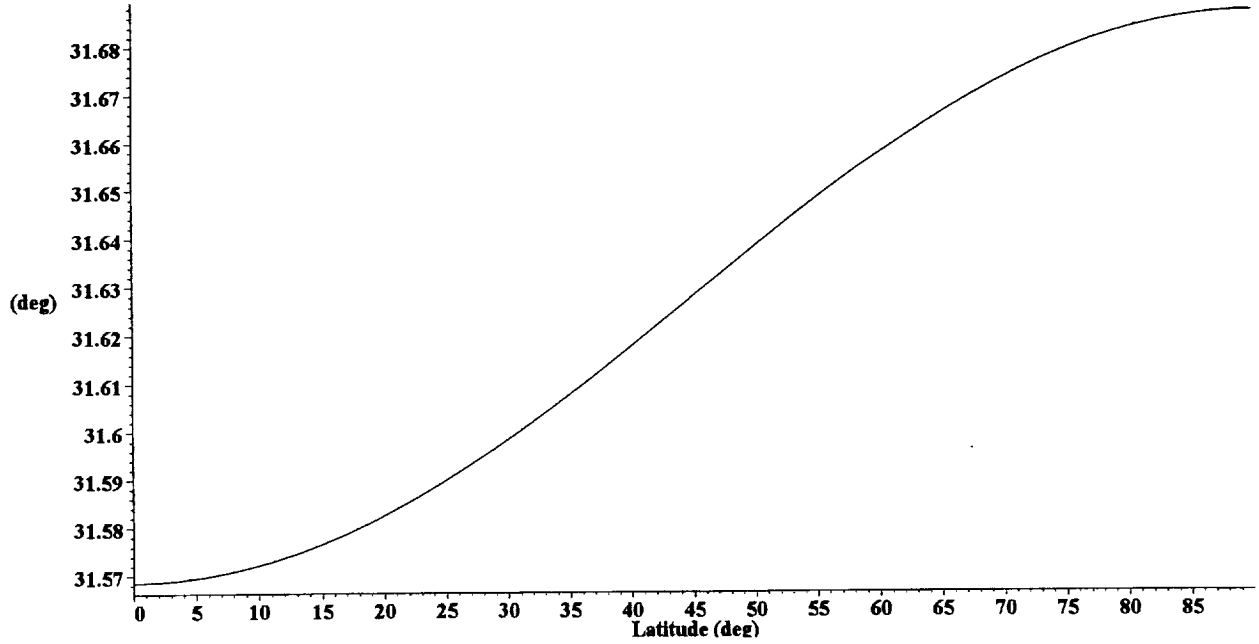

As previously we can show the change in degrees with respect to the nadir angle at the surface near the equator.

Figure A1.21: Variation of the nadir angle at the earth's surface

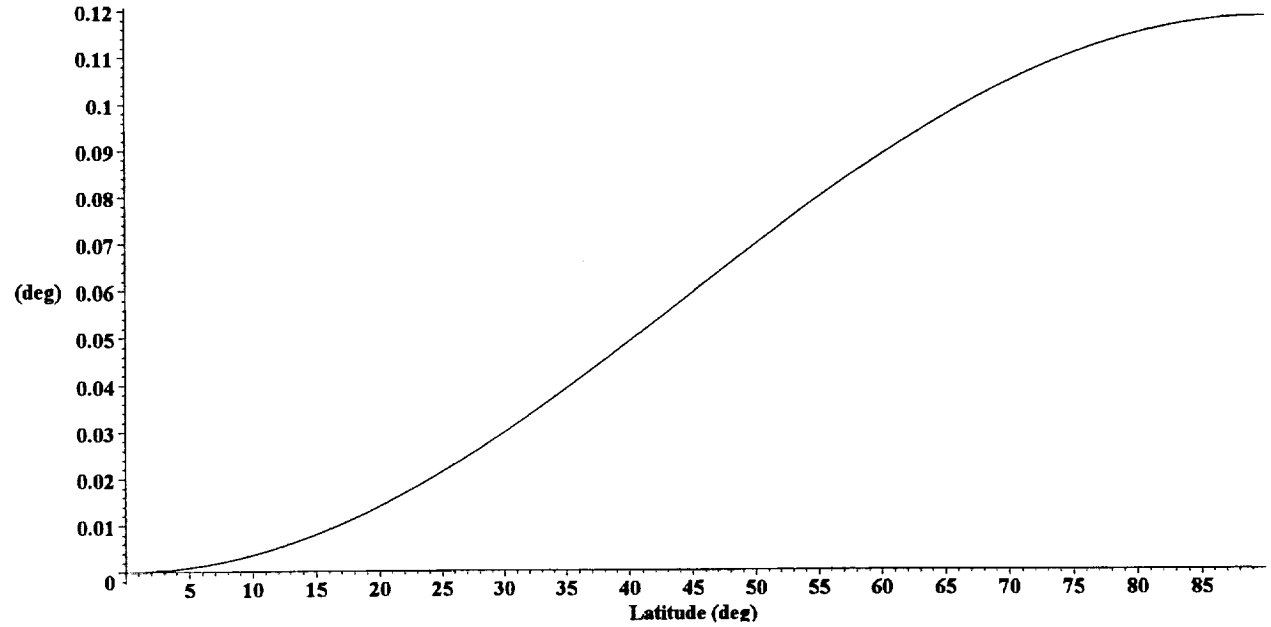

and replot this in milliradians.

Figure A1.22: Variation of the nadir angle at the earth's surface

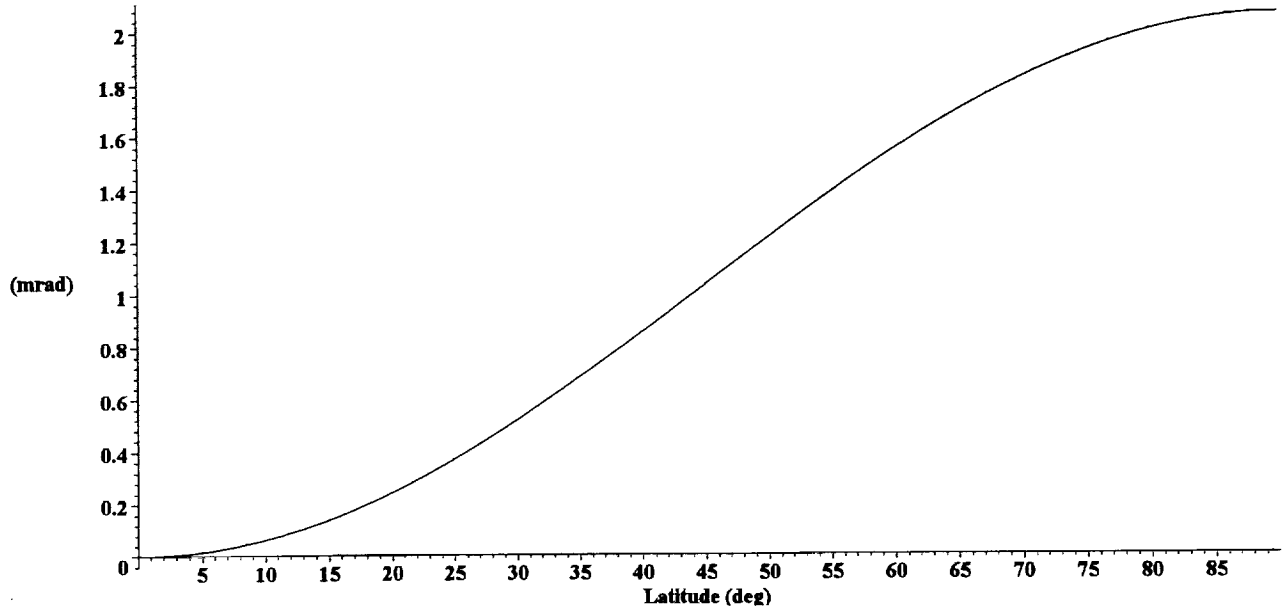

We can also determine the nadir angle at a given target altitude. The following plot is for a latitude of 45 deg.

Figure A1.23: Nadir angle at a given altitude above the surface

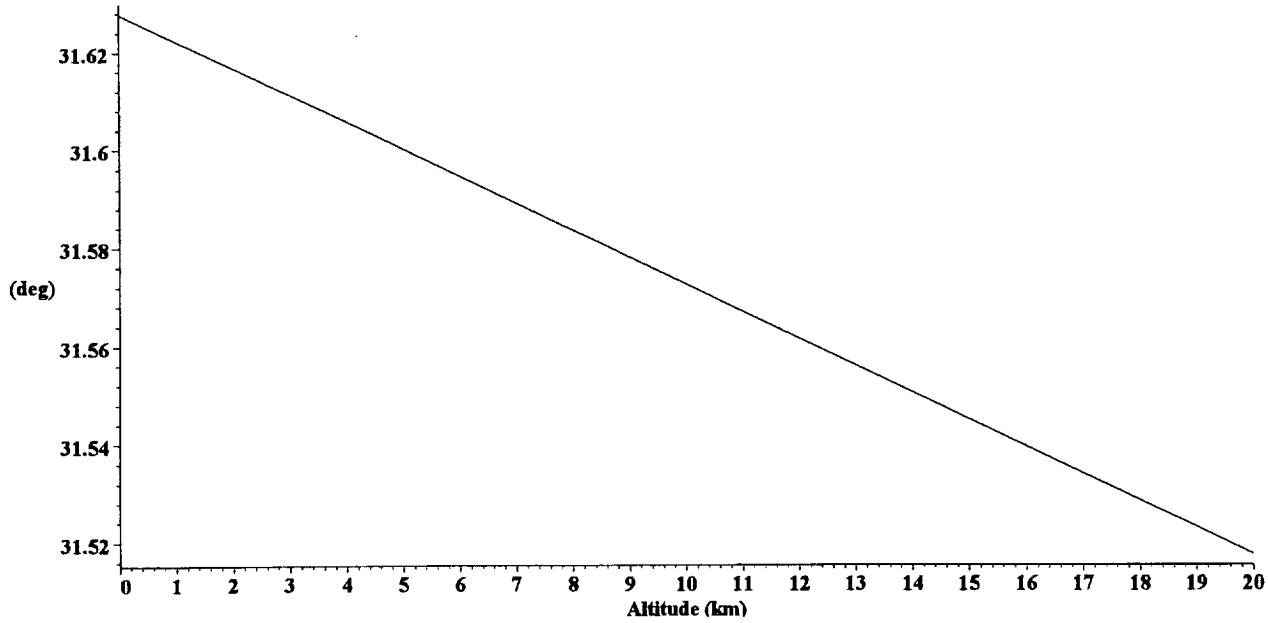

We can combine the altitude and latitude dependencies of the nadir angle at the target:

Figure A1.24: Variation of nadir angle with altitude and latitude

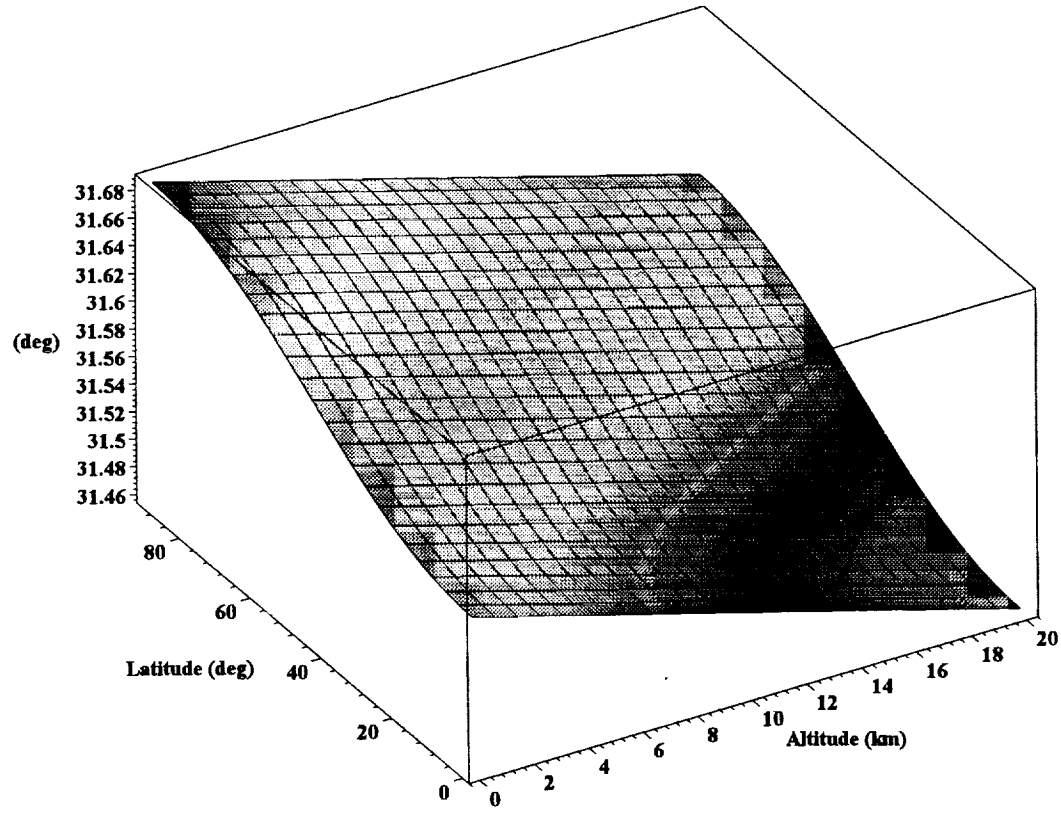

The range from the lidar to a target at an altitude, alt is given by:

```
Range := proc(orbh, nadir, alt, lat)
    sqrt(
    (orbh + a)^2 + (Rlat(lat) + alt)^2 - 2*(orbh + a)*(Rlat(lat) + alt)*cos(nadalt(orbh, nadir, alt, lat) - nadir))
end
```

We can plot this as a function of latitude and target altitude:

Figure A1.25: Range to altitude (wrt WGS84)

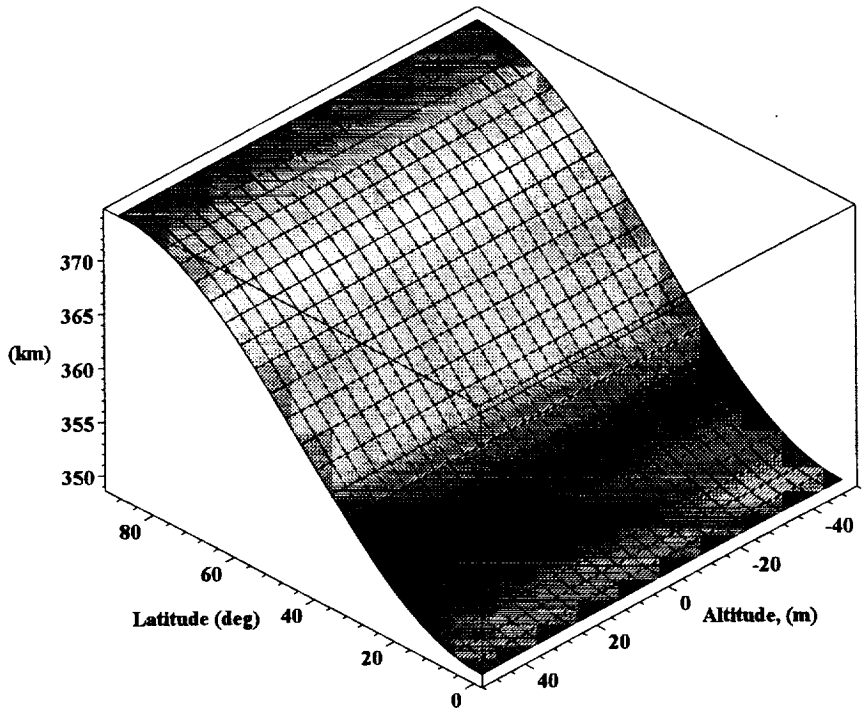

For the orbit conditions documented ealier we can determine the sensitivity of the range to a given altitude by plotting the range as a function of altitude. For the plot shown, a latitude of 45 degrees was used as this is the latitude at which the range is most sensitive to changes in latitude.

Figure A1.26: Error in range to altitude wrt WGS84

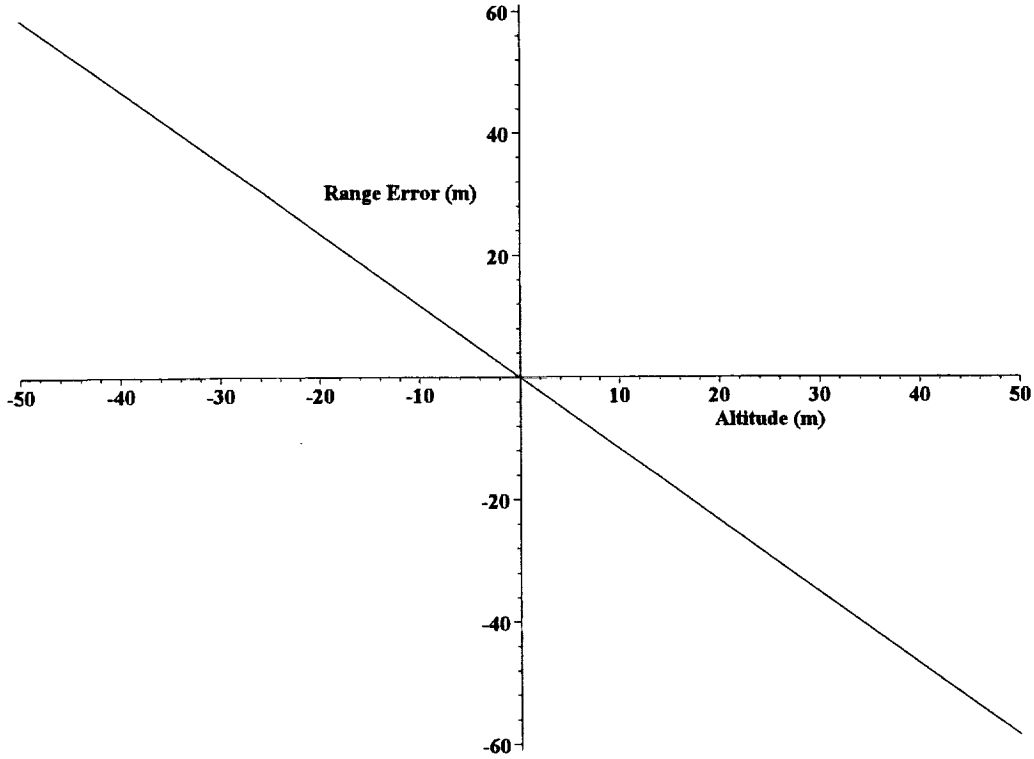

Similarly we can plot the range dependence on variations in orbit height:

Figure A1.27: Error in range (m)

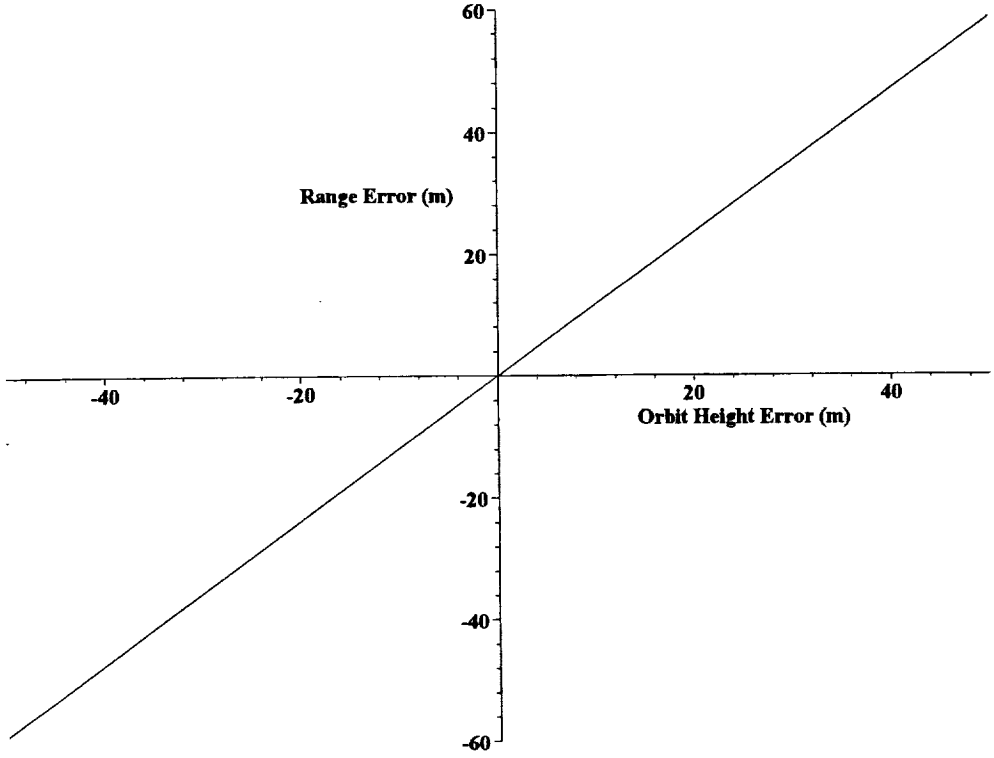

on variations in nadir angle:

Figure A1.28: Error in range (m)

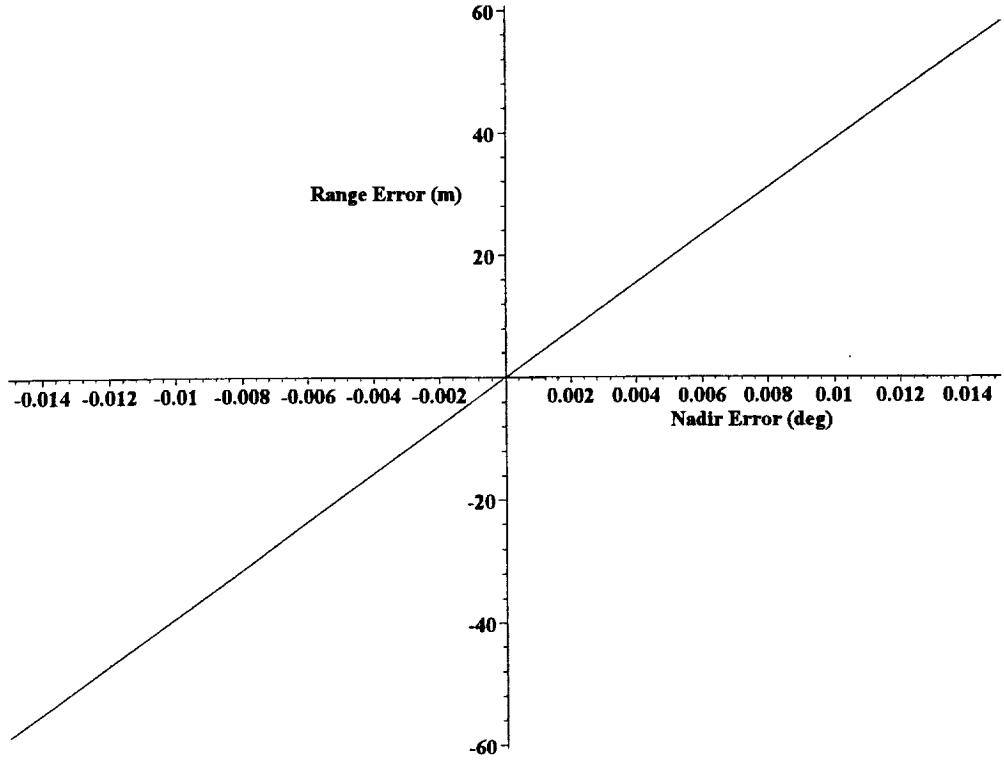

and finally on variations in latitude:

Figure A1.29: Error in range (m)

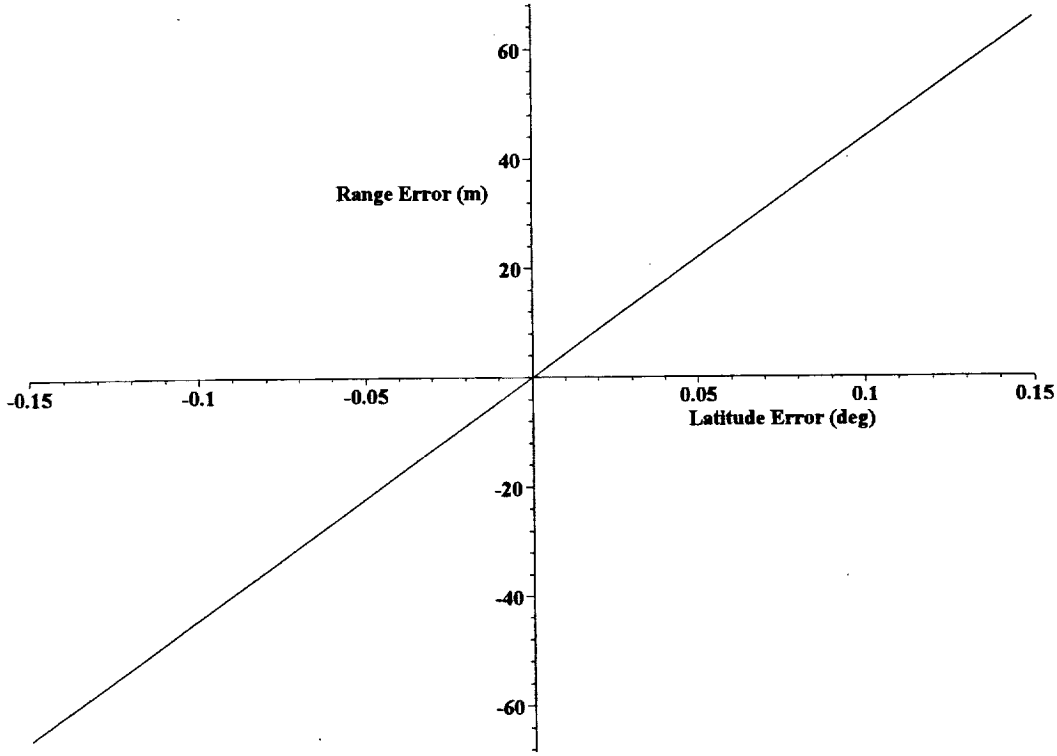

To determine the range from the lidar to a target we measure the round trip time of flight and calculate the range.

t_rtrp := **proc**(*orbh*, *nadir*, *alt*, *lat*) 2*Range(*orbh*, *nadir*, *alt*, *lat*) / *v_c* **end**

Figure A1.30: Round trip time variation with nadir angle

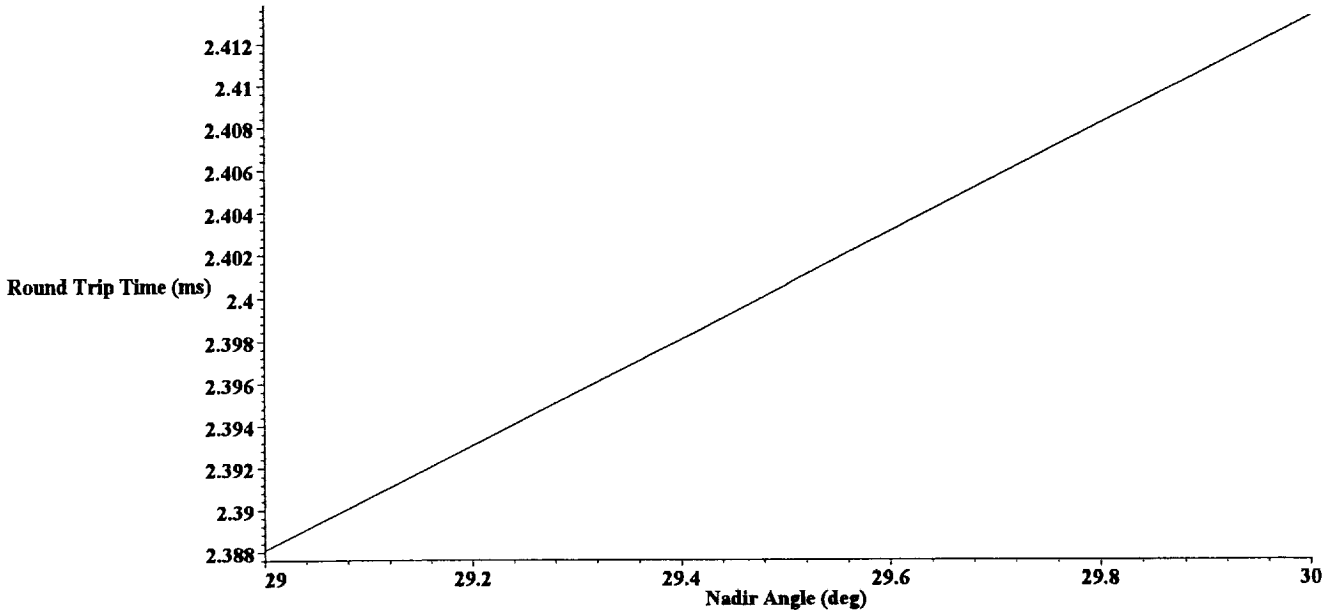

We can plot the round trip time as a function of orbit height and nadir angle to determine the range of round trip times we can anticipate seeing:

Figure A1.31: Lidar Signal Round Trip Time

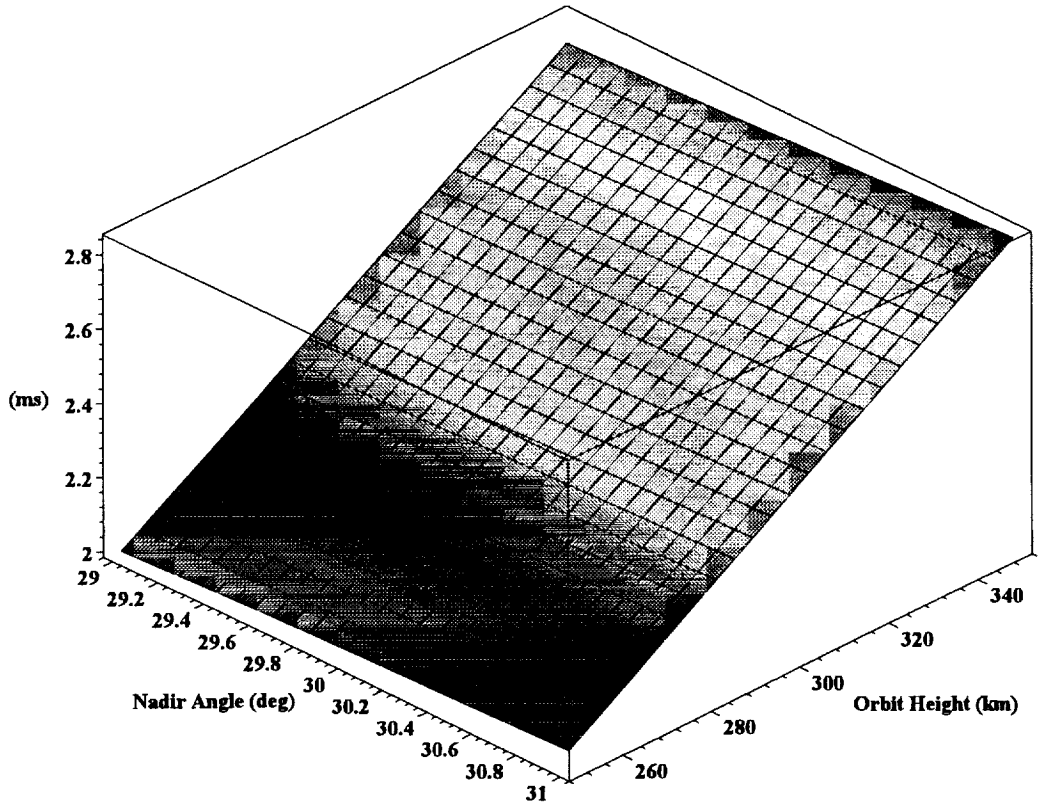

During the round trip time the spacecraft continues to rotate about the planet. This rotation results in a tipping of the nadir angle during the round trip time that translates into a misalignment angle between the transmit and receive optical paths. The round trip time depends on the nadir angle and therefore the nadir tipping angle has a dependence on nadir angle and this is shown in the following plot.

nadirtip := **proc**(*orbh*, *nadir*, *alt*, *lat*) **global** *a*; vsat(*orbh*)*t_rtrp(*orbh*, *nadir*, *alt*, *lat*) / (*orbh* + *a*) **end**

Figure A1.32: Nadir tipping angle dependence on nadir angle

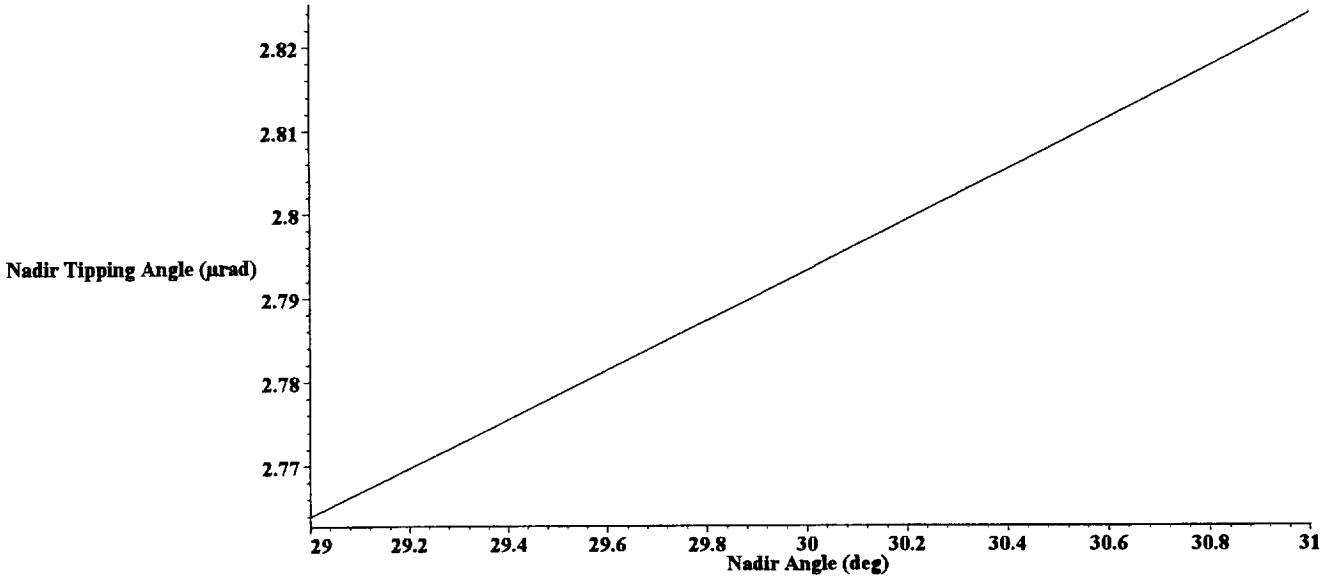

We can see that this is a weak dependence. The dependence on orbit height is much stronger as the next plot shows:

Figure A1.33: Nadir Tipping Angle

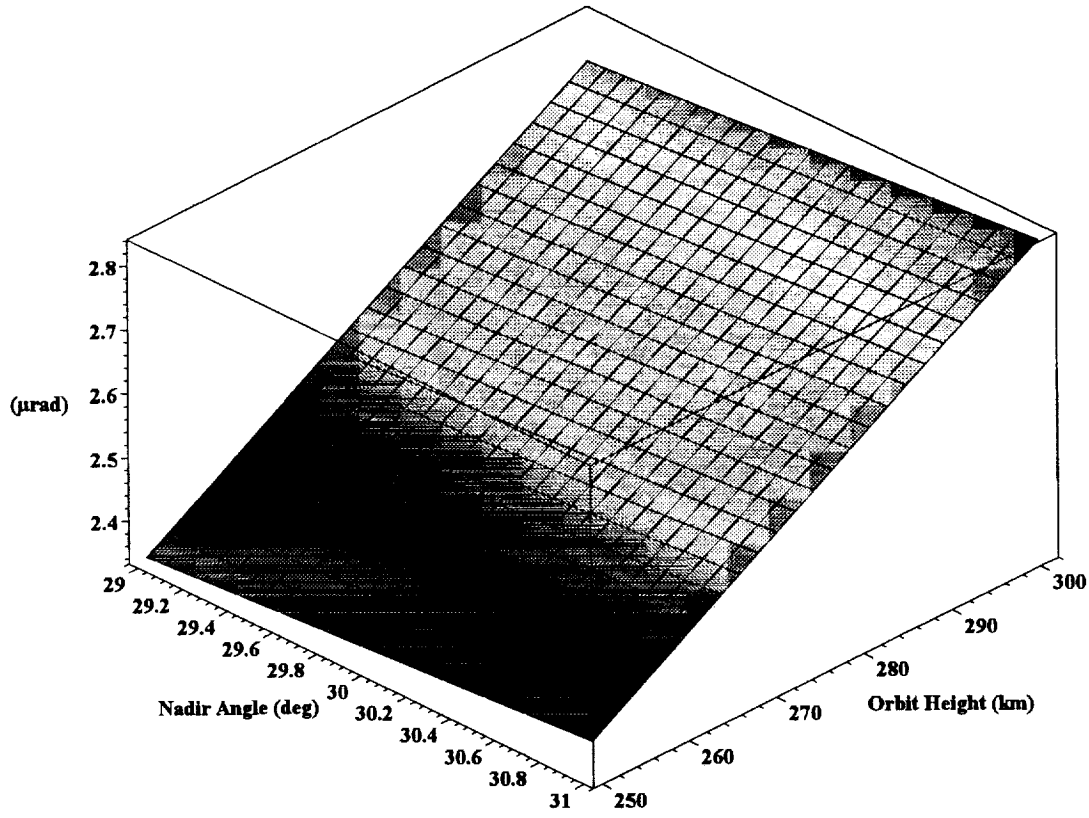

The orbital velocity, in m/s, of a satellite at the orbit height documented earlier is:

7729.187356

The line of sight velocity seen by the satellite is a function of the target, satellite and earth rotation velocities.

los_vel := **proc**(*nadir*, *az*, *alt*, *inc*, *orbh*, *lat*, *trgta*, *vtrgtv*, *htrgtv*, *hsatv*, *vsatv*)
*htrgtv**cos(*az* + orblat(*lat*, *inc*) − *trgta*)*sin(nadalt(*orbh*, *nadir*, *alt*, *lat*))
+ *vtrgtv**cos(nadalt(*orbh*, *nadir*, *alt*, *lat*)) + *hsatv**cos(*az*)*sin(*nadir*) + *vsatv**cos(*nadir*)
+ Vlat(*lat*)*sin(orblat(*lat*, *inc*) + *az*)*sin(nadalt(*orbh*, *nadir*, *alt*, *lat*))
end

where az, trgta, vtrgtv, htrgtv, hsatv, vsatv are the azimuth angle of the line of sight wrt the velocity direction, the azimuthal angle the target velocity makes with respect to the local meridian, the target vertical and horizontal velocities and the satellite horizontal and target velocities respectively. For the orbit and lidar parameters listed at the start of this document the line of sight velocity as a function of azimuth is shown in the following figure for a lidar over the earth's equator .

Figure A1.34: LOS velocity as a function of azimuth

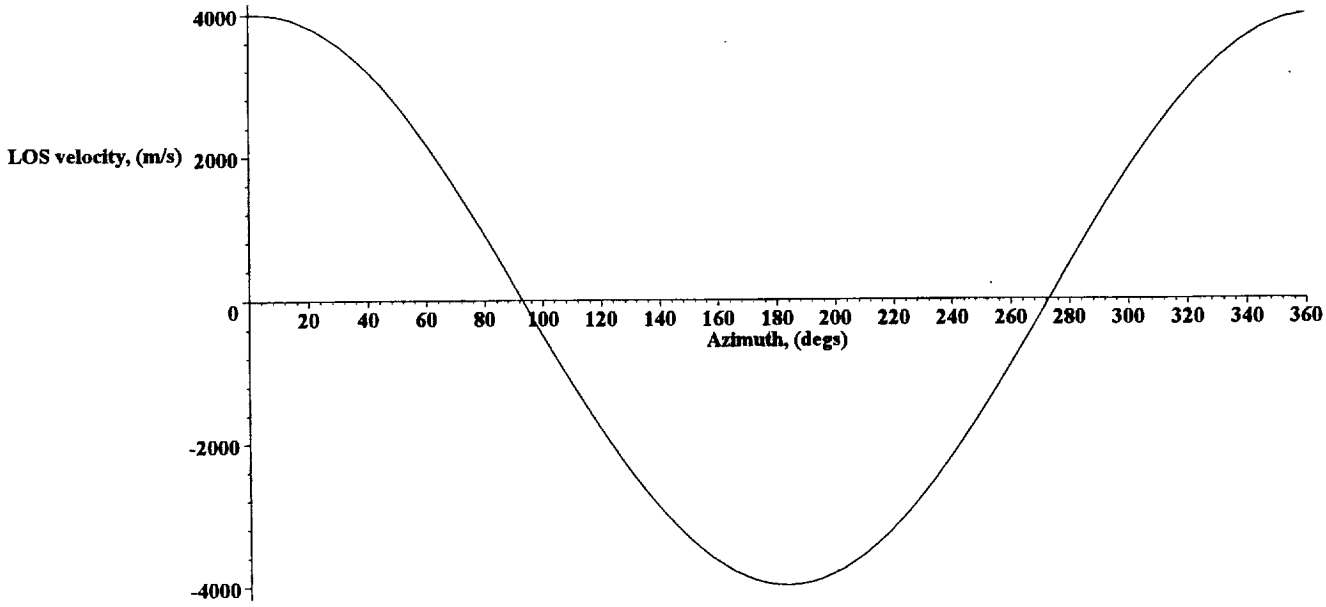

Expanding the region around the first 0 m/s point enables the gradient to be determined.

Figure A1.35: LOS velocity as a function of azimuth

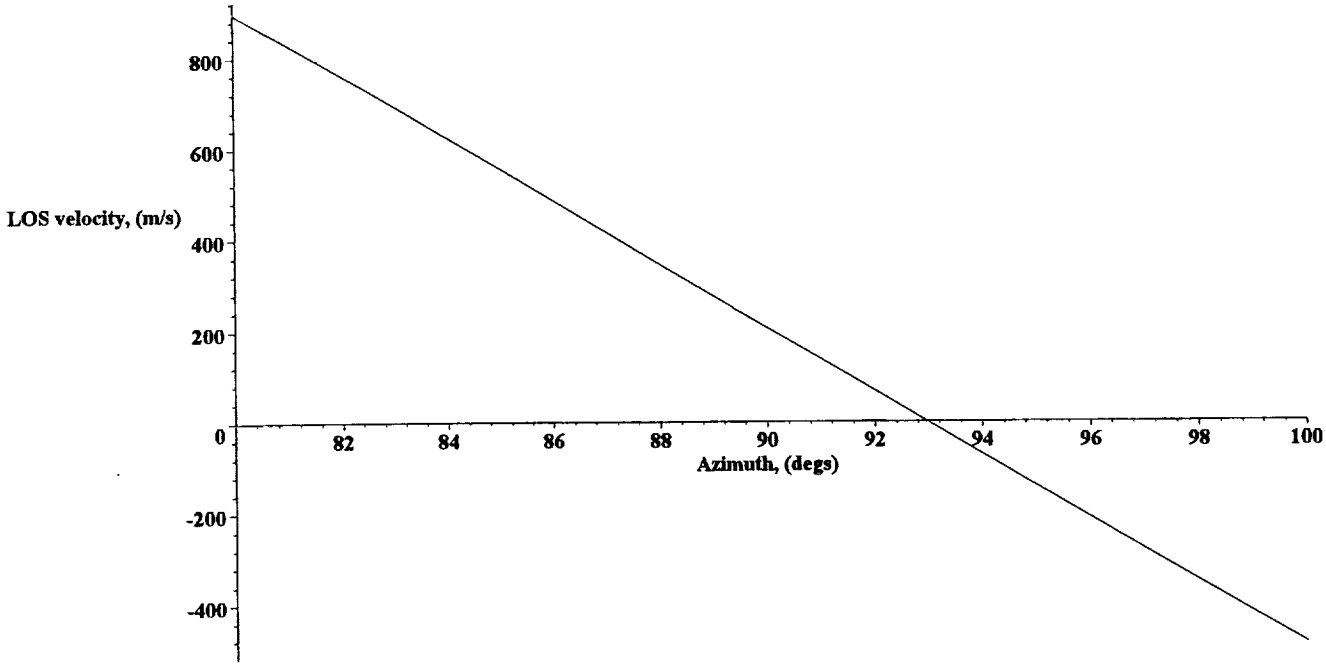

Alternatively plotting the differential of the line of sight velocity with respect to the azimuth angle enables the maximum rate of change to be determined:

Figure A1.36: Rate of change of LOS velocity as a function of azimuth

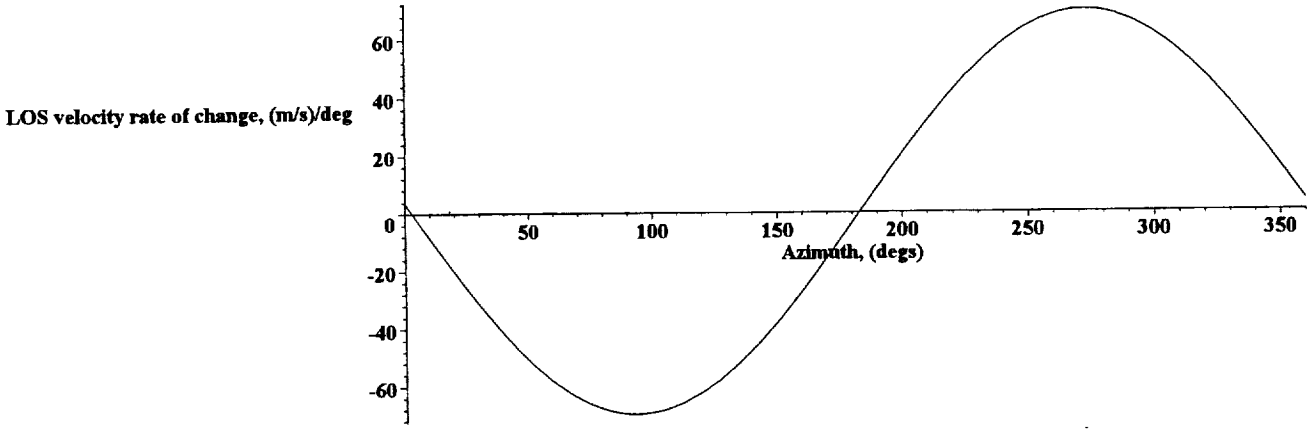

The line of sight velocity is dominated by the spacecraft velocity, if this is removed then we can see the dependence on the earth's rotational velocity:

Figure A1.37: Earth rotation component of the LOS velocity as a function of azimuth

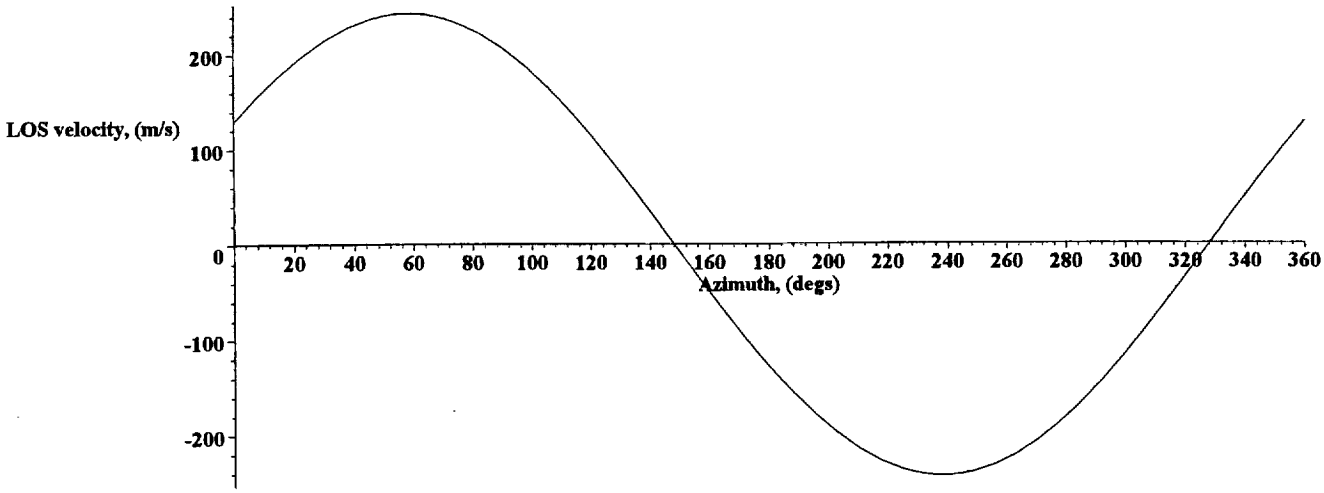

This clearly shows the much smaller magnitude of the earth's rotational contribution. Again we can determine the maximum rate of change with azimuth by plotting the differential with respect to the azimuth angle:

Figure A1.38: Rate of change of the Earth rotation component of the LOS velocity as a function of azimuth

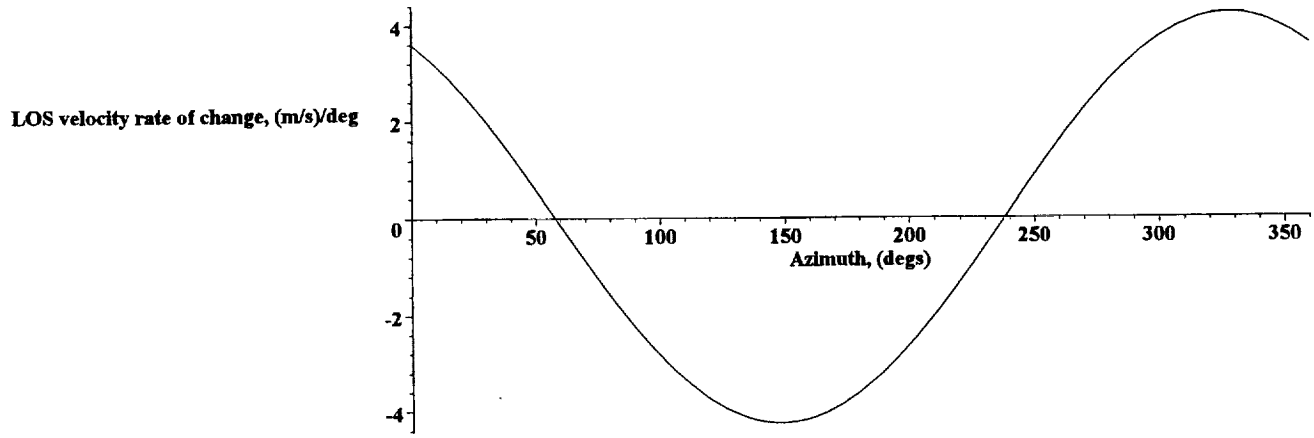

The line of sight velocity also depends on the nadir angle. The following plot shows the line of sight velocity dependence on both nadir and azimuth angle:

Figure A1.39: LOS velocity as a function of azimuth and nadir angles

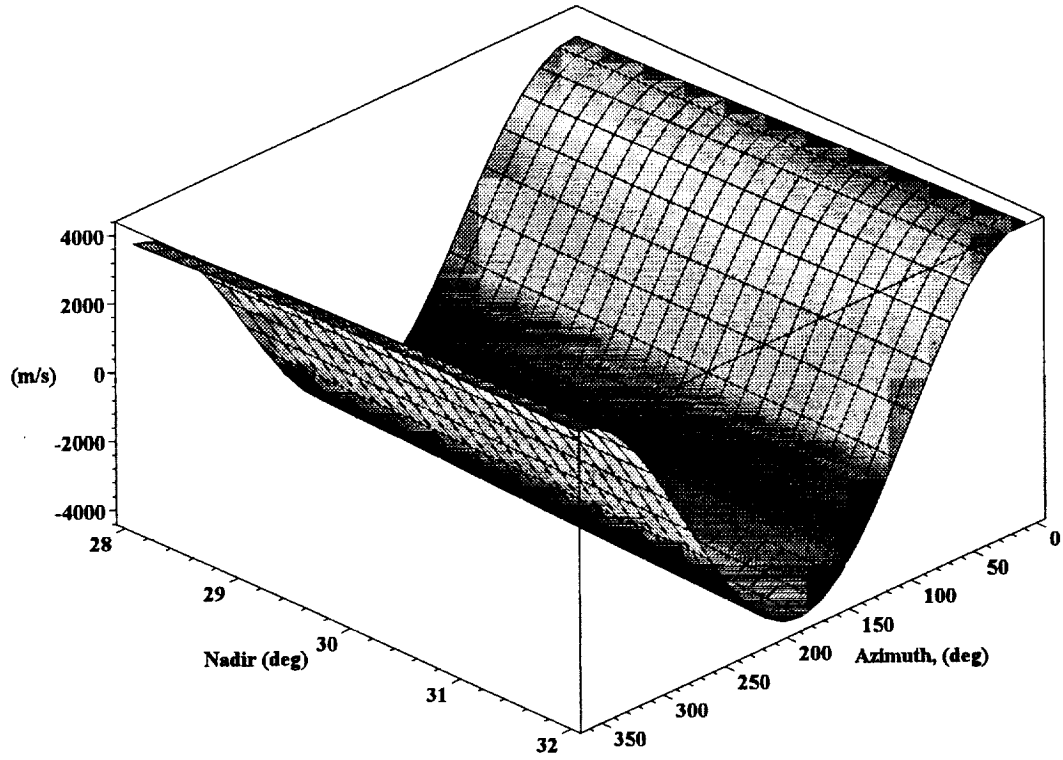

Clearly the azimuthal dependence dominates over the restricted range of nadir angles plotted. The dependence on nadir only becomes clearly visible when a much wider range of nadir angles is considered:

Figure A1.40: LOS velocity as a function of azimuth and nadir angles

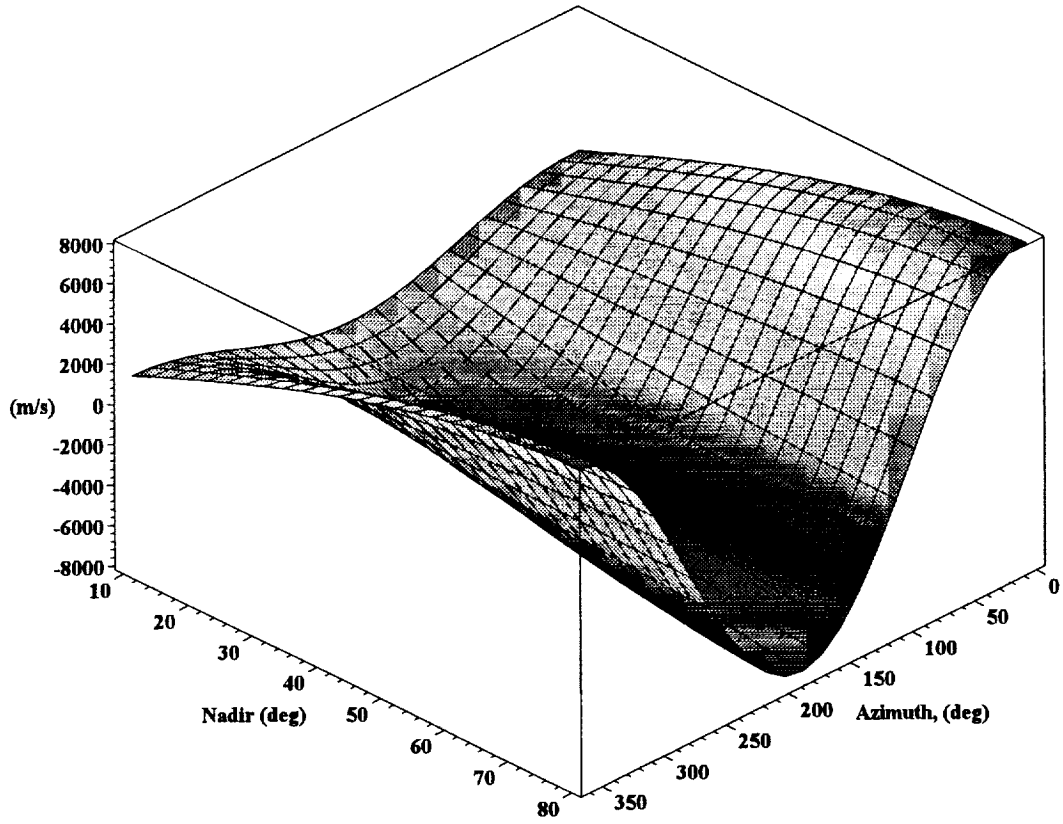

Alternatively the dependence of the line of sight velocity on nadir angle can be obtained by plotting the differential with respect to the nadir angle:

Figure A1.41: Rate of change of LOS velocity with nadir angle

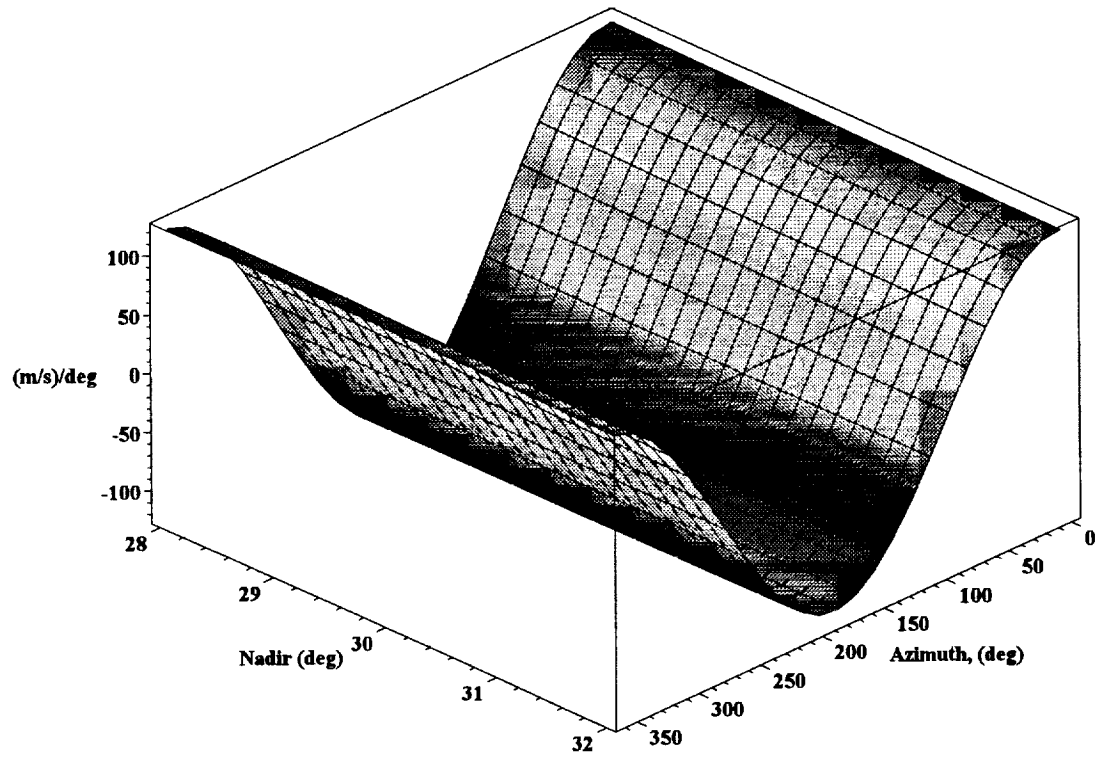

We can see that the rate of change of the line of sight velocity with nadir angle varies between about ± 90 m/s/deg depending on the azimuth angle as expected. The following plot for an azimuth angle of 0 deg clearly shows the gradient as a function of nadir angle:

Figure A1.42: Change of LOS velocity wrt the value at the nominal nadir angle

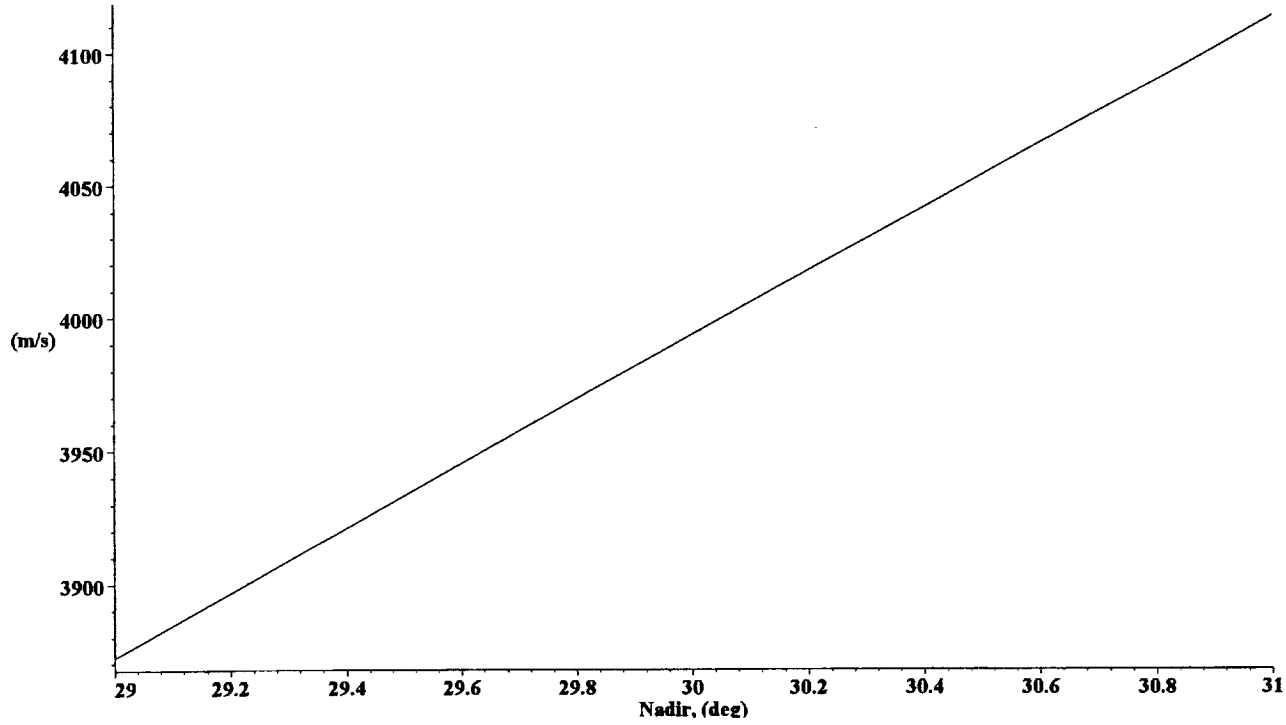

Similarly the following plot shows the variation in the LOS velocity as a function of nadir relative to the LOS velocity at the nominal nadir angle for three azimuth angles of 0 , 45 and 90 degrees respectively.

Figure A1.43: Change of LOS velocity wrt the value at the nominal nadir angle

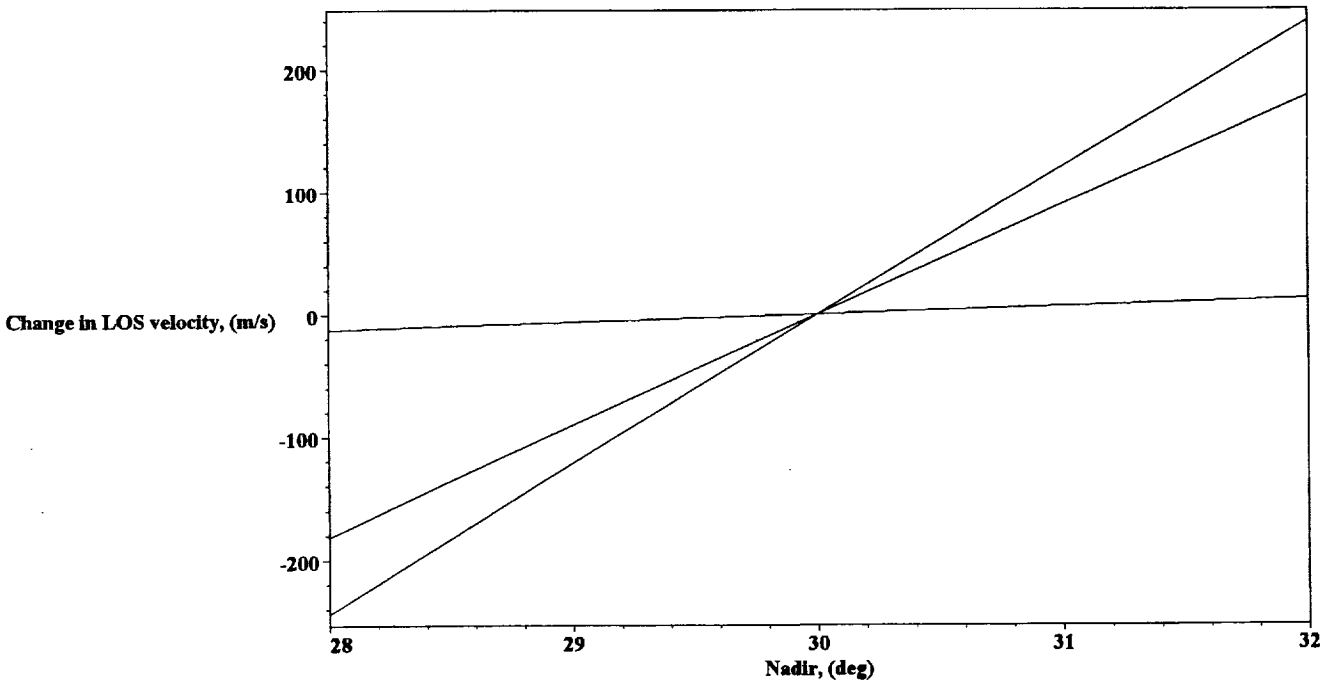

Plotting the change relative to the value at the nominal nadir angle makes the dependence on nadir and azimuth angle easier to see:

Figure A1.44: Change of LOS velocity wrt to the value at the nominal nadir angle

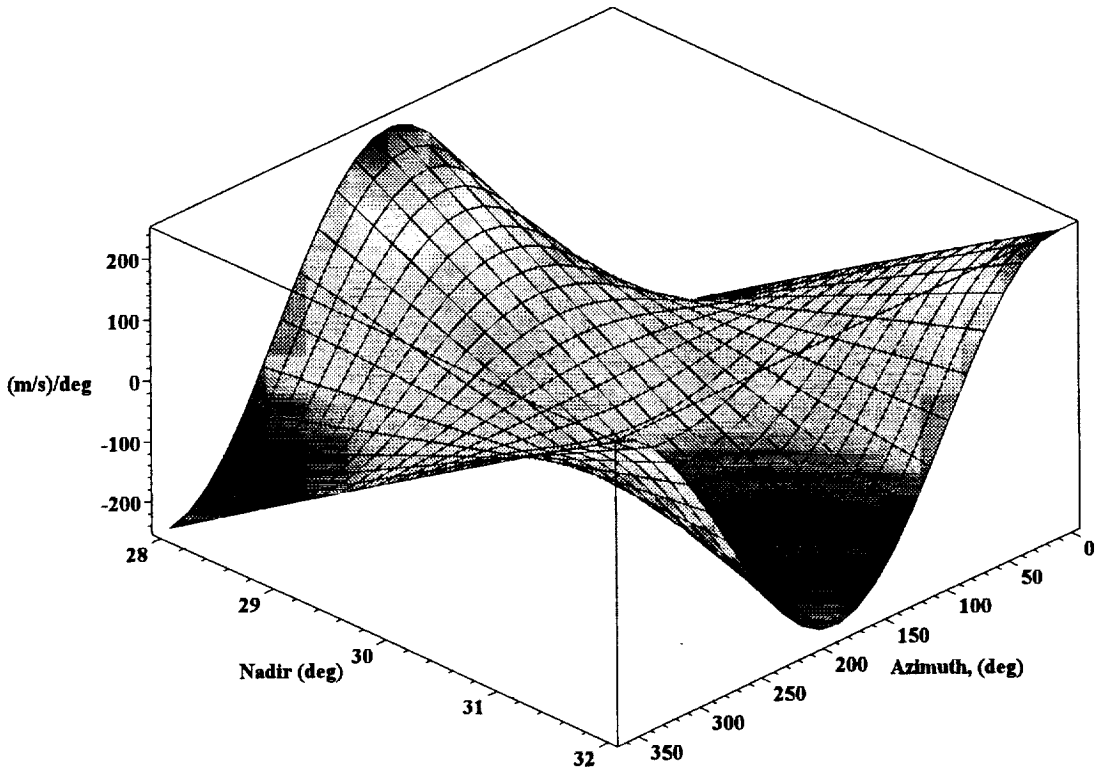

Finally, as a consistency check if we plot the differential of Figure A1.44 with respect to the nadir angle we should get back to Figure A1.41.

Figure A1.45: Rate of change of LOS velocity with nadir angle

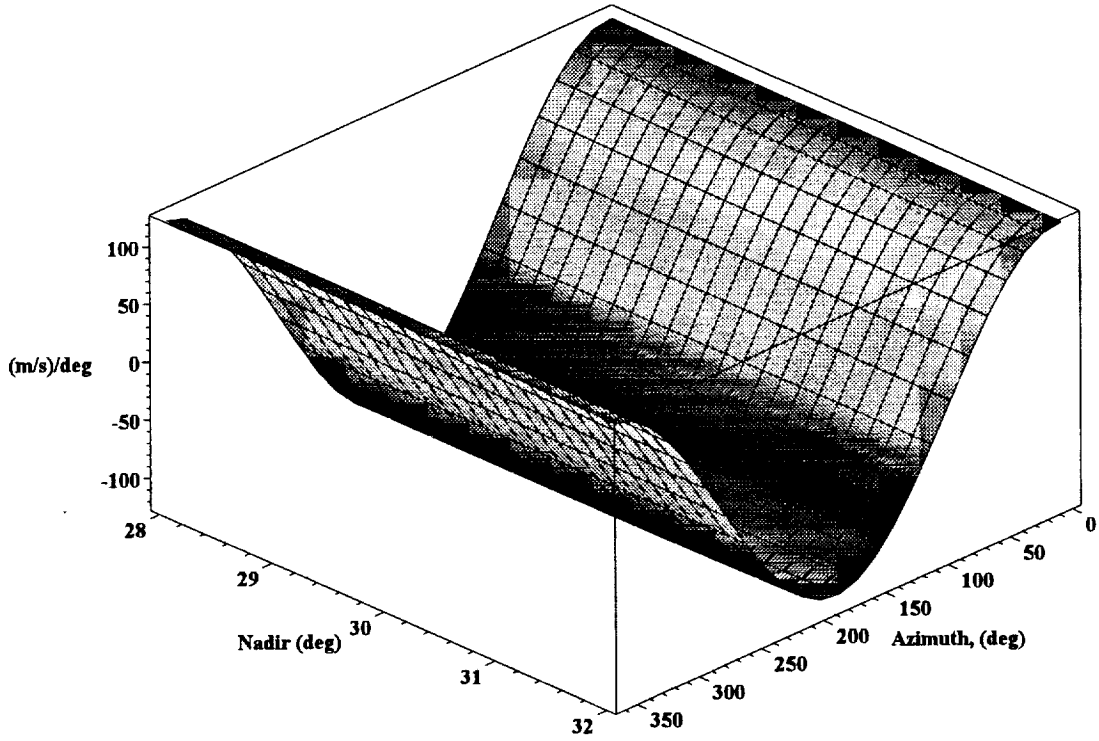

We can find the dependence on latitude by subtracting the value at the equator from the value at some other latitude.

Figure A1.46: Relative change of LOS velocity as a function of latitude

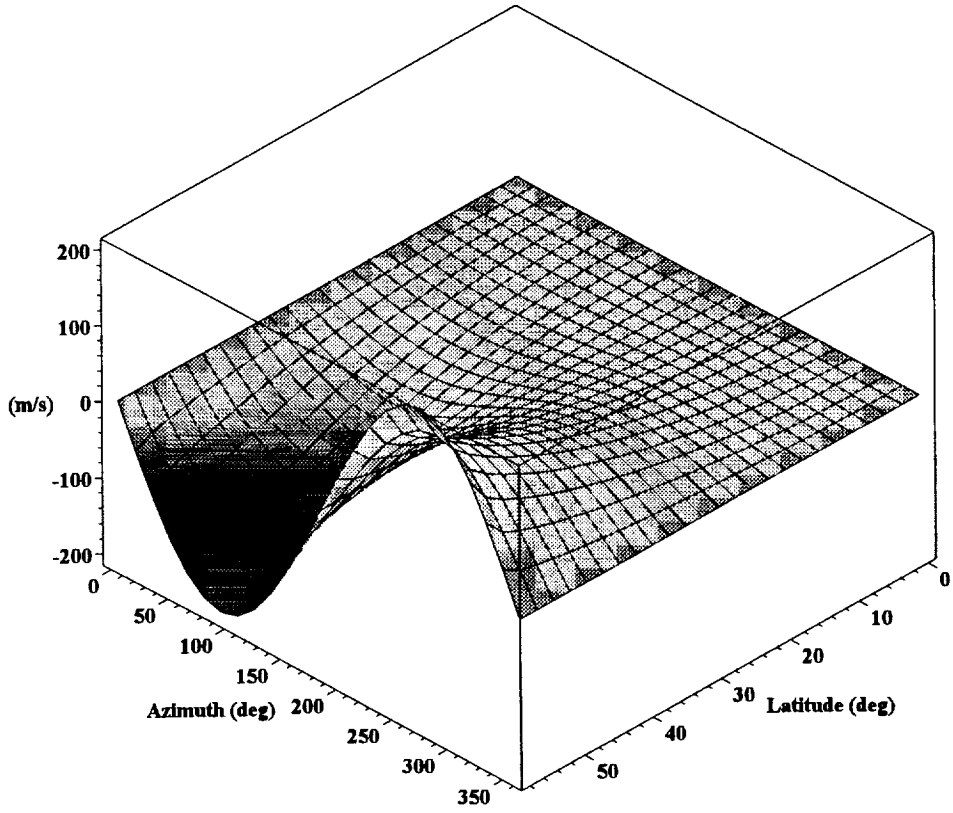

What this figure shows is that as the instrument moves to higher or lower latitudes wrt the equator the component of the line of sight velocity due to the earth's rotation at a given azimuth changes. This occurs because the angle the orbit makes to the local meridian changes as a function of latitude. Plotting the diferential of Figure A1.46 with respect to latitude enables the increase in slope to be determined.

Figure A1.47: Rate of change of LOS velocity as a function of latitude

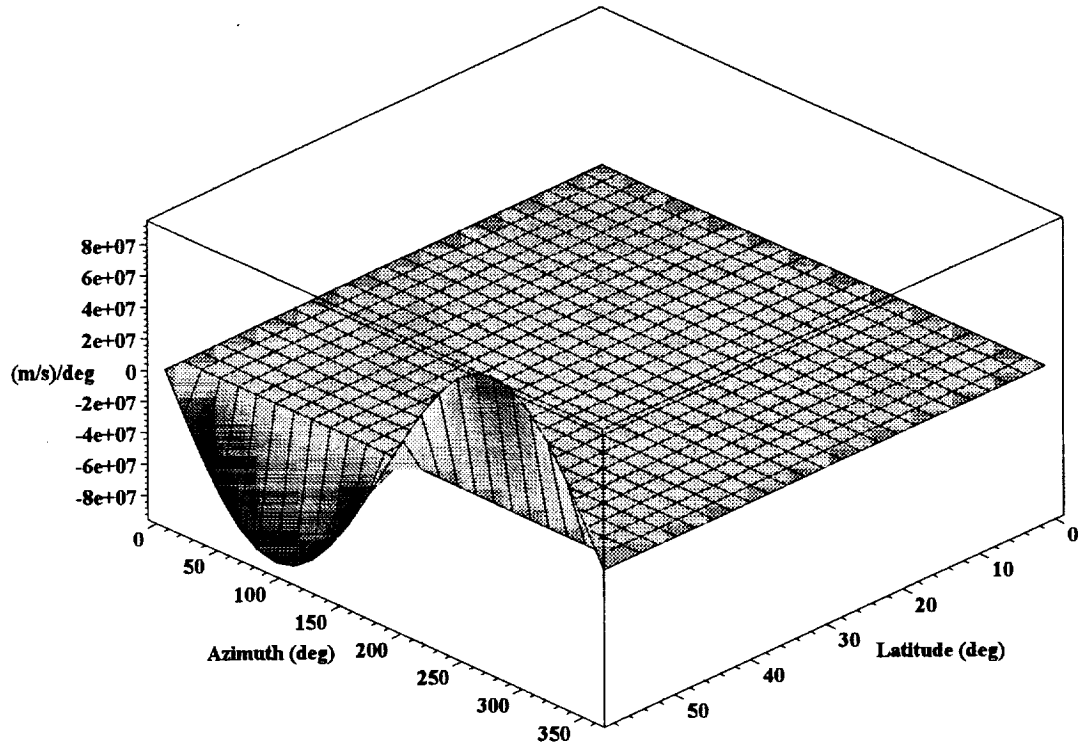

Figure A1.47 clearly show the rapid increase in the sensitivity to latitude at the highest latitudes. The plot above clearly shows the difficulty the numeric routines have near the maximum latitude where the rate of change of line of sight velocity with latitude approaches ± infinity depending on the azimuth angle. We can replot this on a logarithmic scale, using the absolute value of the slope, to get a clearer view of the rate of change and also limit the plot to a latitude slightly below the maximum value. The following plot is for a maximum latitude of 0.001 deg below the true maximum.

Figure A1.48: Rate of change of LOS velocity as a function of latitude (log z-axis)

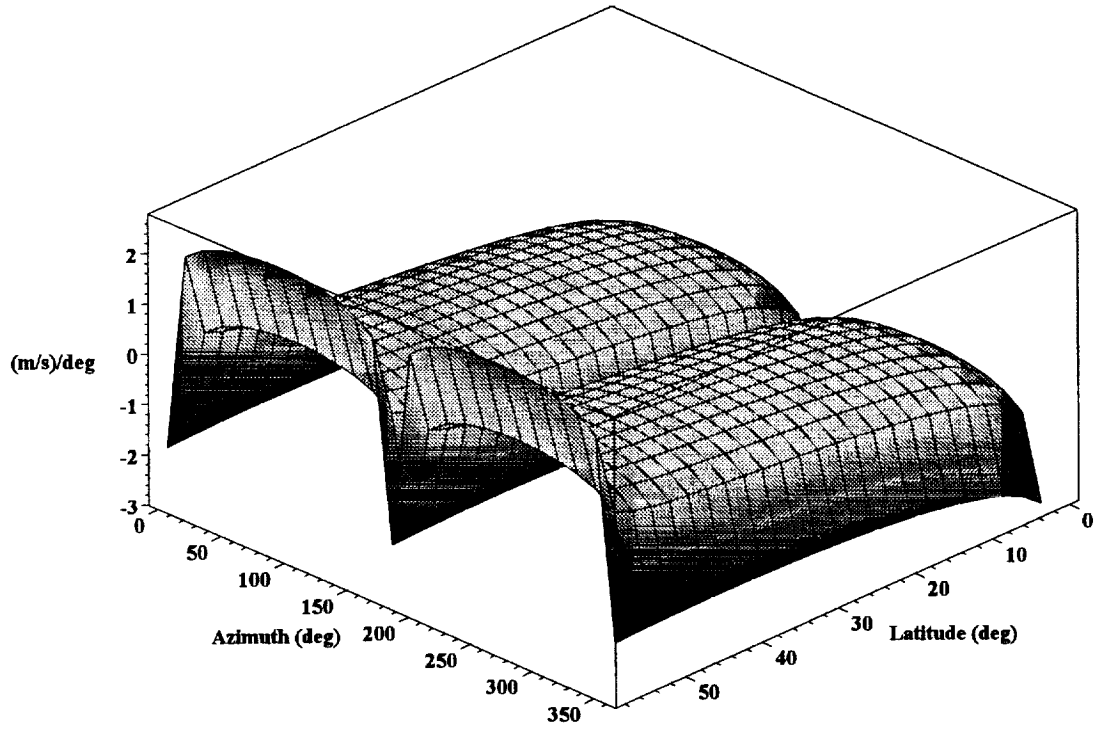

Finally we can plot just the higher latitude portion of this plot:

Figure A1.49: Rate of change of LOS velocity as a function of latitude (log z-axis)

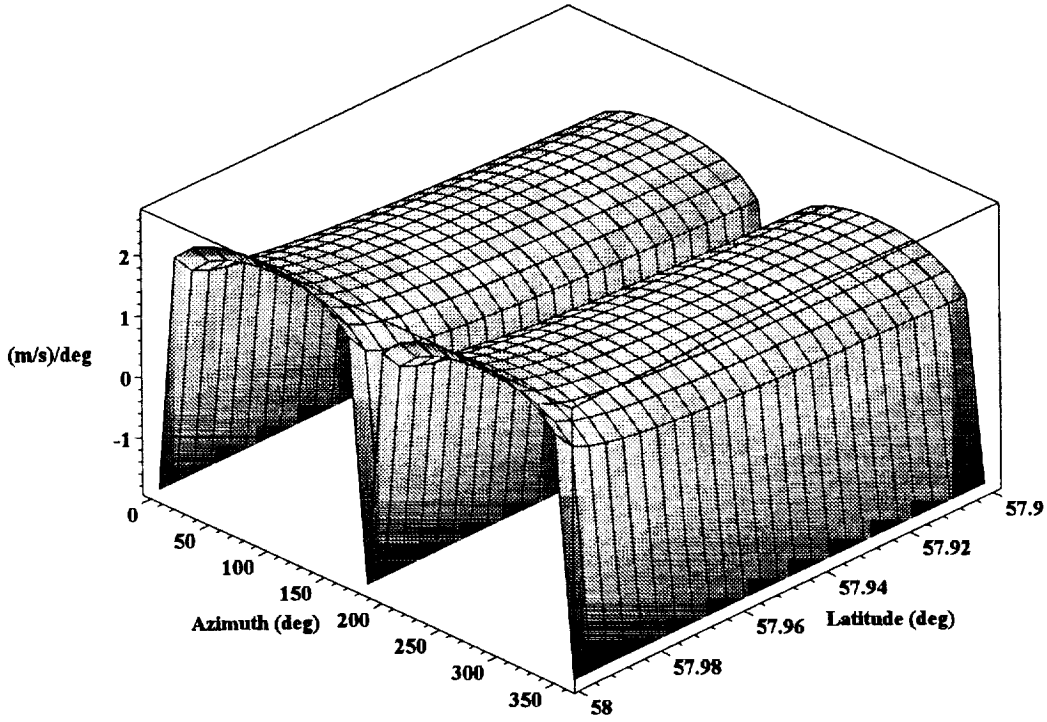

The dependence of the line of sight velocity on orbit inclination is shown below:

Figure A1.50: LOS velocity as a function of orbit inclination

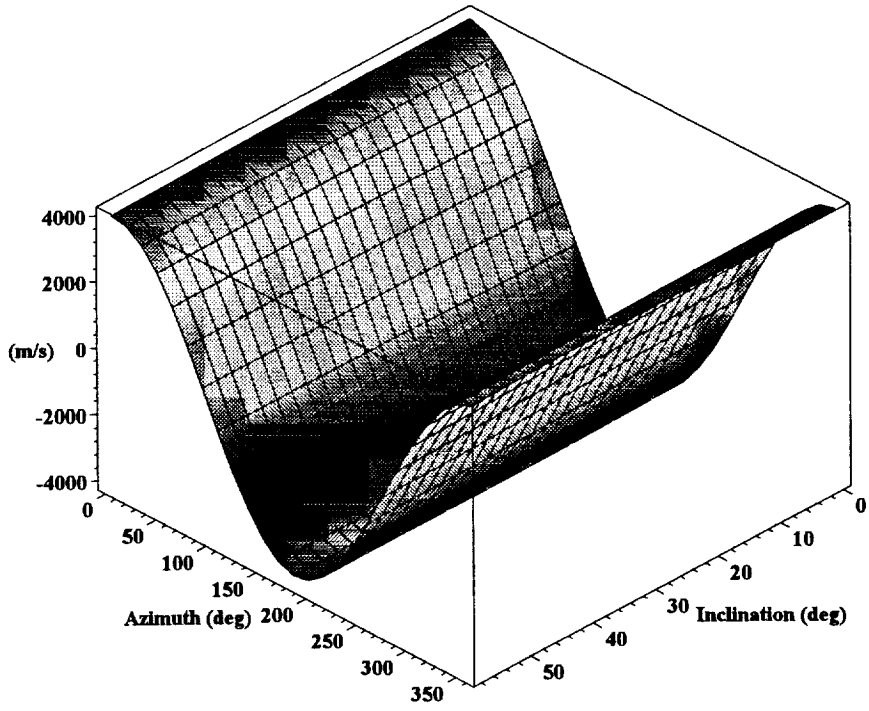

The dependence on azimuth angle is clearly dominant again and we can plot the differential with respect to the inclination angle to more clearly show the dependence on inclination angle.

Figure A1.51: Rate of change of LOS velocity with orbit inclination

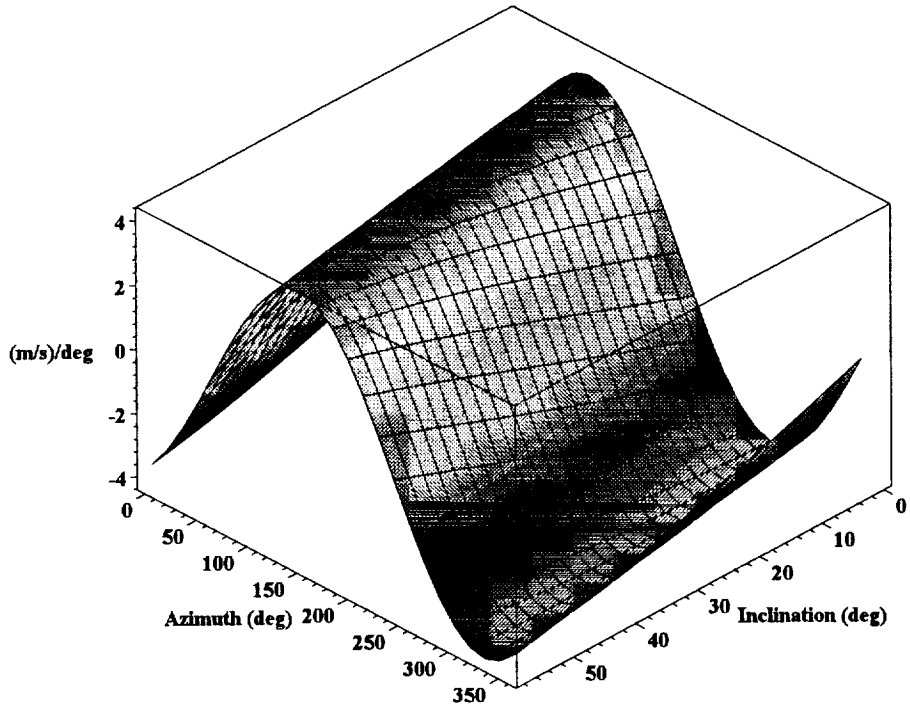

Figure A1.8 showed the satellite velocity as a function of orbit height. The line of sight velocity dependence on orbit height for an azimuth angle of 0 deg will simply be a component of this that depends on the nadir angle. Although the line of sight velocity component contains a contribution from the earth's rotational velocity this is so much smaller than the satellite velocity that it will not be visible in the plot.

Figure A1.52: LOS velocity as a function of orbit height

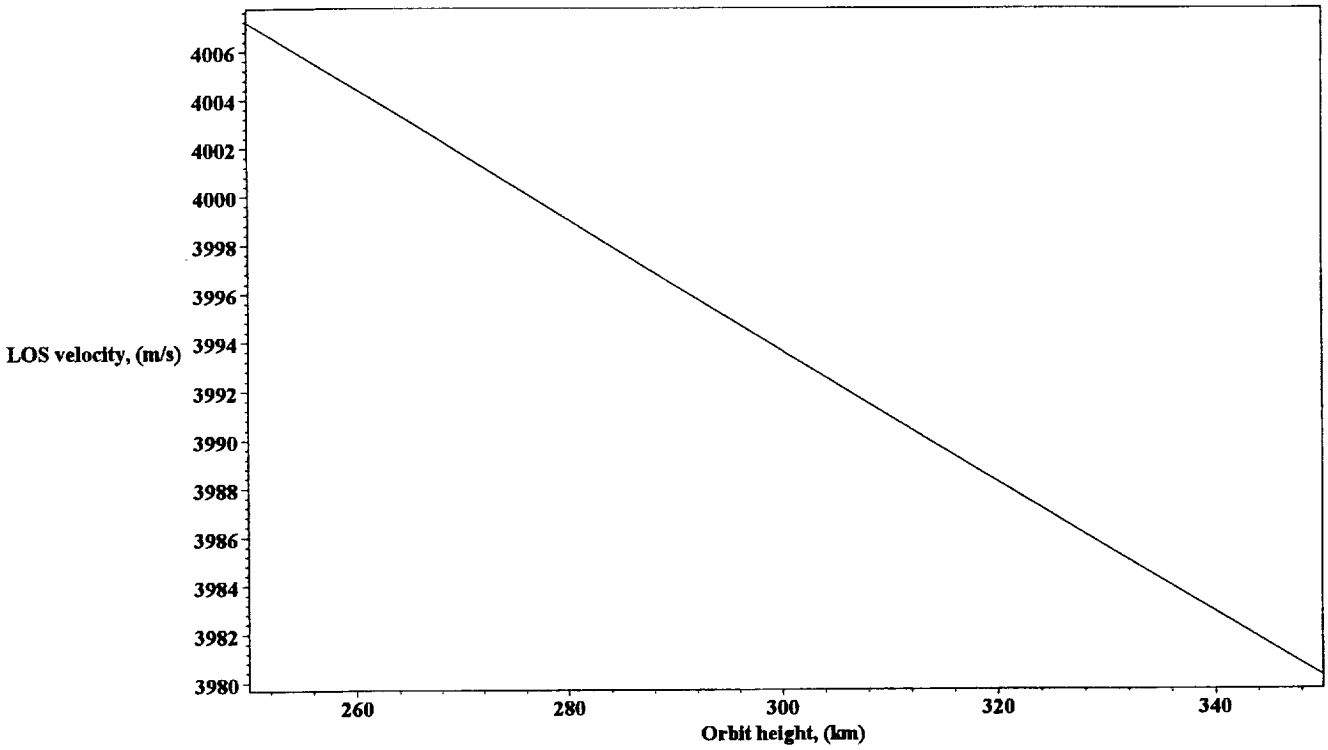

Plotting the differential with respect to the orbit height permits the sensitivity to be easily determined.

Figure A1.53: Rate of change of LOS velocity with orbit height

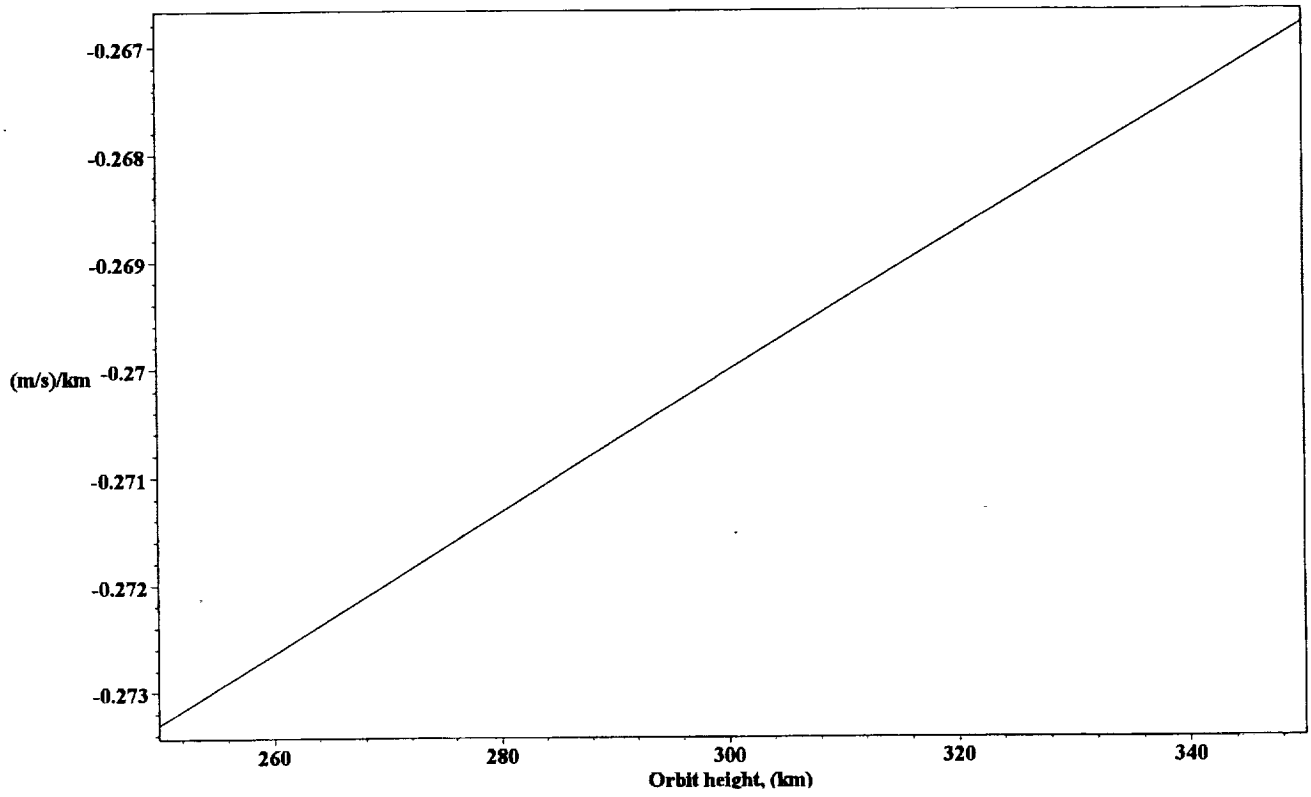

Figure A1.53 assumes an azimuth angle of 0 deg which corresponds to maximising the magnitude of the line of sight component of the spacecraft velocity. At other azimuth angles the dependence will be weaker and this is shown in the following 3D plot.

Figure A1.54: Rate of change of LOS velocity with orbit height

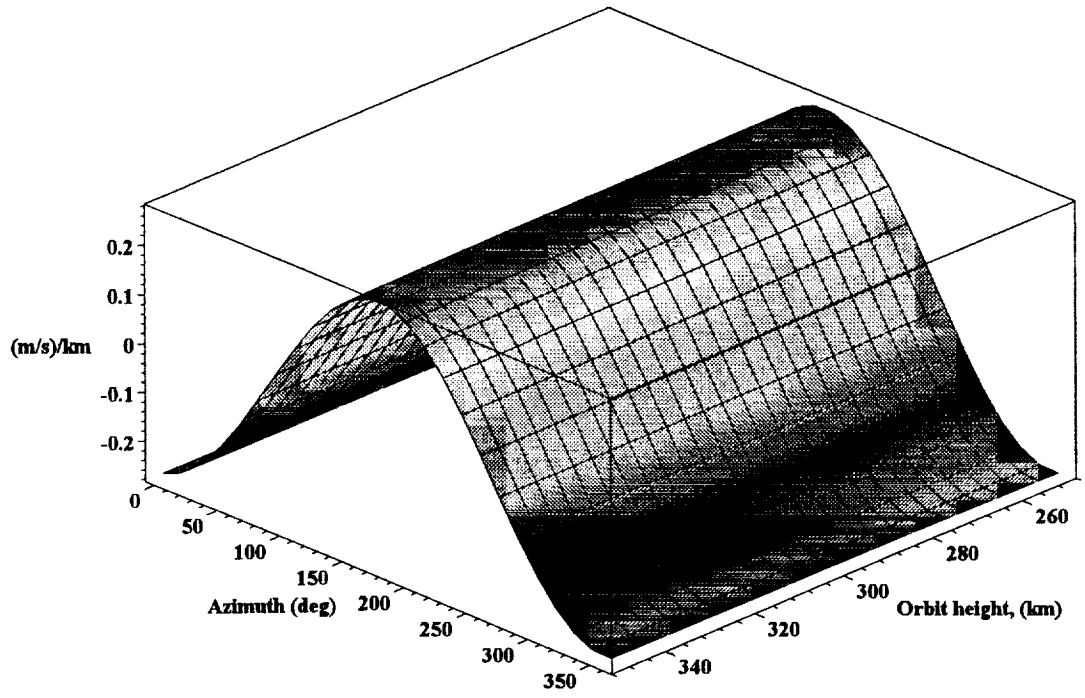

The nadir angle at the target varies as a function of the altitude of the target and so the line of sight velocity has a weak dependence on the target latitude. This is shown below for an azimuth angle of 0 degrees.

Figure A1.55: Rate of change of LOS velocity with target altitude

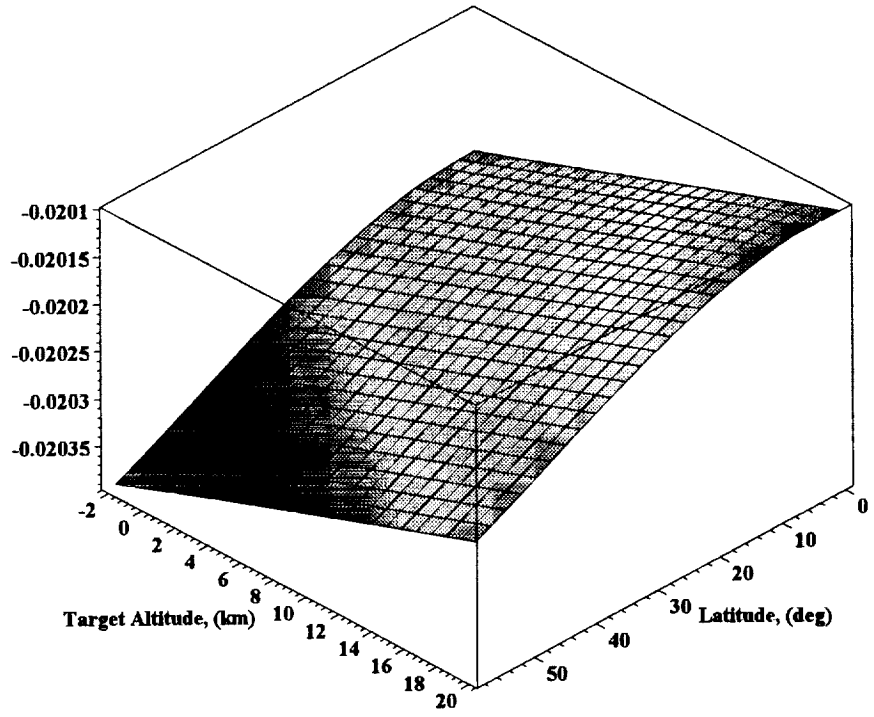

For a fixed azimuth angle the line of sight velocity should be simply proportional to the satellite horizontal and vertical velocities with the constant of proportionality being simply the sine and cosine of the nadir angle respectively. Plotting the differential of the line of sight velocity with respect to the satellite velocity should therefore obtain sin(nadir) and cos(nadir) for the horizontal and vertical velocities respectively.

Figure A1.56: Rate of change of LOS velocity with satellite horizontal velocity

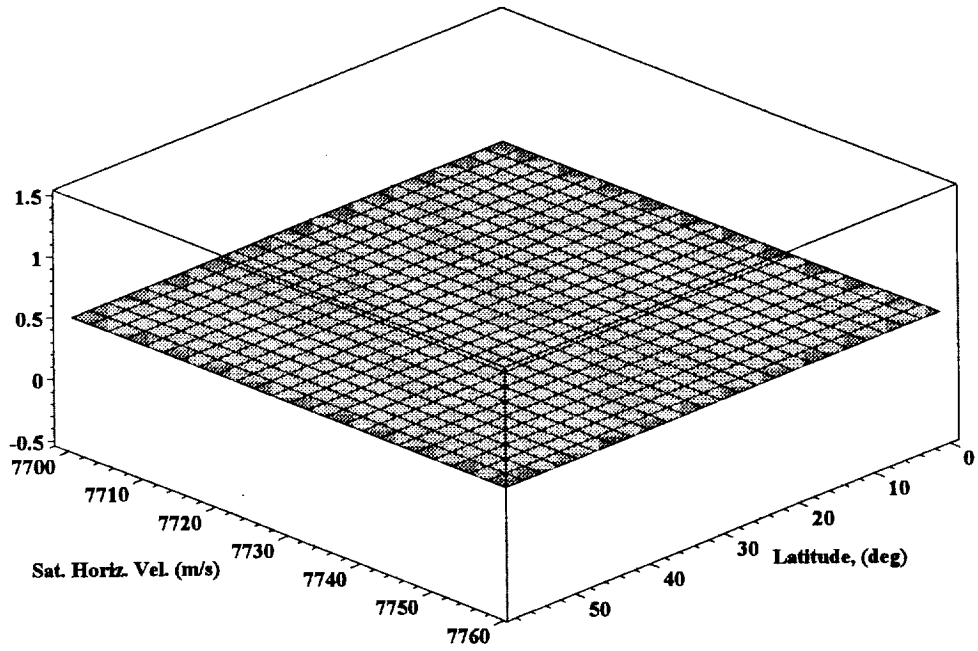

Figure A1.57 Rate of change of LOS velocity with satellite vertical velocity

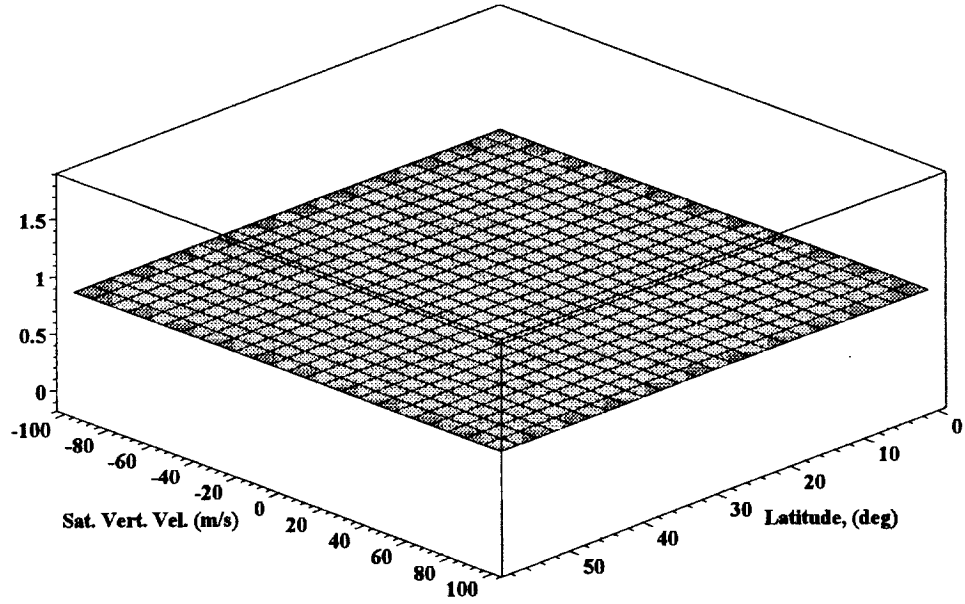

This provides the anticipated result. Plotting as a function of latitude ensures that there are no WGS84 related dependencies. As indicated previously the line of sight velocity includes a component due to the earth's rotational velocity (Figure A1.37). The earth's rotational velocity also depends on the latitude (Figure A1.18) as does the nadir angle at the surface (Figure A1.20). These dependencies combine to create a complex surface that must be accounted for in order to correctly determine the target velocity independent of the latitude and azimuth angle.

Figure A1.58: LOS velocity due to earth rotation

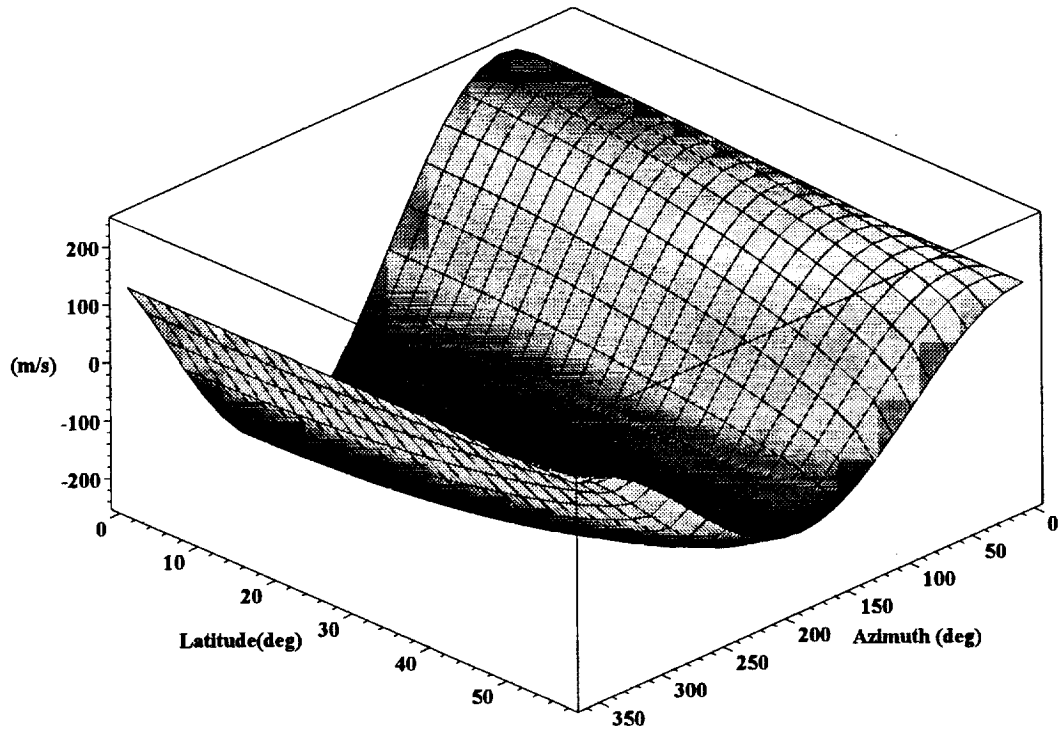

We can plot the differential with respect to the azimuth angle and latitude respectively to determine the sensitivities.

Figure A1.59: Rate of change of line of sight component of the earth's rotational velocity with azimuth

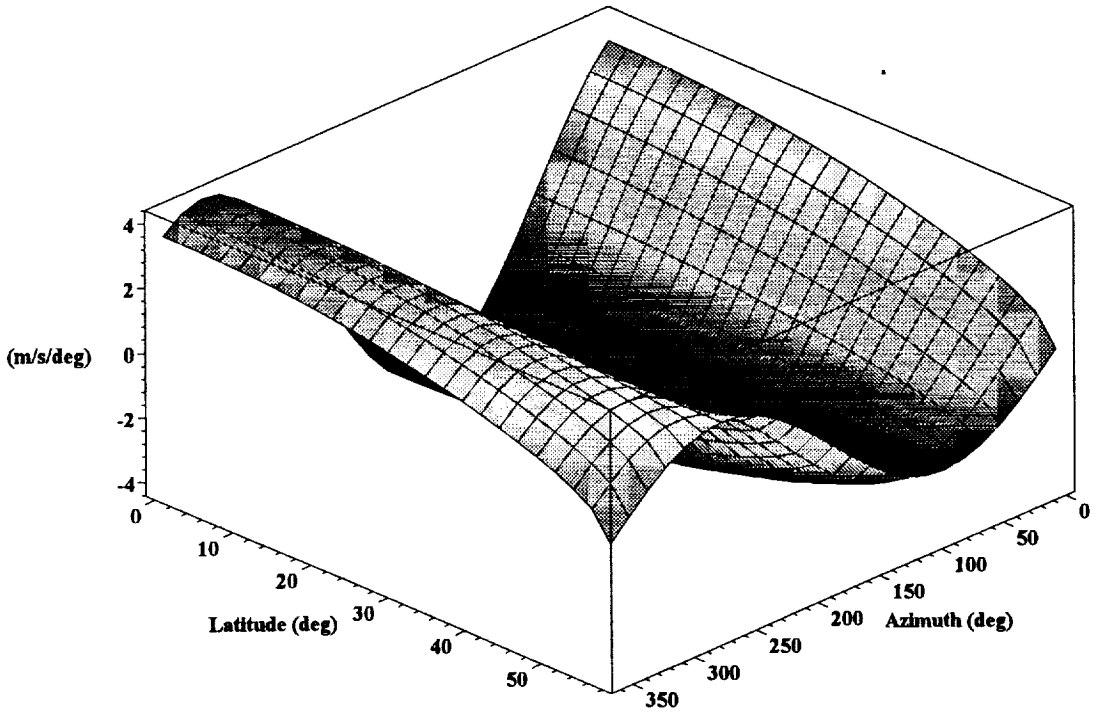

Figure A1.60: Rate of change of line of sight component of the earth's rotational velocity with latitude

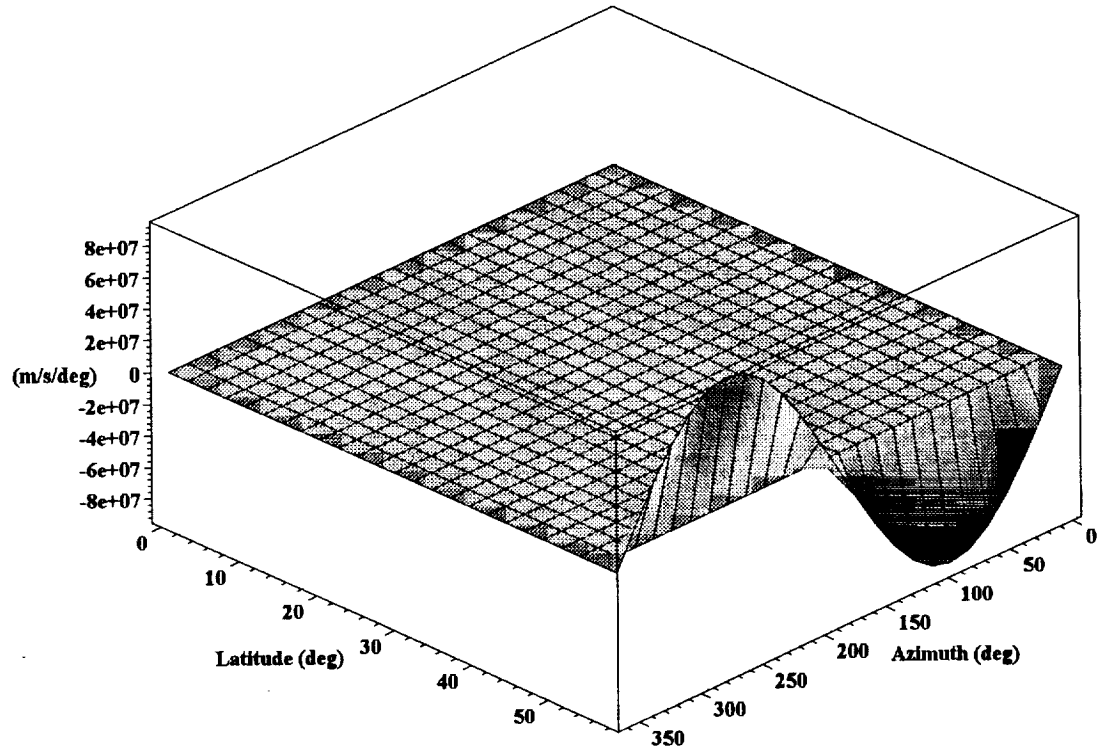

The rate of change of the line of sight component of the earth's rotational velocity with latitude (Figure A1.60) should be the same as for the rate of change of the total line of sight velocity (Figure A1.47).

We now consider the frequencies seen by the lidar. The local oscillator frequency is given by:

```
lo_f := proc(λ) global v_c; v_c / λ end
```

where λ is the wavelength and v_c is the velocity of light. In order to reduce the detector bandwidth we want to tune one of the lasers to track the anticipated Doppler shift from the line of sight velocities due to the spacecraft and earth rotation velocities. The Doppler shift tuning function is given by:

```
tune_f := proc(n, az, alt, inc, orbh, lat, hsatv, vsatv, λ)
    2*(hsatv*cos(az)*sin(n) + vsatv*cos(n) + Vlat(lat)*sin(orblat(lat, inc) + az)*sin(nadalt(orbh, n, alt, lat)))
    / λ
end
```

If we consider the case where the outgoing laser pulse is tuned then the master oscillator tuning function is given by:

```
mo_f := proc(n, az, alt, inc, orbh, lat, hsatv, vsatv, λ, offset_f, deadband, qswitchf)
local a, b, c;
global d2r;
    b := tune_f(n, az, alt, inc, orbh, lat, hsatv, vsatv, λ) + qswitchf;
    if evalf(az < 90*d2r) and evalf(abs(b + offset_f) < deadband) then a := b + offset_f
    elif evalf(90*d2r ≤ az) and evalf(az ≤ 270*d2r) and evalf(deadband ≤ abs(b - offset_f)) then
        a := b - offset_f
    else a := b + offset_f
    fi;
    lo_f(λ) - a
end
```

where offset_f is the desired offset frequency on the atmospheric signal detector for a target velocity of 0 m/s, deadband is the deadband desired to avoid operating the electronics too close to D.C. and qswitchf is the frequency offset that the slave oscillator q-switch introduces. The deadband is primarily required to ensure that the MO/LO offset frequency can be accurately measured. We can plot the master oscillator tuning as a function of azimuth angle for a latitude of 45 deg, a wavelength of 2.051 μm, an offset frequency of 250 MHz, a deadband of 100 MHz and a q-switch frequency shift of 50 MHz.

Figure A1.61: MO Tuning

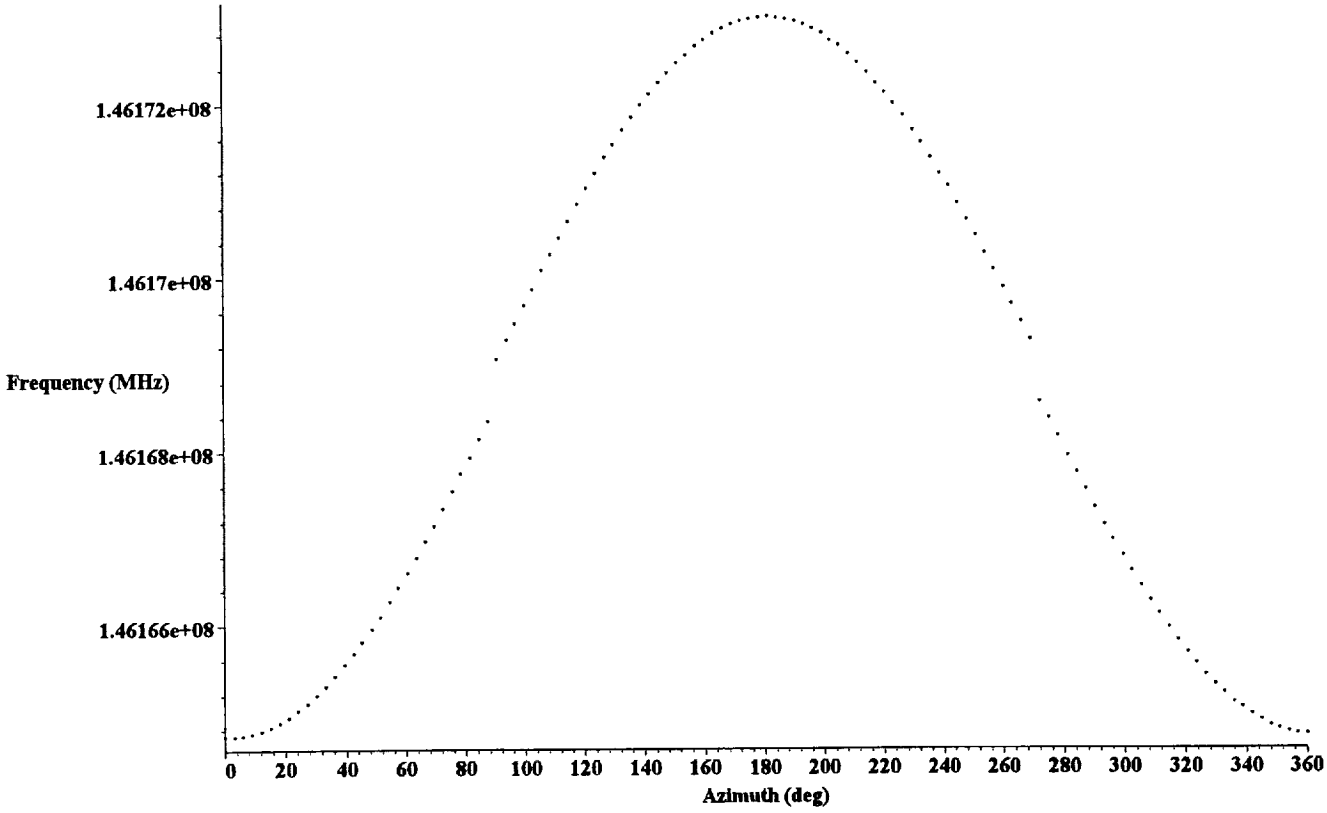

The plot clearly shows the frequency hop in the tuning curve that is required to meet the deadband requirements. The slave oscillator output frequency is simply the master oscillator frequency combined with the slave oscillator frequency shift.

Slave_f := **proc**(*n, az, alt, inc, orbh, lat, hsatv, vsatv,* λ, *offset_f, deadband, qswitchf*)

mo_f(*n, az, alt, inc, orbh, lat, hsatv, vsatv,* λ, *offset_f, deadband, qswitchf*) + *qswitchf*

end

Figure A1.62: Slave oscillator frequency

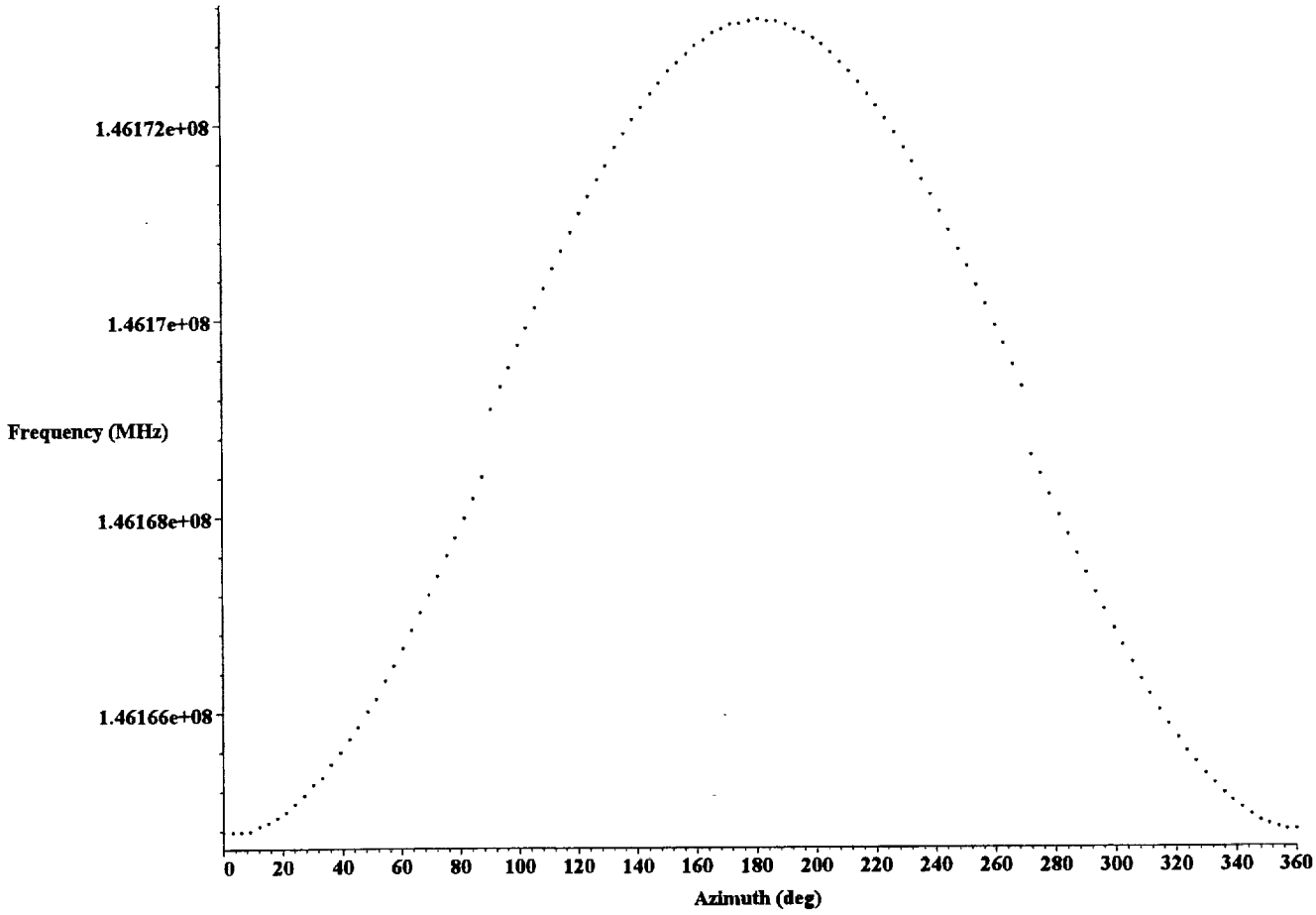

The slave oscillator frequency is Doppler shifted.

Doppler_f := **proc**(*n, az, alt, inc, orbh, lat, trgta, vtrgtv, htrgtv, hsatv, vsatv*, λ, *offset_f, deadband, qswitchf*)
global *v_c*;
    2*los_vel(*n, az, alt, inc, orbh, lat, trgta, vtrgtv, htrgtv, hsatv, vsatv*)*
    Slave_f(*n, az, alt, inc, orbh, lat, hsatv, vsatv*, λ, *offset_f, deadband, qswitchf*) / *v_c*
end

Figure A1.63: Doppler frequency shift

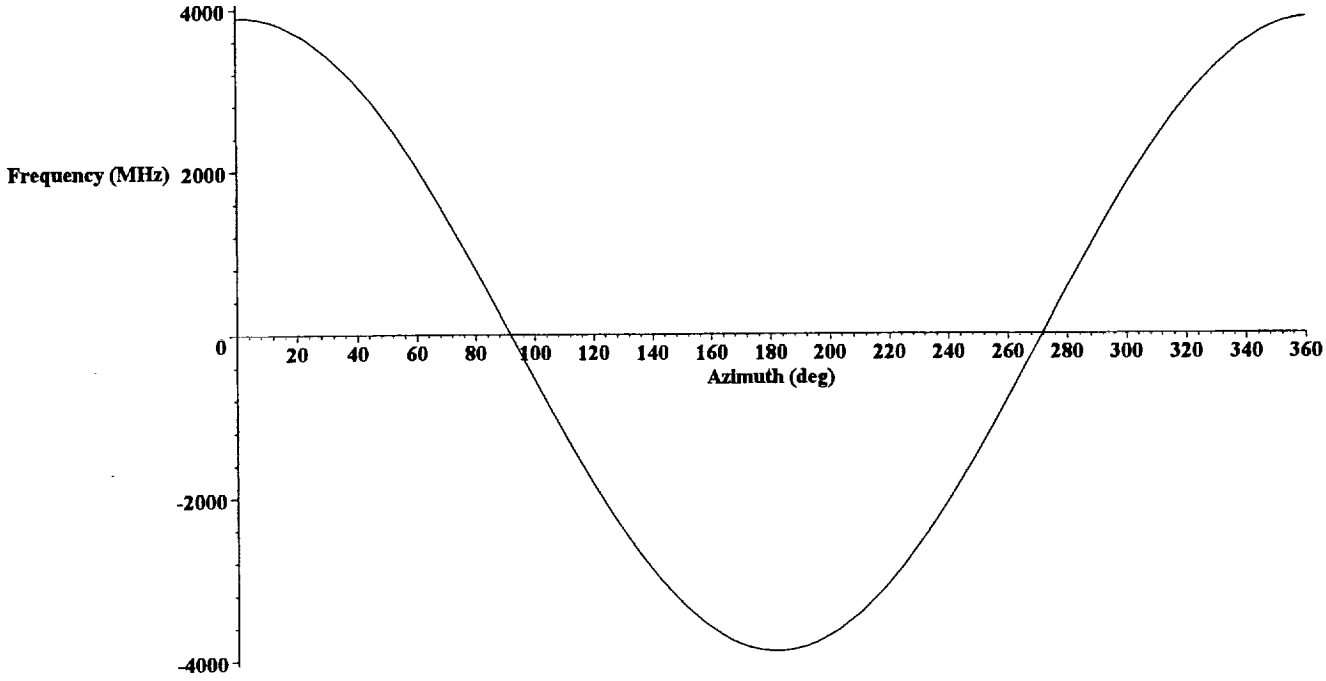

One of the detectors monitors the offset frequency between the master oscillator and the local oscillator. This detector sees the full bandwidth of possible signals and is the one that requires the deadband frequency to ensure adequate measurement of the MO/LO offset frequency. The MO/LO frequency difference is given by:

molo_f := **proc**(*n, az, alt, inc, orbh, lat, hsatv, vsatv*, λ, *offset_f, deadband, qswitchf*)
    lo_f(λ) − mo_f(*n, az, alt, inc, orbh, lat, hsatv, vsatv*, λ, *offset_f, deadband, qswitchf*)
end

The return signal is mixed with the local oscillator on the signal detector and the return signal/LO frequency difference is given by:

det_f := **proc**(*n, az, alt, inc, orbh, lat, trgta, vtrgtv, htrgtv, hsatv, vsatv*, λ, *offset_f, deadband, qswitchf*)
    Slave_f(*n, az, alt, inc, orbh, lat, hsatv, vsatv*, λ, *offset_f, deadband, qswitchf*)
    + Doppler_f(*n, az, alt, inc, orbh, lat, trgta, vtrgtv, htrgtv, hsatv, vsatv*, λ, *offset_f, deadband, qswitchf*)
    − lo_f(λ)
end

Figure A1.64: LO/MO frequency difference

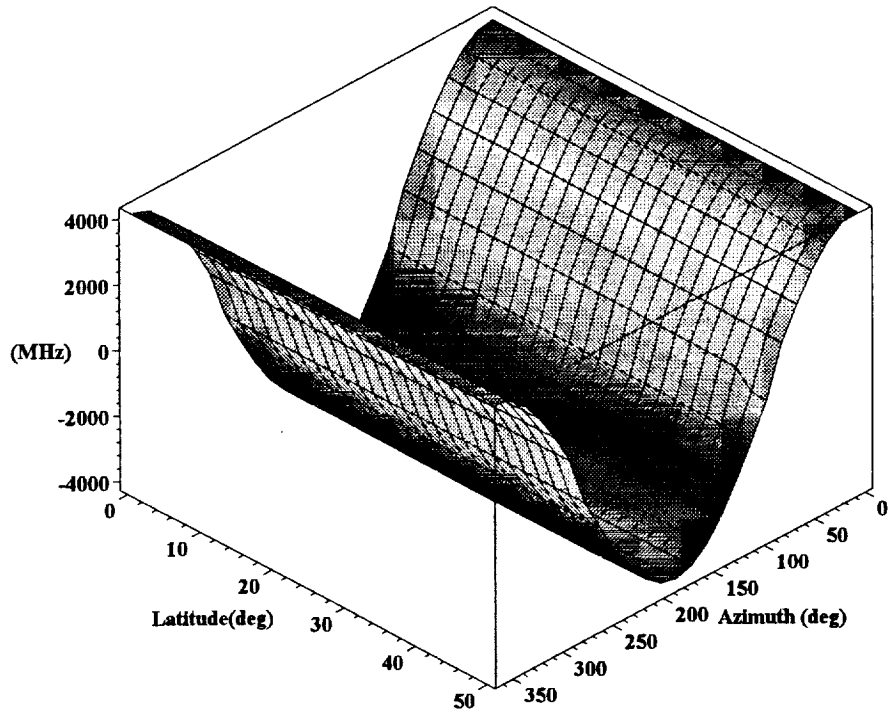

Note that the plot above is discontinuous about 0 MHz due to the frequency jump that is introduced by the tuning algorithm however this discontinuity does not show up in the plot because of the plotting routine. In order to clearly show the discontinuity we can plot a slice through the above plot at a fixed latitude value (45 deg).

Figure A1.65: LO/MO frequency difference

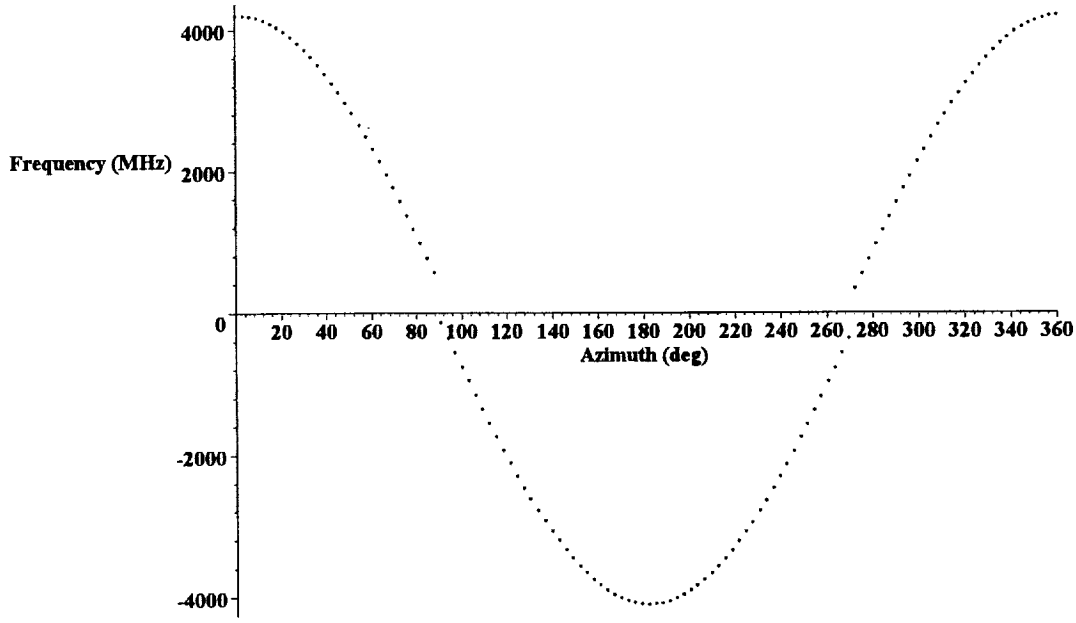

The frequencies from the MO/LO detector are simply given by:

molodet_f := **proc**(*nadir, az, alt, inc, orbh, lat, hsatv, vsatv, λ, offset_f, deadband, qswitchf*)
abs(molo_f(*nadir, az, alt, inc, orbh, lat, hsatv, vsatv, λ, offset_f, deadband, qswitchf*))
end

Figure A1.66: LO/MO detector frequency

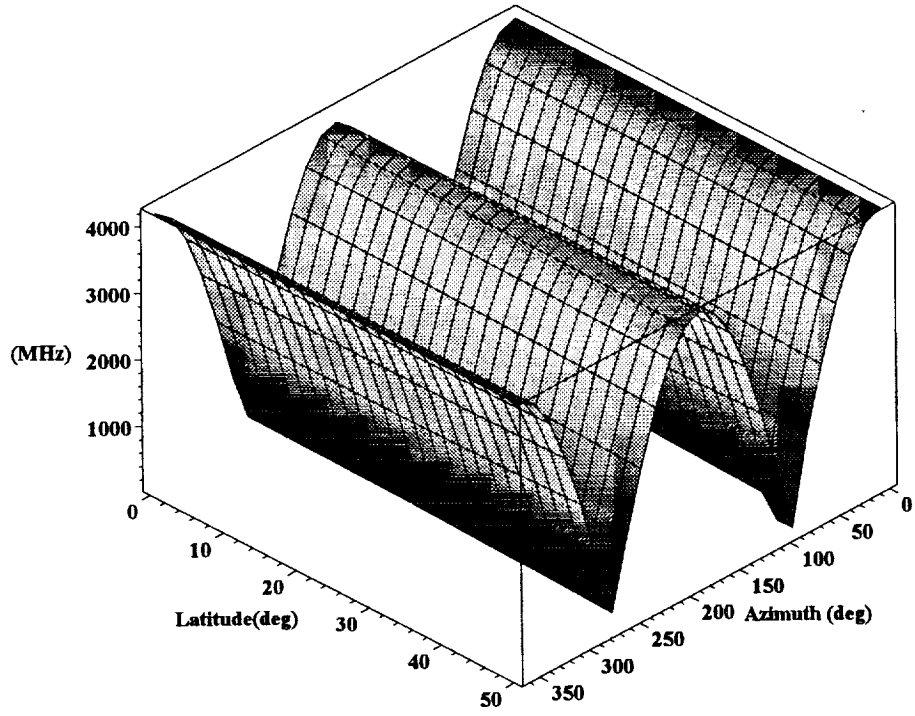

The minimum frequency (MHz) in this plot is:

119.3498471

which is greater than the deadband frequency desired. Thus the algorithm correctly maintains the deadband requirements on the MO/LO detector. The Q-switch introduces a frequency offset of the slave oscillator frequency with respect to the master oscillator frequency. Taking the beat frequency between the two should result in the Q-switch frequency shift independent of azimuth angle or latitude.

Figure A1.67: MO/SO frequency difference

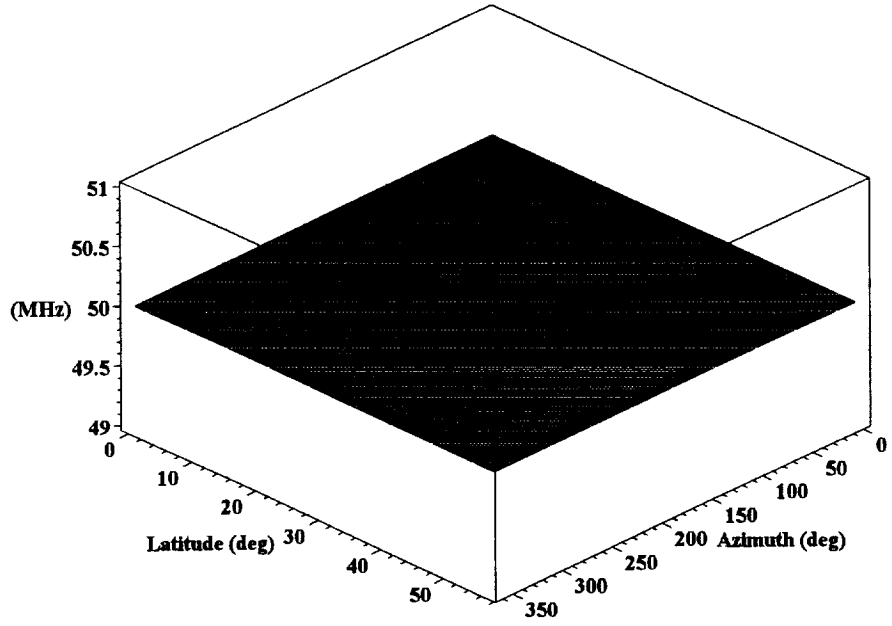

This figure clearly shows that the MO/SO frequency difference is independent of the azimuth angle and latitude. The following figure shows the actual frequency transmitted as a function of azimuth angle and latitude.

Figure A1.68: Outgoing slave oscillator frequency

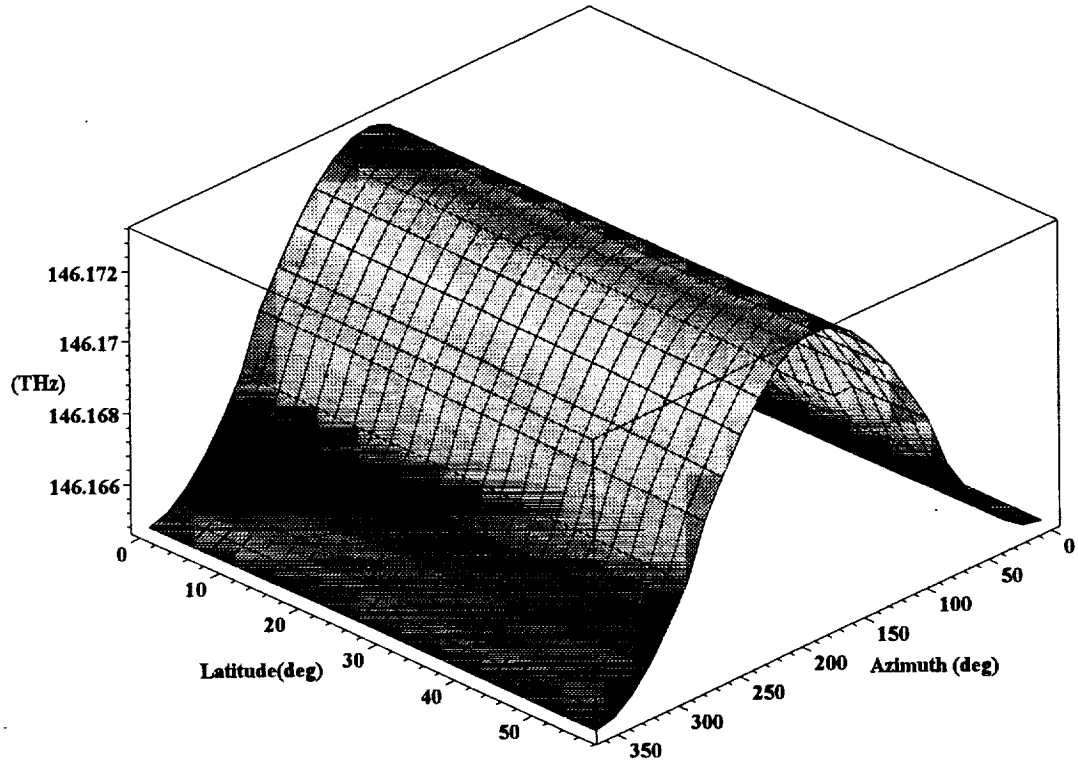

The transmitted frequency is Doppler shifted by the line of sight components of the satellite, earth rotation and target velocities and returns to the spacecraft where it is mixed with the local oscillator. The frequency difference between the local oscillator and the return signal is:

Figure A1.69: Return signal/LO frequency difference

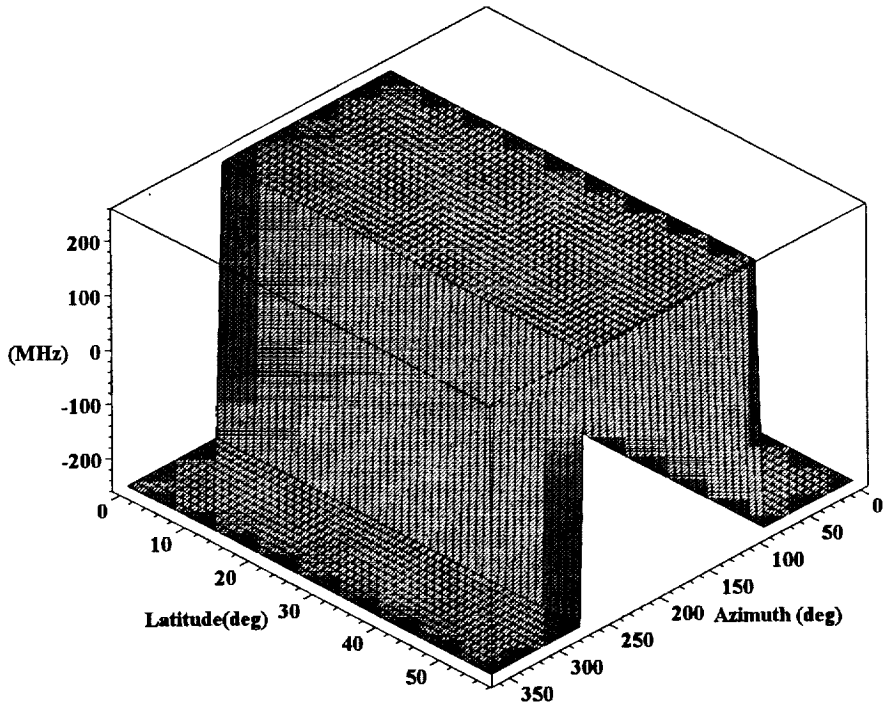

Figure A1.69 clearly shows the signal center frequency hop from -(Offset frequency) to +(Offset frequency) as the tuning algorithm accounts for the MO/LO detector deadband requirements. The frequencies actually seen on the signal detector are the absolute values of Figure A1.69:

Figure A1.70: Signal detector frequency

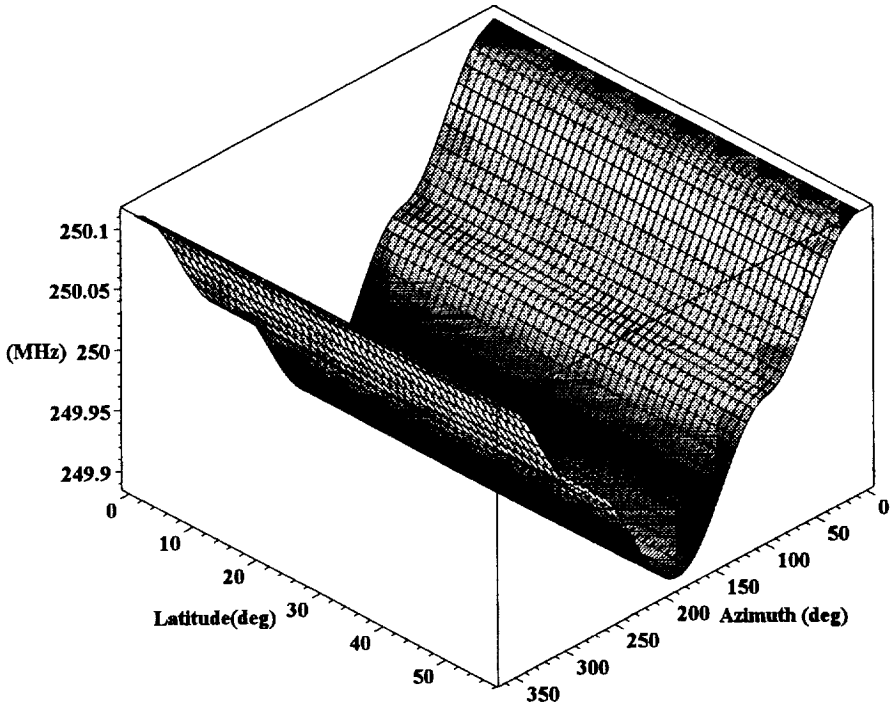

We can see from this figure that the signal floor is not completely flat but varies by ~± 0.1 MHz. This occurs because the Doppler frequency shift for tuning the MO is calculated from the center frequency of the laser but the actual Doppler frequency shift seen is the shift for a frequency of (center frequency of the laser +calculated offset) and this means there is a small error attributable to the method by which the offset is determined. This error, if not accounted for, introduces the small frequency/velocity error seen in Figure A1.70. The following figure shows the absolute value of this offset error as a function of azimuth and latitude relative to the 'ideal' value. Knowing this effect it is, in principle, possible to remove it in post-processing.

Figure A1.71: Magnitude of the uncompensated Doppler Frequency

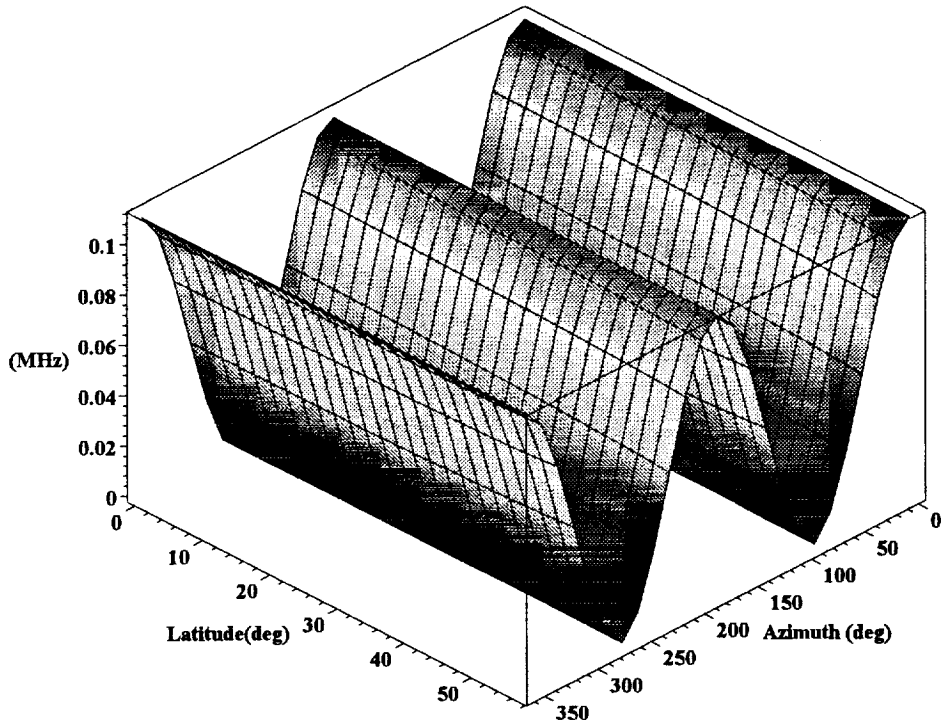

We can plot a series of views of the frequency on the detector as a function of latitude and azimuth for target horizontal velocities of -100 m/s, -50 m/s, 0 m/s, +50 m/s and 100 m/s. This first series of plots is for the velocity always being aligned to the azimuth angle. This ensures that the maximum component of the target velocity is always seen and should result in a frequency independent of latitude and azimuth except for the difference due to maintaining the deadband on the MO/LO detector. Note that there appears to be steps in the following plots in the region around azimuth angles of 90 - 100 degrees. This is an artifact of the plotting grid used - at higher grid resolutions these artifacts dissappear. Figure A1.69 shows how these plots appear with higher resolution plotting grids.

Figures A1.72 - A1.76: Frequency on the detector for target velocities of -100,-50 ,0,50,100 m/s into the line of sight

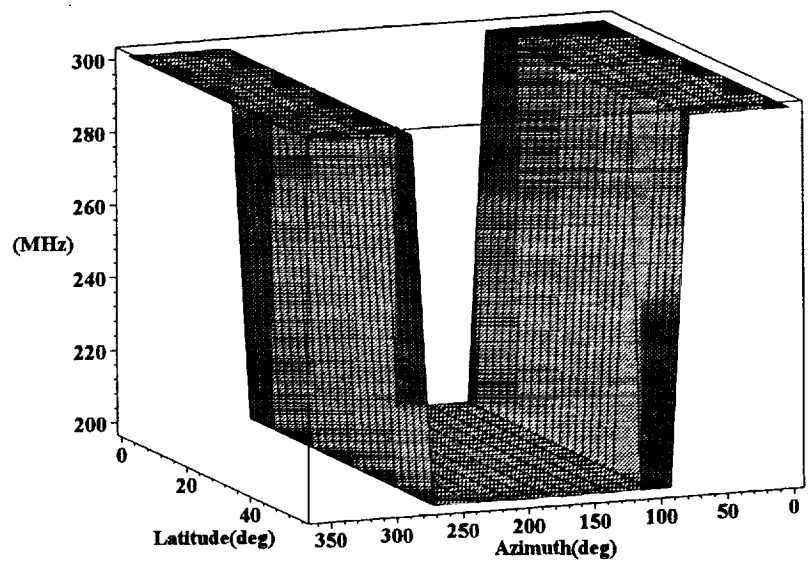

Fig. A1.72
-100 m/s

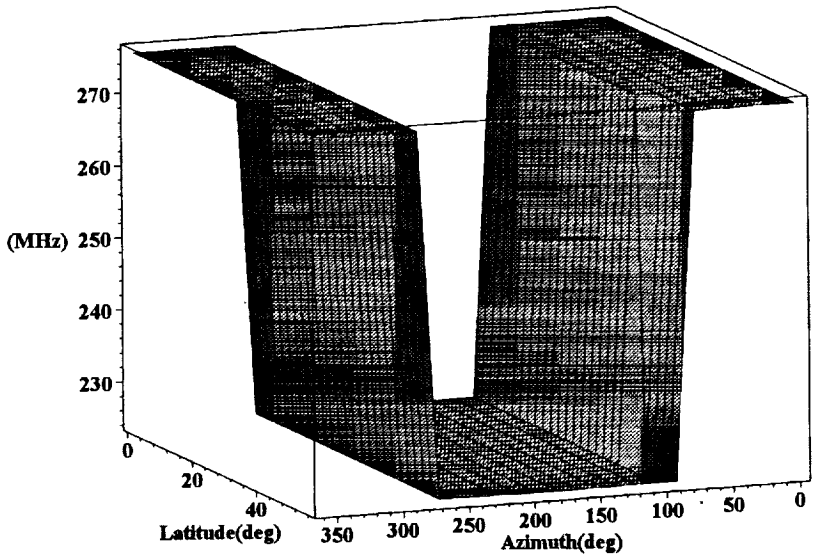

Fig. A1.73
-50 m/s

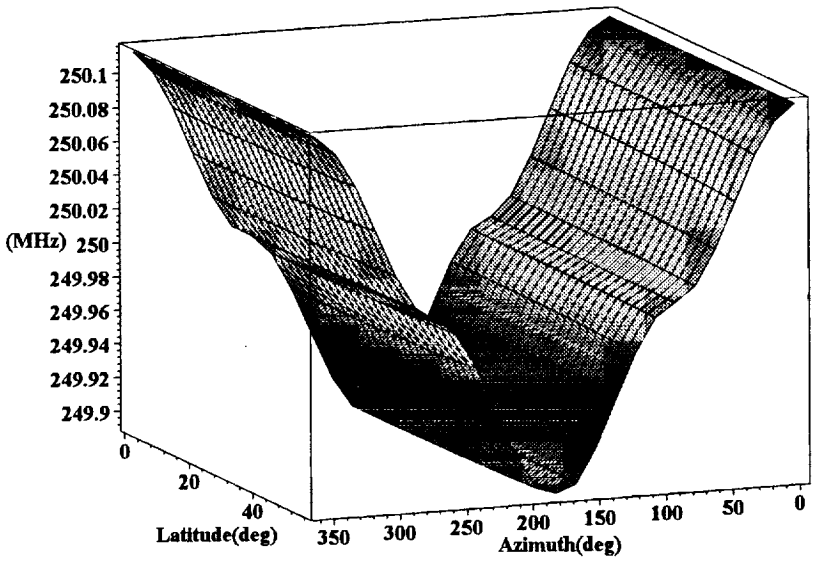

Fig. A1.74
0 m/s

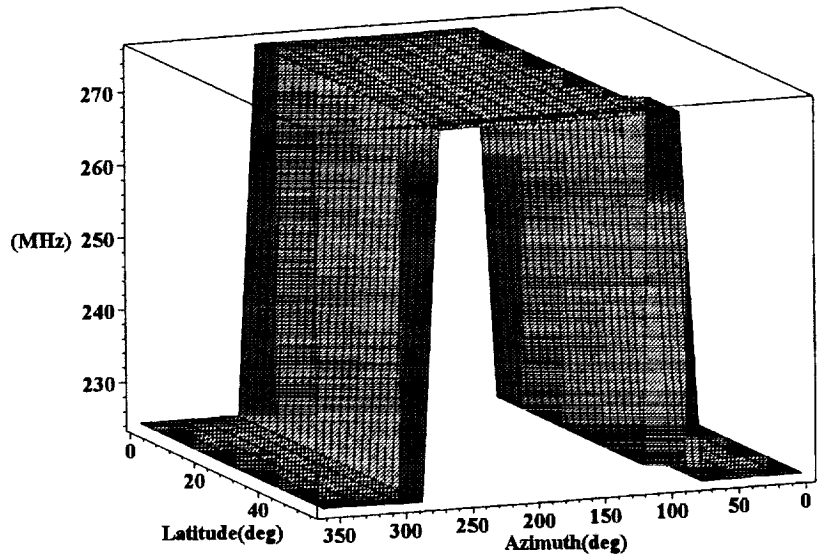

Fig. A1.75
50 m/s

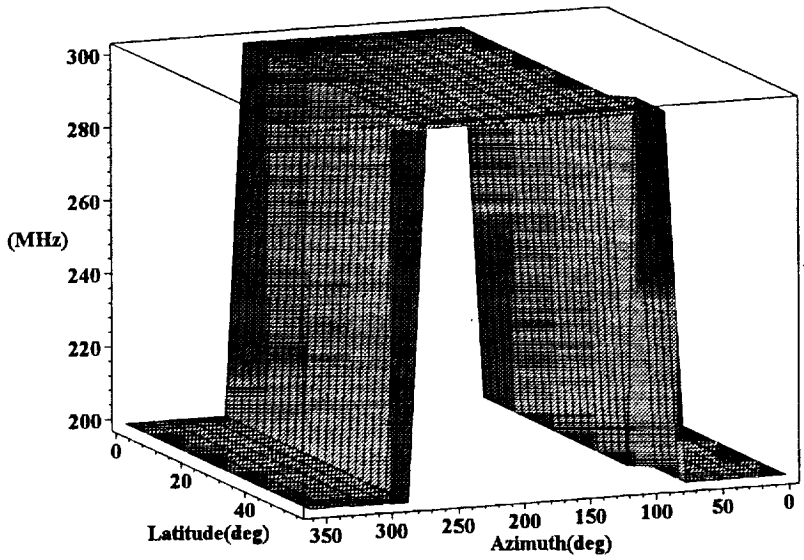

Fig. A1.76
100 m/s

This set of plots shows that as the target velocity varies between the minimum and maximum velocities the signal frequency is independent of the latitude and azimuth angle. The clear separation of the two portions of the signal ensures that in post-processing it will be clearly distinguishable where the frequency hop required to maintain the deadband occured. For comparison purposes the next set of plots is for the same target velocities except that the target velocity is always oriented at a fixed angle, parallel to the lines of latitude. In this case the line of sight component of the target velocity will have an azimuthal dependence. Note that there appears to be steps in the following plots in the region around azimuth angles of 90 - 100 degrees. As in the prior plots this is an artifact of the plotting grid used - at higher grid resolutions these artifacts dissappear.

Figures A1.77 - A1.81: Frequency on the detector for target velocities of -100,-50,0,50,100 m/s parallel to the lines of latitude

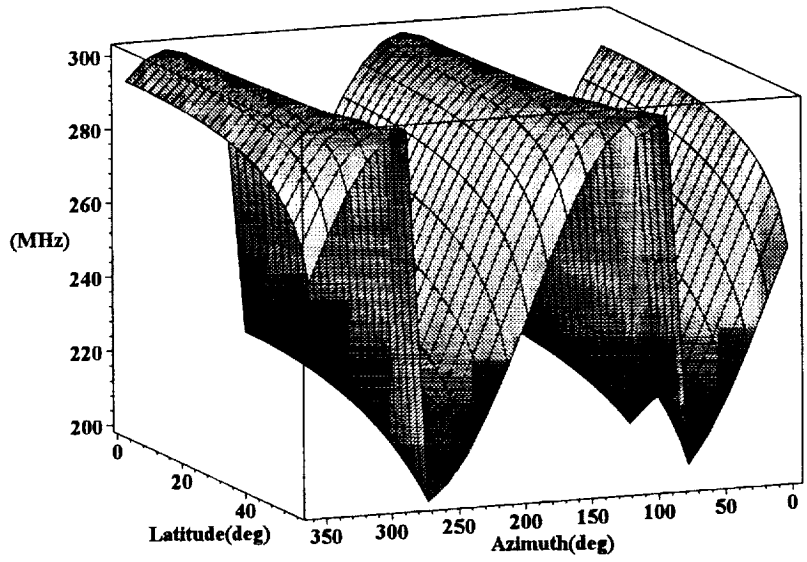

Fig. A1.77
-100 m/s

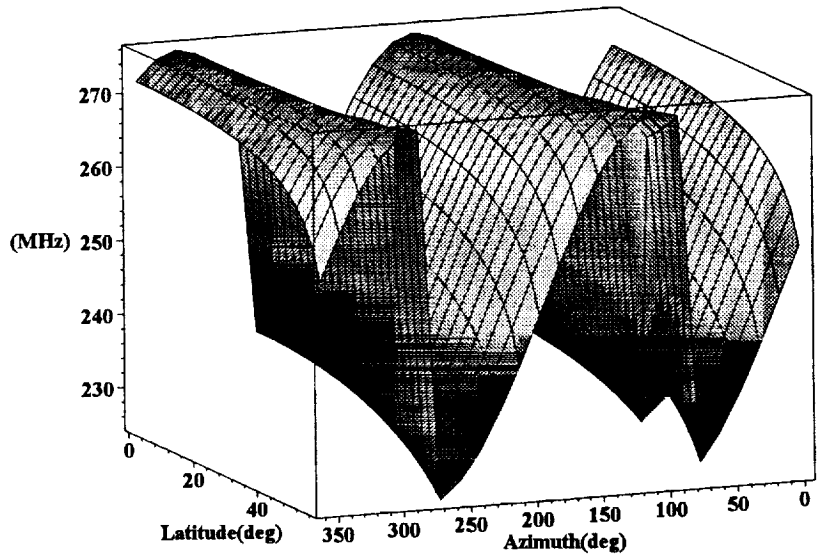

Fig. A1.78
-50 m/s

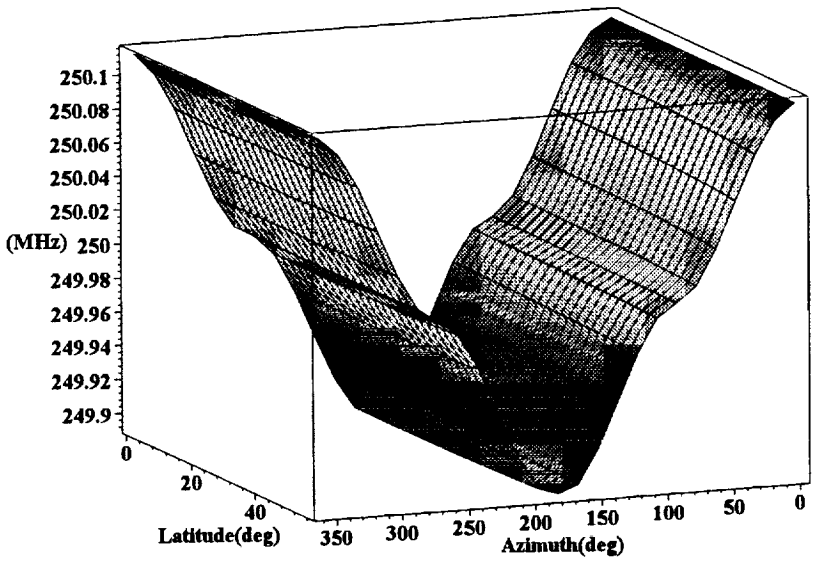

Fig. A1.79
0 m/s

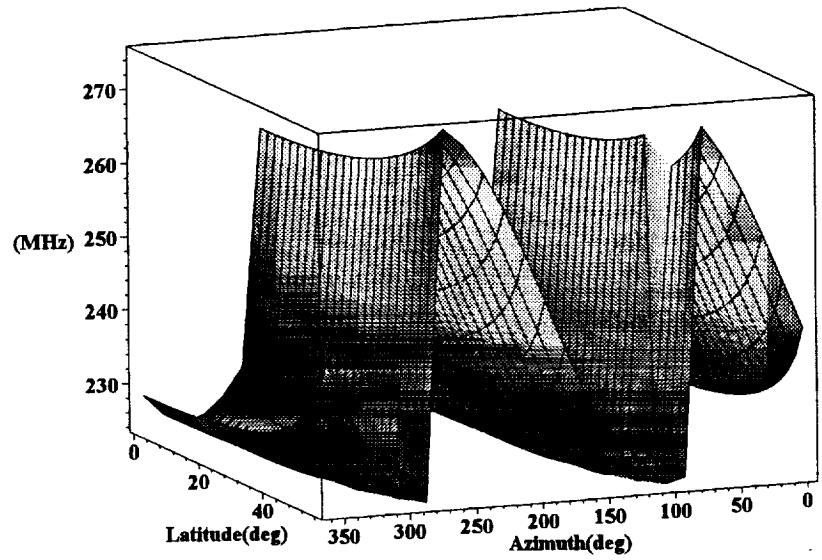

Fig A1.80
50 m/s

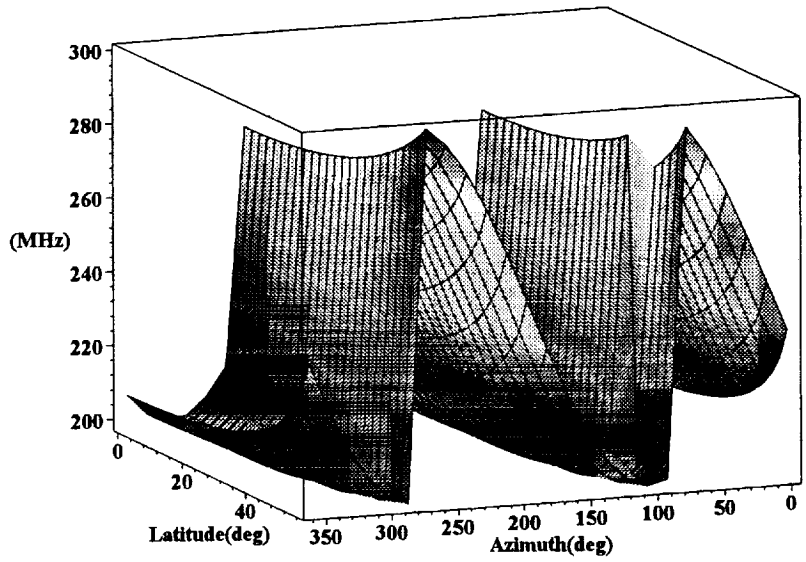

Fig. A1.81
100 m/s

Appendix A2: Satellite Lidar Sensitivity Analyses

833 km, 89 deg inclination orbit, 45 deg nadir instrument

The equations in this document are in MAPLE, a symbolics mathematics package format. Define some constants:

$$r2d := 180\,\frac{1}{\pi}$$

$$d2r := \frac{1}{180}\,\pi$$

$$v\_c := .2997924590\ 10^{9}$$

$$G := .6672590000\ 10^{-10}$$

$$Me := .5979000000\ 10^{25}$$

where r2d and d2r are constants for converting between degrees and radians, v_c is the velocity of light in m/s , G is the Gravitational constant in N m^2/kg^2 and Me is the mass of the earth in kg. Now define the WGS84 ellipsoid parameters:

$$a := .63781370\ 10^{7}$$

$$b := .63567523142\ 10^{7}$$

$$We := .00007292115$$

$$ee := .0818191908426$$

$$ee2 := .00669437999013$$

where a and b are the semimajor (equatorial) and semiminor (polar) radii respectively, We is the angular velocity of the earth, ee and ee2 are the first eccentricity and its square respectively.
Finally define the parameters for this analysis:

$$maxlat := 89$$

$$orbit1 := 833000$$

$$nadir1 := 45$$

where maxlat is the highest latitude that the orbit passes over, orbit1 is the orbit height with respect to the equatorial earth radius, a and nadir1 is the instrument nadir at the spacecraft. We now define a procedure to calculate the radius of the oblate earth with respect to the geodetic latitude. Note that the expression for calculating the geodetic latitude breaks down at the poles and so a check must be made for a latitude of Pi/2 radians.

```
Rlat := proc(lat)
global a, b;
    if lat = 1 / 2*π or lat = - 1 / 2*π then b else 1 / (sqrt(1 / a^2 + tan(lat)^2 / b^2)*cos(lat)) fi
end
```

This next procedure calculates the differential of the earths radius as a function of latitude.

```
dRlat := proc(lat)
global a, b;
    sin(lat) / (cos(lat)^2*sqrt(1 / a^2 + tan(lat)^2 / b^2))
    - 2*tan(lat)*(1 + tan(lat)^2) / (cos(lat)*(1 / a^2 + tan(lat)^2 / b^2)^3*b^2)
end
```

This procedure calculates the earth's rotational velocity at a latitude, lat :

```
Vlat := proc(lat) global We, a, ee2; We*a*cos(lat) / sqrt((1 - ee2)*sin(lat)^2 + cos(lat)^2) end
```

Consider a satellite at some latitude, lat in an orbit of inclination, inc then the angle the satellite orbit makes to a meridian line at latitude, lat is:

```
orblat := proc(lat, inc) arcsin(cos(inc) / cos(lat)) end
```

Plot the angle between orbit and meridian as a function of latitude for the parameters above.

Figure A2.1: Angle between orbit and meridian

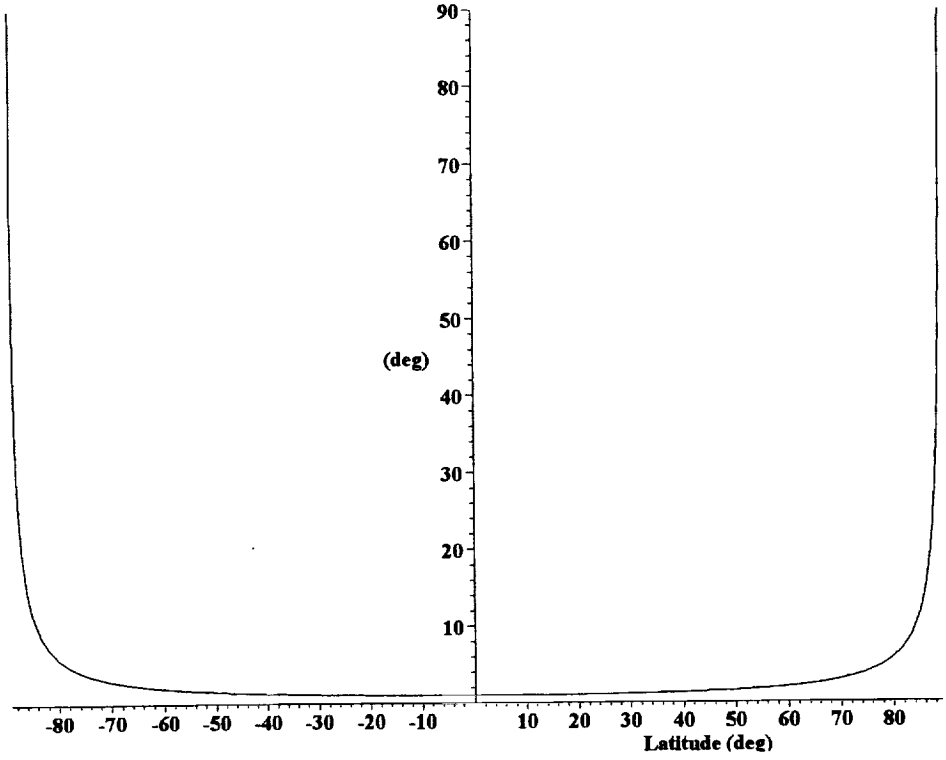

We can also plot the rate of change of the angle between the orbit and meridian as a function of latitude.

Figure A2.2: Rate of change of angle to local meridian

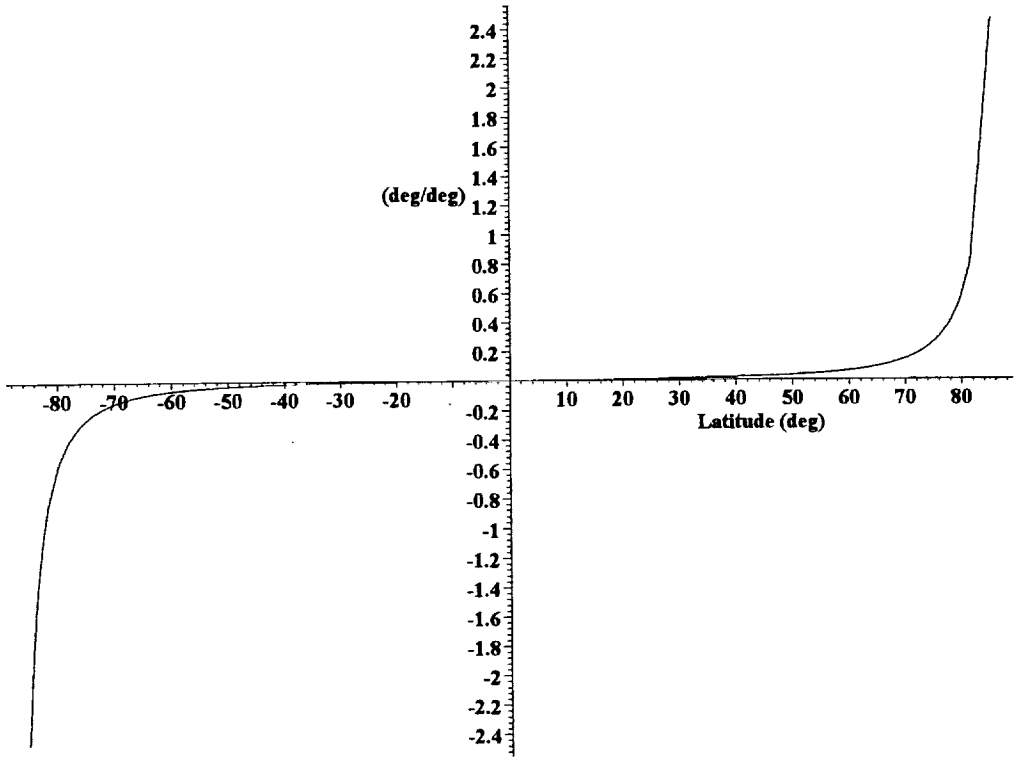

Plot the change in WGS84 earth radius with respect to the equatorial radius as a function of latitude.

Figure A2.3: Variation in the earth's radius as a function of latitude

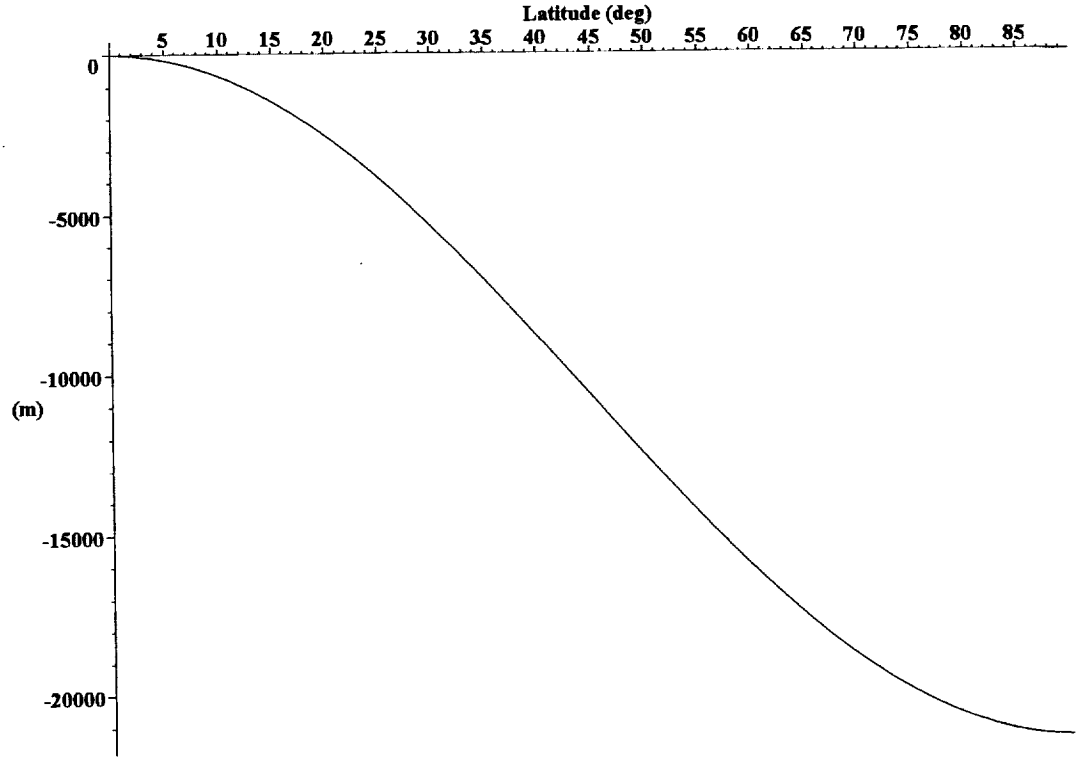

This clearly shows the 20 km difference between the two radii. Plot the distance moved along the surface for one degree

change in latitude.

Figure A2.4: Latitude surface distance

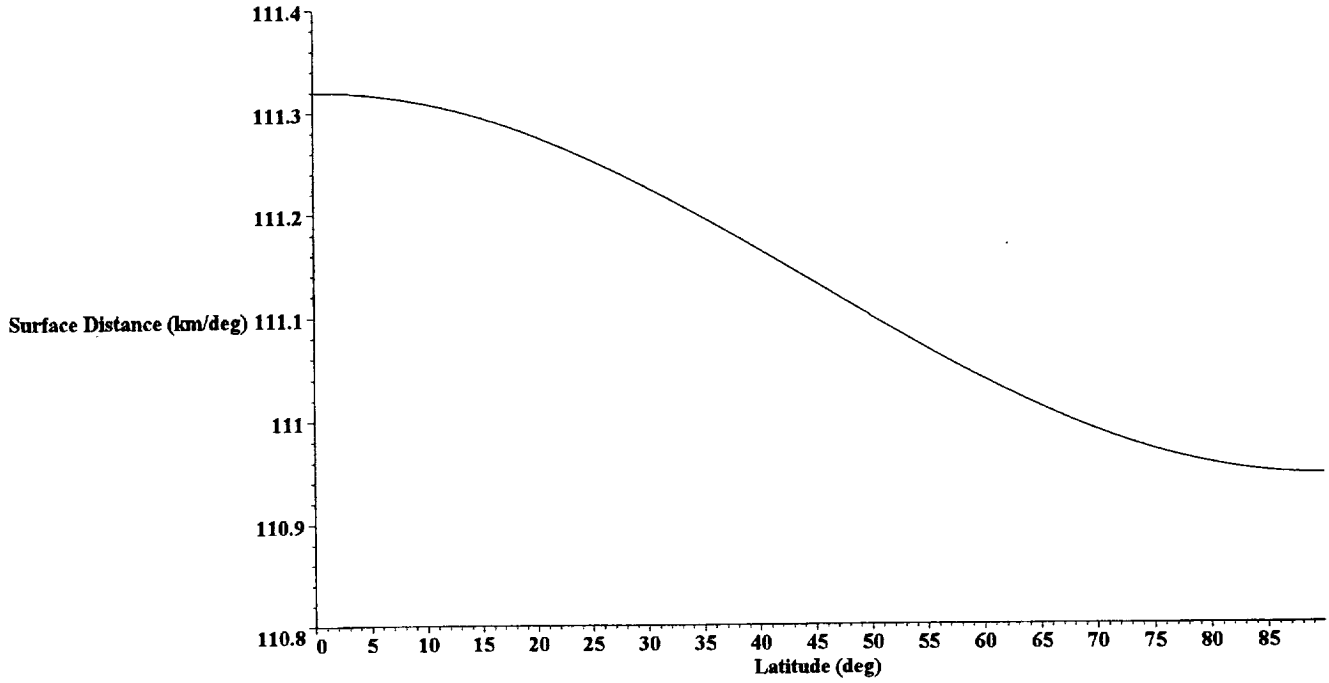

We can replot this as a delta change from the value at the equator.

Figure A2.5: Delta change in Latitude surface distance

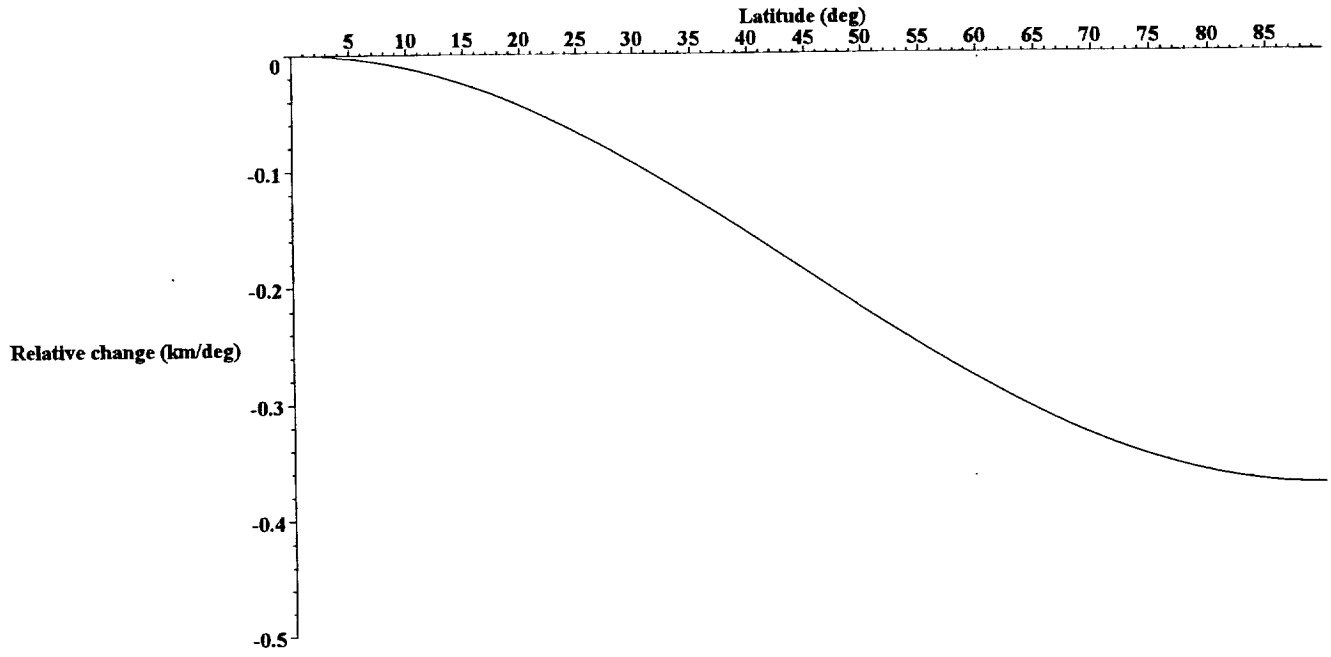

The rate of change of the WGS84 ellipsoid radius is given by:

```
dRlat := proc(lat)
global a, b;
    sin(lat) / (cos(lat)^2*sqrt(1 / a^2 + 1 / (cos(lat)^2*b^2) - 1 / b^2))
    - sin(lat) / (cos(lat)^4*(1 / a^2 + 1 / (cos(lat)^2*b^2) - 1 / b^2)^(3 / 2)*b^2)
end
```

and we can also plot it:

Figure A2.6: Rate of change of the WGS84 ellipsoid radius

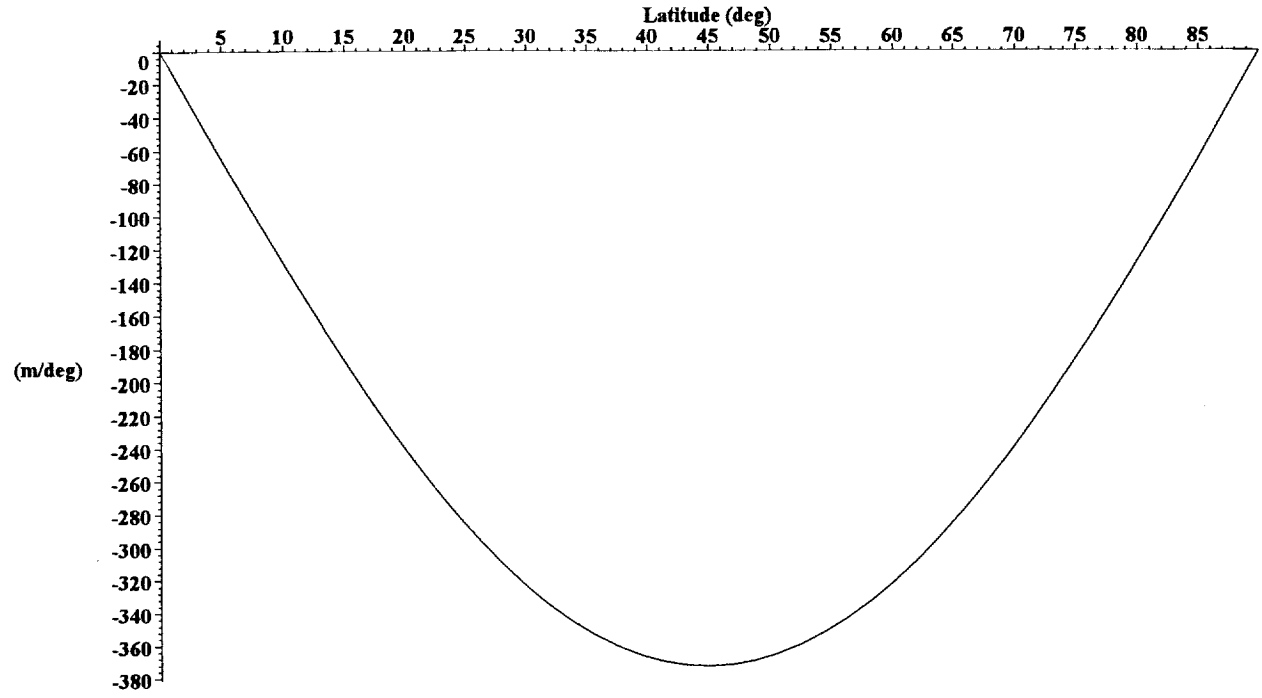

If we plot the integral of the rate of change of the WGS84 ellipsoid with latitude we should get back to the initial plot.

Figure A2.7: Integral of dWGS84/dlat as a fn of lat (sanity check)

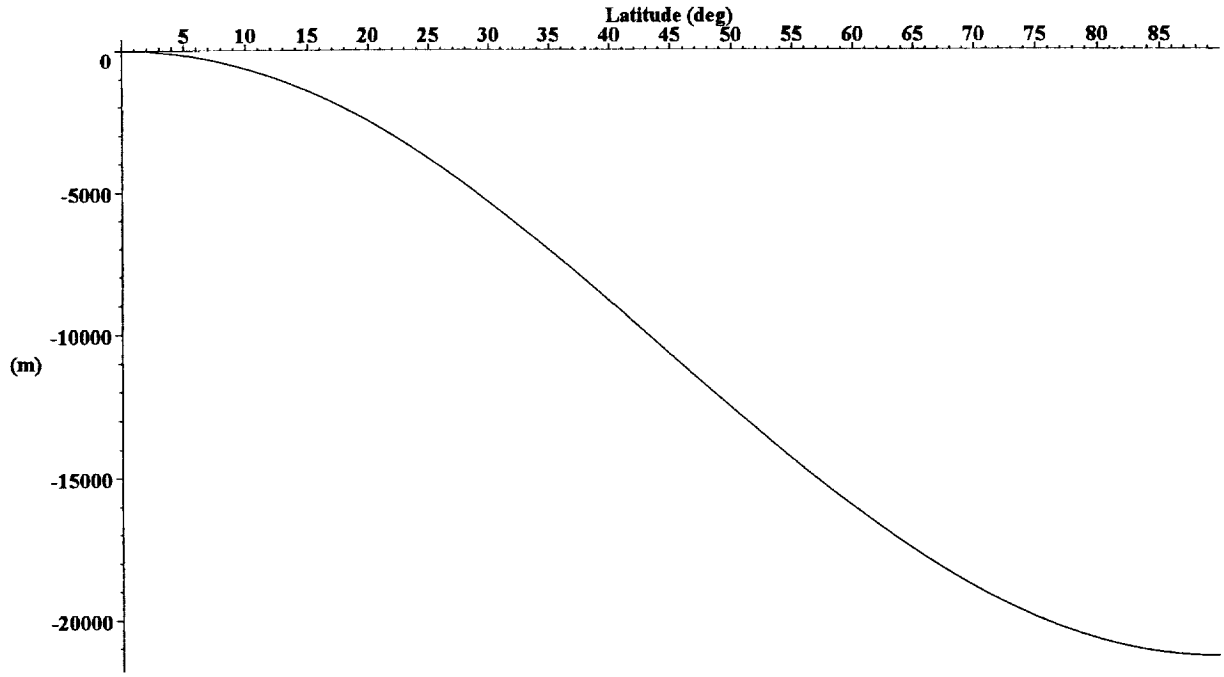

A satellite in a circular orbit around the earth with an orbit radius of (orbh + a), where orbh is the height of the orbit above the equator, has a velocity given by:

vsat := **proc**(*orbh*) **global** *a*, *b*, *G*, *Me*; sqrt(*G***Me* / (*orbh* + *a*)) **end**

The following plot shows the variation in velocity over the orbit heights within 50 km of the nominal orbit height.

Figure A2.8: Satellite Velocity

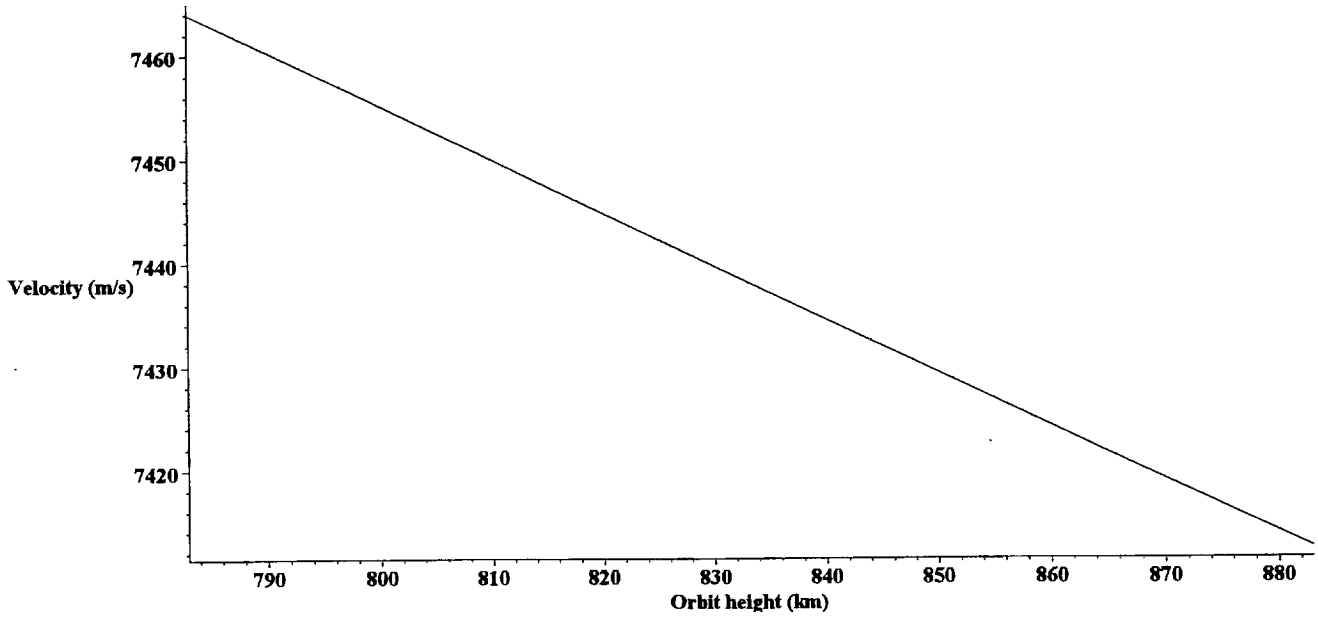

We can replot this as a change in satellite velocity relative to the nominal orbit height.

Figure A2.9: Change in Satellite Velocity

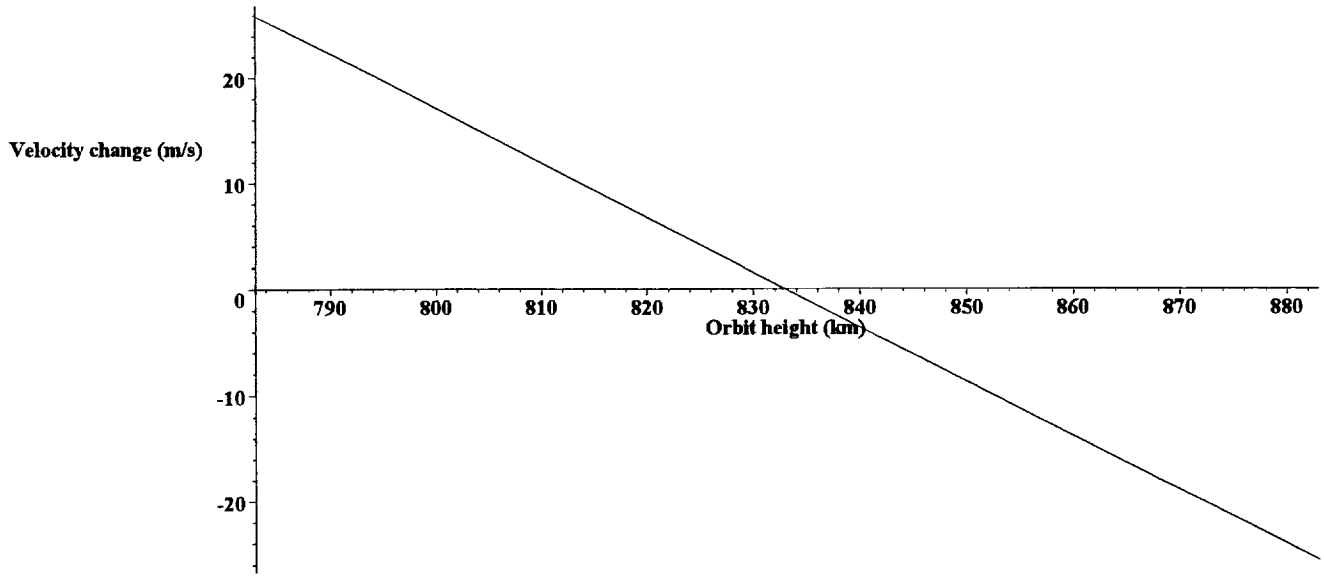

The sensitivity of the satellite velocity to changes in orbit height can be determined by plotting the differential wrt the orbit height:

Figure A2.10: Rate of change in satellite velocity vs. orbit height

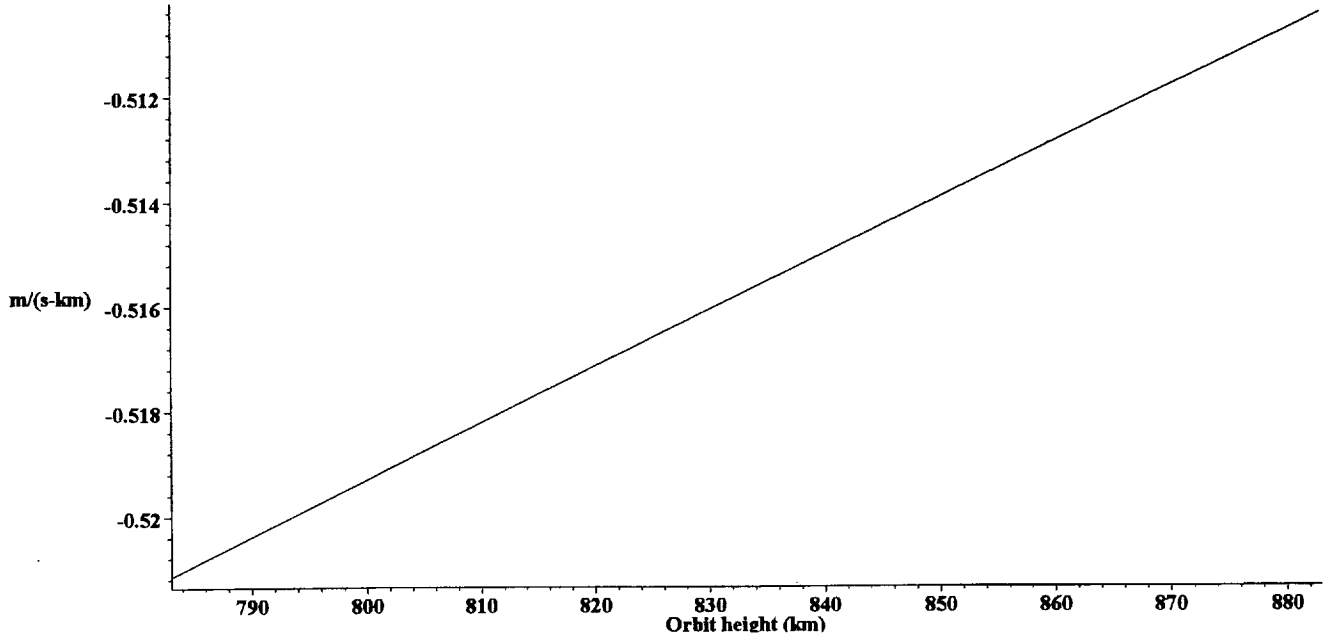

The time for one orbit is simply given by:

torbit := **proc**(*orbh*) **global** *a*, *b*; 2*π*(*orbh* + *a*) / vsat(*orbh*) **end**

and the variation in orbit period over the orbit heights of interest is shown in the following plot:

Figure A2.11: Orbit Period

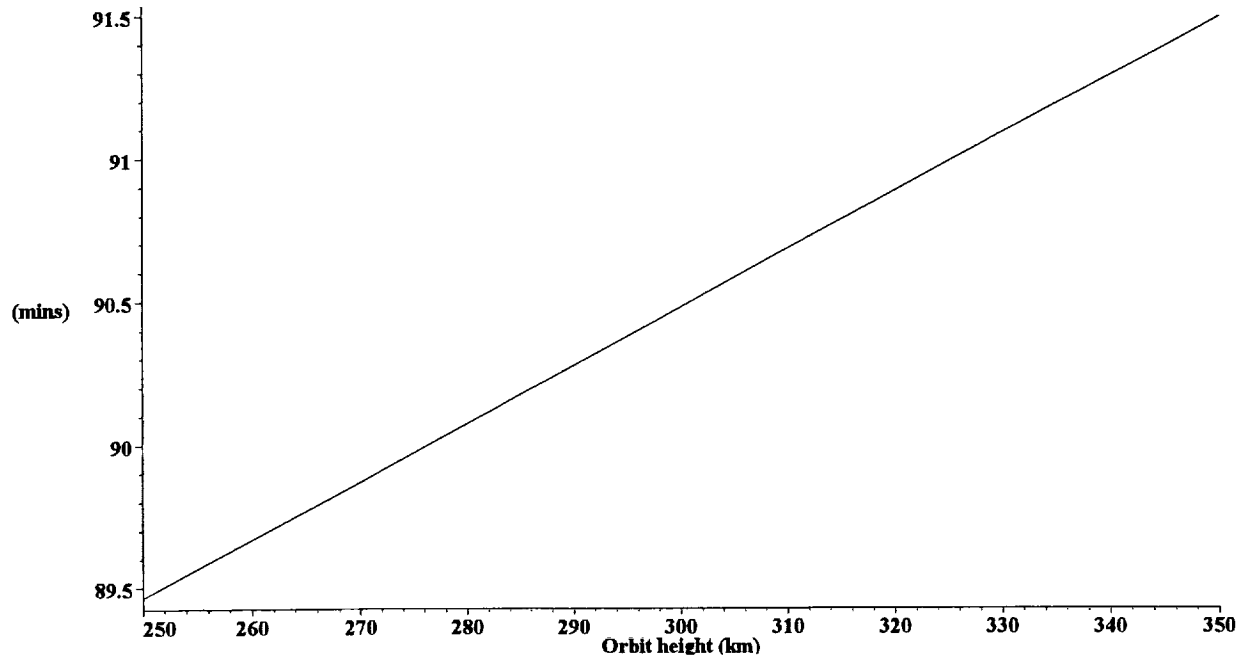

We can modify this to show a delta change wrt the lowest orbit height:

Figure A2.12: Change in orbit period with orbit height

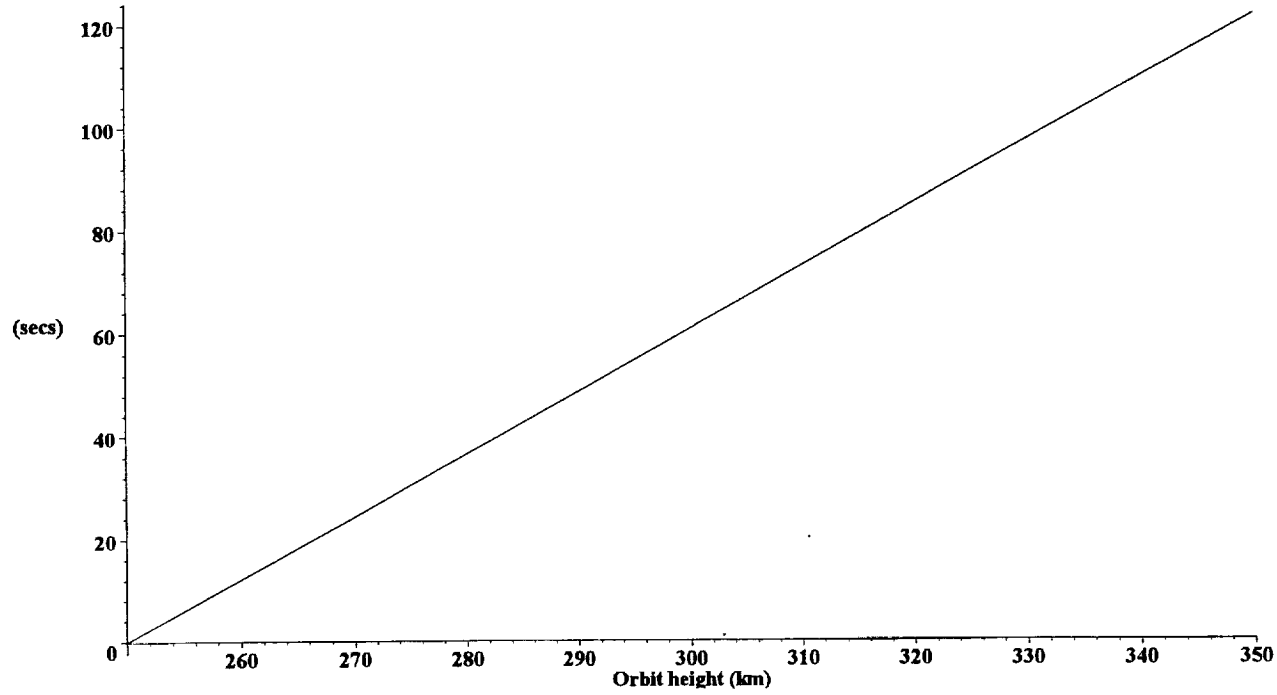

For the orbit conditions specified at the beginning of this document the component of the satellite velocity parallel to the local line of meridian at a given latitude is:

vlat := **proc**(*lat*, *orbh*, *inc*) **global** *a*, *b*; vsat(*orbh*)*cos(orblat(*lat*, *inc*)) **end**

Figure A2.13: Satellite velocity parallel to lines of meridian

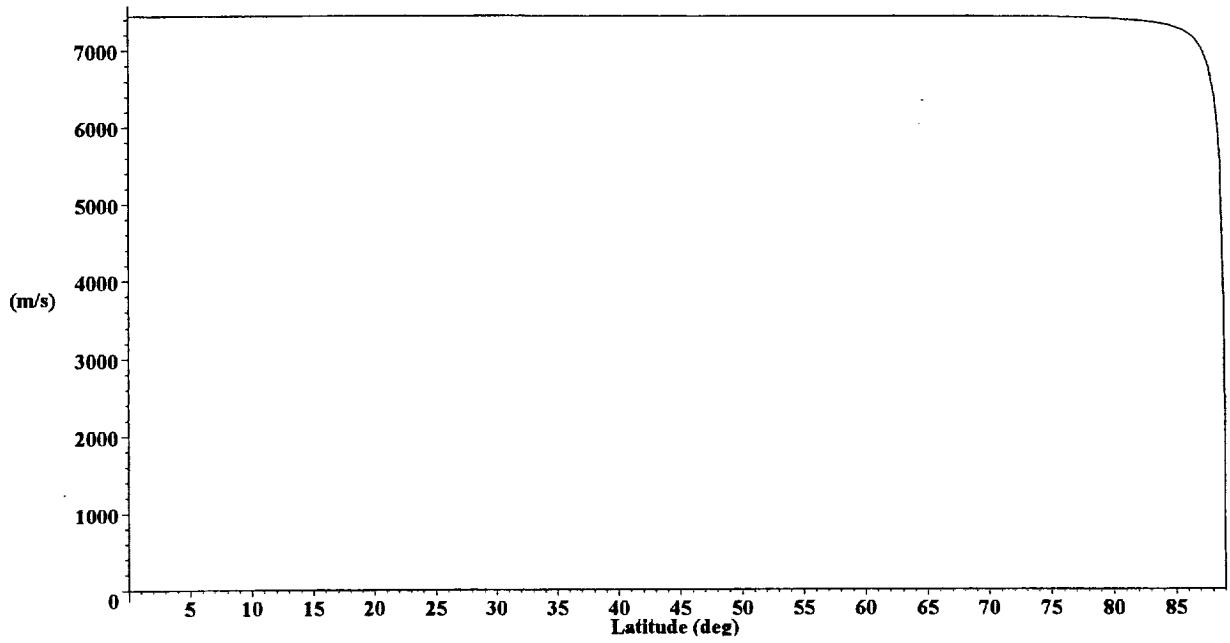

Similarly the component of the satellite velocity parallel to the lines of longitude at a given latitude is:

vlong := **proc**(*lat*, *orbh*, *inc*) **global** *a*, *b*; vsat(*orbh*)*sin(orblat(*lat*, *inc*)) **end**

Figure A2.14: Satellite velocity parallel to lines of longitude

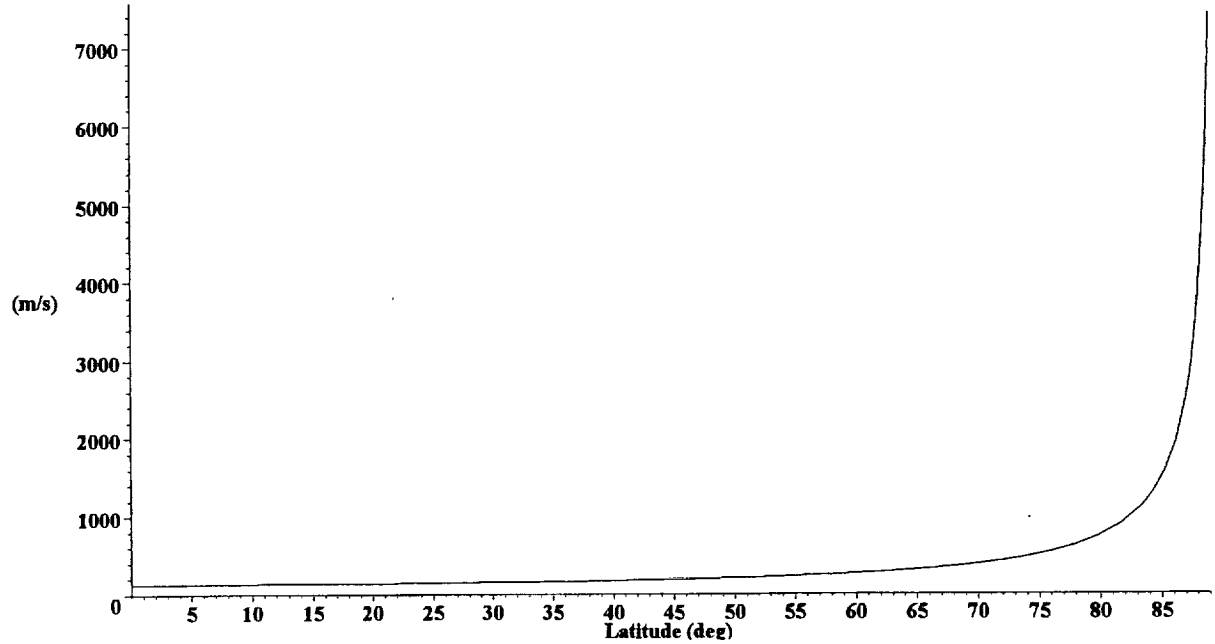

Recombining these we should get a constant satellite velocity independent of latitude:

Figure A2.15: Sqrt(Vlong^2+Vlat^2) (sanity/numerics check)

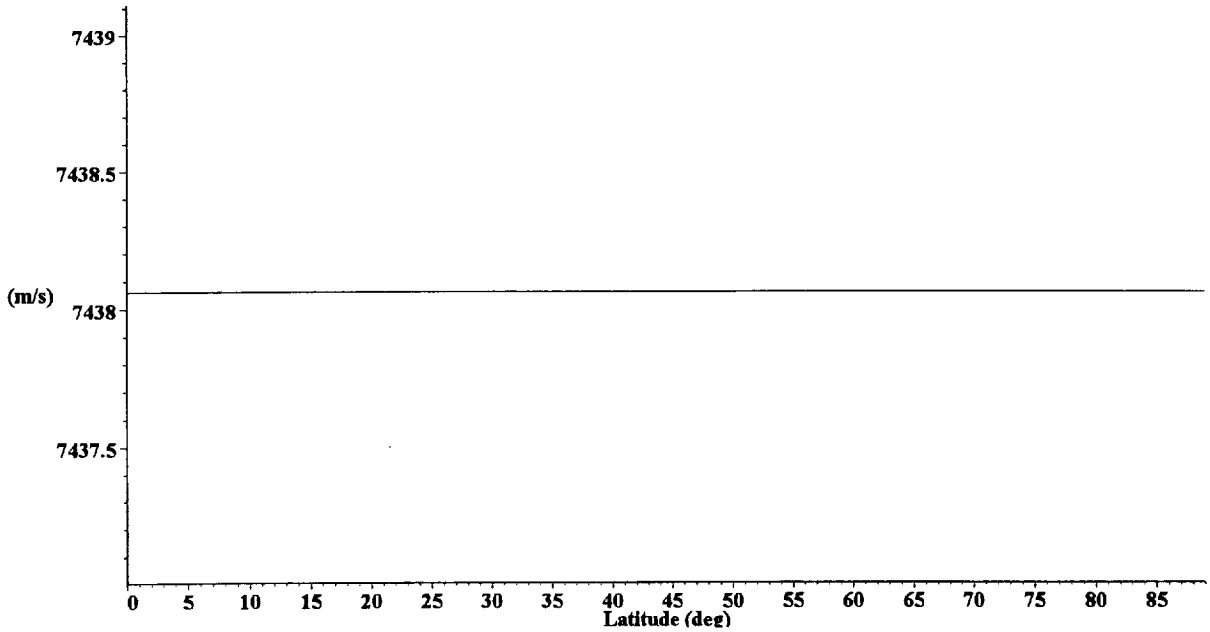

Once we know the component of the velocity along the lines of latitude we can determine the rate of change of latitude as a function of latitude for any given orbit.

dlatdt := **proc**(*lat*, *orbh*, *inc*) **global** *a*, *b*; vlat(*lat*, *orbh*, *inc*)**r2d* / (*orbh* + *a*) **end**

For the orbit under consideration this gives:

Figure A2.16: Rate of change of latitude

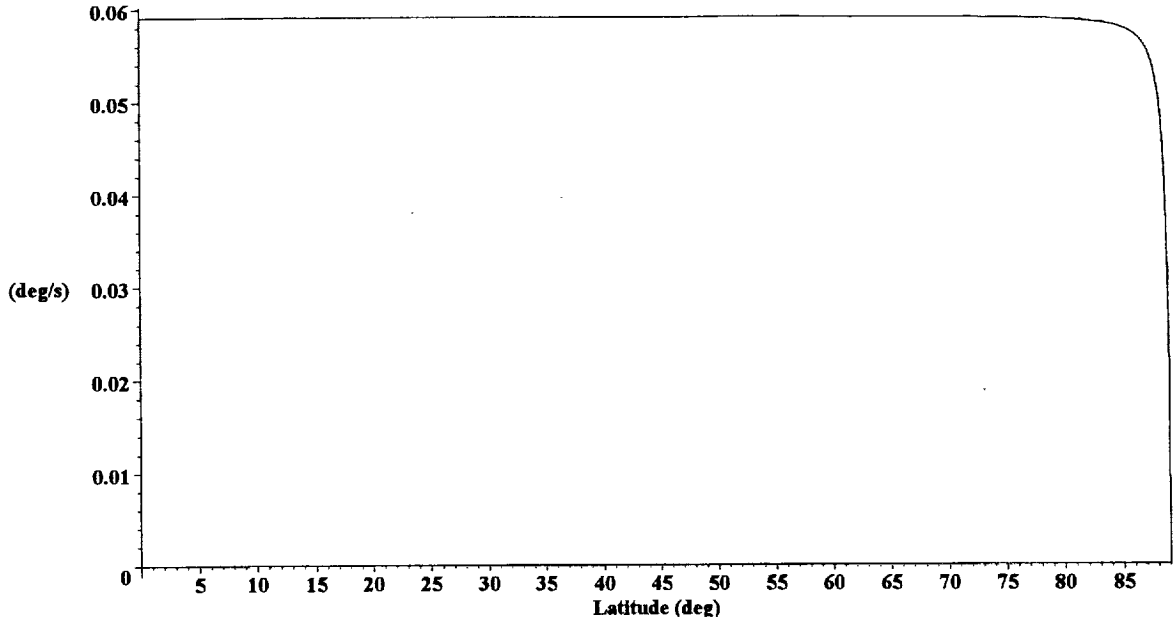

We can then combine this with the WGS84 ellipsoid radius to get the time rate of change of the Earth's radius as a function of latitude for this orbit configuration.

dRlatdt := **proc**(*lat*, *orbh*, *inc*) **global** *a*, *b*; dlatdt(*lat*, *orbh*, *inc*)*dRlat(*lat*)**d2r* **end**

Figure A2.17: Rate of change of the Earth's radius

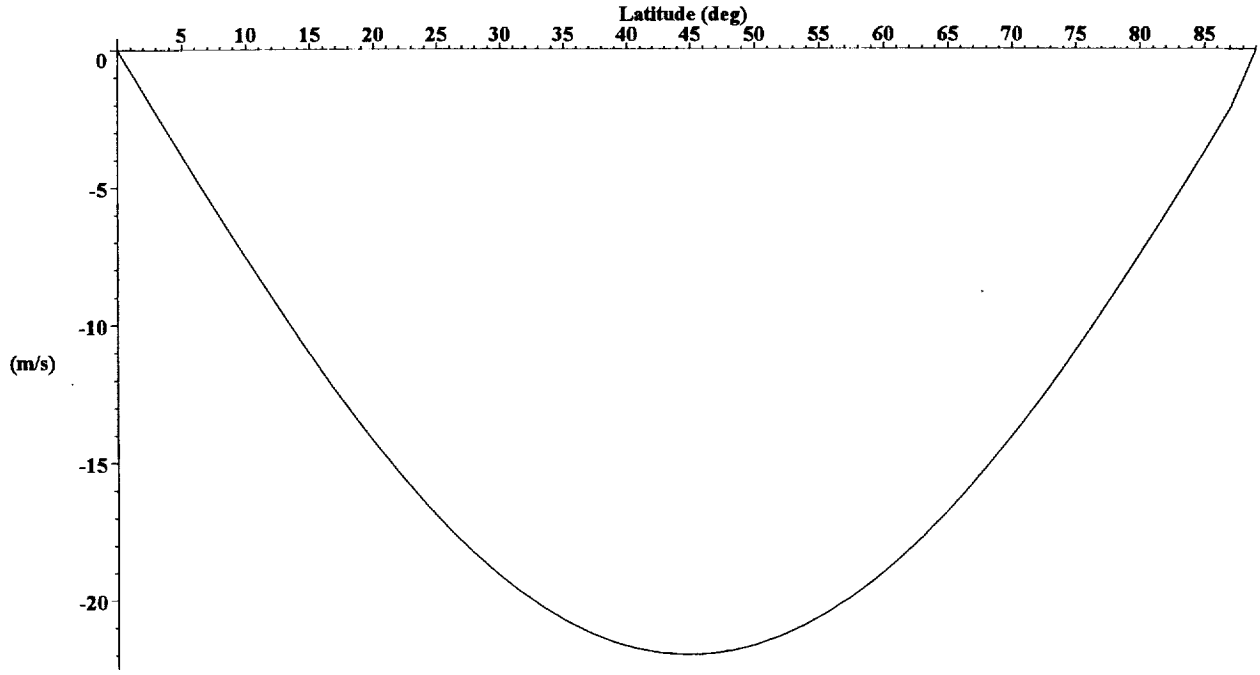

We can look at the earth's rotational velocity as a function of latitude:

Figure A2.18: Earth's rotational velocity at the WGS84 ellipsoid radius

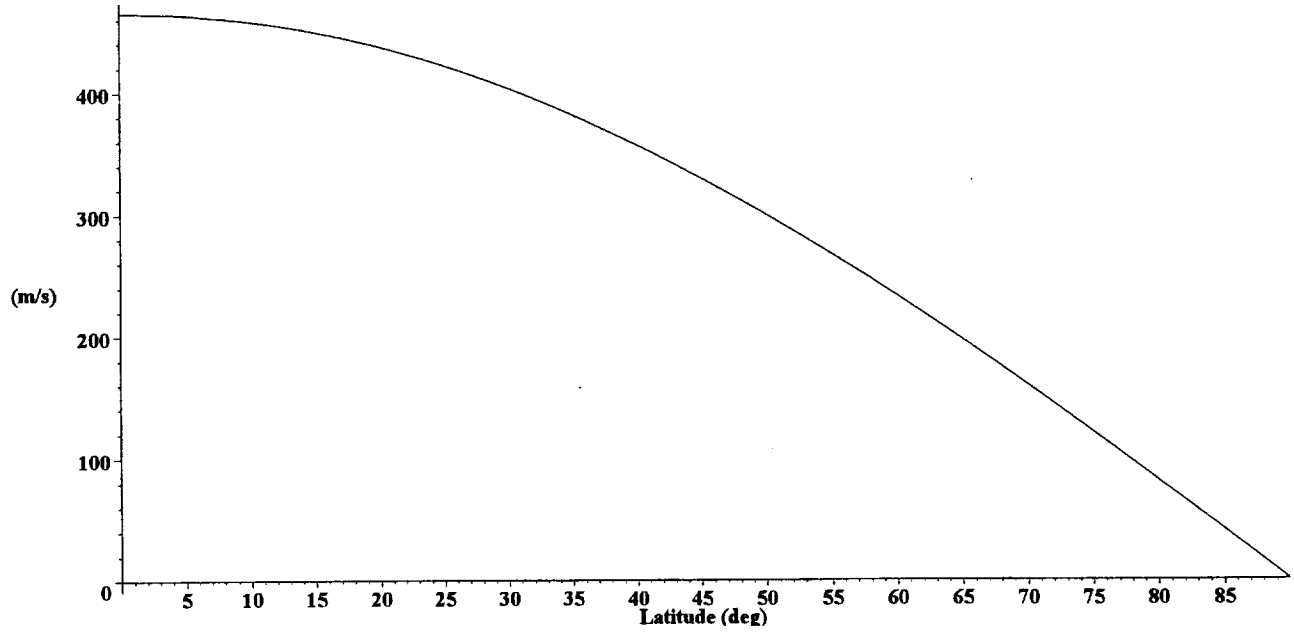

and the rate of change of the earth's rotational velocity with latitude:

Figure A2.19: Rate of change of Earth's rotational velocity with latitude

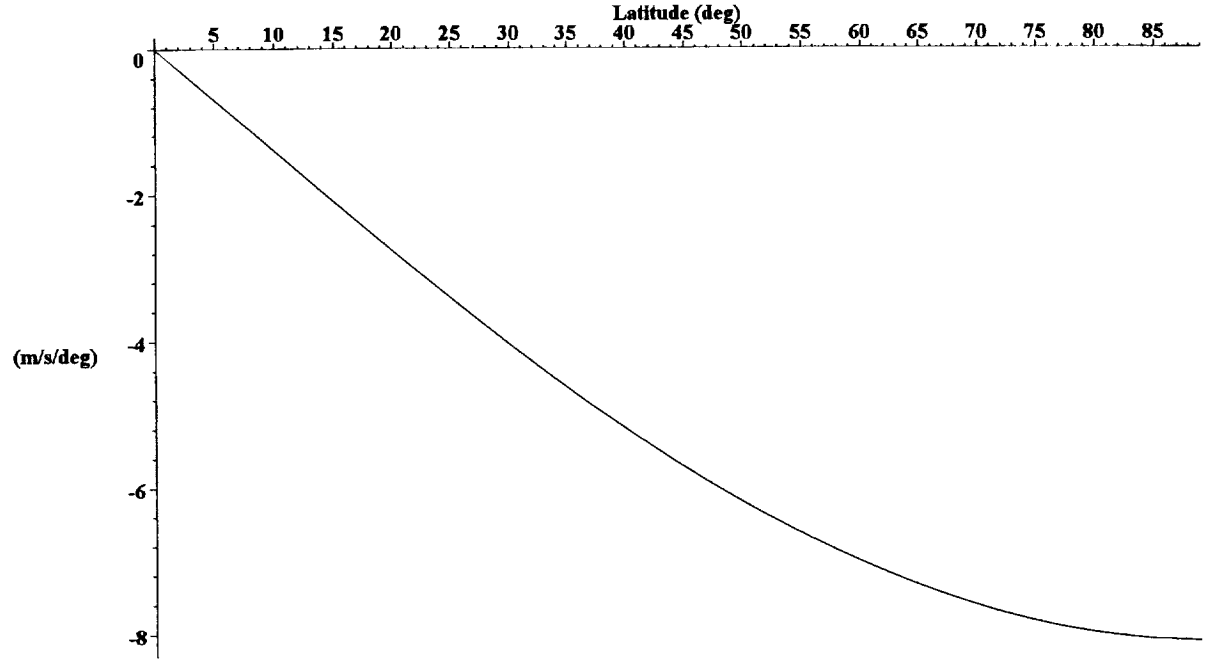

The nadir angle at a target height, alt above the ground is given by:

nadalt := **proc**(*orbh*, *nadir*, *alt*, *lat*) **global** *a*; arcsin(((*orbh* + *a*)*sin(*nadir*)) / (Rlat(*lat*) + *alt*)) **end**

where nadir is the nadir angle at the spacecraft. We can then plot the change in nadir angle at the earth's surface, for the current orbit height and nadir angle as a function of latitude.

Figure A2.20: Nadir angle at the earth's surface

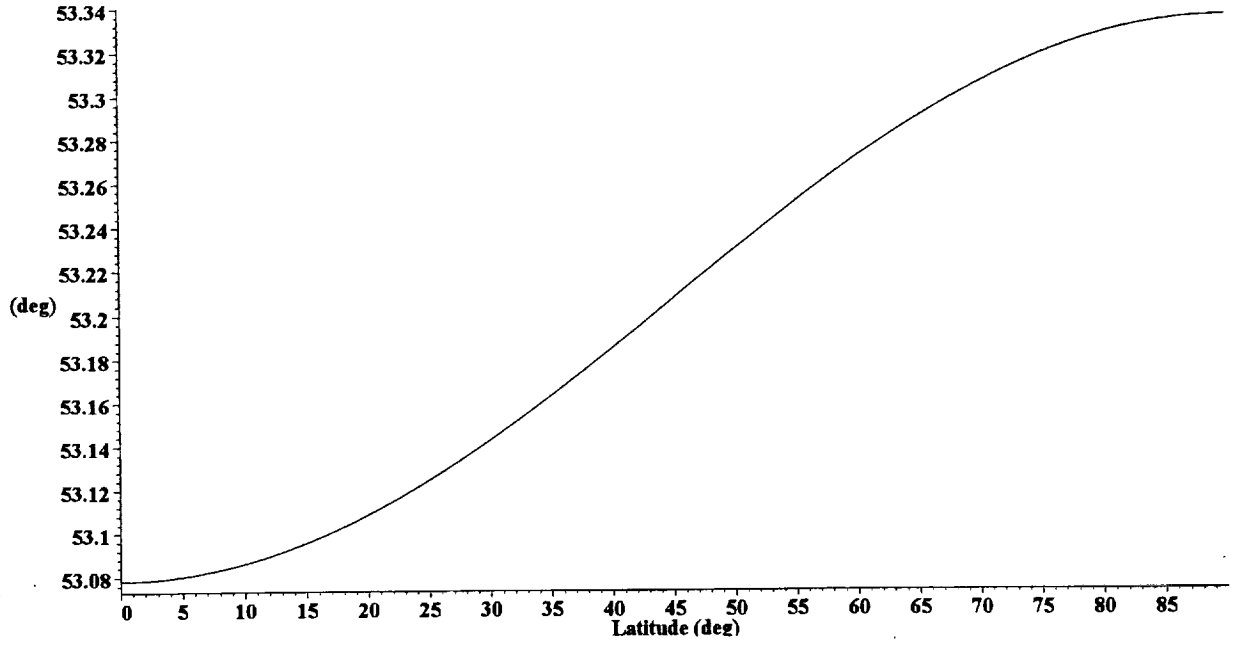

As previously we can show the change in degrees with respect to the nadir angle at the surface near the equator.

Figure A2.21: Variation of the nadir angle at the earth's surface

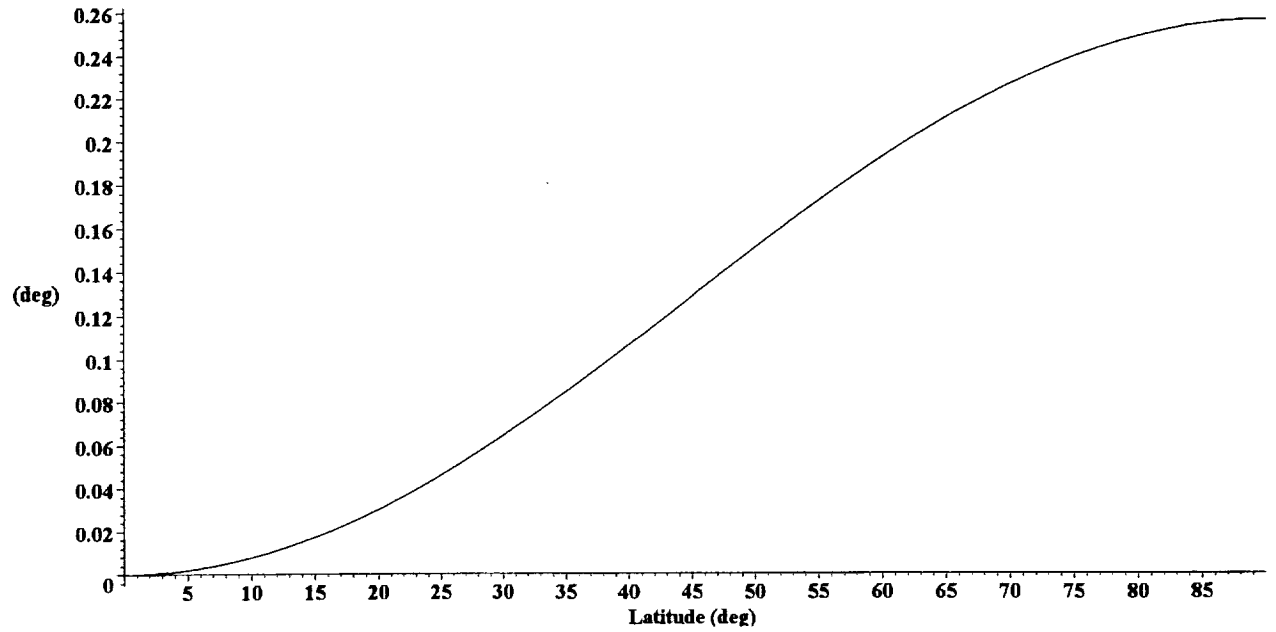

and replot this in milliradians.

Figure A2.22: Variation of the nadir angle at the earth's surface

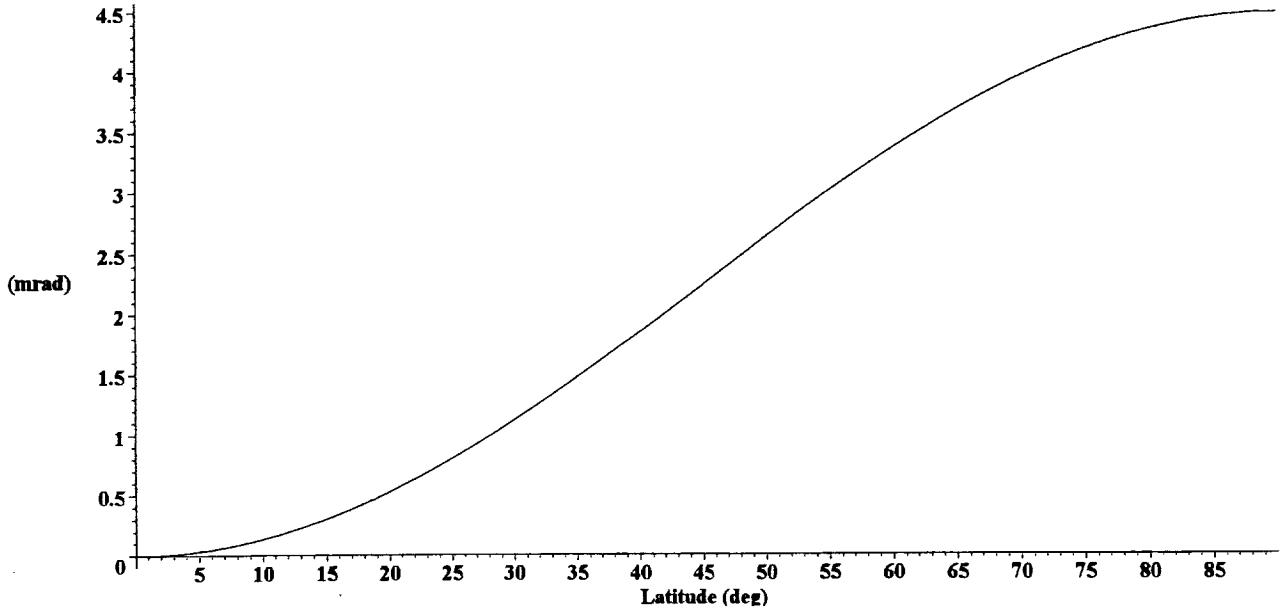

We can also determine the nadir angle at a given target altitude. The following plot is for a latitude of 45 deg.

Figure A2.23: Nadir angle at a given altitude above the surface

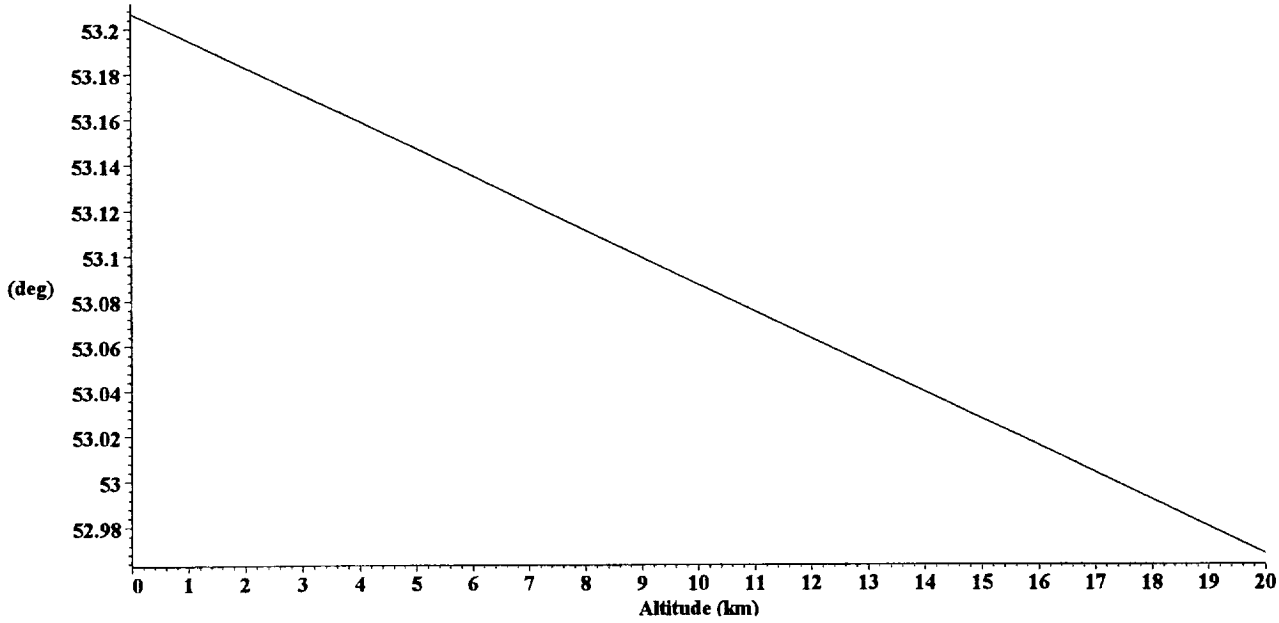

We can combine the altitude and latitude dependencies of the nadir angle at the target:

Figure A2.24: Variation of nadir angle with altitude and latitude

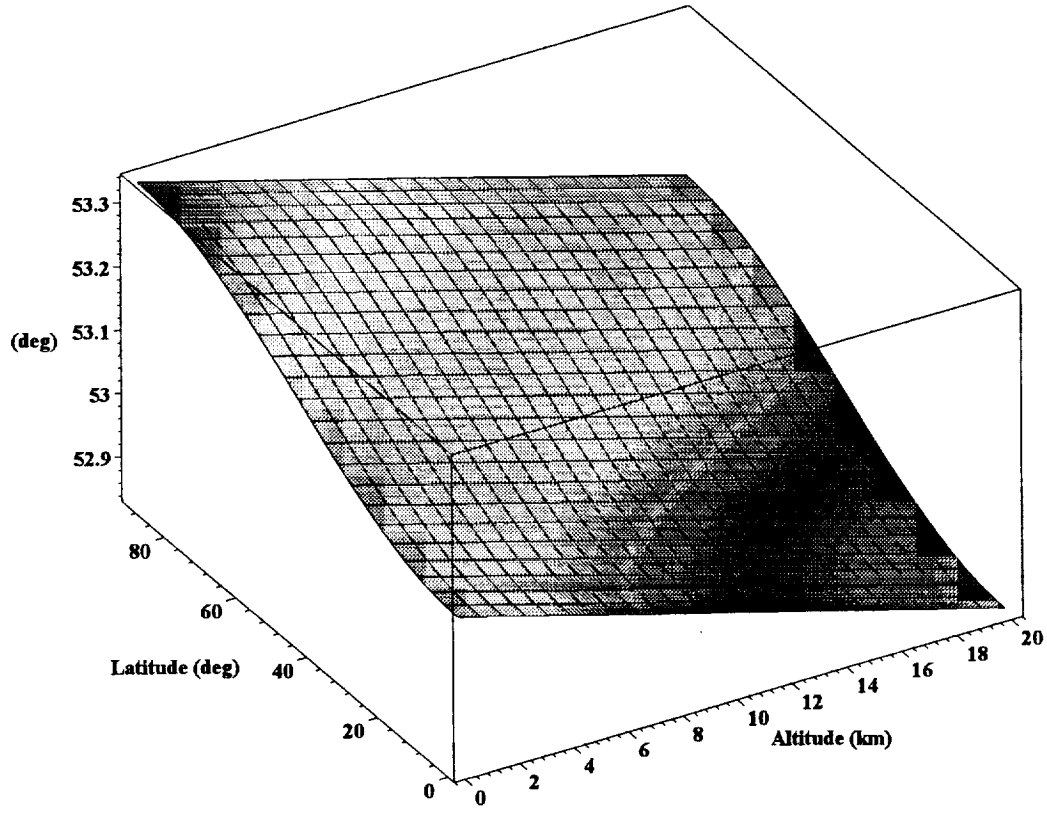

The range from the lidar to a target at an altitude, alt is given by:

Range := **proc**(*orbh*, *nadir*, *alt*, *lat*)

sqrt(

(*orbh* + *a*)^2 + (Rlat(*lat*) + *alt*)^2 − 2*(*orbh* + *a*)*(Rlat(*lat*) + *alt*)*cos(nadalt(*orbh*, *nadir*, *alt*, *lat*) − *nadir*))

end

We can plot this as a function of latitude and target altitude:

Figure A2.25: Range to altitude (wrt WGS84)

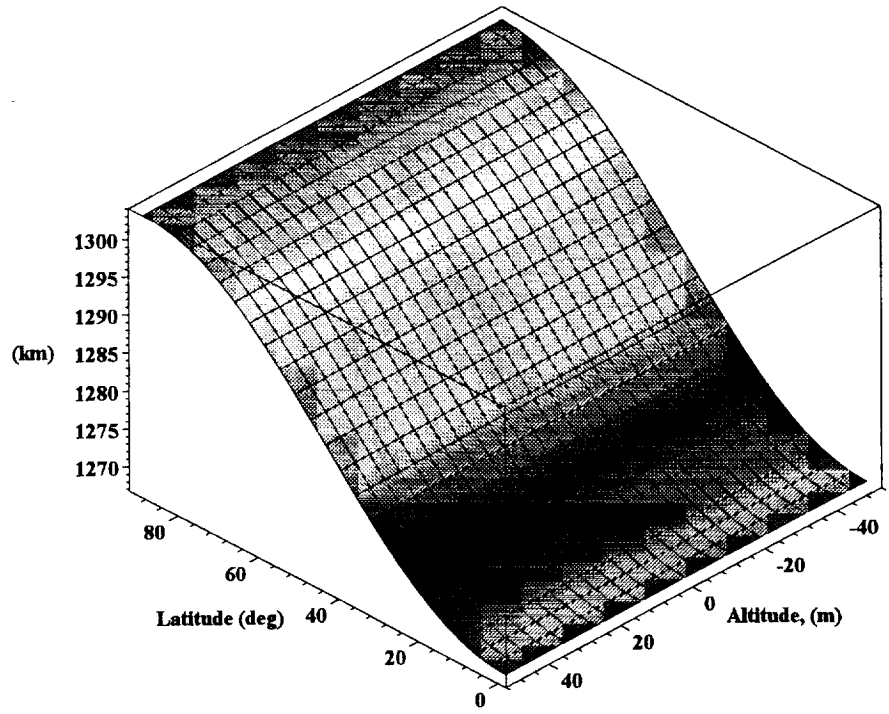

For the orbit conditions documented ealier we can determine the sensitivity of the range to a given altitude by plotting the range as a function of altitude. For the plot shown, a latitude of 45 degrees was used as this is the latitude at which the range is most sensitive to changes in latitude.

Figure A2.26: Error in range to altitude wrt WGS84

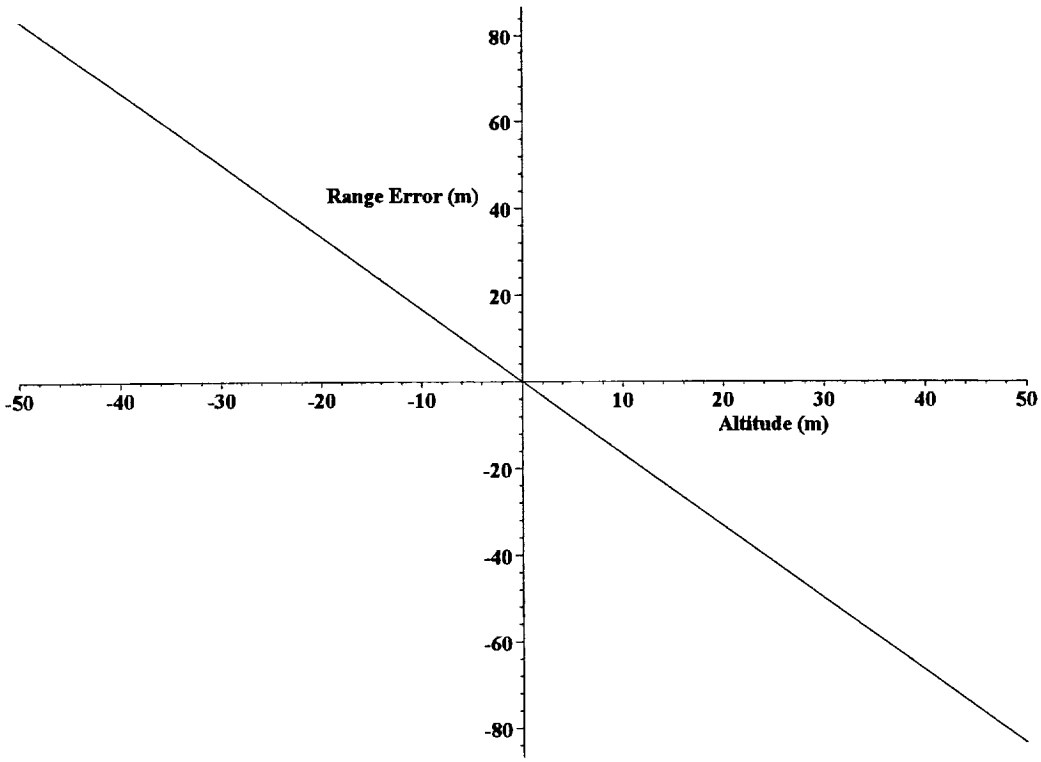

Similarly we can plot the range dependence on variations in orbit height:

Figure A2.27: Error in range (m)

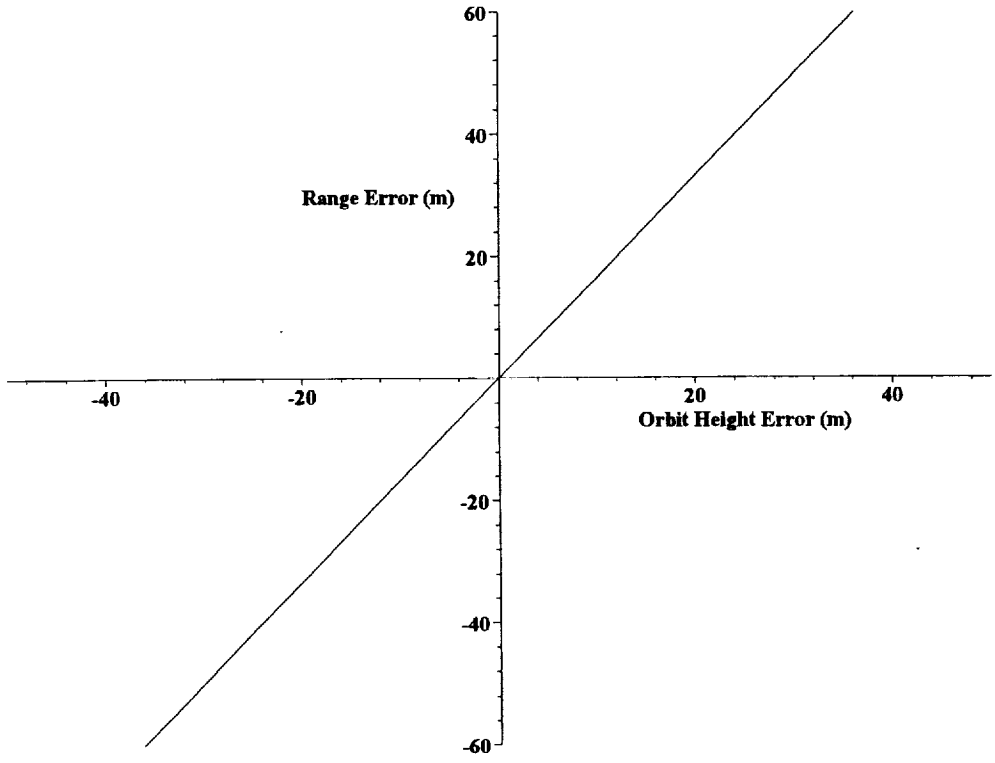

on variations in nadir angle:

Figure A2.28: Error in range (m)

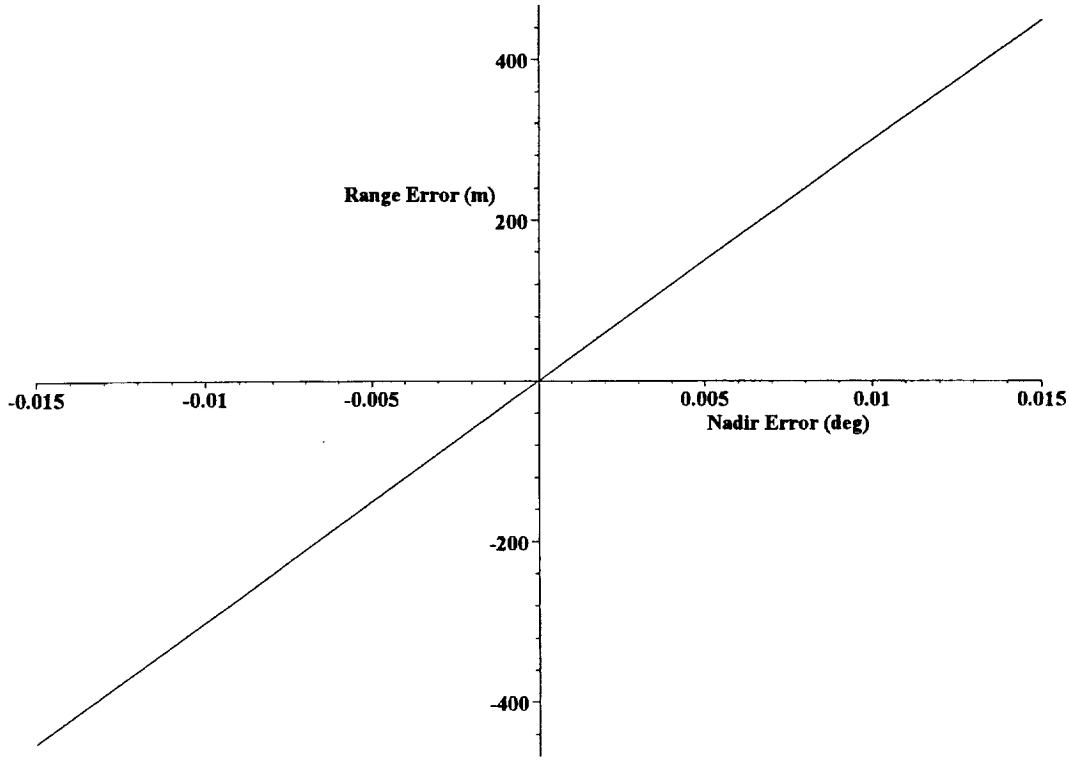

and finally on variations in latitude:

Figure A2.29: Error in range (m)

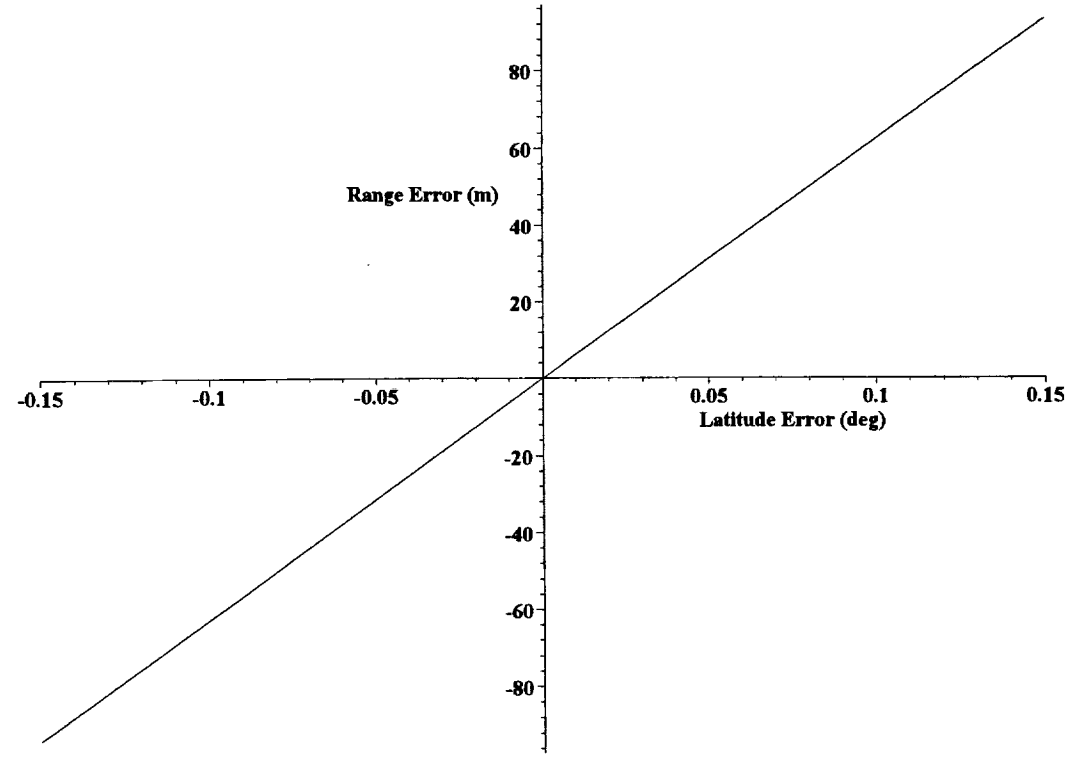

To determine the range from the lidar to a target we measure the round trip time of flight and calculate the range.

t_rtrp := **proc**(*orbh*, *nadir*, *alt*, *lat*) 2*Range(*orbh*, *nadir*, *alt*, *lat*) / *v_c* **end**

Figure A2.30: Round trip time variation with nadir angle

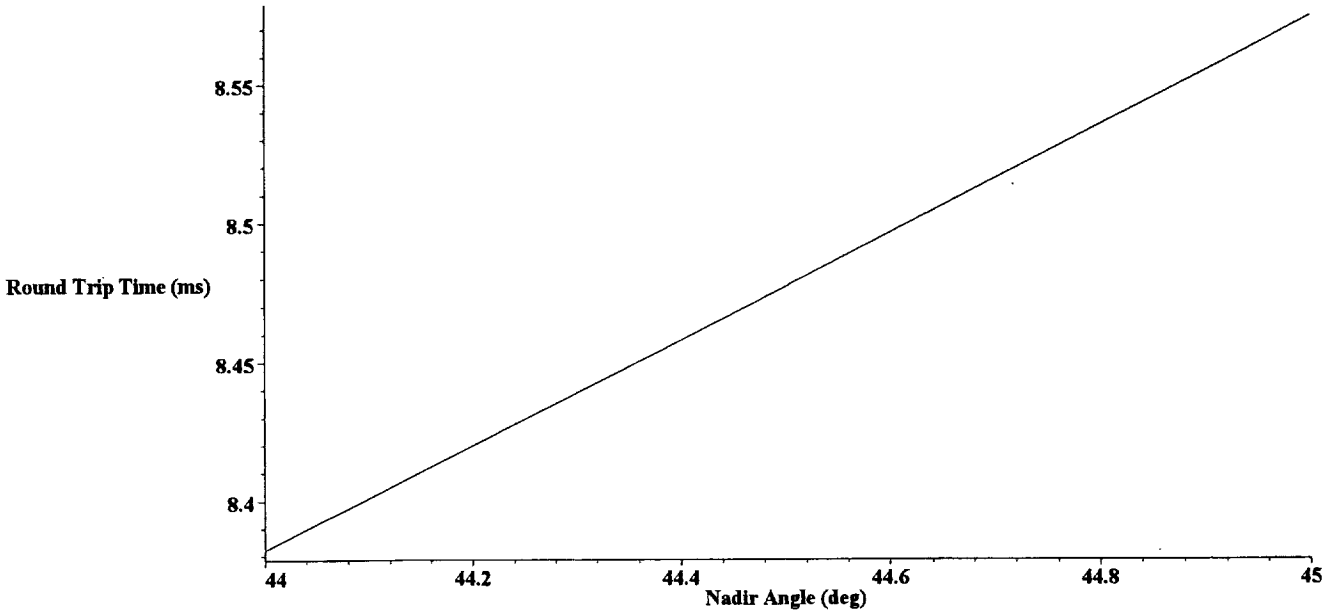

We can plot the round trip time as a function of orbit height and nadir angle to determine the range of round trip times we can anticipate seeing:

Figure A2.31: Lidar Signal Round Trip Time

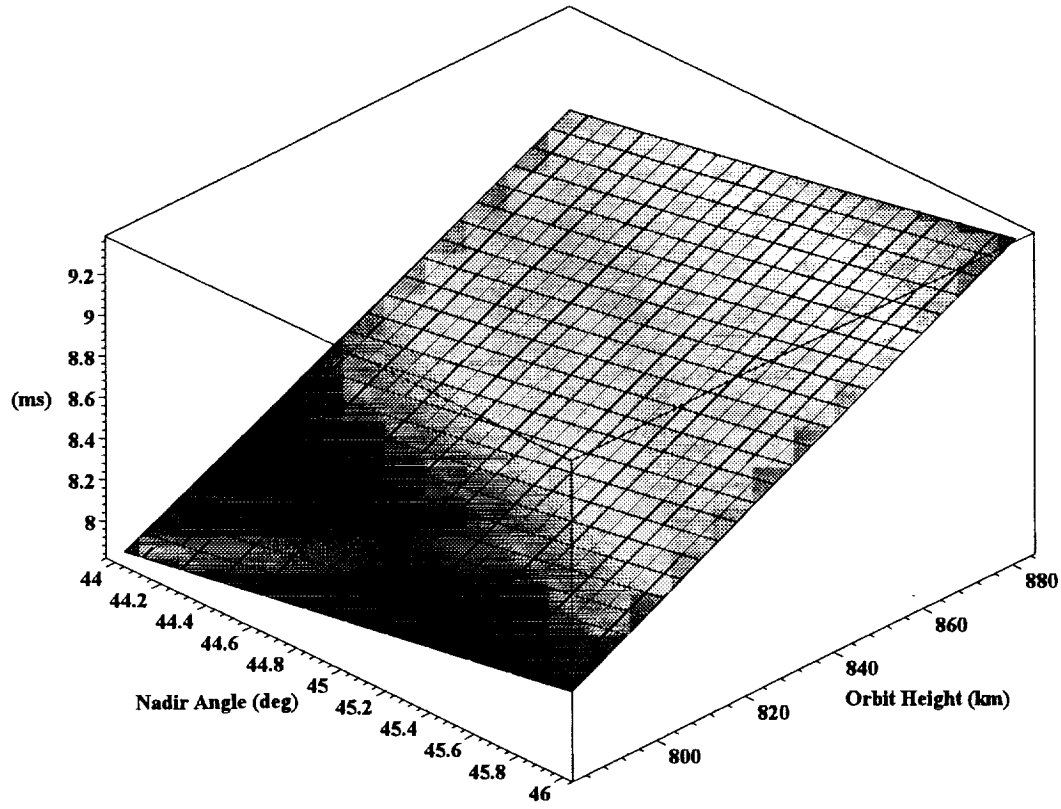

During the round trip time the spacecraft continues to rotate about the planet. This rotation results in a tipping of the nadir angle during the round trip time that translates into a misalignment angle between the transmit and receive optical paths. The round trip time depends on the nadir angle and therefore the nadir tipping angle has a dependence on nadir angle and this is shown in the following plot.

nadirtip := **proc**(*orbh*, *nadir*, *alt*, *lat*) **global** *a*; vsat(*orbh*)*t_rtrp(*orbh*, *nadir*, *alt*, *lat*) / (*orbh* + *a*) **end**

Figure A2.32: Nadir tipping angle dependence on nadir angle

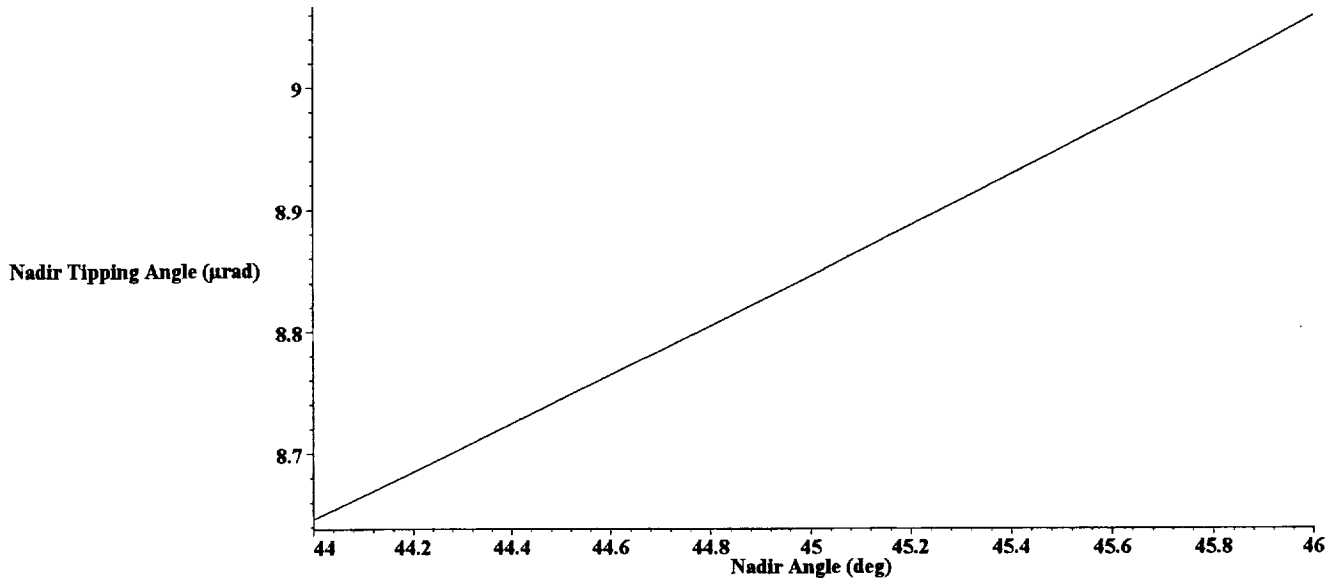

We can see that this is a weak dependence. The dependence on orbit height is much stronger as the next plot shows:

Figure A2.33: Nadir Tipping Angle

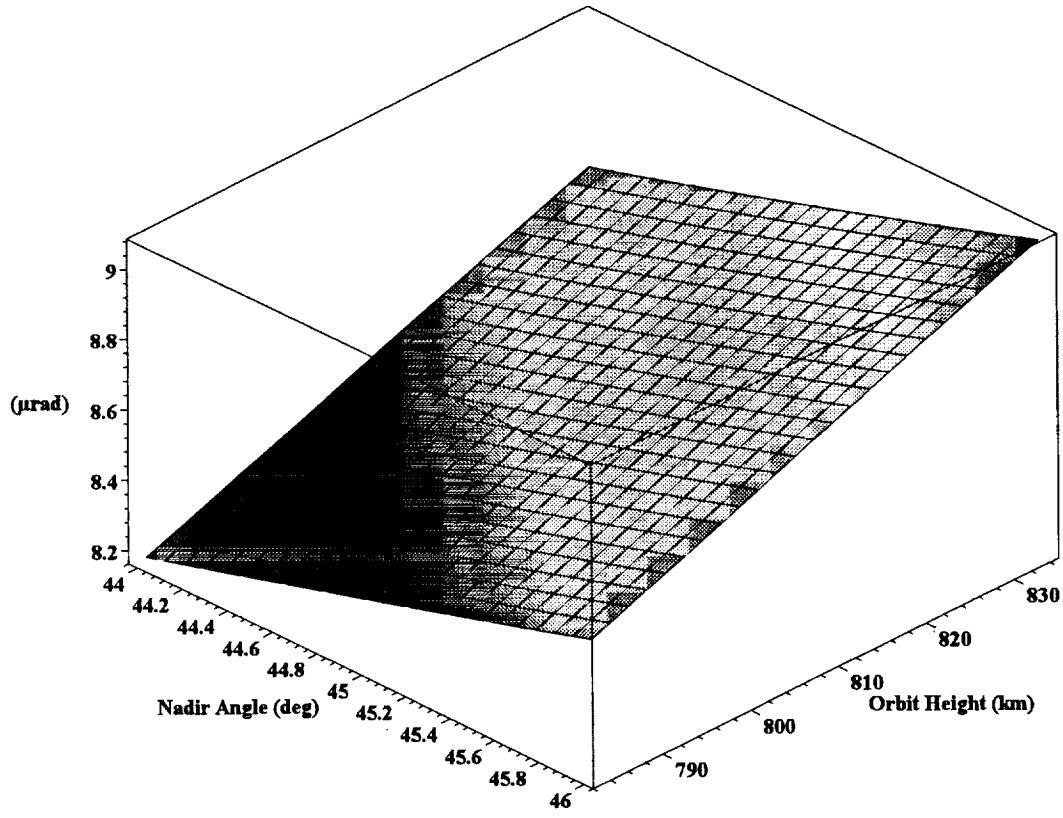

The orbital velocity, in m/s, of a satellite at the orbit height documented earlier is:

7438.059079

The line of sight velocity seen by the satellite is a function of the target, satellite and earth rotation velocities.

```
los_vel := proc(nadir, az, alt, inc, orbh, lat, trgta, vtrgtv, htrgtv, hsatv, vsatv)
    htrgtv*cos(az + orblat(lat, inc) - trgta)*sin(nadalt(orbh, nadir, alt, lat))
     + vtrgtv*cos(nadalt(orbh, nadir, alt, lat)) + hsatv*cos(az)*sin(nadir) + vsatv*cos(nadir)
     + Vlat(lat)*sin(orblat(lat, inc) + az)*sin(nadalt(orbh, nadir, alt, lat))
end
```

where az, trgta, vtrgtv, htrgtv, hsatv, vsatv are the azimuth angle of the line of sight wrt the velocity direction, the azimuthal angle the target velocity makes with respect to the local meridian, the target vertical and horizontal velocities and the satellite horizontal and target velocities respectively. For the orbit and lidar parameters listed at the start of this document the line of sight velocity as a function of azimuth is shown in the following figure for a lidar over the earth's equator .

Figure A2.34: LOS velocity as a function of azimuth

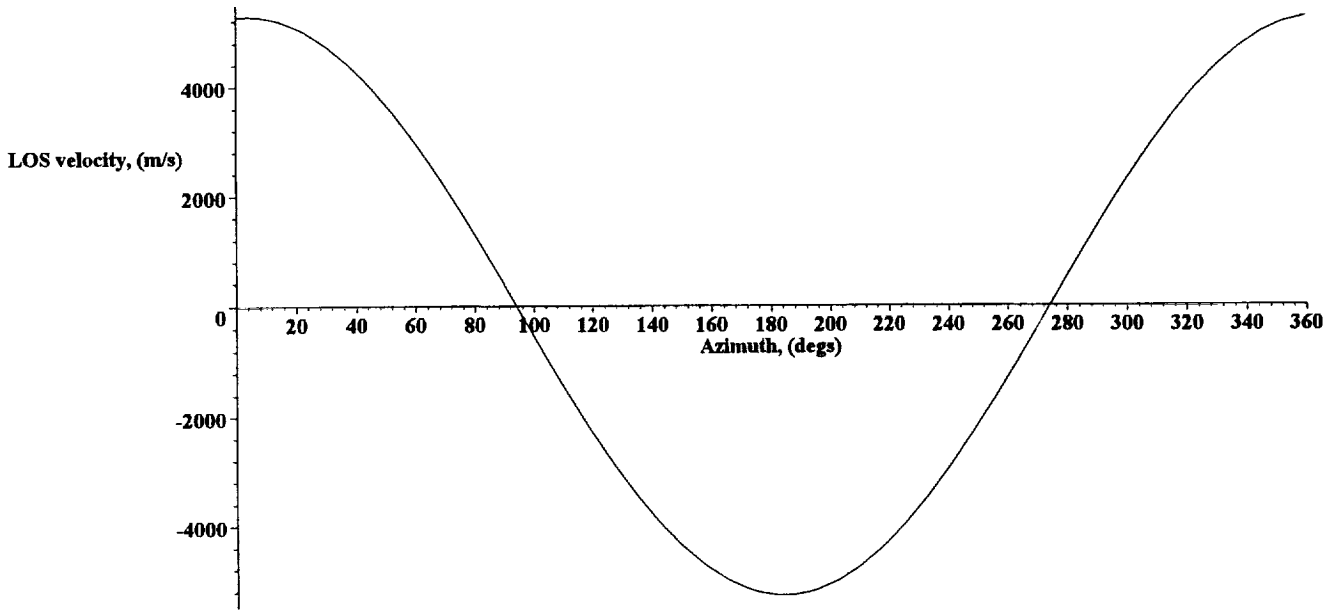

Expanding the region around the first 0 m/s point enables the gradient to be determined.

Figure A2.35: LOS velocity as a function of azimuth

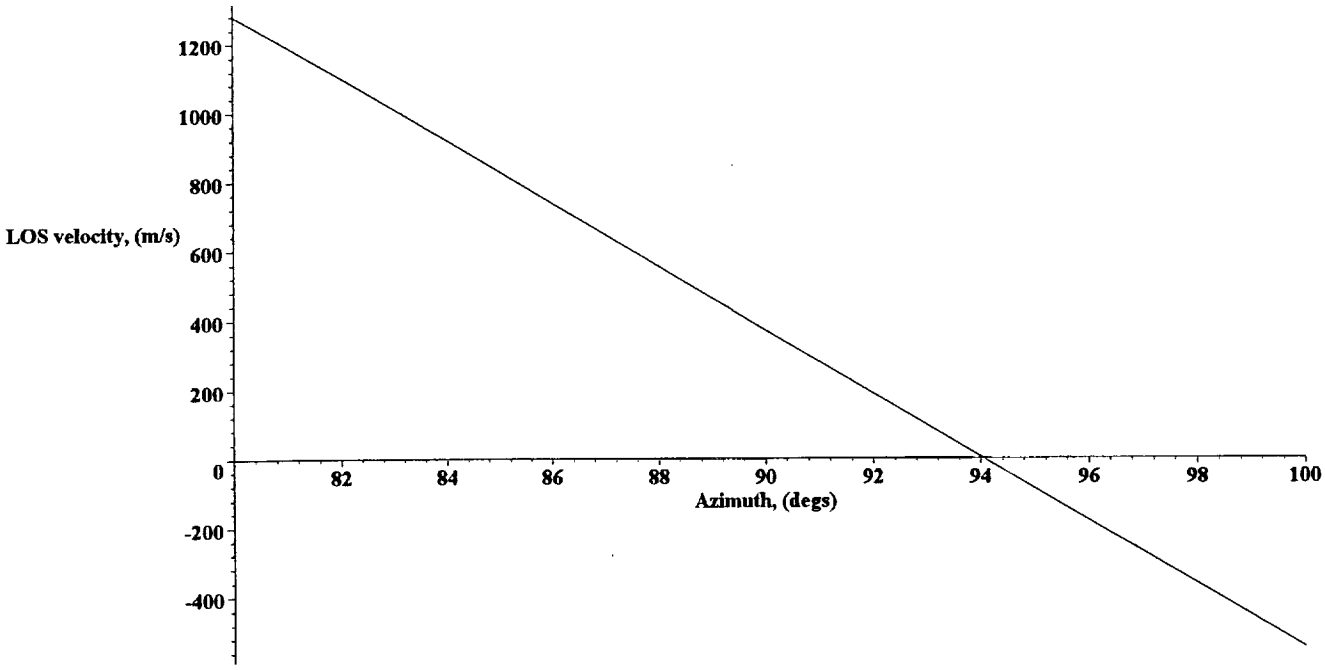

Alternatively plotting the differential of the line of sight velocity with respect to the azimuth angle enables the maximum rate of change to be determined:

Figure A2.36: Rate of change of LOS velocity as a function of azimuth

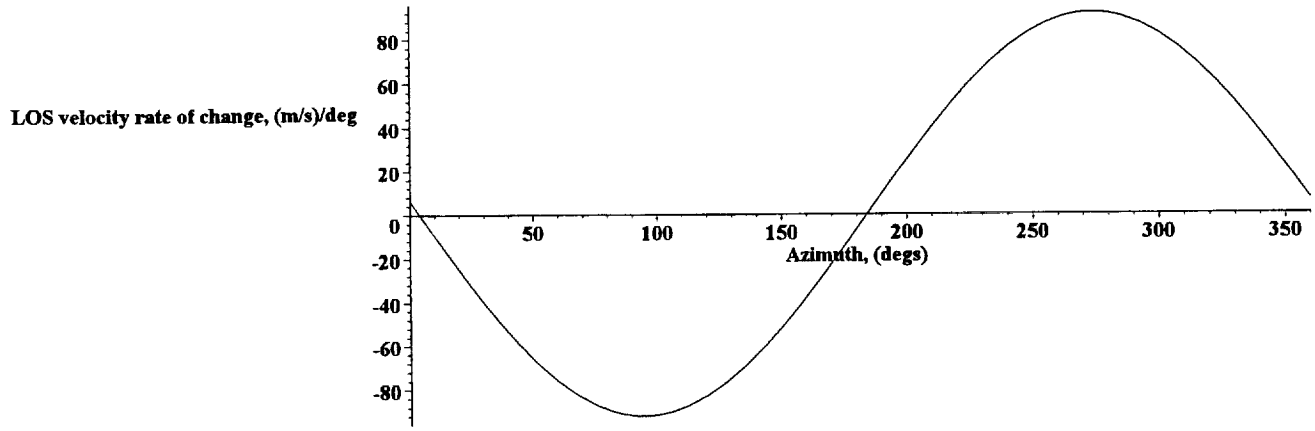

The line of sight velocity is dominated by the spacecraft velocity, if this is removed then we can see the dependence on the earth's rotational velocity:

Figure A2.37: Earth rotation component of the LOS velocity as a function of azimuth

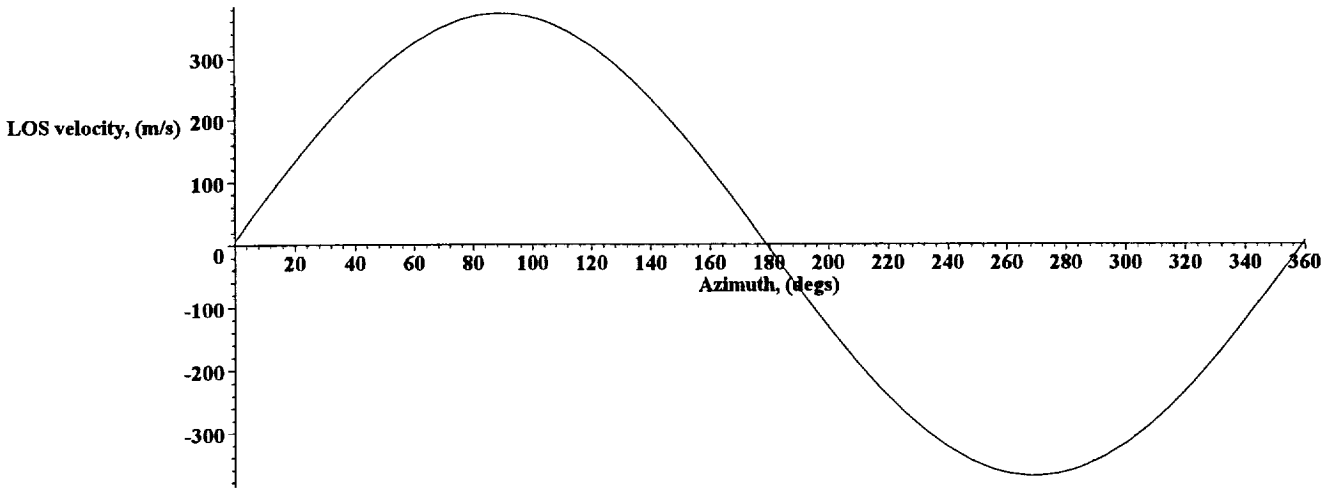

This clearly shows the much smaller magnitude of the earth's rotational contribution. Again we can determine the maximum rate of change with azimuth by plotting the differential with respect to the azimuth angle:

Figure A2.38: Rate of change of the Earth rotation component of the LOS velocity as a function of azimuth

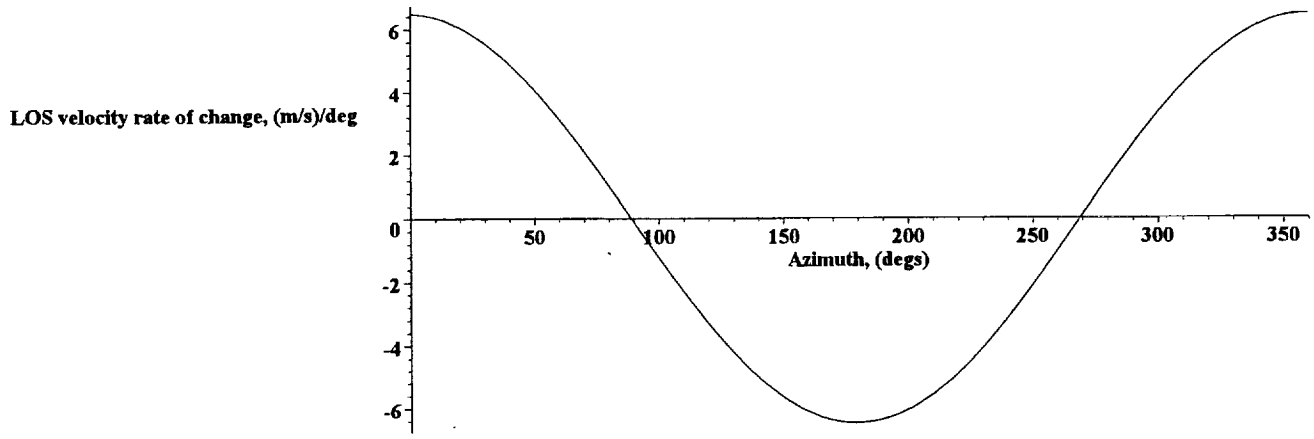

The line of sight velocity also depends on the nadir angle. The following plot shows the line of sight velocity dependence on both nadir and azimuth angle:

Figure A2.39: LOS velocity as a function of azimuth and nadir angles

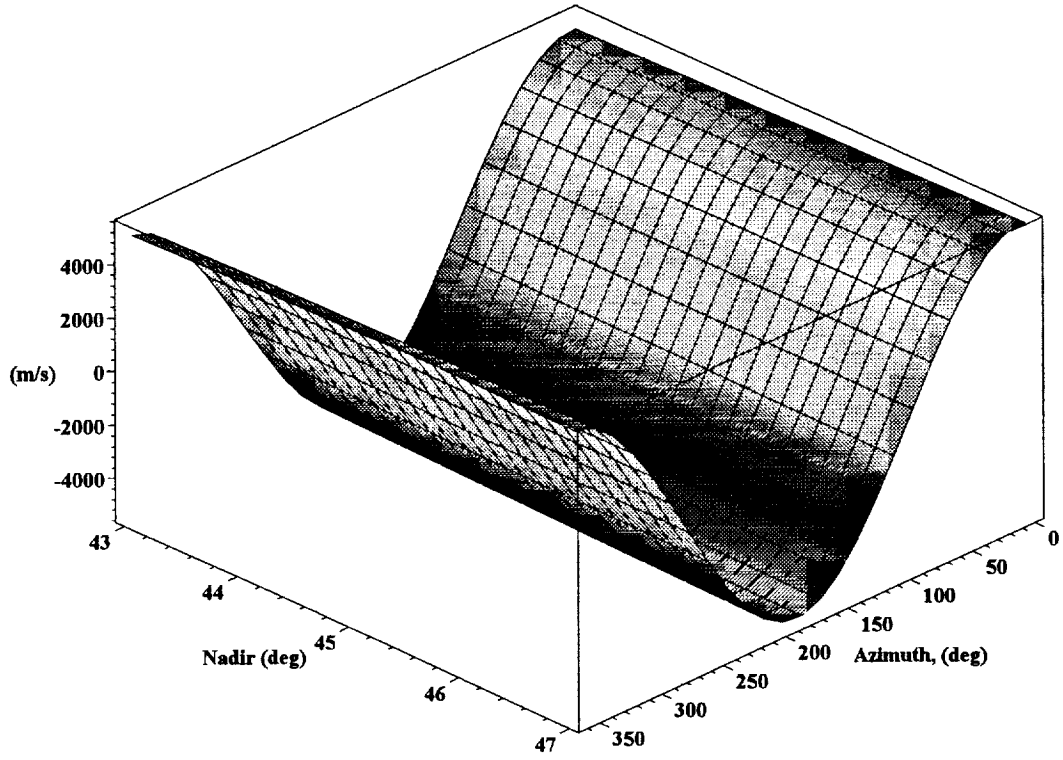

Clearly the azimuthal dependence dominates over the restricted range of nadir angles plotted. The dependence on nadir only becomes clearly visible when a much wider range of nadir angles is considered:

Figure A2.40: LOS velocity as a function of azimuth and nadir angles

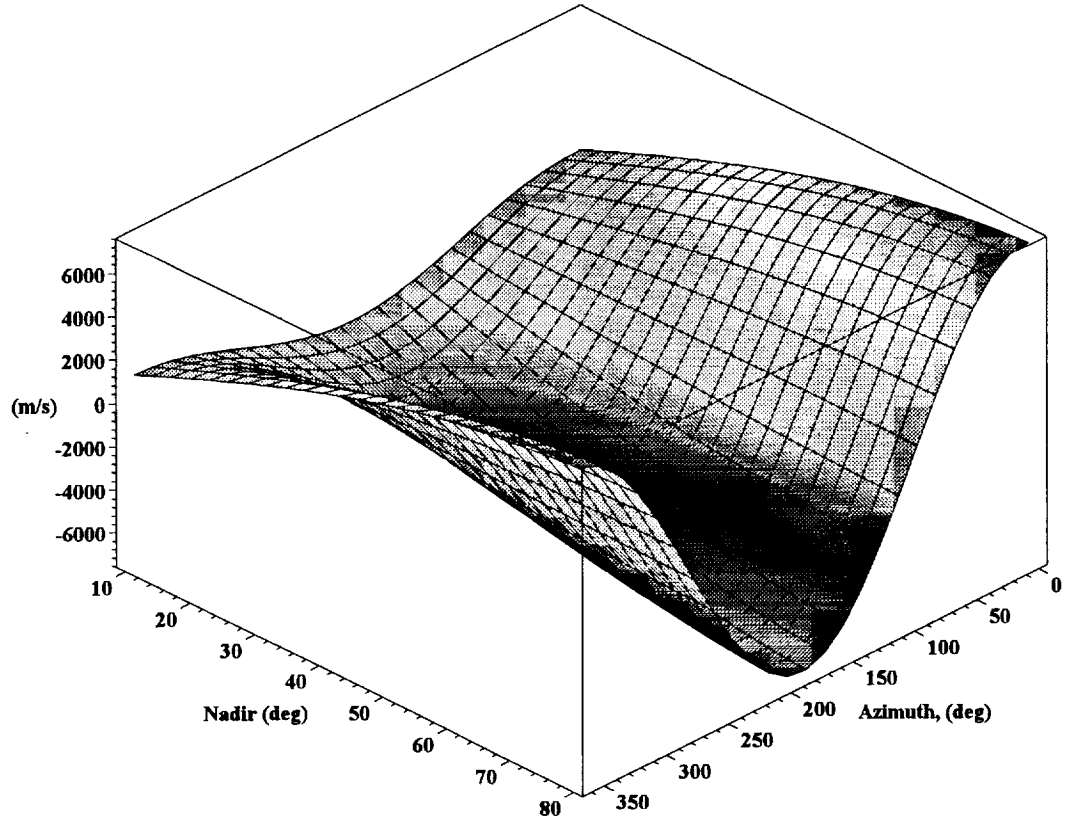

Alternatively the dependence of the line of sight velocity on nadir angle can be obtained by plotting the differential with respect to the nadir angle:

Figure A2.41: Rate of change of LOS velocity with nadir angle

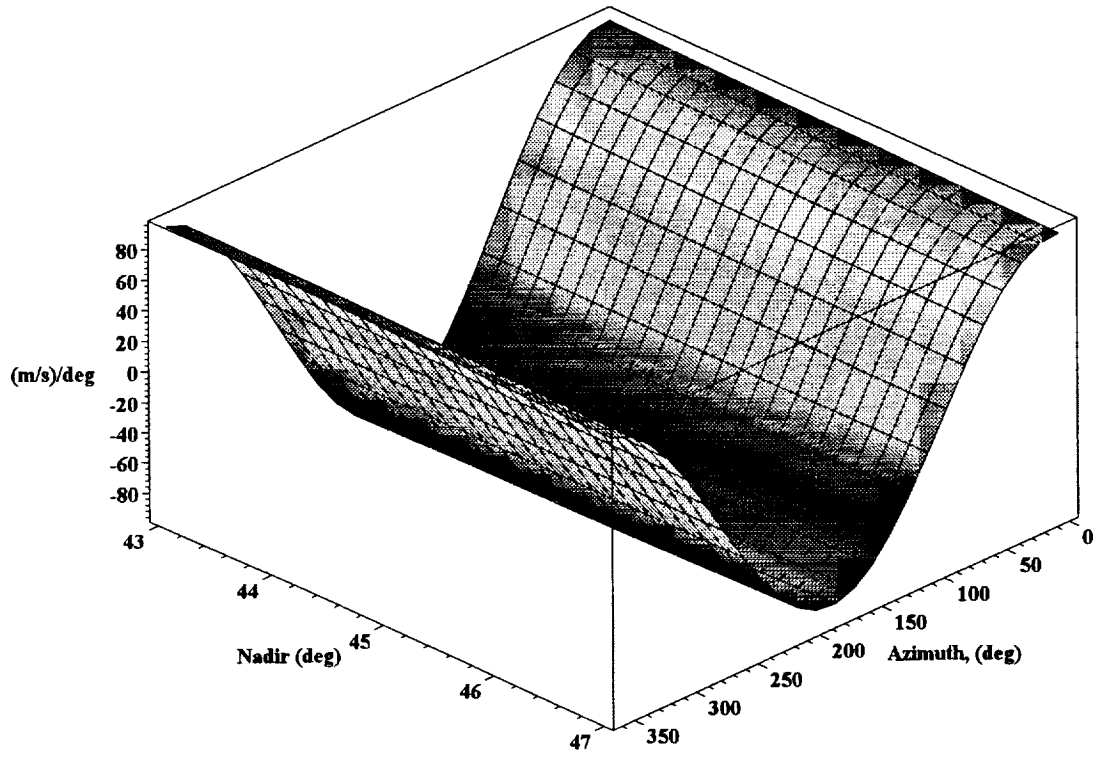

We can see that the rate of change of the line of sight velocity with nadir angle varies between about ± 90 m/s/deg depending on the azimuth angle as expected. The following plot for an azimuth angle of 0 deg clearly shows the gradient as a function of nadir angle:

Figure A2.42: Change of LOS velocity wrt the value at the nominal nadir angle

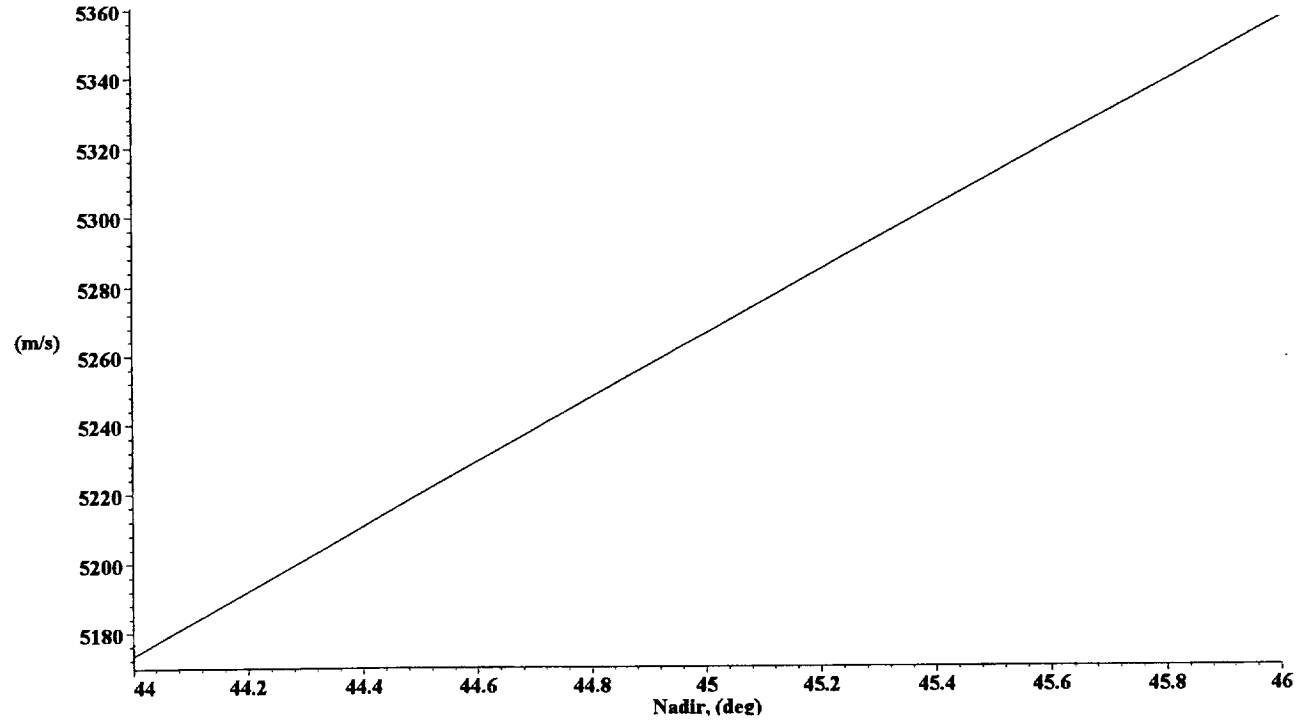

Similarly the following plot shows the variation in the LOS velocity as a function of nadir relative to the LOS velocity at the nominal nadir angle for three azimuth angles of 0 , 45 and 90 degrees respectively.

Figure A2.43: Change of LOS velocity wrt the value at the nominal nadir angle

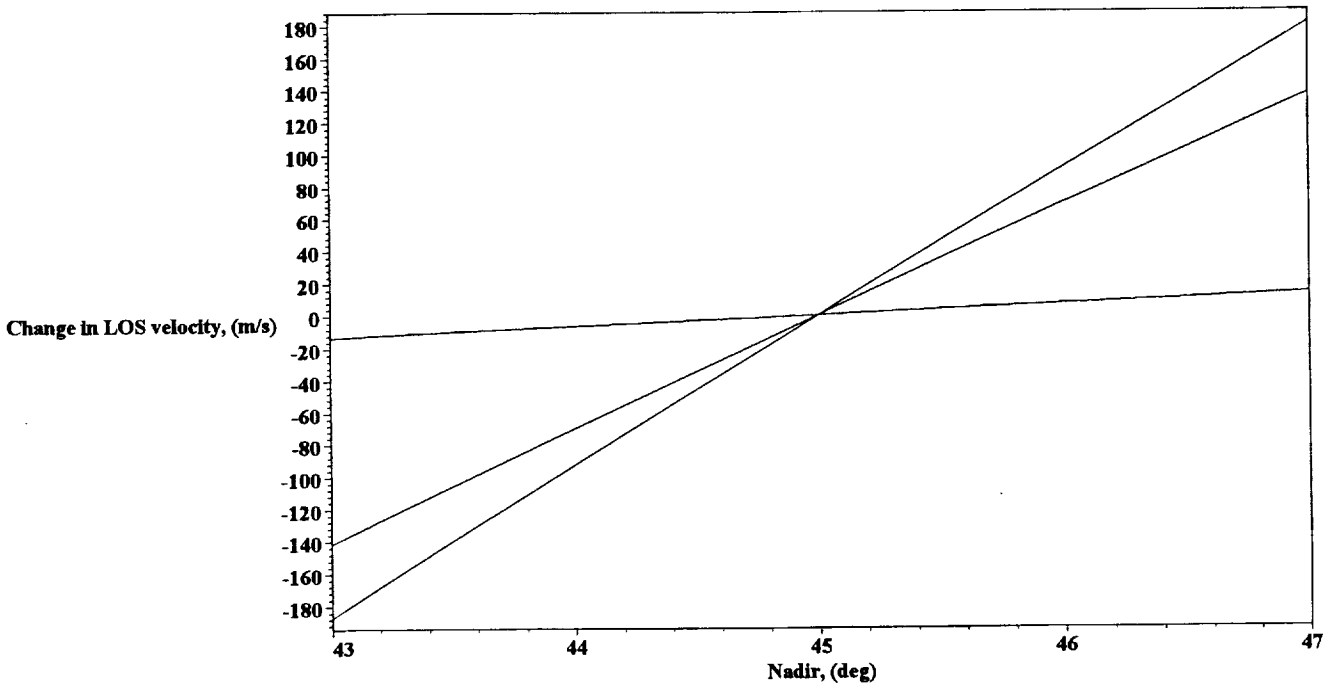

Plotting the change relative to the value at the nominal nadir angle makes the dependence on nadir and azimuth angle easier to see:

Figure A2.44: Change of LOS velocity wrt to the value at the nominal nadir angle

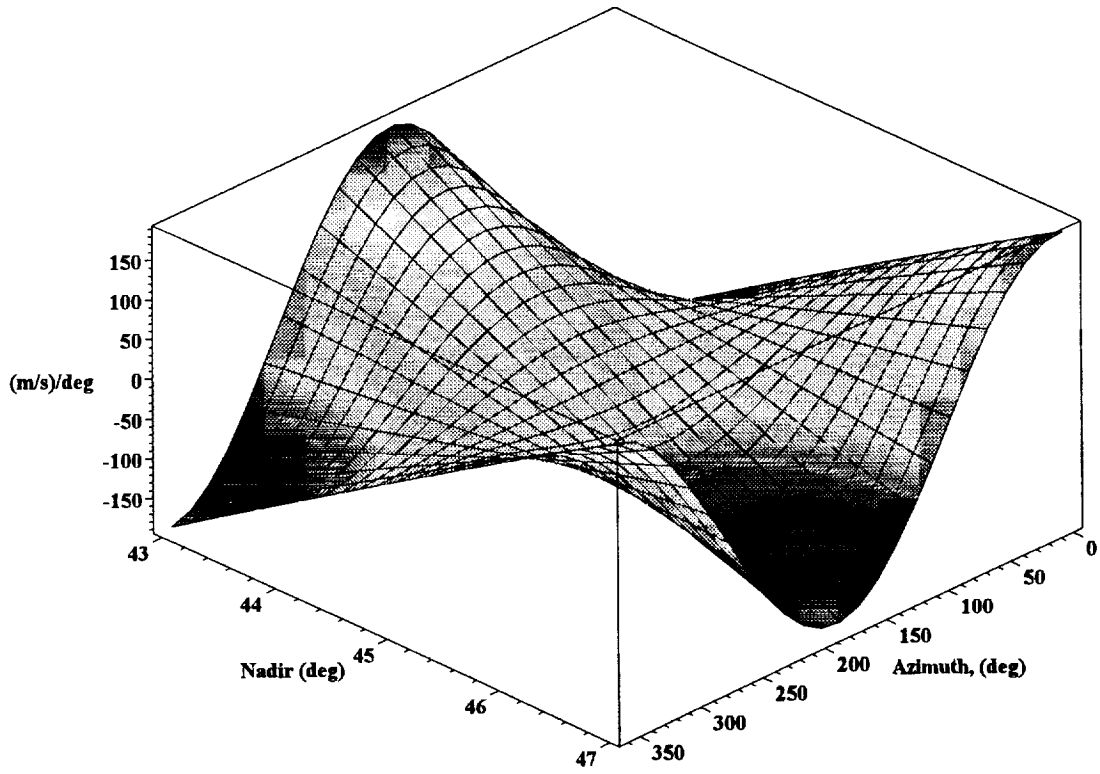

Finally, as a consistency check if we plot the differential of Figure A2.44 with respect to the nadir angle we should get back to Figure A2.41.

Figure A2.45: Rate of change of LOS velocity with nadir angle

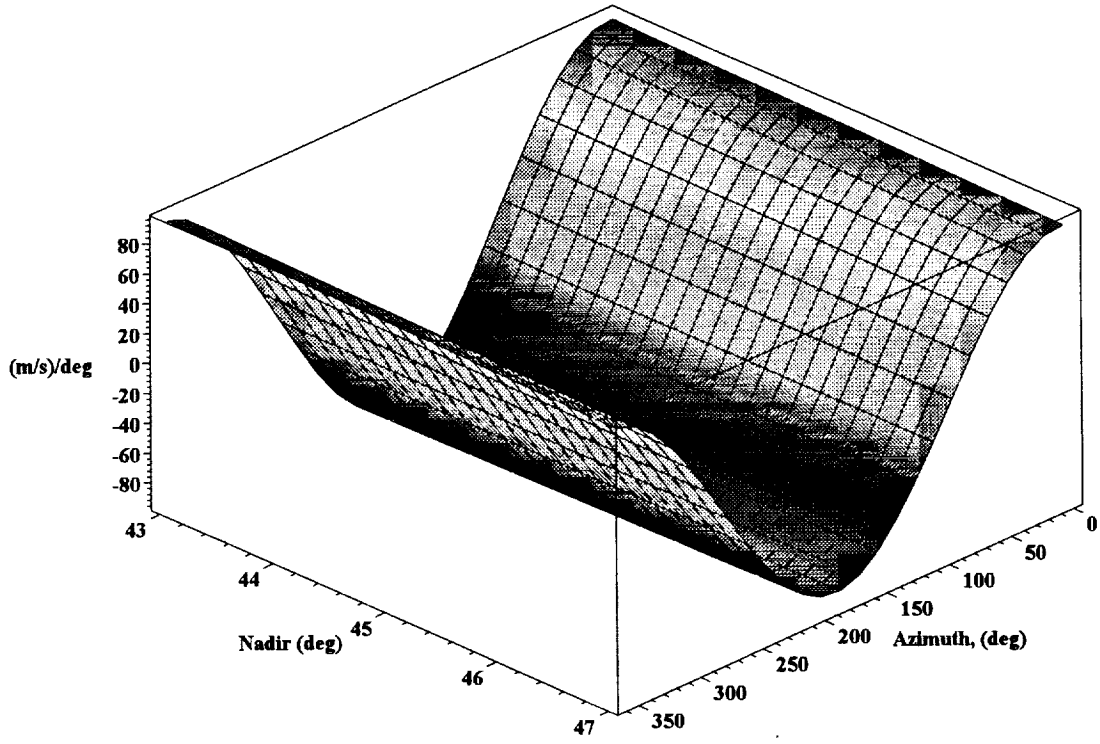

We can find the dependence on latitude by subtracting the value at the equator from the value at some other latitude.

Figure A2.46: Relative change of LOS velocity as a function of latitude

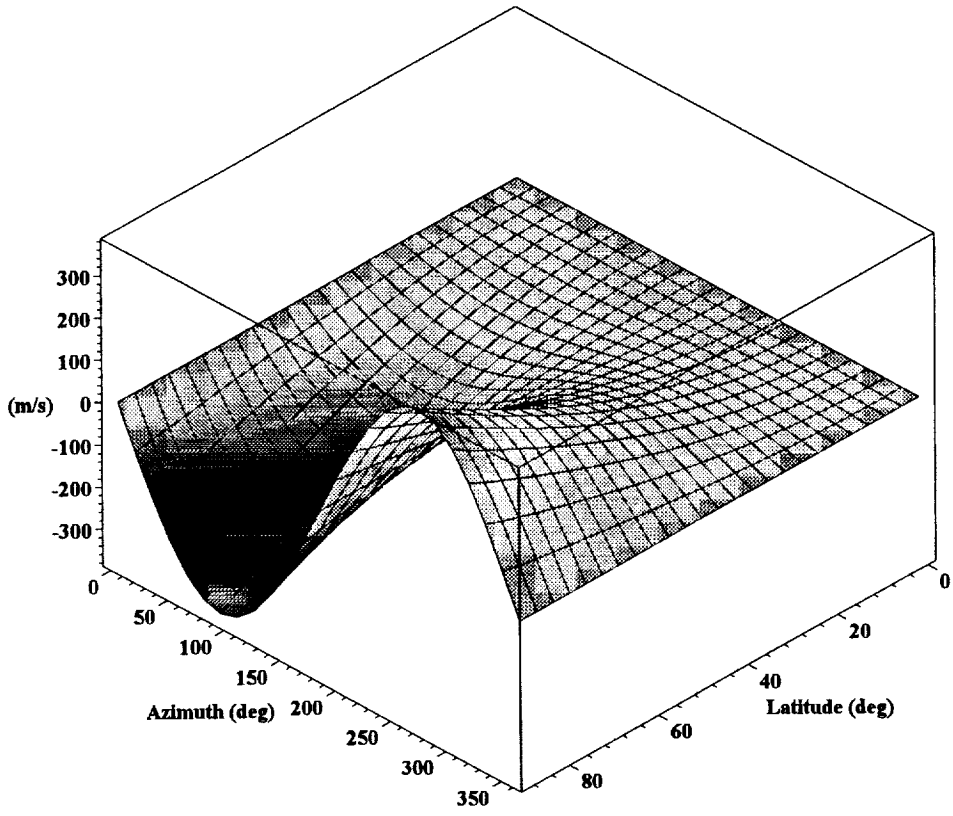

What this figure shows is that as the instrument moves to higher or lower latitudes wrt the equator the component of the line of sight velocity due to the earth's rotation at a given azimuth changes. This occurs because the angle the orbit makes to the local meridian changes as a function of latitude. Plotting the diferential of Figure A2.46 with respect to latitude enables the increase in slope to be determined.

Figure A2.47: Rate of change of LOS velocity as a function of latitude

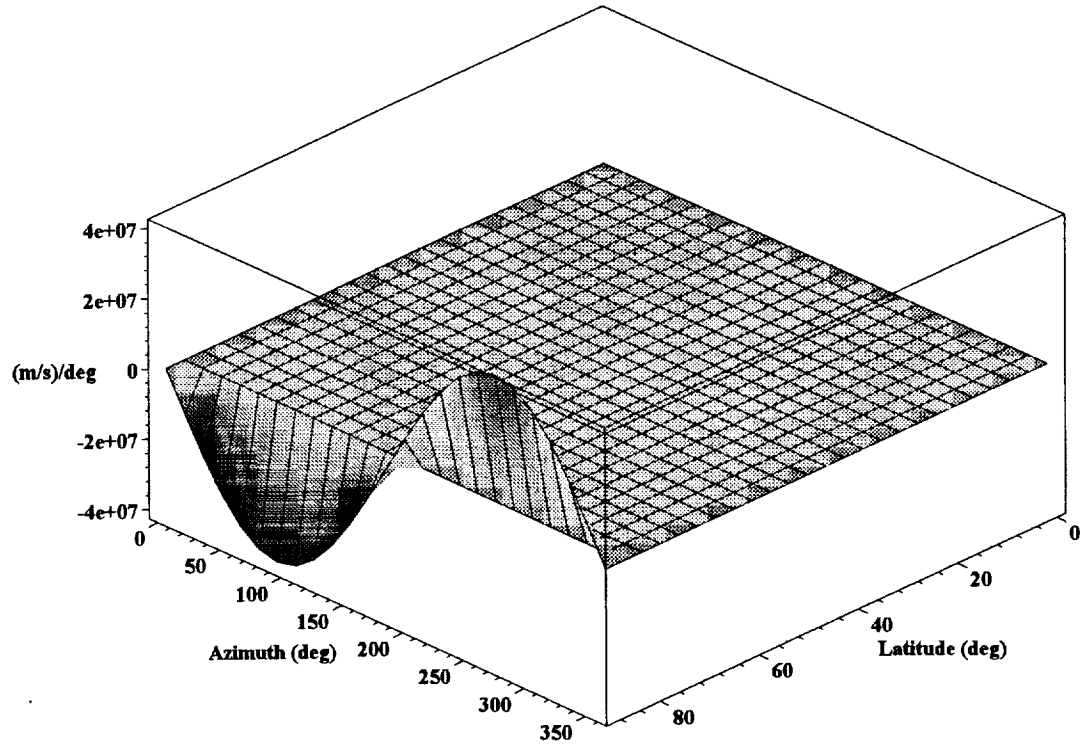

Figure A2.47 clearly show the rapid increase in the sensitivity to latitude at the highest latitudes. The plot above clearly shows the difficulty the numeric routines have near the maximum latitude where the rate of change of line of sight velocity with latitude approaches ± infinity depending on the azimuth angle. We can replot this on a logarithmic scale, using the absolute value of the slope, to get a clearer view of the rate of change and also limit the plot to a latitude slightly below the maximum value. The following plot is for a maximum latitude of 0.001 deg below the true maximum.

Figure A2.48: Rate of change of LOS velocity as a function of latitude (log z-axis)

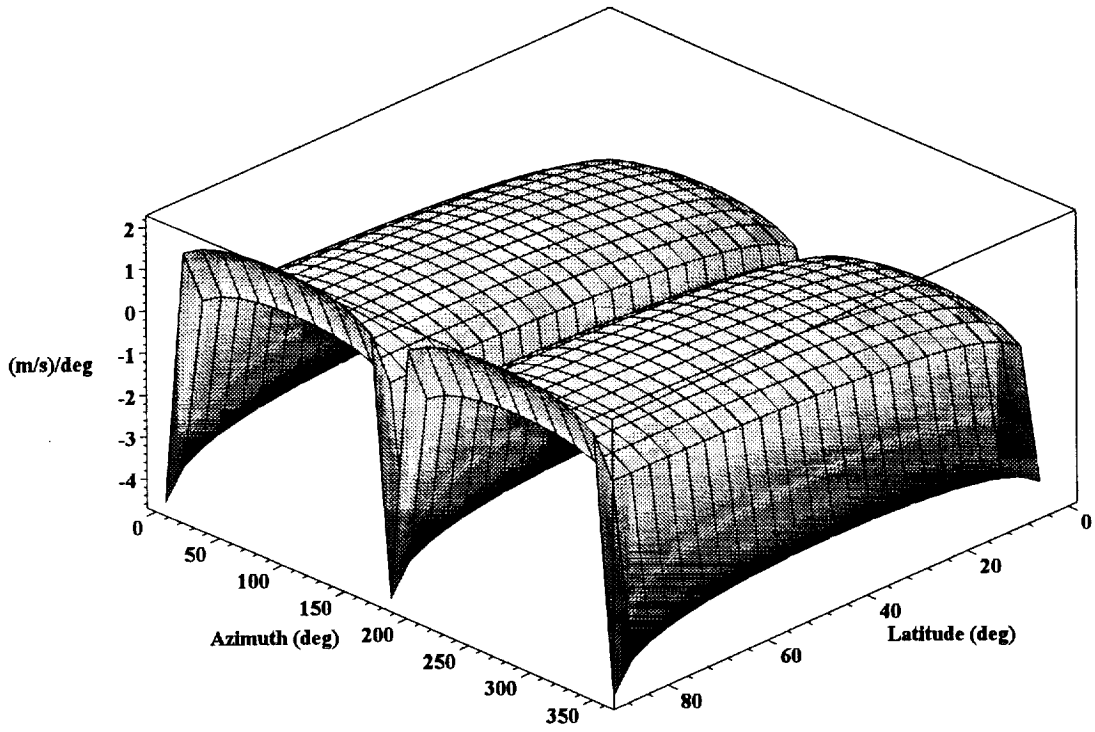

Finally we can plot just the higher latitude portion of this plot:

Figure A2.49: Rate of change of LOS velocity as a function of latitude (log z-axis)

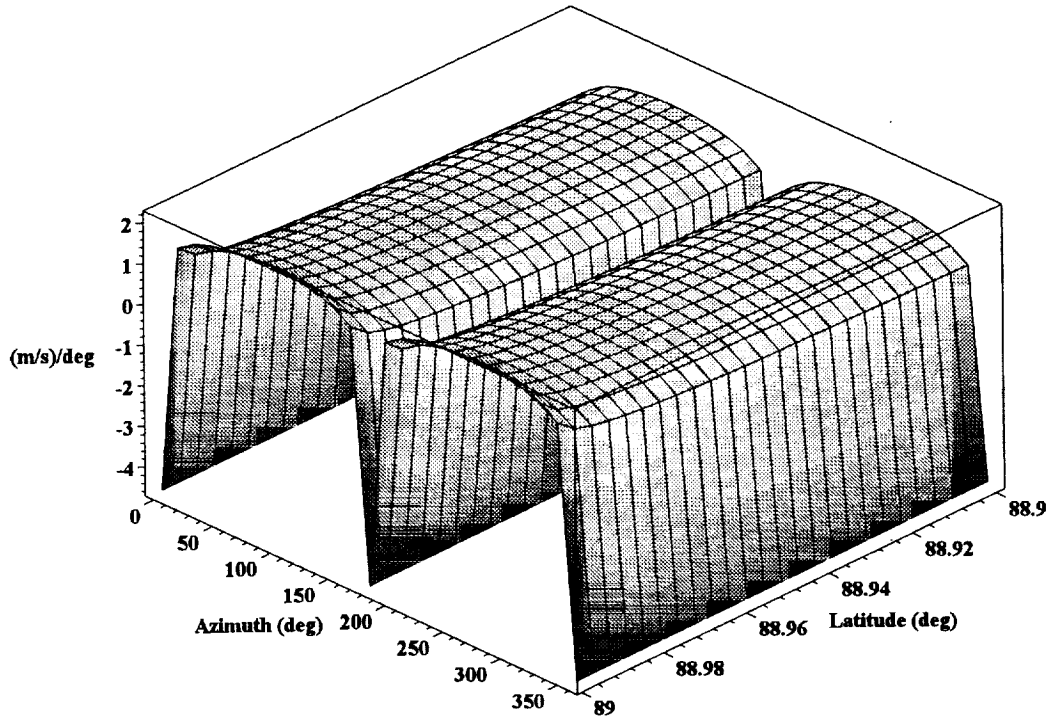

The dependence of the line of sight velocity on orbit inclination is shown below:

Figure A2.50: LOS velocity as a function of orbit inclination

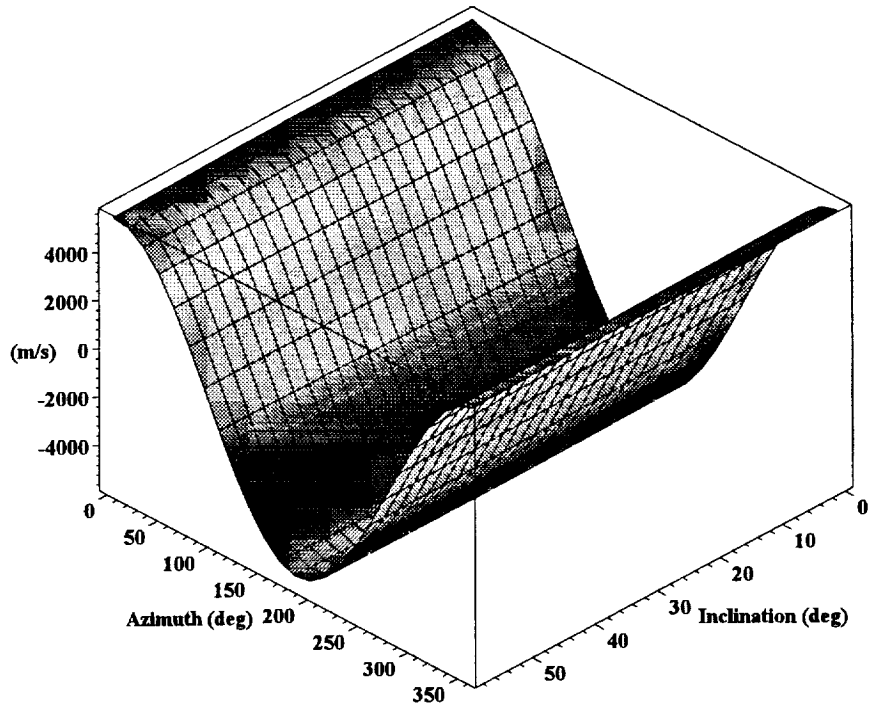

The dependence on azimuth angle is clearly dominant again and we can plot the differential with respect to the inclination angle to more clearly show the dependence on inclination angle.

Figure A2.51: Rate of change of LOS velocity with orbit inclination

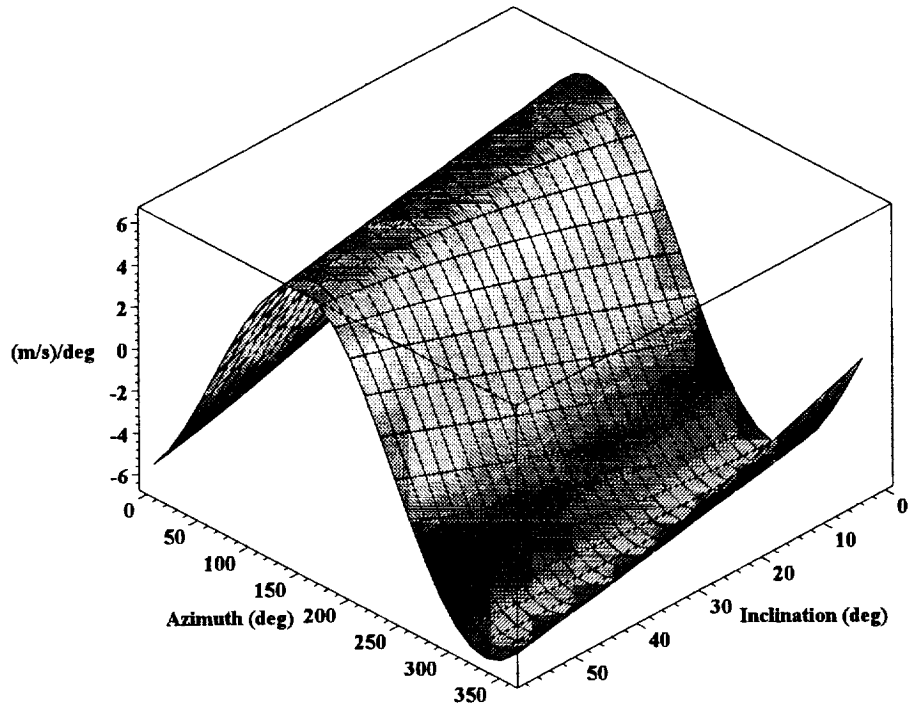

Figure A2.8 showed the satellite velocity as a function of orbit height. The line of sight velocity dependence on orbit height for an azimuth angle of 0 deg will simply be a component of this that depends on the nadir angle. Although the line of sight velocity component contains a contribution from the earth's rotational velocity this is so much smaller than the satellite velocity that it will not be visible in the plot.

Figure A2.52: LOS velocity as a function of orbit height

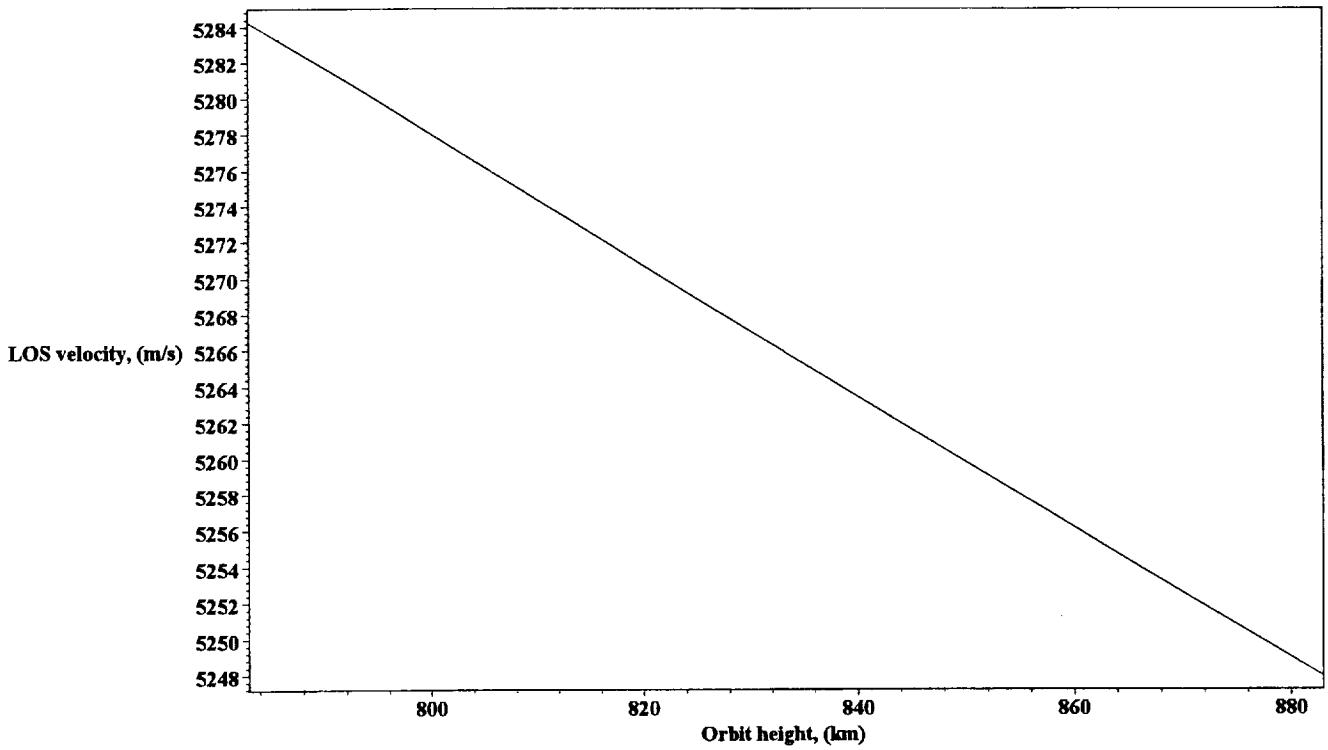

Plotting the differential with respect to the orbit height permits the sensitivity to be easily determined.

Figure A2.53: Rate of change of LOS velocity with orbit height

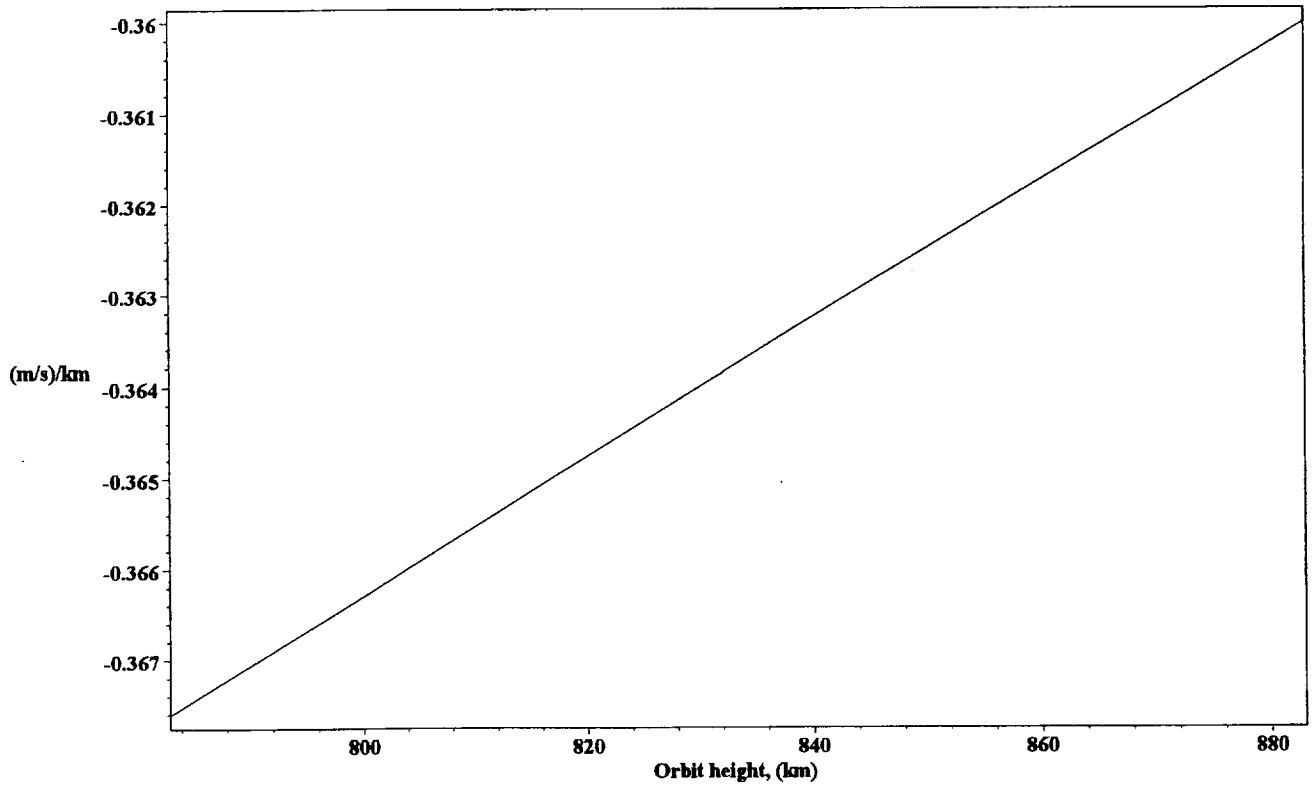

Figure A2.53 assumes an azimuth angle of 0 deg which corresponds to maximising the magnitude of the line of sight component of the spacecraft velocity. At other azimuth angles the dependence will be weaker and this is shown in the following 3D plot.

Figure A2.54: Rate of change of LOS velocity with orbit height

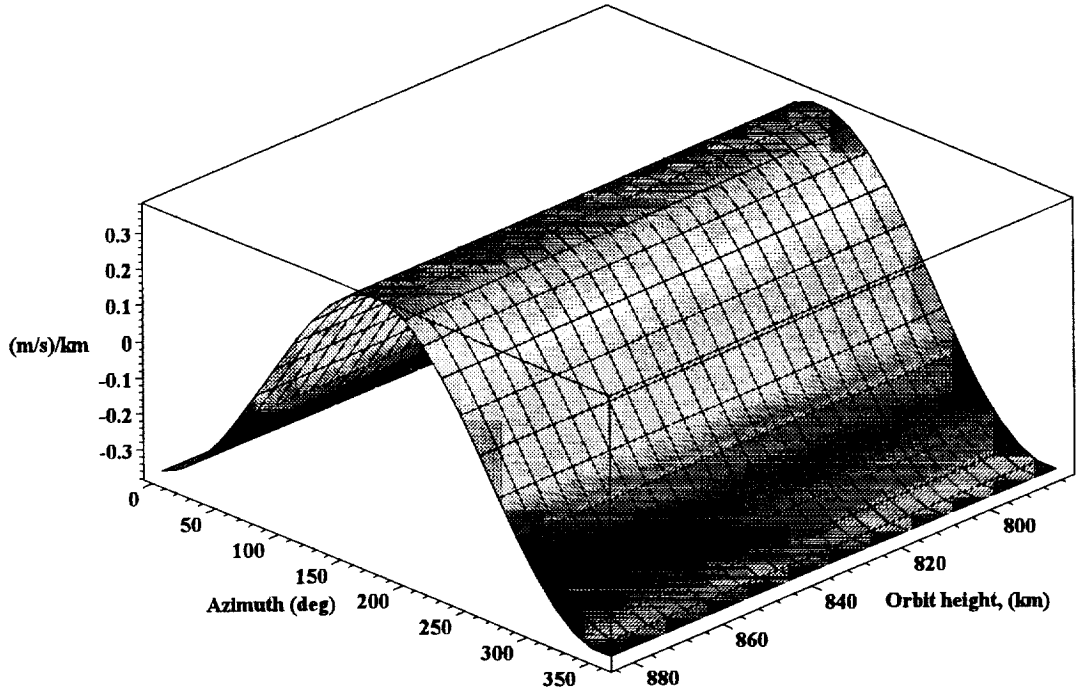

The nadir angle at the target varies as a function of the altitude of the target and so the line of sight velocity has a weak dependence on the target latitude. This is shown below for an azimuth angle of 0 degrees.

Figure A2.55: Rate of change of LOS velocity with target altitude

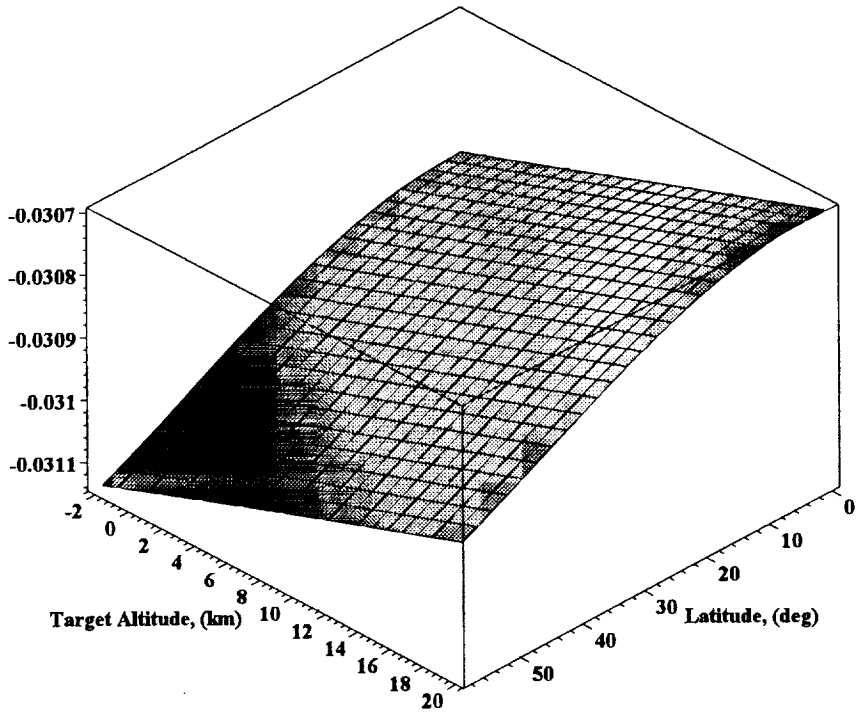

For a fixed azimuth angle the line of sight velocity should be simply proportional to the satellite horizontal and vertical velocities with the constant of proportionality being simply the sine and cosine of the nadir angle respectively. Plotting the differential of the line of sight velocity with respect to the satellite velocity should therefore obtain sin(nadir) and cos(nadir) for the horizontal and vertical velocities respectively.

Figure A2.56: Rate of change of LOS velocity with satellite horizontal velocity

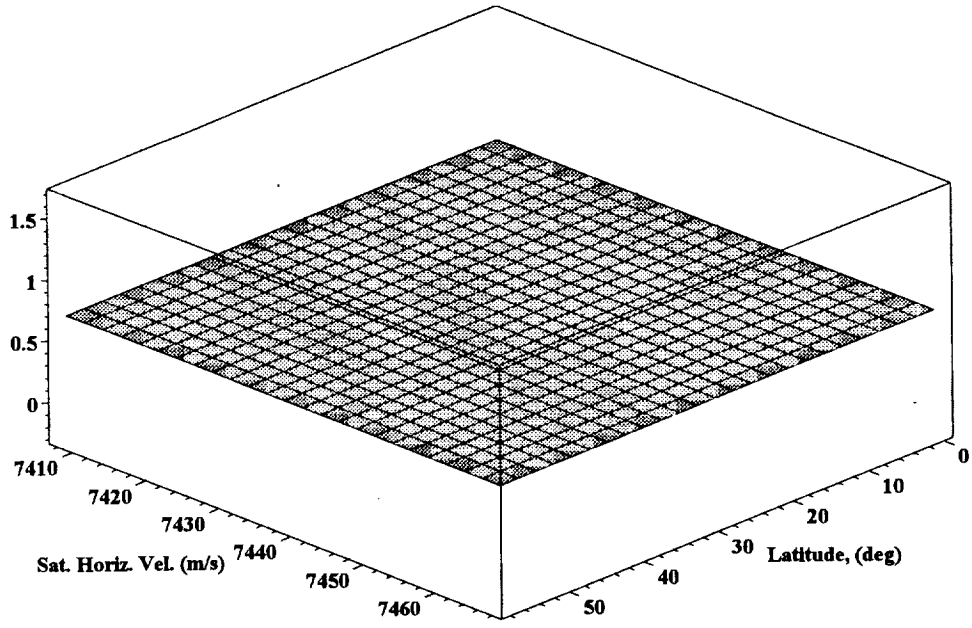

Figure A2.57 Rate of change of LOS velocity with satellite vertical velocity

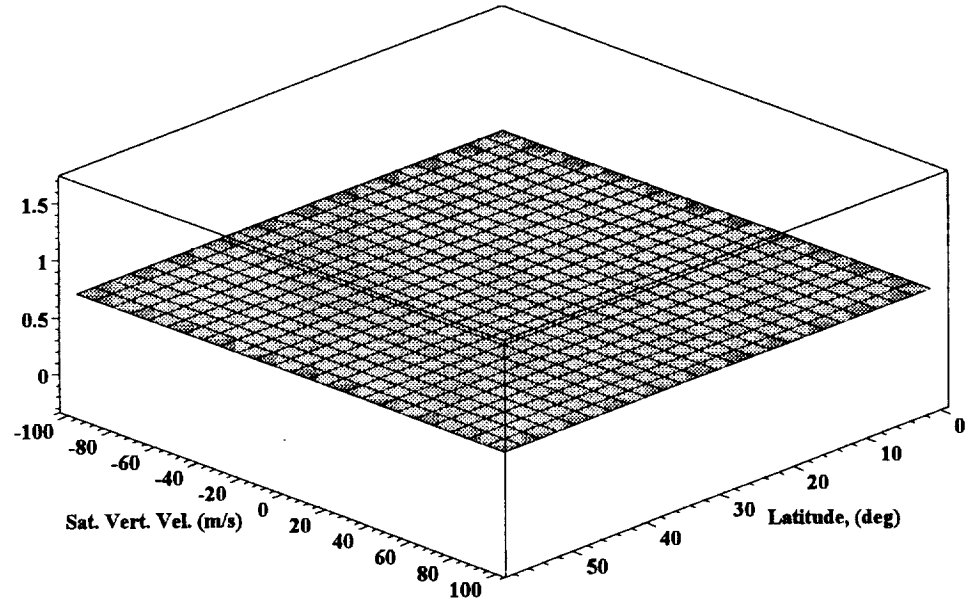

This provides the anticipated result. Plotting as a function of latitude ensures that there are no WGS84 related dependencies. As indicated previously the line of sight velocity includes a component due to the earth's rotational velocity (Figure A2.37). The earth's rotational velocity also depends on the latitude (Figure A2.18) as does the nadir angle at the surface (Figure A2.20). These dependencies combine to create a complex surface that must be accounted for in order to correctly determine the target velocity independent of the latitude and azimuth angle.

Figure A2.58: LOS velocity due to earth rotation

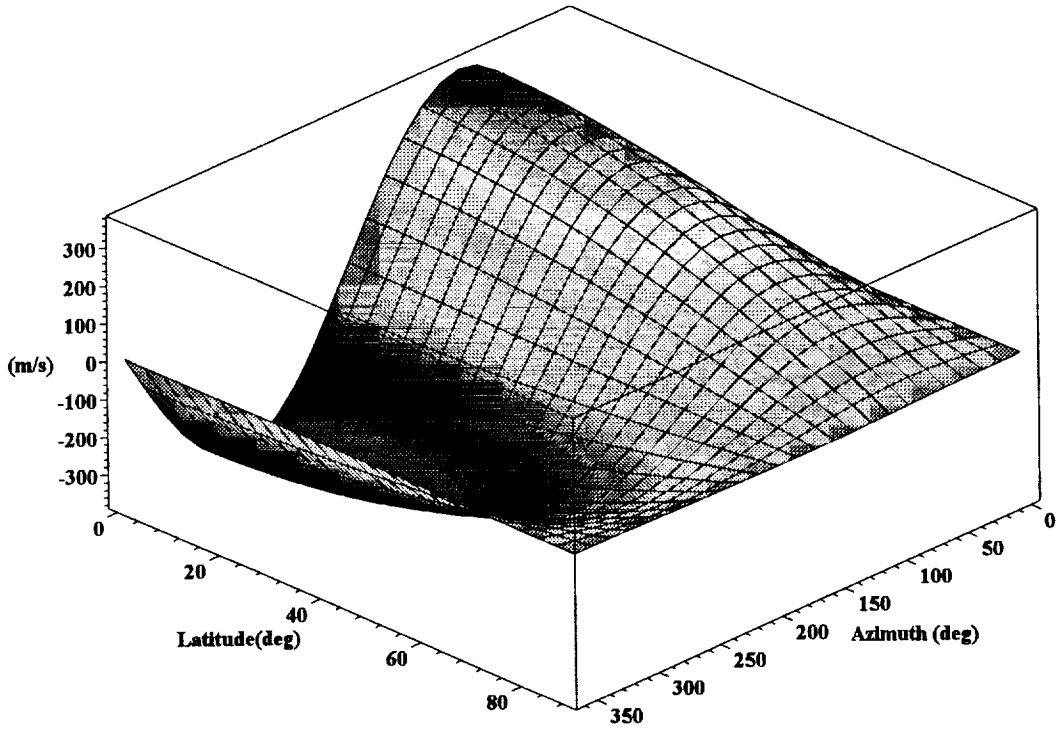

We can plot the differential with respect to the azimuth angle and latitude respectively to determine the sensitivities.

Figure A2.59: Rate of change of line of sight component of the earth's rotational velocity with azimuth

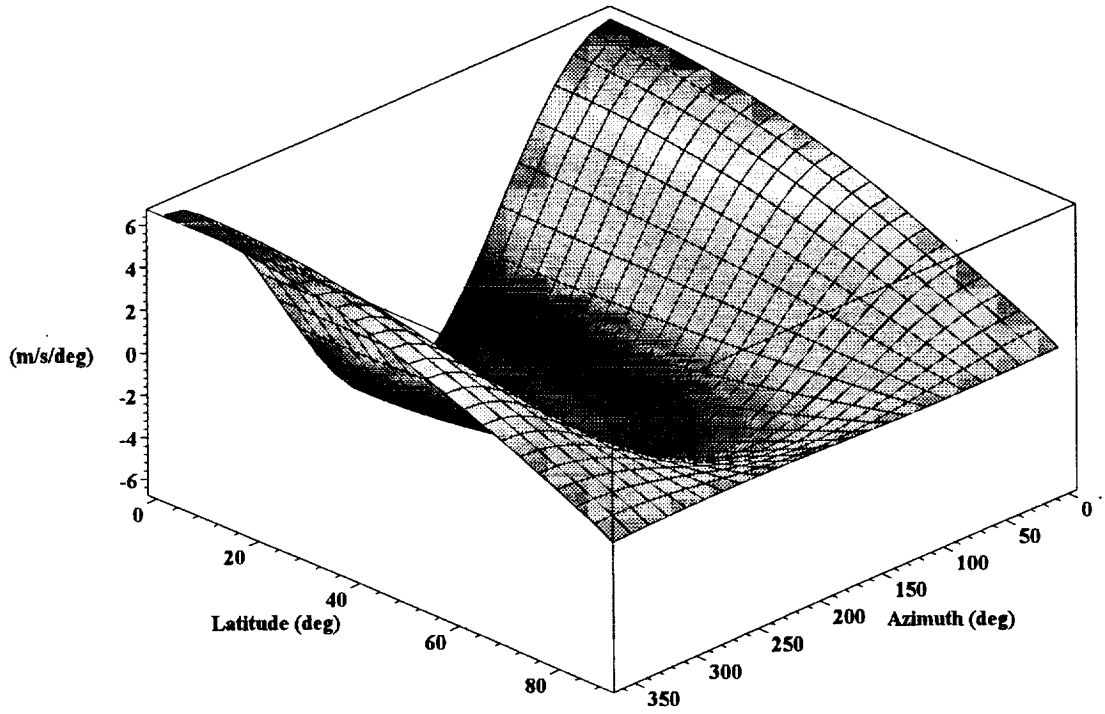

Figure A2.60: Rate of change of line of sight component of the earth's rotational velocity with latitude

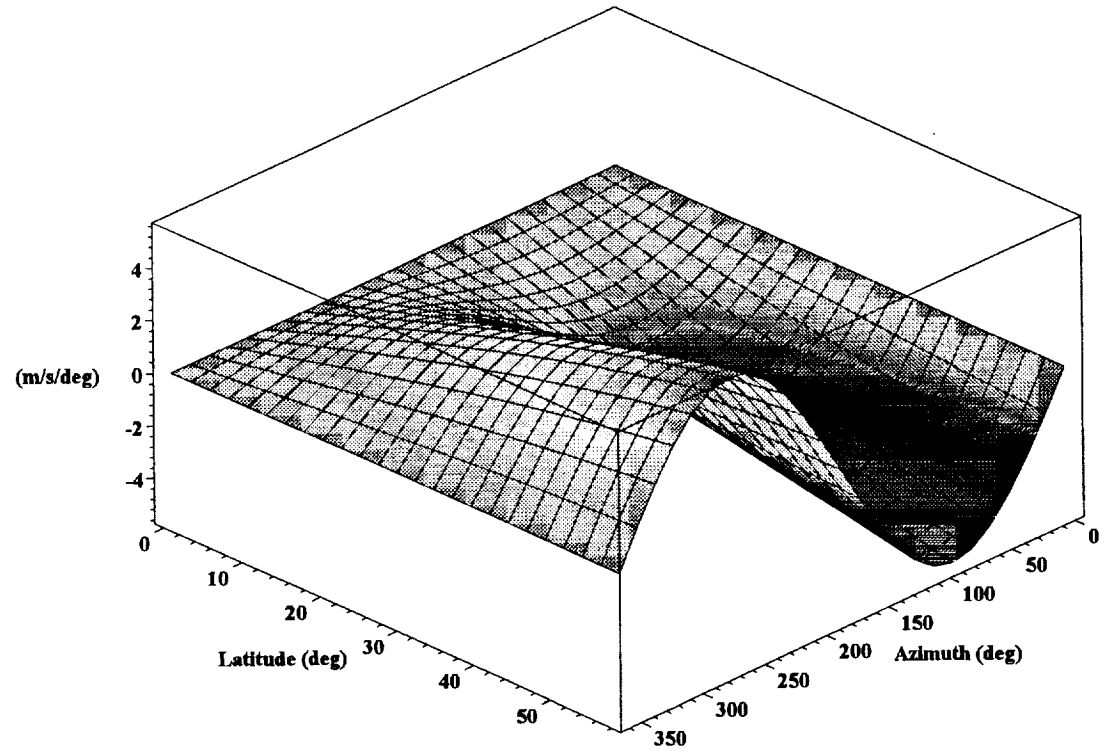

The rate of change of the line of sight component of the earth's rotational velocity with latitude (Figure A2.60) should be the same as for the rate of change of the total line of sight velocity (Figure A2.47).

We now consider the frequencies seen by the lidar. The local oscillator frequency is given by:

```
lo_f := proc(λ) global v_c; v_c / λ end
```

where λ is the wavelength and v_c is the velocity of light. In order to reduce the detector bandwidth we want to tune one of the lasers to track the anticipated Doppler shift from the line of sight velocities due to the spacecraft and earth rotation velocities. The Doppler shift tuning function is given by:

```
tune_f := proc(n, az, alt, inc, orbh, lat, hsatv, vsatv, λ)
    2*(hsatv*cos(az)*sin(n) + vsatv*cos(n) + Vlat(lat)*sin(orblat(lat, inc) + az)*sin(nadalt(orbh, n, alt, lat)))
    / λ
end
```

If we consider the case where the outgoing laser pulse is tuned then the master oscillator tuning function is given by:

```
mo_f := proc(n, az, alt, inc, orbh, lat, hsatv, vsatv, λ, offset_f, deadband, qswitchf)
local a, b, c;
global d2r;
    b := tune_f(n, az, alt, inc, orbh, lat, hsatv, vsatv, λ) + qswitchf;
    if evalf(az < 90*d2r) and evalf(abs(b + offset_f) < deadband) then a := b + offset_f
    elif evalf(90*d2r ≤ az) and evalf(az ≤ 270*d2r) and evalf(deadband ≤ abs(b - offset_f)) then
        a := b - offset_f
    else a := b + offset_f
    fi;
    lo_f(λ) - a
end
```

where offset_f is the desired offset frequency on the atmospheric signal detector for a target velocity of 0 m/s, deadband is the deadband desired to avoid operating the electronics too close to D.C. and qswitchf is the frequency offset that the slave oscillator q-switch introduces. The deadband is primarily required to ensure that the MO/LO offset frequency can be accurately measured. We can plot the master oscillator tuning as a function of azimuth angle for a latitude of 45 deg, a wavelength of 2.051 μm, an offset frequency of 250 MHz, a deadband of 100 MHz and a q-switch frequency shift of 50 MHz.

Figure A2.61: MO Tuning

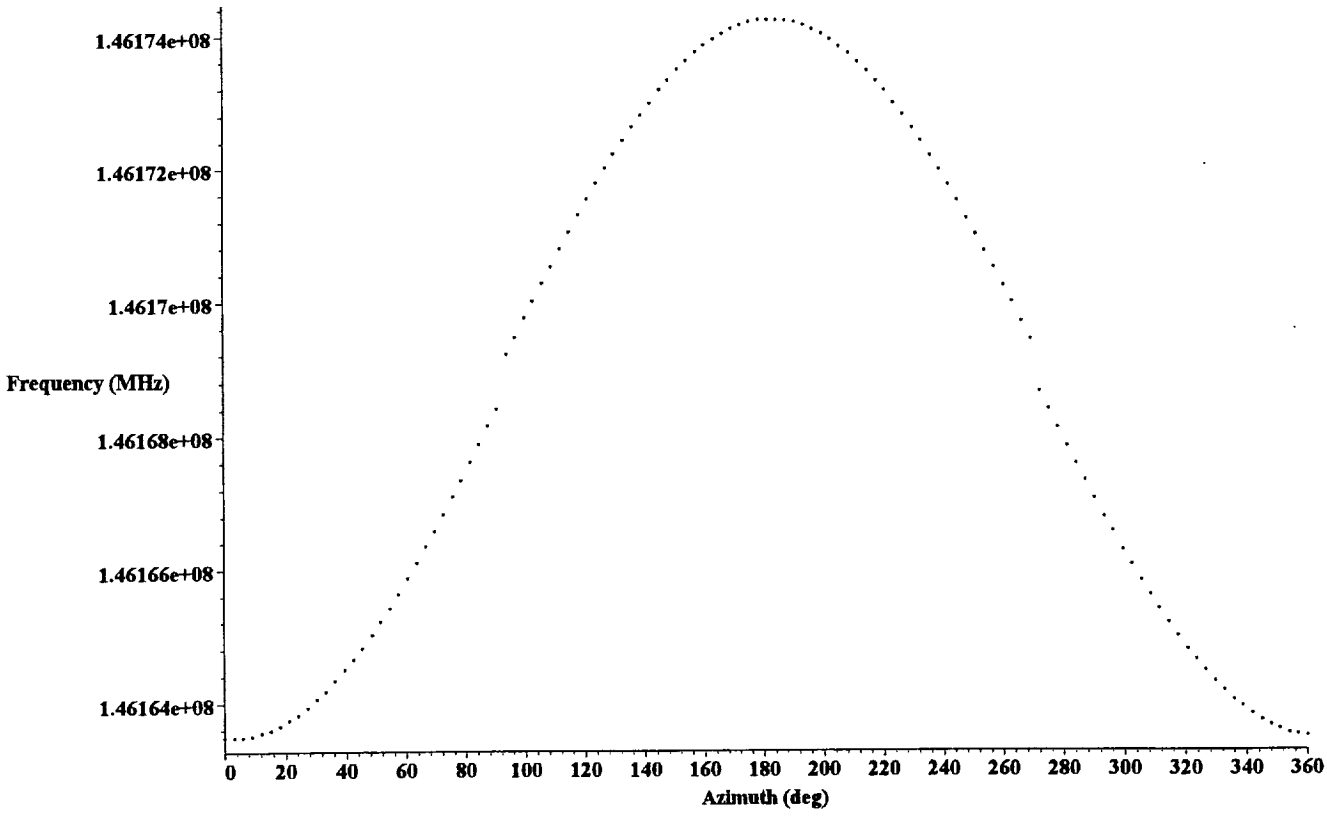

The plot clearly shows the frequency hop in the tuning curve that is required to meet the deadband requirements. The slave oscillator output frequency is simply the master oscillator frequency combined with the slave oscillator frequency shift.

Slave_f := **proc**(*n*, *az*, *alt*, *inc*, *orbh*, *lat*, *hsatv*, *vsatv*, λ, *offset_f*, *deadband*, *qswitchf*)

mo_f(*n*, *az*, *alt*, *inc*, *orbh*, *lat*, *hsatv*, *vsatv*, λ, *offset_f*, *deadband*, *qswitchf*) + *qswitchf*

end

Figure A2.62: Slave oscillator frequency

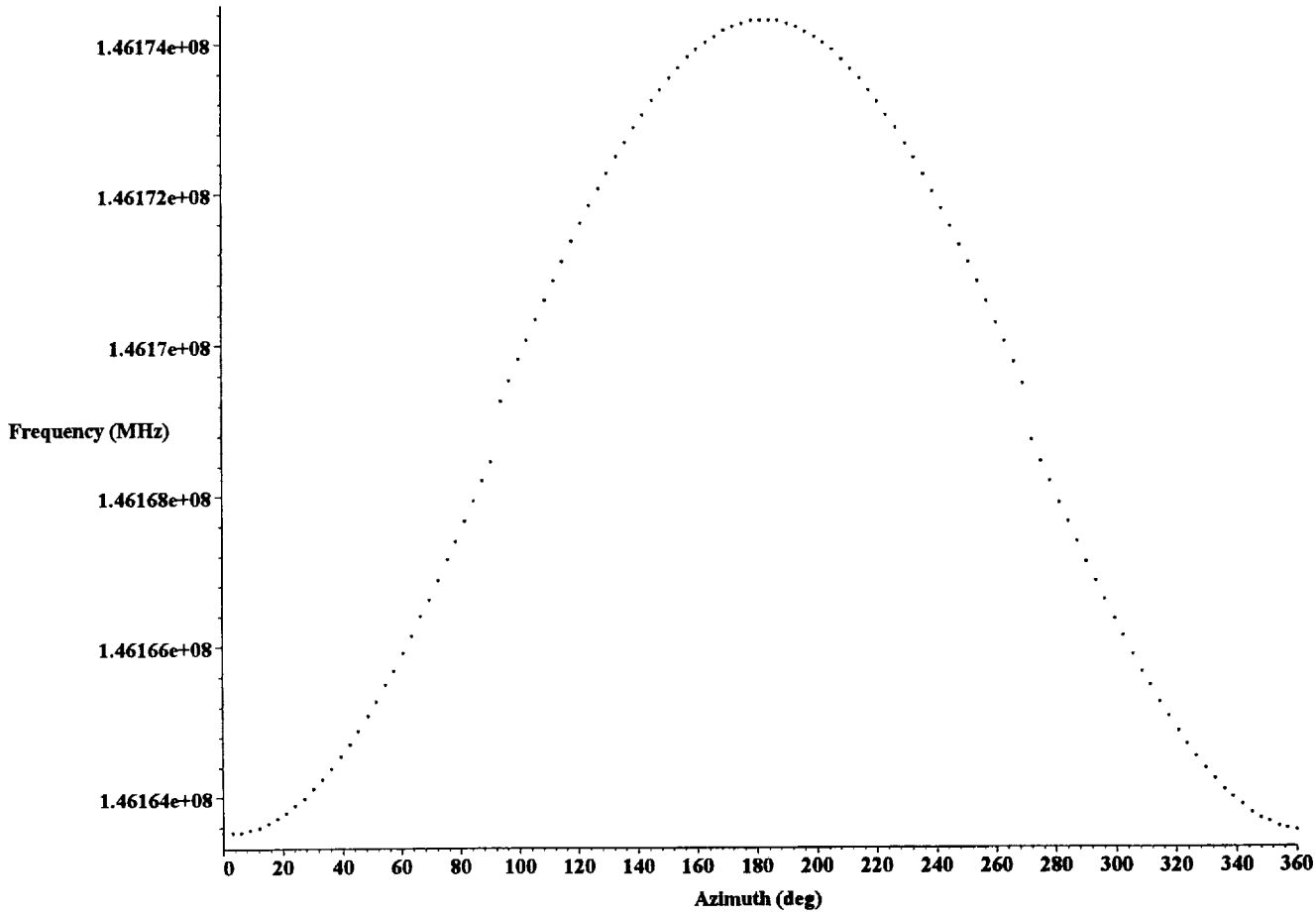

The slave oscillator frequency is Doppler shifted.

Doppler_f := **proc**(*n, az, alt, inc, orbh, lat, trgta, vtrgtv, htrgtv, hsatv, vsatv*, λ, *offset_f, deadband, qswitchf*)
global *v_c*;
    2*los_vel(*n, az, alt, inc, orbh, lat, trgta, vtrgtv, htrgtv, hsatv, vsatv*)*
    Slave_f(*n, az, alt, inc, orbh, lat, hsatv, vsatv*, λ, *offset_f, deadband, qswitchf*) / *v_c*
end

Figure A2.63: Doppler frequency shift

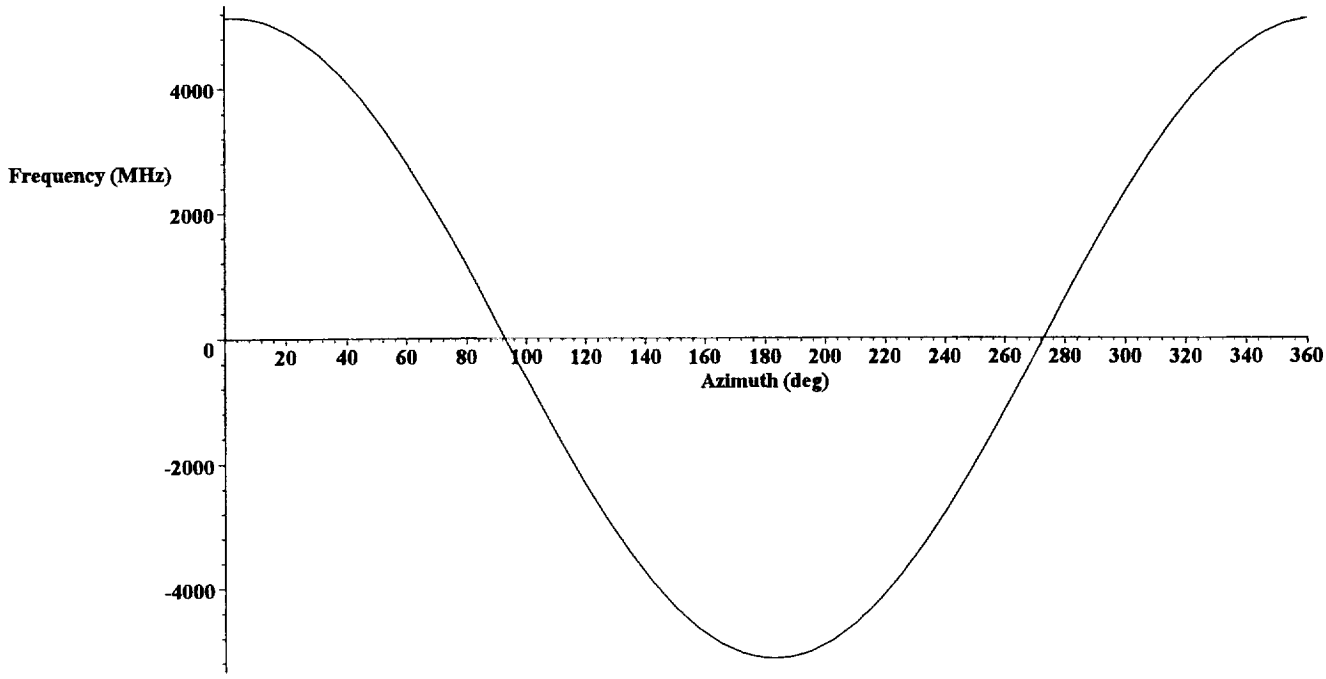

One of the detectors monitors the offset frequency between the master oscillator and the local oscillator. This detector sees the full bandwidth of possible signals and is the one that requires the deadband frequency to ensure adequate measurement of the MO/LO offset frequency. The MO/LO frequency difference is given by:

molo_f := **proc**(*n, az, alt, inc, orbh, lat, hsatv, vsatv*, λ, *offset_f, deadband, qswitchf*)
    lo_f(λ) – mo_f(*n, az, alt, inc, orbh, lat, hsatv, vsatv*, λ, *offset_f, deadband, qswitchf*)
end

The return signal is mixed with the local oscillator on the signal detector and the return signal/LO frequency difference is given by:

det_f := **proc**(*n, az, alt, inc, orbh, lat, trgta, vtrgtv, htrgtv, hsatv, vsatv*, λ, *offset_f, deadband, qswitchf*)
    Slave_f(*n, az, alt, inc, orbh, lat, hsatv, vsatv*, λ, *offset_f, deadband, qswitchf*)
    + Doppler_f(*n, az, alt, inc, orbh, lat, trgta, vtrgtv, htrgtv, hsatv, vsatv*, λ, *offset_f, deadband, qswitchf*)
    – lo_f(λ)
end

Figure A2.64: LO/MO frequency difference

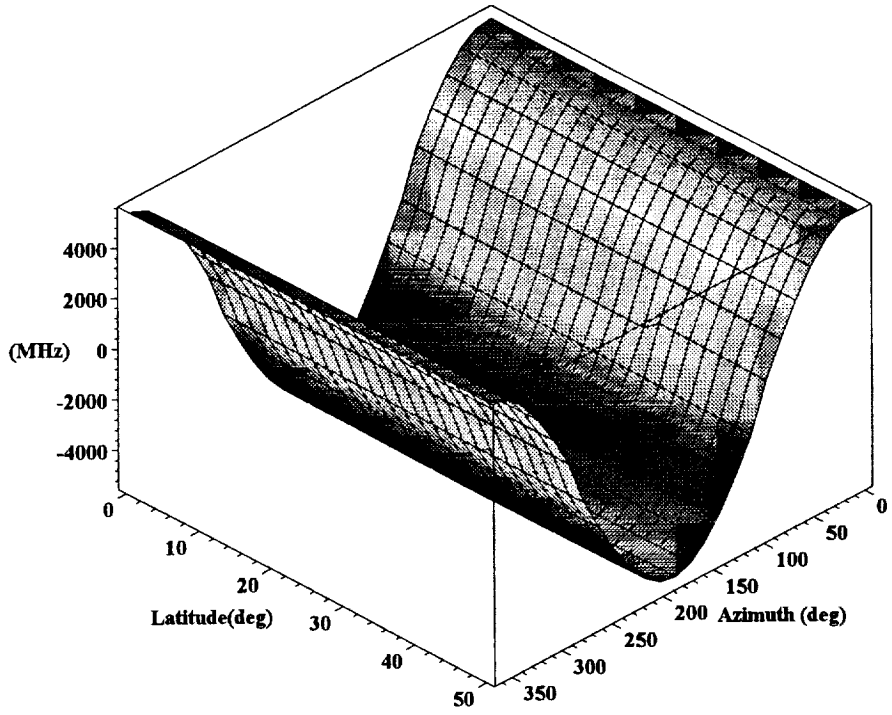

Note that the plot above is discontinuous about 0 MHz due to the frequency jump that is introduced by the tuning algorithm however this discontinuity does not show up in the plot because of the plotting routine. In order to clearly show the discontinuity we can plot a slice through the above plot at a fixed latitude value (45 deg).

Figure A2.65: LO/MO frequency difference

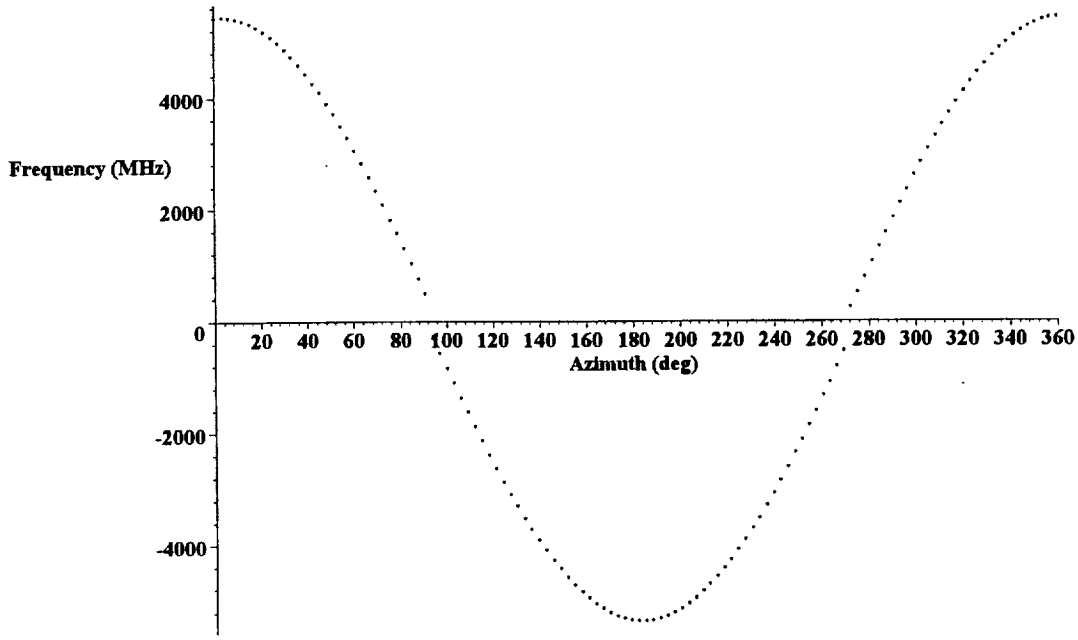

The frequencies from the MO/LO detector are simply given by:

molodet_f := **proc**(*nadir, az, alt, inc, orbh, lat, hsatv, vsatv, λ, offset_f, deadband, qswitchf*)
    abs(molo_f(*nadir, az, alt, inc, orbh, lat, hsatv, vsatv, λ, offset_f, deadband, qswitchf*))
end

Figure A2.66: LO/MO detector frequency

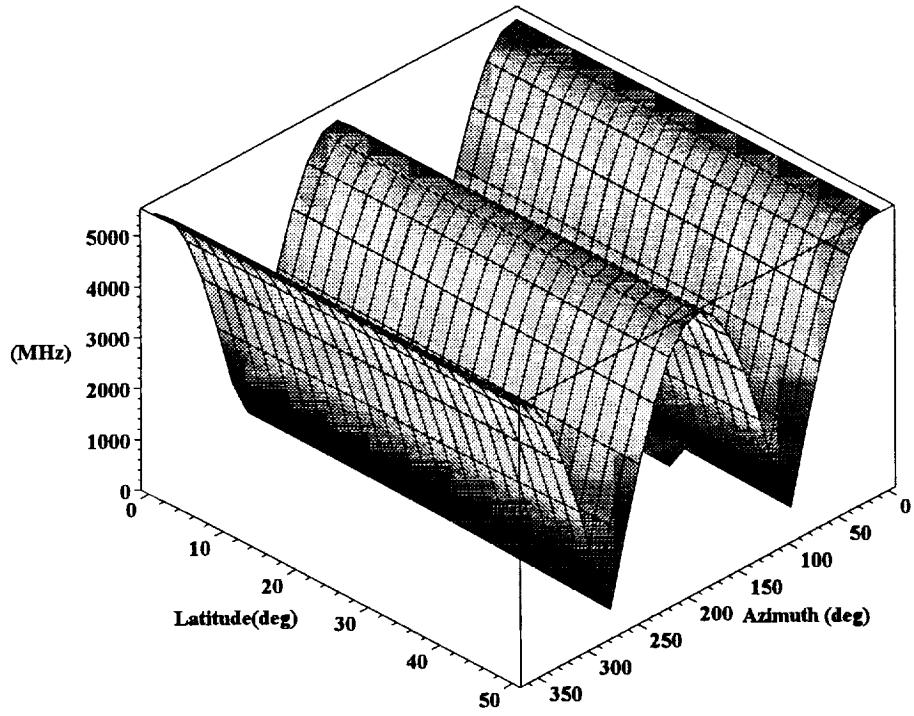

The minimum frequency (MHz) in this plot is:

100.9270462

which is greater than the deadband frequency desired. Thus the algorithm correctly maintains the deadband requirements on the MO/LO detector. The Q-switch introduces a frequency offset of the slave oscillator frequency with respect to the master oscillator frequency. Taking the beat frequency between the two should result in the Q-switch frequency shift independent of azimuth angle or latitude.

Figure A2.67: MO/SO frequency difference

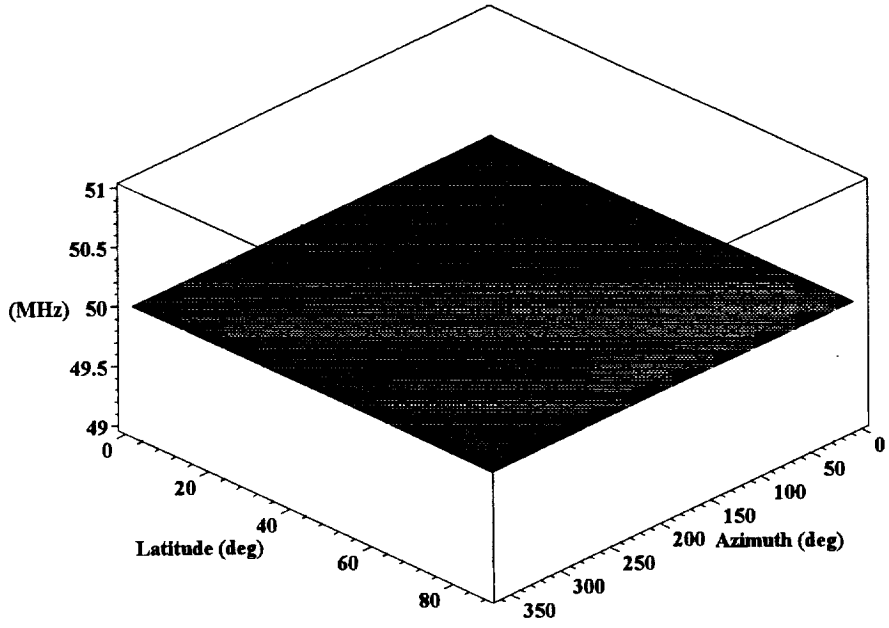

This figure clearly shows that the MO/SO frequency difference is independent of the azimuth angle and latitude. The following figure shows the actual frequency transmitted as a function of azimuth angle and latitude.

Figure A2.68: Outgoing slave oscillator frequency

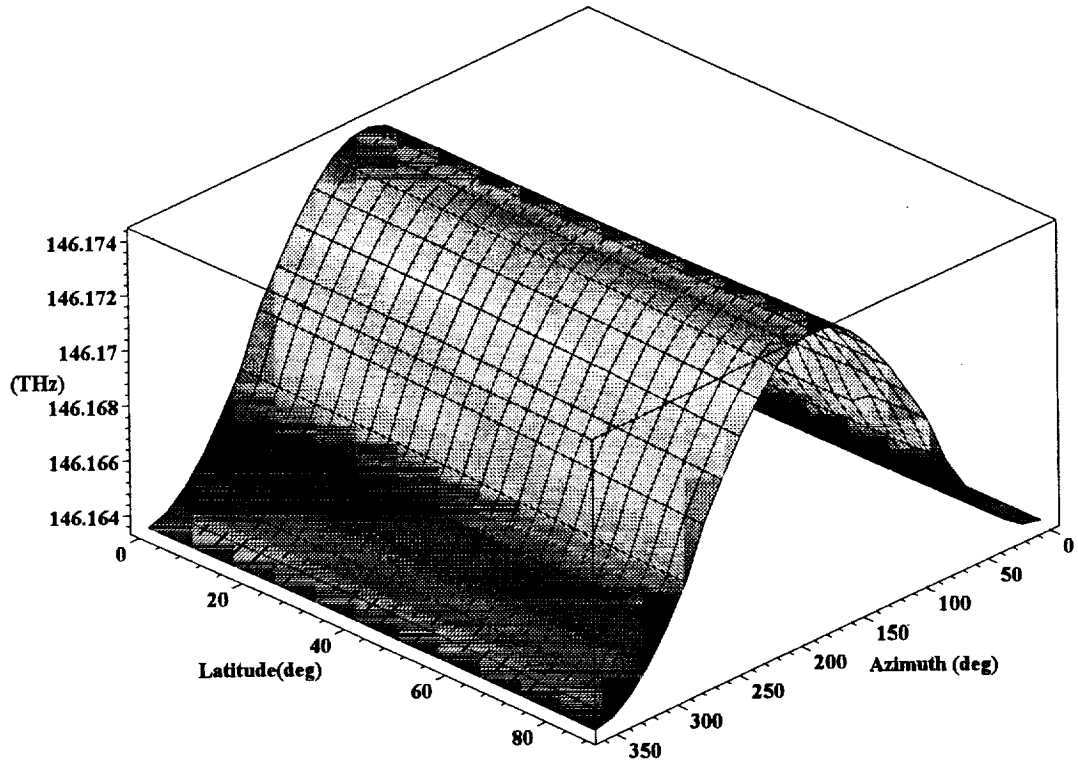

The transmitted frequency is Doppler shifted by the line of sight components of the satellite, earth rotation and target velocities and returns to the spacecraft where it is mixed with the local oscillator. The frequency difference between the local oscillator and the return signal is:

Figure A2.69: Return signal/LO frequency difference

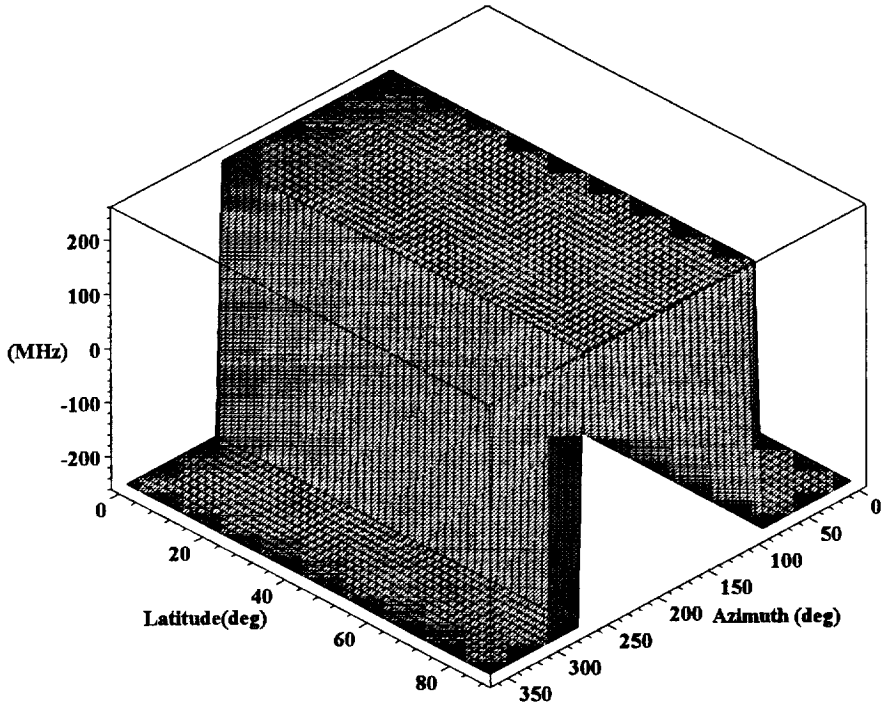

Figure A2.69 clearly shows the signal center frequency hop from -(Offset frequency) to +(Offset frequency) as the tuning algorithm accounts for the MO/LO detector deadband requirements. The frequencies actually seen on the signal detector are the absolute values of Figure A2.69:

Figure A2.70: Signal detector frequency

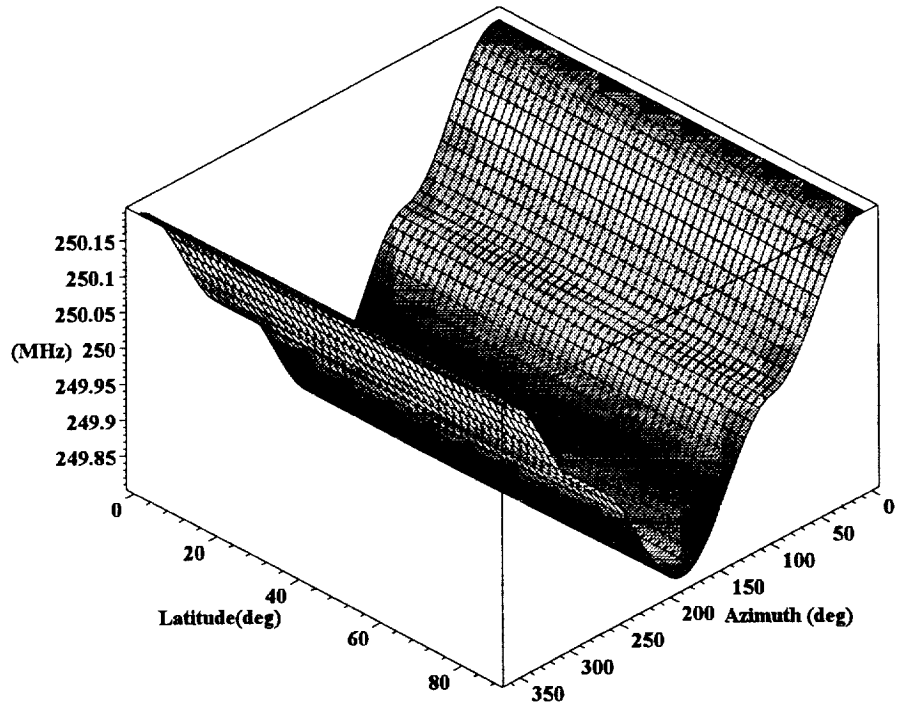

We can see from this figure that the signal floor is not completely flat but varies by ~± 0.2 MHz. This occurs because the Doppler frequency shift for tuning the MO is calculated from the center frequency of the laser but the actual Doppler frequency shift seen is the shift for a frequency of (center frequency of the laser +calculated offset) and this means there is a small error attributable to the method by which the offset is determined. This error, if not accounted for, introduces the small frequency/velocity error seen in Figure A2.70. The following figure shows the absolute value of this offset error as a function of azimuth and latitude relative to the 'ideal' value. Knowing this effect it is, in principle, possible to remove it in post-processing.

Figure A2.71: Magnitude of the uncompensated Doppler Frequency

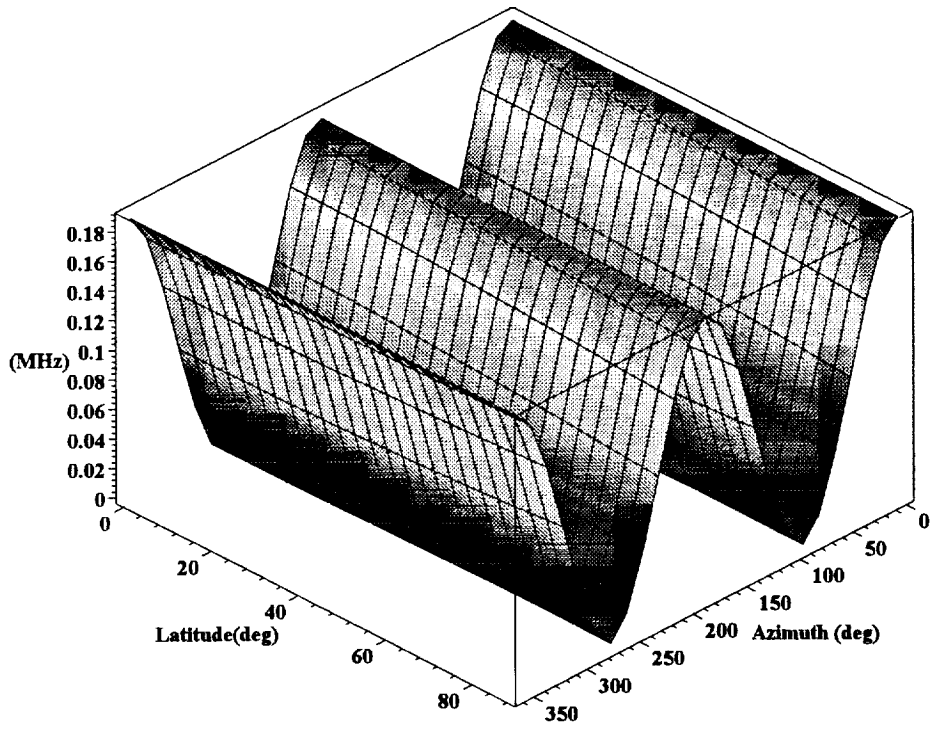

We can plot a series of views of the frequency on the detector as a function of latitude and azimuth for target horizontal velocities of -100 m/s, -50 m/s, 0 m/s, +50 m/s and 100 m/s. This first series of plots is for the velocity always being aligned to the azimuth angle. This ensures that the maximum component of the target velocity is always seen and should result in a frequency independent of latitude and azimuth except for the difference due to maintaining the deadband on the MO/LO detector. Note that there appears to be steps in the following plots in the region around azimuth angles of 90 - 100 degrees. This is an artifact of the plotting grid used - at higher grid resolutions these artifacts dissappear. Figure A2.69 shows how these plots appear with higher resolution plotting grids.

Figures A2.72 - A2.76: Frequency on the detector for target velocities of -100,-50 ,0,50,100 m/s into the line of sight

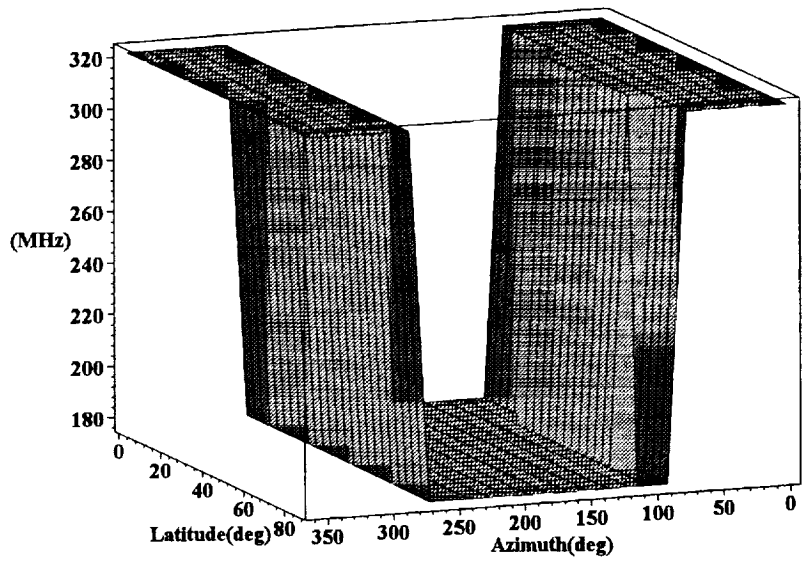

Fig. A2.72
-100 m/s

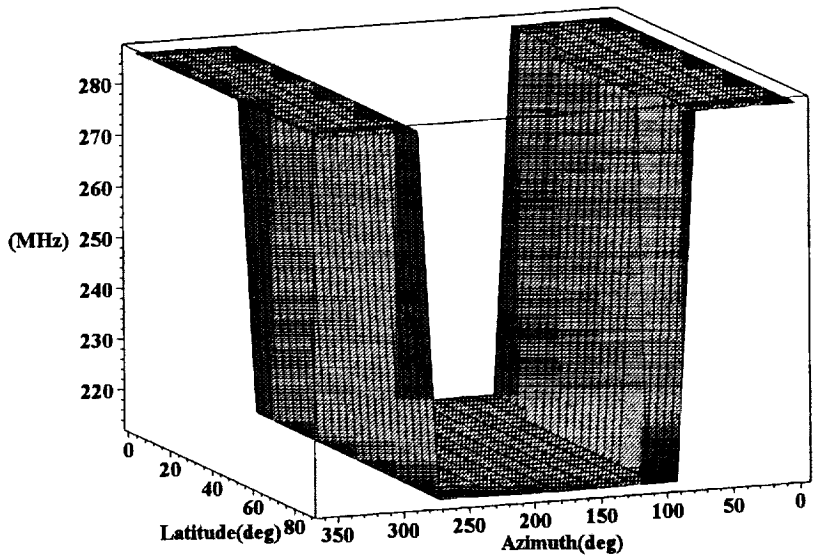

Fig. A2.73
-50 m/s

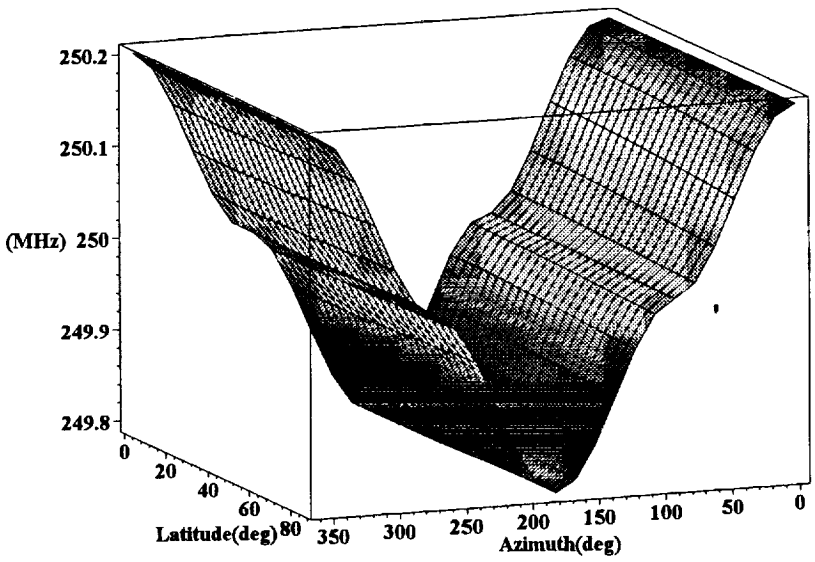

Fig. A2-74
0 m/s

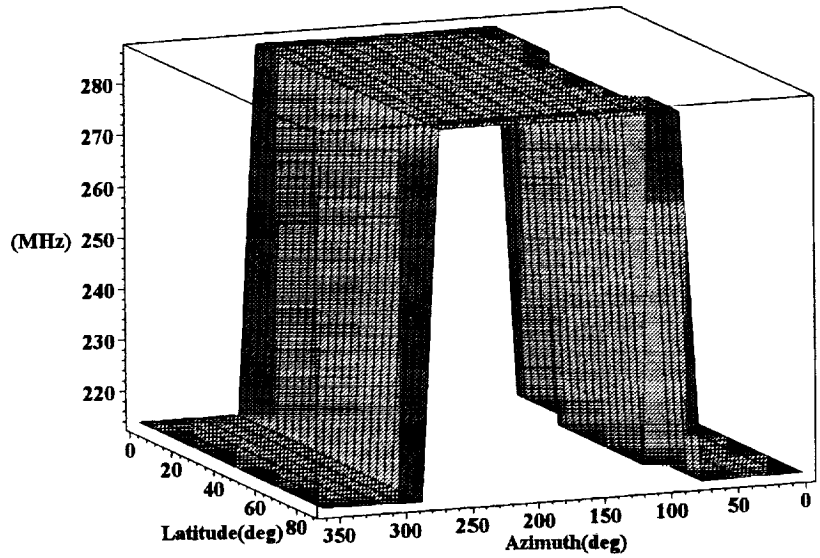

Fig. A2-75
50 m/s

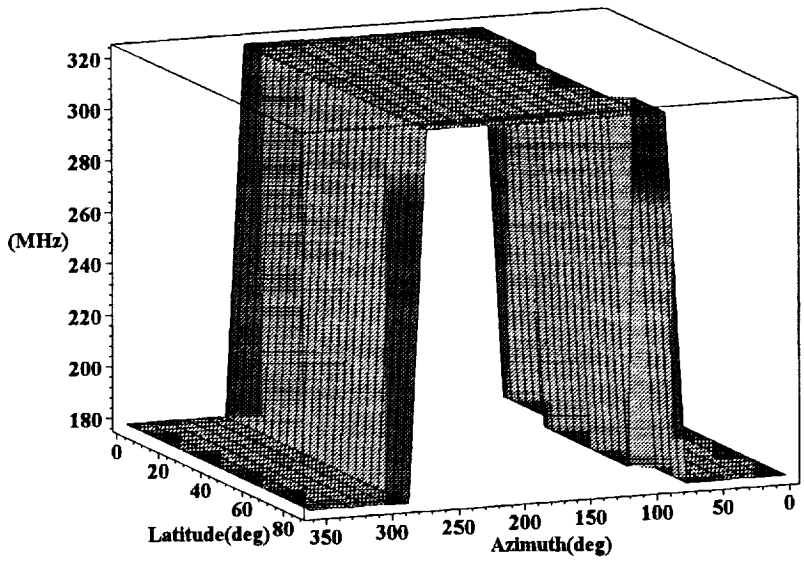

Fig. A2.76
100 m/s

This set of plots shows that as the target velocity varies between the minimum and maximum velocities the signal frequency is independent of the latitude and azimuth angle. The clear separation of the two portions of the signal ensures that in post-processing it will be clearly distinguishable where the frequency hop required to maintain the deadband occured. For comparison purposes the next set of plots is for the same target velocities except that the target velocity is always oriented at a fixed angle, parallel to the lines of latitude. In this case the line of sight component of the target velocity will have an azimuthal dependence. Note that there appears to be steps in the following plots in the region around azimuth angles of 90 - 100 degrees. As in the prior plots this is an artifact of the plotting grid used - at higher grid resolutions these artifacts dissappear.

Figures A2.77 - A2.81: Frequency on the detector for target velocities of -100,-50,0,50,100 m/s parallel to the lines of latitude

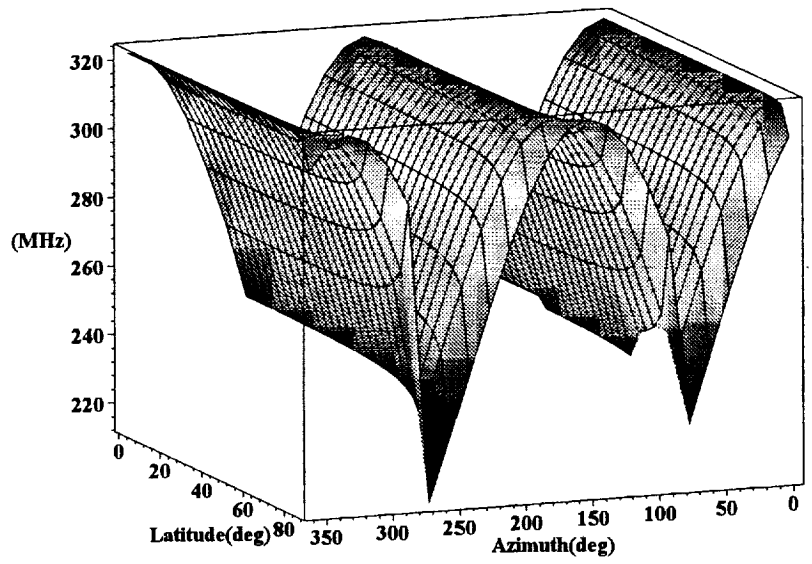

Fig. A2.77
-100 m/s

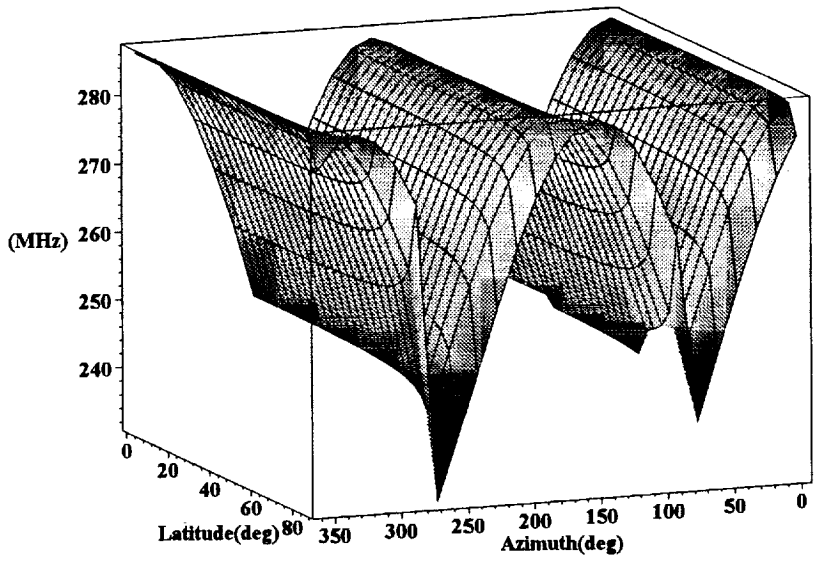

Fig. A2.78
-50 m/s

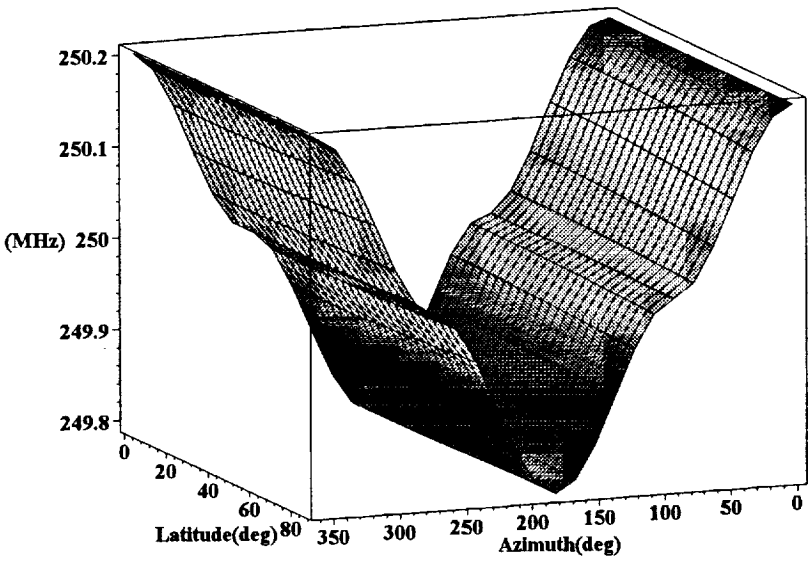

Fig. A2.79
0 m/s

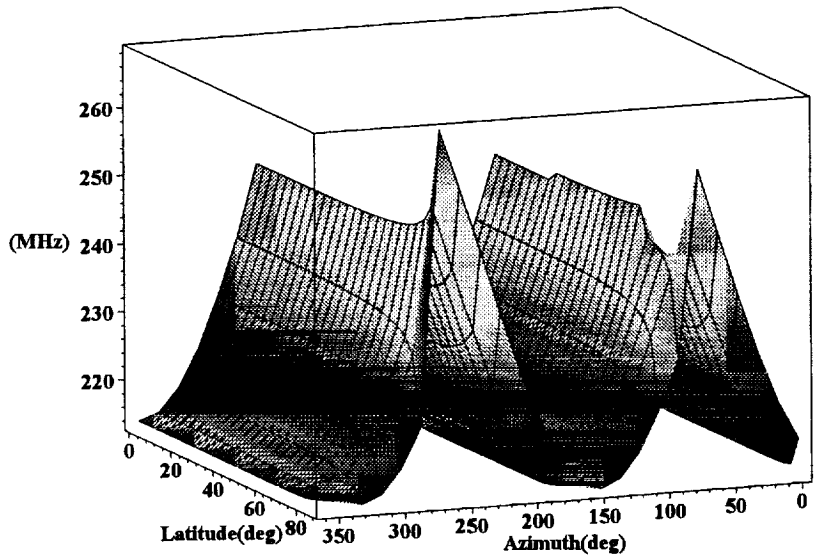

Fig. A2.80
50 m/s

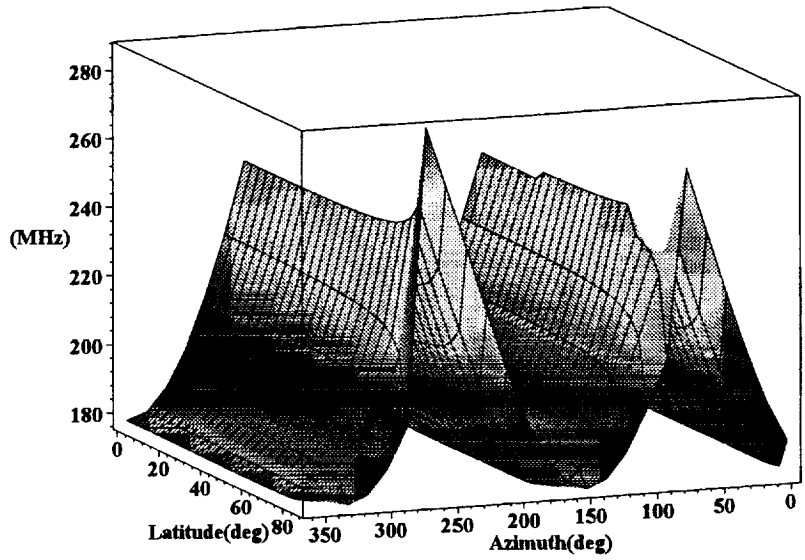

Fig. A2.81
100 m/s

National Aeronautics and
Space Administration

George C. Marshall Space Flight Center
Marshall Space Flight Center, Alabama 35812

MSFC
SPACE READINESS COHERENT LIDAR EXPERIMENT (SPARCLE)

PRELIMINARY DESIGN REVIEW SYSTEM PERFORMANCE ANALYSIS REPORT

CENTER FOR APPLIED OPTICS
UNIVERSITY OF ALABAMA IN HUNTSVILLE
HUNTSVILLE, AL 35899

MSFC - Form 454 (Rev. October 1992)

A3a

r

Release Date: ___/___/___	**Marshall Space Flight Center** **SPECIFICATION/DOCUMENT CHANGE INSTRUCTION** **Spec./Doc. No.** MSFC-DOC-????	Page 1 of 1 Copy No.:

Change No./Date	SCN/DCN No./Date	CCBD No./Date	Replacement Page Instructions

MSFC-Form 4140 (Revised September 1990)

NOTE: After revising the document, file this sheet in document preceding Table of Contents

A3b

MSFC
SPACE READINESS COHERENT LIDAR EXPERIMENT (SPARCLE)
PRELIMINARY DESIGN REVIEW
SYSTEM PERFORMANCE ANALYSIS REPORT
MSFC-DOC-????
September 1998

Prepared by: Date
Gary D. Spiers
UAH SPARCLE Lidar Systems Engineer

Approved by: Date
Allen S. Bacskay
MSFC SPARCLE Project Chief Engineer

Approved by: Date
Jimmie E. Johnson
MSFC SPARCLE Project Manager

A3c

SPARCLE PRELIMINARY DESIGN REVIEW
SYSTEM PERFORMANCE ANALYSIS

TABLE OF CONTENTS

LIST OF FIGURES

FIGURE PAGE

LIST OF TABLES

TABLE PAGE

APPENDICES

SPARCLE PRELIMINARY DESIGN REVIEW
SYSTEMS PERFORMANCE ANALYSIS

1. SCOPE

This document provides the results of an analysis of the ability of the SPARCLE experiment to meet the line of sight velocity accuracy and sensitivity requirements documented in MSFC-RQMT-2797 SPARCLE Science/Mission Requirements Document. It also documents the error budgets associated with the instrument.

2. REFERENCE DOCUMENTS

MSFC-RQMT-2828	SPARCLE Mission Science Requirements
MSFC-RQMT-2797	SPARCLE System Requirements Document
DMA-TR-8350.2	Department of Defense World Geodetic System 1984

Copies of the MSFC reference documents are available from the MSFC Repository.

3. ACRONYMS/DEFINITIONS

The following are acronyms/definitions used in this document.

CAO	Center for Applied Optics
CI	Co-Investigator
GHCC	Global Hydrology and Climate Center
GIS	Goddard Internal Simulation
GPS	Global Positioning System
GSE	Ground Support Equipment
GSFC	Goddard Space Flight Center
HH	Hitchhiker
INS	Inertial Navigation System
JIS	Joint Integrated Simulation
JSC	Johnson Space Center

LIDAR	Light Detection And Ranging
LOS	Line of Sight
MSFC	Marshall Space Flight Center
MTPE	Mission to Planet Earth
NMP	New Millennium Program
PI	Principal Investigator
SPARCLE	SPAce Readiness Coherent Lidar Experiment
SRD	System Requirements Document
SSP	Space Shuttle Program
STS	Space Transportation System
TBD	To Be Determined
TDRS	Tracking and Data Relay Satellite
UAH	University of Alabama in Huntsville
WGS84	World Geodetic System 1984
WSC	White Sands Complex
-ZLV	The Shuttle payload bay is in an earth viewing attitude.

4. INSTRUMENT DESCRIPTION

The SPARCLE instrument is intended as a technology validation/demonstration of the ability of a space-based coherent Doppler lidar to measure wind velocity from space. The SPARCLE instrument operates at a nominal wavelength of 2.051 microns. The instrument will be mounted to a cross-bay bridge in the payload bay of an STS orbiter. The instrument consists of three Hitchhiker canisters that will be mounted to the side of the bridge and a radiator that will be mounted to the top of the bridge.

5. REQUIREMENTS AND ERROR BUDGETS

5.1 Introduction

The error budgets documented here are intended to reflect the instrument's ability to meet the requirements documented in MSFC-RQMT-2797. The requirements in MSFC-RQMT-2797 were intended to separate out the effect of instrument errors on the measurement from errors resulting from the choice of platform. The performance of the combined instrument and platform will be addressed in section 6. Performance Analysis.

5.2 Line of sight velocity accuracy

5.2.1 Requirement

This is identified in 3.2.1.11 of MSFC-RQMT-2797 and states:

"The instrument contribution to the line of sight velocity measurement accuracy excluding the velocity estimator and assuming perfect instrument velocity, position and attitude knowledge shall be better than 1 m/s."

5.2.2 Discussion of the requirement

The SPARCLE instrument measures wind velocity by calculating the frequency difference between the transmitted laser beam and the return signal. This frequency difference is due to the transmitted frequency being Doppler shifted by the line of sight velocity seen by the instrument. The line of sight velocity is comprised of velocity components due to the satellite velocity, the earth's rotational velocity and the velocity of the target. Figure (1) shows the velocities that contribute to the line of sight velocity in the horizontal plane and Figure (2) shows the geometry in the vertical plane.

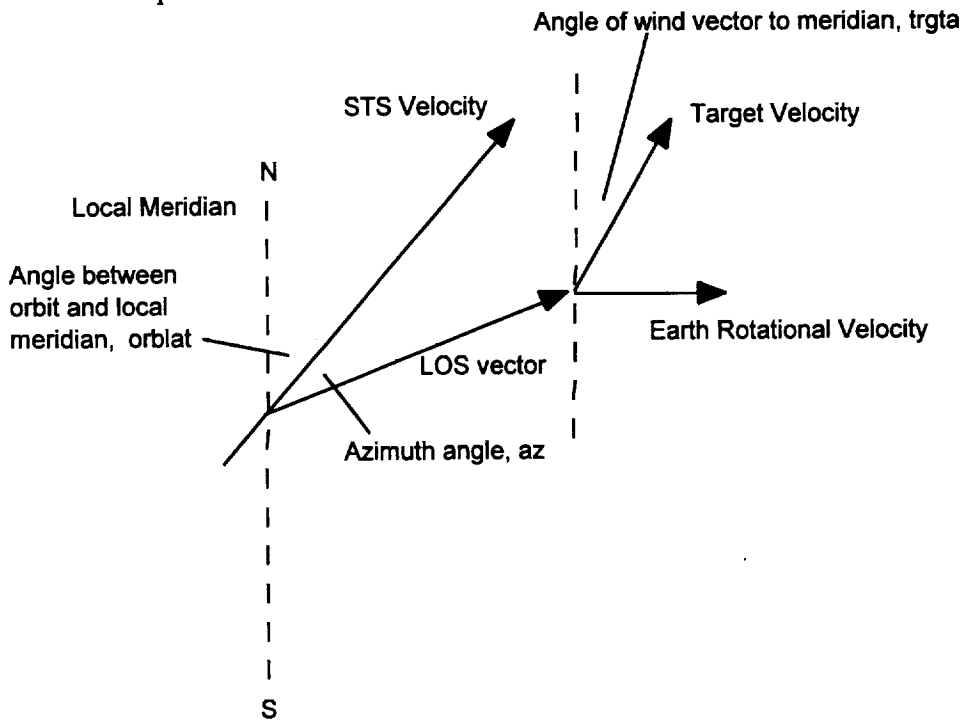

Figure 1) The velocities contributing to the line of sight velocity.

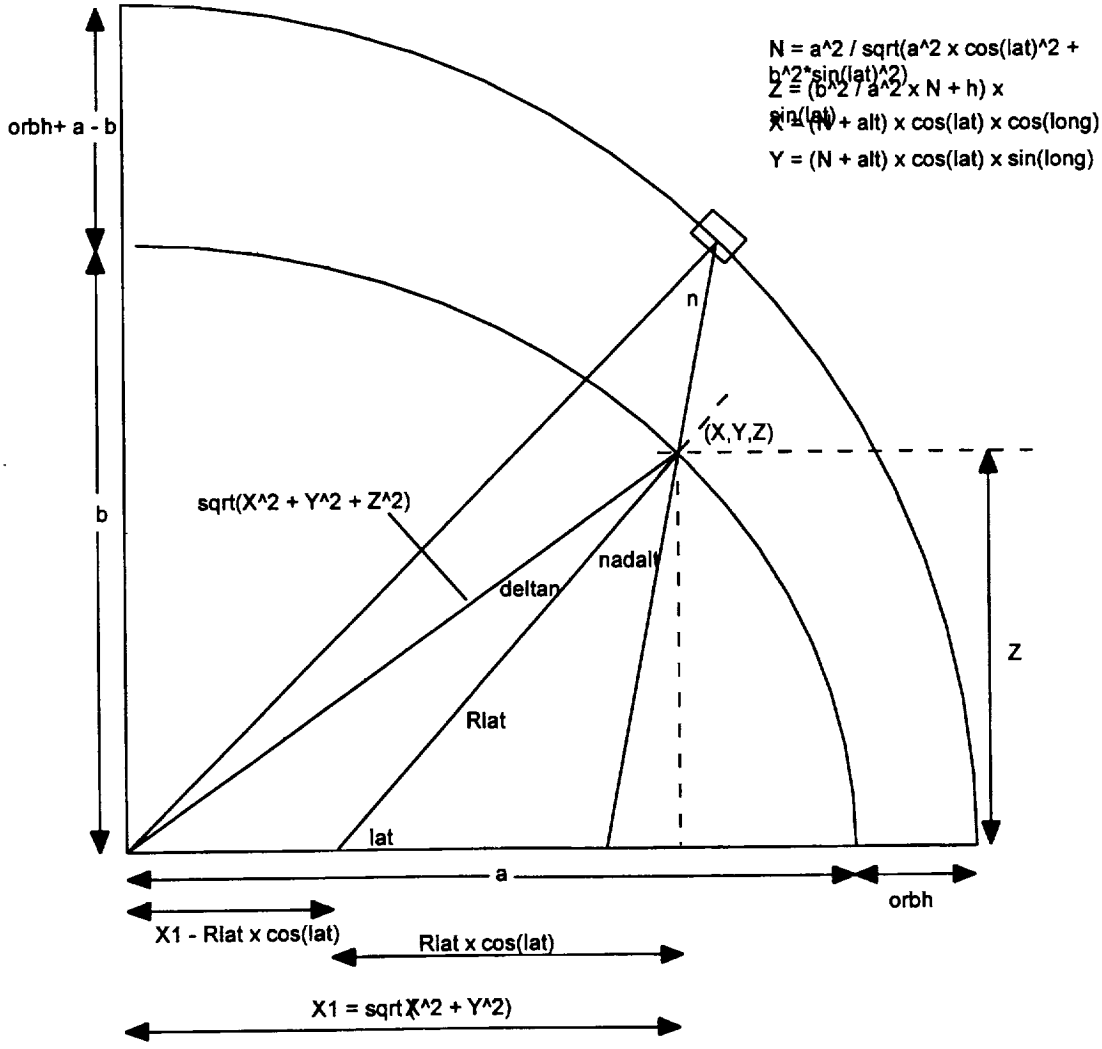

Figure 2) The measurement geometry in the 'vertical' plane.

The combined line of sight velocity is given by:

$$\begin{aligned} los\_vel := {} & htrgtv\ \cos(-az - \mathrm{orblat}(lat, inc) + trgta)\ \sin(\mathrm{nadalt}(orbh, n, alt, lat)) \\ & + vtrgtv\ \cos(\mathrm{nadalt}(orbh, n, alt, lat)) + hsatv\ \cos(az)\ \sin(n) + vsatv\ \cos(n) \\ & + \mathrm{Vlat}(lat)\ \sin(\mathrm{orblat}(lat, inc) + az)\ \sin(\mathrm{nadalt}(orbh, n, alt, lat)) \end{aligned} \qquad \text{EQ(1)}$$

where the first and second terms are the line of sight components of the target velocity with respect to the local WGS84 earth ellipsoid surface. The third and fourth terms are the line of sight components of the STS horizontal and vertical velocities. The final term is the component of the earth's rotational velocity along the line of sight. Table 1 lists the 11 base parameters listed in this equation while Table 2 identifies the functions called out in equation (1):

Symbol	Parameter

htrgtv	target horizontal velocity
vtrgtv	target vertical velocity
trgta	angle of the target velocity with respect to the local meridian
az	azimuth angle with respect to the STS velocity vector
lat	latitude of the STS
inc	orbit inclination angle
orbh	orbit height
n	instrument nadir angle
alt	altitude of the target with respect to the local WGS84 ellipsoid surface
hsatv	horizontal component of the STS velocity
vsatv	vertical component of the STS velocity

Table 1) Fundamental parameters.

Function	Purpose
orblat(lat,inc)	The angle of the STS velocity vector to the local meridian
nadalt(orbh,n,alt,lat)	The nadir angle the line of sight makes with the target with respect to the local WGS84 ellipsoid surface
Vlat(lat)	The earth's rotational velocity at a latitude, lat

Table 2) Functions referred to in equation 1.

5.2.3 Sensitivity analysis

For the purposes of assessing the line of sight performance of the instrument we look at the velocity returns from the earth ground return ie the first two terms of equation (1) are zero. We can look at the sensitivity of the line of sight velocity as a function of the parameters in table (1). The analyses shown here also include the dependencies of the functions listed in Table (2) on the parameters listed in Table (1) as well as any dependencies on the WGS84 ellipsoid model. Unless otherwise stated these analyses used the baseline parameter values listed in Table (3).

Parameter	Value
htrgtv, (m/s)	0
vtrgtv, (m/s)	0
trgta, (m/s)	0
az, (deg)	varies
lat, (deg)	45
inc, (deg)	58
orbh, (km)	300
n, (deg)	30
alt, (m)	0
hsatv, (m/s)	sqrt(Me x G /(orbh+a))
vsatv	0

Table 3) Baseline parameter values used for analyses.

For the purpose of the analyses the STS horizontal velocity was calculated using the equation given in Table 4, where Me is the earth's mass, G is the gravitational constant and a is the WGS84 semimajor ellipsoid axis. The sensitivity of the line of sight velocity to each of the parameters is summarised in table 4.

Parameter	Maximum Error Rate	Error required to give 1 m/s los error
Azimuth angle	68 (m/s)/deg	256 microradians
Nadir angle	140 (m/s)/deg	125 microradians
Orbit height	0.31 (m/s)/km	3.22 km
Latitude	24 (m/s)/deg	725 microradians
Orbit inclination	3.7 (m/s)/deg	4.7 milliradians
Target altitude	0.02 (m/s)/km	50 km
STS horiz. velocity	0.5 (m/s)/(m/s)	2 (m/s)
STS vert. velocity	0.87 (m/s)/(m/s)	1.15 (m/s)

Table 4) LOS velocity sensitivities.

Note that the error due to each of the parameters is generally a complex function of other parameters (typically azimuth and/or latitude) and the values in table (4) represent the worst case analysis. Appendix 1 contains plots of the variation of the line of sight velocity with each of these parameters and with combinations of each of these parameters.

All structural/ mechanical errors that affect the instrument line of sight velocity performance are contained within the nadir and azimuth requirements listed above. Additional errors arise from the actual measurement of the laser and return signal frequencies.

5.2.4 The line of sight velocity error budget
The following table lists the breakout of the line of sight velocity error for the conditions stipulated in MSFC-RQMT-2797. Parameters affected by these conditions have been highlighted.

SRD Requirement		(m/s)	(m/s)	(m/s)	Notes
Line of sight velocity error				0.75	
Frequency measurement error			0.57		
MO/LO		0.14			
Algorithm (m/s)	0.1				
Receiver contribution (m/s)	0.1				
SO/MO		0.51			
Algorithm (m/s)	0.5				
Receiver contribution (m/s)	0.1				
LO drift		0.15			< 200 kHz in 4 ms
Signal		0.10			
Velocity algorithm (m/s)	0				
Receiver contribution (m/s)	0.1				
Doppler correction error (MHz)	0.08	0.08			
Position knowledge error			0.37		
Latitude		0.00			24 m/s per deg
INS/GPS position knowledge (m)	0				8.6x10^(-6) deg/m
Structure	0.1				
Orbit inclination		0.37			
Knowledge (deg)	0.1				
Orbit height		0.00			0.31 (m/s)/km
Position measurement (m)	0				
Attitude knowledge error			0.32		
Nadir angle		0.29			
Attitude knowledge (microradians)	0				
GPS/INS performance	0				
Structural misalignment wrt optical axis					
Lidar instrument (microradians)	30				
Optics canister structure (microradians)	20				from 3.5.4.2 of SRD
Azimuth angle		0.14			
Attitude knowledge (microradians)	0				
GPS/INS performance	0				
Structural misalignment wrt optical axis					
Lidar instrument (microradians)	30				
Optics canister structure (microradians)	20				from 3.5.4.2 of SRD
Velocity measurement error			0.00		
STS horizontal velocity		0.00			
INS/GPS accuracy (m/s)	0				
STS vertical velocity		0.00			
INS/GPS accuracy (m/s)	0				

Table 5) The line of sight velocity error budget to meet MSFC-RQMT-2797 3.2.1.11

The optical subsystem contributions to the nadir and azimuth errors documented in Table 5) are listed in Table 6) of section 5.3.

5.3 Position accuracy

5.3.1 Requirement

This is defined in MSFC-RQMT-2797 3.2.1.3 which states:

"Knowledge accuracy of the instrument position shall be better than 500 meters."

5.3.2 Discussion

Knowledge of the instrument position is required in order to be able to correctly assign a position to the velocity measurement. From Figure we can conceptually see that errors in the azimuth or nadir angle causes the line of sight to describe a cone about the 'true' or 'ideal' value. The position of the measurement relative to the instrument is simply:

$$Z_{lvlh} := \frac{1}{2} c\, t_{rtrp} \cos(n) \qquad \text{EQ(2)}$$

in the vertical and

$$R_{lvlh} := \frac{1}{2} c\, t_{rtrp} \sin(n) \qquad \text{EQ(3)}$$

is the radial distance from the sub-instrument point to the target location, c and t_{rtrp} are the velocity of light and the round trip time of flight respectively. Finally we must constrain the azimuthal direction such that the circumferential distance from the 'true position' can be determined. This distance is simply (R_{lvlh} x daz) where daz is the error in azimuth angle. This provides the target position in a local coordinate frame which can then be transformed to obtain the target position with respect to WGS84.

5.3.3 Sensitivity Analysis
Appendix 2 contains the sensitivity plots used to obtain the following tables.

Parameter	Error Rate	Error required to give 1m error
Instrument vertical position	1 m /m	1 m
Nadir angle	44 m / 200 μrad	4.55 μrad
Round trip time	40 m / 300 ns	7.5 ns

Table 6) Vertical position assignment sensitivity

Parameter	Error Rate	Error required to give 1m error
Instrument horizontal position	1 m /m	1 m
Nadir angle	40 m / 100 μrad	2.5 μrad
Round trip time	24 m / 300 ns	12.5 ns
Azimuth angle	24 m/ 100 μrad	4.17 μrad

Table 7) Horizontal position assignment sensitivity

5.3.4 Position Accuracy Error Budget

There is an ambiguity in this requirement. This requirement, like the line of sight velocity accuracy requirement depends on the position and attitude knowledge. For consistency with the prior requirement, the following error budget assumes the same conditions as for the line of sight velocity accuracy i.e. perfect knowledge of position, velocity and attitude. Section 6 will address the situation when this is not assumed.

SRD Requirement		m	m	m
Position error				29.82574
Horizontal radial position error			20.65842	
Instrument position knowledge		0.1		
INS/GPS position knowledge (m)	0			
Structure	0.1			
Attitude knowledge error				
Nadir angle		14.42221		
GPS/INS performance	0			
Structural misalignment wrt optical axis				
Lidar instrument (microradians)	30			
Optics canister structure (microradians)	20			
Azimuth angle		8.646406		
GPS/INS performance	0			
Structural misalignment wrt optical axis				
Lidar instrument (microradians)	30			
Optics canister structure (microradians)	20			
Range measurement error		12		
Round trip timing accuracy (ns)	150			
Vertical position error			21.51289	
Instrument position knowledge		0.1		
INS/GPS position knowledge (m)	0			
Structure	0.1			
Attitude knowledge error				
Nadir angle		7.924289		
GPS/INS performance	0			
Structural misalignment wrt optical axis				
Lidar instrument (microradians)	30			
Optics canister structure (microradians)	20			
Range measurement error		20		
Round trip timing accuracy (ns)	150			

Table 8) The position error budget to meet MSFC-RQMT-2797 3.2.1.3

5.4 Instrument nadir and azimuth angle knowledge
5.4.1 Requirement
These are defined in MSFC-RQMT-2797 3.2.1.1 and 3.2.1.2 for nadir and azimuth angle respectively and state:

"Knowledge accuracy of the instrument nadir angle relative to the optical axis shall be better than 90 microradians (one sigma)."

and

"Knowledge accuracy of the instrument azimuth angle in a plane orthogonal to the optical axis shall be better than 90 microradians (one sigma)."

5.4.2 Discussion
This requirement consists of components from the optical subsystem and the structural subsystem.

5.4.3 Instrument nadir and azimuth angle error budgets
The contributions assigned to the optical components are documented in Table 9. The contribution from the structure is also included from MSFC-RQMT-2797 3.5.4.2 which states:

"The total contribution to the pointing error from structural components within the optics can shall not exceed 20 microradians tilt during any 30 minute operational time period."

Error Source	Azimuth (μrad)	Nadir (μrad)
Telescope output beam pointing measurement	10	10
Relative error between the actual transmitter beam and the alignment beam	5	5
Long term thermal and mechanical displacement of the top plate and structure	10	10
Long term laser beam pointing drift	2	2
Long term pointing error due to thermal induced displacements of telescope mirrors and optical wedge	15	15
Thermally induced birefringence in the optical window	10	10
Scanner positioning error in azimuth	6	
Pointing error due to scanner wobble of 25 μrad		3
Total (RSS of individual)	24.3	23.7
Contribution from structural components (2797 3.5.4.2)	20	20
Total (Combined optical and structural)	31.5	31

Table 9) The nadir and azimuth angle error budgets to meet MSFC-RQMT-2797 3.2.1.1 and 3.2.1.2.

5.5 Instrument attitude knowledge
5.5.1 Requirements
These are documented in MSFC-RQMT-2797 3.2.1.4, Instrument Attitude Accuracy and 3.2.1.5, Instrument Attitude Resolution which state:

"The instrument knowledge of its attitude shall be better than 0.05 degrees (RMS) over a nine hour period assuming no initial condition errors"

and

"The instrument attitude resolution shall be less than or equal to 100 microradians."

5.5.2 Discussion

The SIGI GPS/INS that is to be flown as part of the SPARCLE payload is specified to meet these requirements when provided with continuous GPS satellite coverage. There are two issues associated with this:

1) Initialization of the INS portion of the SIGI unit.
2) Quality of the solution when adequate GPS satellite coverage is not available.

These issues will be addressed further in Section 6.

5.6 Signal to noise ratio
5.6.1 Requirement
This is requirement 3.2.1.8 from MSFC-RQMT-2797 which states :

"The Signal to Noise Ratio over the line of sight velocity search bandwidth equivalent to the horizontal velocity search bandwidth shall be greater than -7.2 dB for the conditions defined in section A.6 of MSFC-RQMT-2828."

Where section A.6 of MSFC-RQMT-2828 states:

"The following parameters were assumed in the calculation of the aerosol backscatter sensitivity requirement given in item 9 of Table 1, and any revisions to these should be used only after consultation with the PIs. It should be noted that the calculation assumed a spherical earth, and for purposes of verification appropriate changes may be made due to latitudinal effects of a more realistic earth shape.

Range to aerosol target = 348 km (assumes spherical earth)
Aerosol target altitude = 1 km above ground level
Nadir angle at target = 31.56 deg. (assumes spherical earth)
Vertical resolution of processed data = 250 m
1-way intensity transmission through atmosphere = 0.84
Horizontal wind velocity search space = ±10 m/s
Single shot velocity estimate
Probability of estimate being good = 0.5"

5.6.2 Analysis
For the conditions provided above and the additional parameters documented in Table 10)

Subsystem	Parameter	Value
Transceiver (CTI)	Wavelength	2.051 μm
Transceiver (CTI)	Pulse energy	100 mJ
Transceiver (CTI)	Pulse length (FWHM)	0.17 μs
Transceiver (CTI)	Receiver efficiency	0.25
Optics (UAH)	Optics clear aperture diameter	0.233 m
Optics (UAH)	Transmit beam $1/e^2$ diameter	0.2 m
Optics (UAH)	Optics transmission	0.64
Optics (UAH)	Wavefront aberrations (mainly coma)	0.69
System	Truncated/untruncated correction	0.53

System	Misalignment efficiency	0.622
Optics (UAH)	Polarisation efficiency	0.9
System	Margin	0.5

Table 10) Parameters used in the SNR analysis.

we obtain a system efficiency, including margin of 0.11 and a searchband SNR of –7.7 dB. This corresponds to a β(50%) sensitivity of 5.8 x 10^{-6} /m-sr if a Capon velocity estimator is used (b0=75.36, alpha=1.08, gamma=17.45, chi=0.568, g0=18.25, epsilon=1.8, delta=0.765, mu=0.301). This does not meet the requirement in MSFC-RQMT-2797.

This can be traced to a discrepancy in the output diameter $1/e^2$ radius from the telescope. There is an optimum value for this radius and for the SPARCLE clear aperture of 0.233 m this needs to be 0.1867 m. The diameter in the table is consequently too large and results in a lowering of the truncated/untruncated correction factor. The diameter in the table is the optimum diameter for a 25 cm clear aperture.

5.7 Round trip pointing jitter

5.7.1 Requirement

The round trip pointing jitter requirement is 3.2.1.10 from MSFC-RQMT-2797 which states:

"The instrument pointing stability shall be less than 6 microradians (one sigma) over a 4 millisecond time period."

5.7.2 Discussion

The round trip pointing jitter is a critical requirement. It directly affects the sensitivity of the lidar instrument. Figure shows how the lidar efficiency falls off as a function of the lidar jitter during the round trip time. Any jitter of the lidar, including spacecraft motion, during the round trip time contributes to this loss in efficiency.

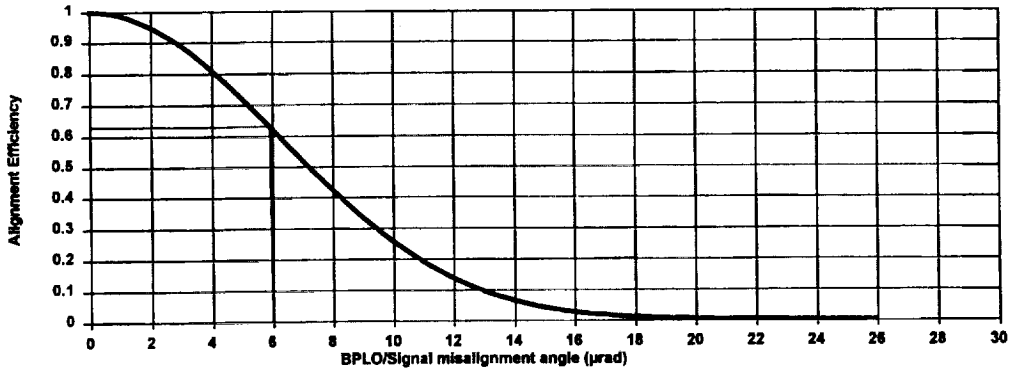

Figure 3. The lidar system efficiency dependence on jitter during the signal round trip time.

5.7.3 Round trip pointing jitter budget

Table lists currently identified sources of jitter and their magnitude.

Parameter	Allocated amount
Laser jitter (pulse to pulse at telescope output)	1 μrad
STS drift	2.8 μrad max. (< 0.04 deg/sec deadband rate)
Optical subsystem jitter	3 μrad
Scanner stability	4 μrad
Other sources	1.5 μrad
RMS Total	6 μrad

Table 11) The round trip pointing jitter budget

Note that the requirement is 6 μrad jitter over a 4 ms signal round trip time. This is to ensure that the instrument will work at the maximum orbit height of 350 km. At 300 km the round trip time is 2.3 ms and this reduces the contribution from orbiter drift to 1.6 μrad permitting the 'other sources' contribution to increase to 2.2 μrad.

6. PERFORMANCE ANALYSIS

The overall performance of the SPARCLE mission is directly linked to the accurate knowledge of position, velocity, attitude and timing. The SPARCLE instrument is currently carrying a Honeywell SIGI GPS/INS unit to provide this data however a number of concerns have arisen with this approach.

6.1 SIGI performance

The SIGI unit has the following performance specifications.

Parameter	SPS Mode	PPS Mode
Position	500m SEP each axis	100 - 150 m SEP each axis
Velocity accuracy	3 m/s RMS each axis	0.3 m/s 1 sigma each axis
Attitude accuracy	0.05 deg RMS cumulative for 9 hour time span	
Attitude rate error	0.01 deg/hour per axis	
Attitude drift rate	0.05 deg each axis per 9 hours 0.01 deg/hr maximum	
Attitude readout precision	~95 microradians (15 bit A/D, Pi rad full scale.)	
Update rates	50 Hz or 64 Hz	
Timing clock accuracy	155 ns	100 ns

Table 12) SIGI performance (see text)

The use of the PPS GPS mode to reduce position errors on orbit has not been demonstrated with the SIGI unit. There was an on-orbit test but due to a 1553 communications problem, no data was collected. There was another test on STS 91 (May 21st) . Until data from this test is fully analysed Honeywell is not prepared to predict what the performance in PPS mode will be, the numbers in

the PPS column are preliminary estimates provided by them that they will not defend. The analyses referred to here do not use the PPS estimates.

The attitude error of the SIGI unit consists of two components, a random walk component and a drift. The drift component is usually the dominant error but Honeywell does not characterise or select individual units according to their error characteristics. The random error component is the one of greatest concern in ensuring that the velocity accuracy requirement in the SRD can be met. Honeywell indicated that this error is highly dependent on temperature and that characterisation of the error on a bench prior to use would be of no benefit unless the

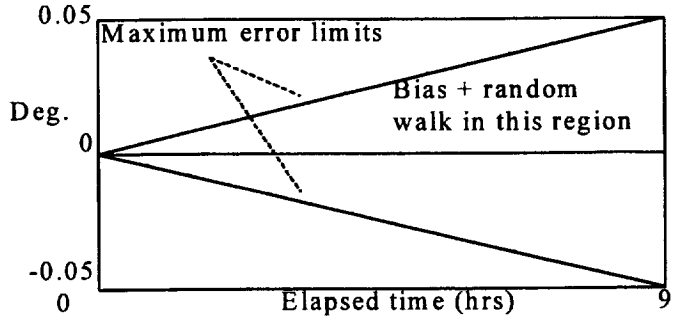

Figure 4) Representation of SIGI time dependent attitude error

environment the INS/GPS was operated in was strictly controlled. Figure (4) schematically shows the definition for the errors provided by Honeywell.

6.1.1 Concerns with the SIGI
There are a number of concerns associated with use of the SIGI unit.

6.1.1.1 SIGI performance
The documented position and velocity performance specifications are inadequate to meet the science requirements without ground post-processing of the data. Improved position and velocity data can be obtained in post processing using additional data. This was the approach taken by the SLA, Shuttle Laser Altimeter experiment. A second source of position and velocity data is the MAGR unit on board the orbiter. The MAGR unit provides 0.1 m/s 3 sigma velocity, 32m vertical, 36m horizontal 3 sigma position error but MAGR data is not always available.

The time dependent drift specification puts a limitation on the length of time between reinitialisations to ~30 minutes. This will be discussed further in the next section.

6.1.1.2 SIGI INS initialisation
The SIGI unit is designed to be initialised on the ground and remain on through launch. This is not available to a Hitchhiker payload and so we will need to initialise the INS portion of the SIGI once

we are on orbit. A method to initialise the unit was developed. It consists of waiting for an orbiter IMU alignment and then providing the SIGI unit with the current (known) orbiter attitude. Once initialised the orbiter can roll over into the –ZLV attitude and the SPARCLE instrument can be used to refine the attitude knowledge. A key concern here is that the SIGI unit must be aligned to the orbiter IMU and to the SPARCLE instrument sufficiently well that the initial signal collected by the SPARCLE lidar is within the capture bandwidth of the SPARCLE receiver. The SPARCLE receiver is designed to accommodate up to a 1 deg error. The Hitchhiker carrier system permits can alignment to +/- 0.1 deg. This enables the following preliminary alignment budget to be assessed:

Parameter	Alignment degrees
SIGI unit to can structure	0.2
SIGI can to cross bay bridge	0.1
Optics canister to cross bay bridge	0.1
Cross bay bridge to orbiter	TBD
Can movement during launch	TBD
Optical axis to optics canister	0.1
Orbiter thermal distortion on orbit	<< 0.1
Orbiter IMU to Orbiter	0.1
RSS total (excluding TBDs)	0.31

Table 13) SIGI INS alignment budget

At the present time most of the alignment parameters documented in the table must be regarded as preliminary due to insufficient verification of these values.

The lidar determines the SIGI INS offset by analysing the Doppler shifted ground velocity from an 8 point scan. The science co-investigator, Dr. Emmitt has demonstrated a working proof of concept attitude extraction algorithm for this purpose.

The SIGI INS drift specification requires that one of these lidar calibration scans be conducted every 30 minutes of operation. A number of issues potentially limit the usefulness of the lidar for updating the SIGI:

a) The calibration ideally needs to be conducted over land.
b) Cloud obscuration may prevent the scan from being conducted.

The calibration scan oversamples to try to limit the effect of cloud cover. The first calibration scan for the initial determination of the SPARCLE SIGI offsets must be successful. If subsequent scans are not successful then the instrument will still be able to collect data but the INS uncertainty will mean that reduction of the velocity error to the 1-2 m/s level would be unlikely. Subsequent post processing and access to secondary sources (cloud track winds) may enable subsequent improvement but should not be relied upon.

6.1.1.3 GPS signal accessibility
It is likely that the GPS antennas on the orbiters will be unavailable to payloads by the time SPARCLE flies as they will be designated criticality 1. Two methods were identified to potentially overcome this:

a) use a SPARCLE specific antenna.

This is still under investigation. The issues relating to this have been addressed in the pointing knowledge document.

b) Obtain position, velocity data from the orbiter and just use the SIGI unit for SPARCLE attitude determination.

The MAGR position and velocity data can be made available to the SPARCLE instrument while on orbit. Unfortunately the data will be time delayed by between 2- 7 seconds. The delay on this data has only been conveyed by JSC verbally at this point in time. Initially the delay was specified as being 2 s which made the data potentially useful but as the delay increases it becomes difficult to assess reliably the value (if any) of the data as the orbital dynamics of the SPARCLE mission becoming important.

6.2 Summary

The current SPARCLE design requires continuous GPS coverage with post processing of the data in order to meet the position and velocity accuracies required to demonstrate wind velocity measurement with an accuracy of 1-2 m/s. The attitude knowledge to meet these velocity accuracies requires the use of the lidar as an attitude calibration sensor. The use of the lidar as an attitude calibration sensor will result in some collected data not meeting the velocity accuracy requirements.

DRAFT

SPARCLE
APPENDIX E INPUTS
NASA HITCHHIKER PROGRAM
CUSTOMER PAYLOAD REQUIREMENTS (CPR)

HITCHHIKER PROGRAM: Hitchhiker Payload

CUSTOMER PAYLOAD: SPARCLE

CUSTOMER: MSFC - Attention Jimmie Johnson (JA51)

DATE: 8-14-98

CUSTOMER APPROVAL NASA APPROVAL

TABLE E.1
CUSTOMER DATA

Customer Payload Name:	SPAce Readiness Coherent Lidar Experiment
Customer Payload Acronym:	SPARCLE
Customer Name, Address, And Telephone Number:	SPARCLE Project Office Mail Code JA51 (Attn: J. Johnson) MSFC, AL 35812 (256)544-0852 or (256)544-7455

Names And Phone numbers Of Customer contacts:

Program Manager:	Ray Arnold (MSFC-HR01) (256)922-5861
Payload Manager:	Jimmie Johnson (MSFC-JA51) (256)544-0852 or (256)544-7455
Project Engineer:	Allen Bacskay (MSFC-EJ43) (256)544-0993 or (256)544-7406
Safety:	Norm Batson (MSFC-CR80) (256)544-1504
Electrical:	Eric Corder (MSFC-EB53) (256)544-3473
Software:	Geoffry Hintze (MSFC-EB43) (256)544-3792
Mechanical:	Deborah Bagdigian (MSFC-ED52) (256)544-7092
Thermal:	John Sharp (MSFC-ED63) (256)544-5156
Operations:	Nelda Hiley (MSFC-EO27) (256)544-5774
Science:	Tim Miller (MSFC-HR01) (256)922-5882

Calendar Interval During Which Flight Is Requested:	March of 2001
Earliest date At Which Qualified Payload Will Be Available:	November of 2000

2.0 PAYLOAD DESCRIPTION

The SPARCLE payload is a coherent Doppler lidar for the measurement of wind velocity. It consists of three physically separate assemblies; the lidar instrument transmitter, telescope and receiver subassemblies will be carried in a Hitchhiker canister, referred to as The Optics Canister. The Optics Canister will be equipped with a standard Motorized Door Assembly (MDA). The computer, mass storage devices, electronics receiver and a portion of the power distribution unit will be housed in a second canister referred to as The Computer Support can. A third can will house the other portion of the power distribution unit, support electronics for the scanner and laser transceiver in addition to the GPS/INS unit. The third can is referred to as The Transceiver Support can. The SPARCLE system will also include a fluid loop pump and radiator that will be mounted to the top of the Cross Bay Bridge.

PAYLOAD FUNCTIONAL DESCRIPTION AND METHOD

The following is a brief functional description of the payload covering methods, techniques, and hardware elements used to obtain the mission objectives. The instrument functions are divided into three canisters, the Optics Canister which contains the optical subsystem, the Computer Support Can which contains a portion of the power supply, computer and mass storage devices and the Transeiver Support Canister which contains the support electronics for the scanner and laser transceiver and the second portion of the power supplies. The three canisters are connected by umbilical cords that provides power and data connections between the three cans. A representation of the integrated SPARCLE system on the GSFC provided Cross Bay Bridge is shown in Figure 1. A schematic representation of the major lidar elements in the Optics Canister is given in Figure 2 and a block diagram of the instrument's major subsystems is shown in Figure 3.

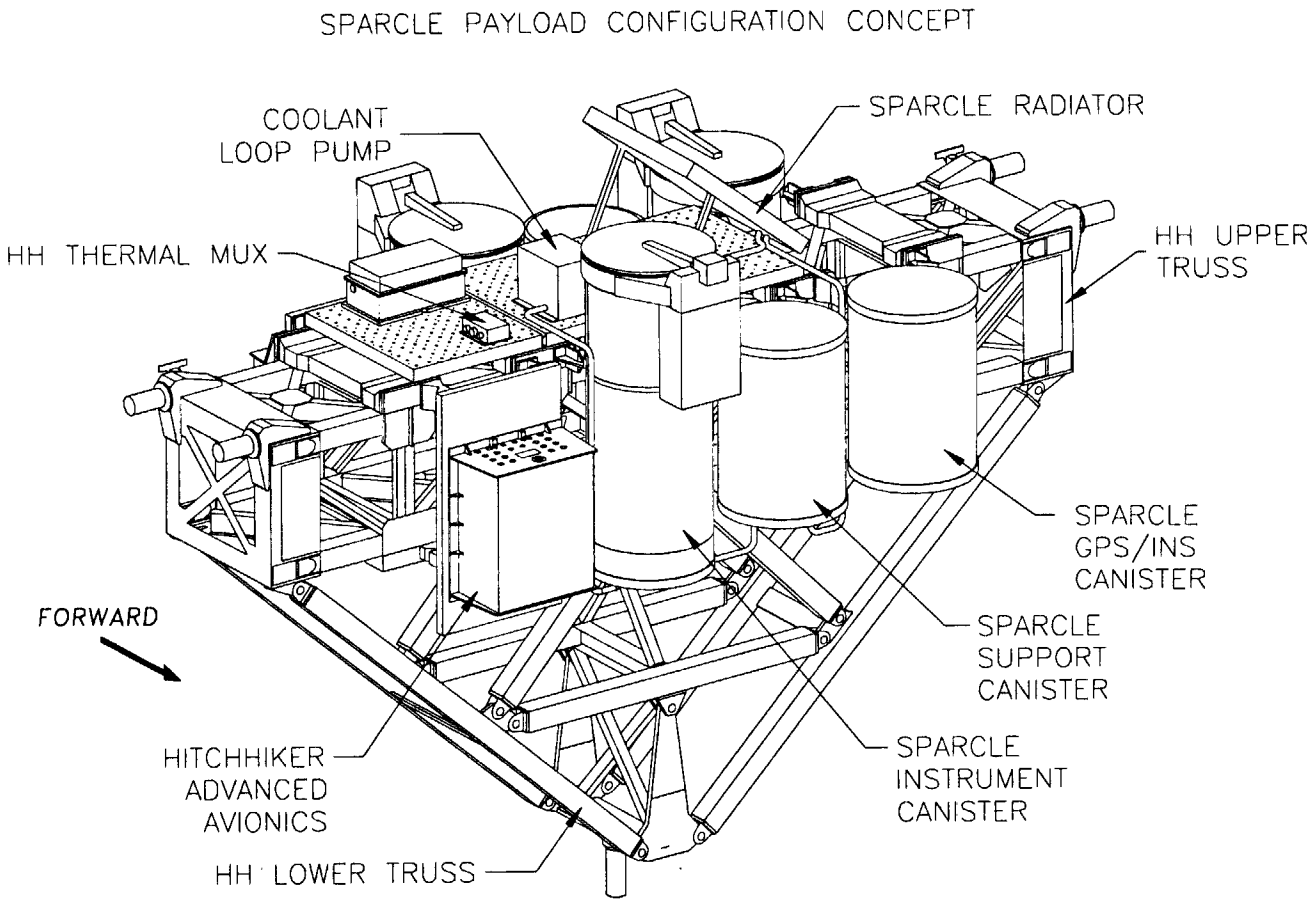

FIGURE 1 SPARCLE CROSS BAY BRIDGE CONFIGURATION

A4.5

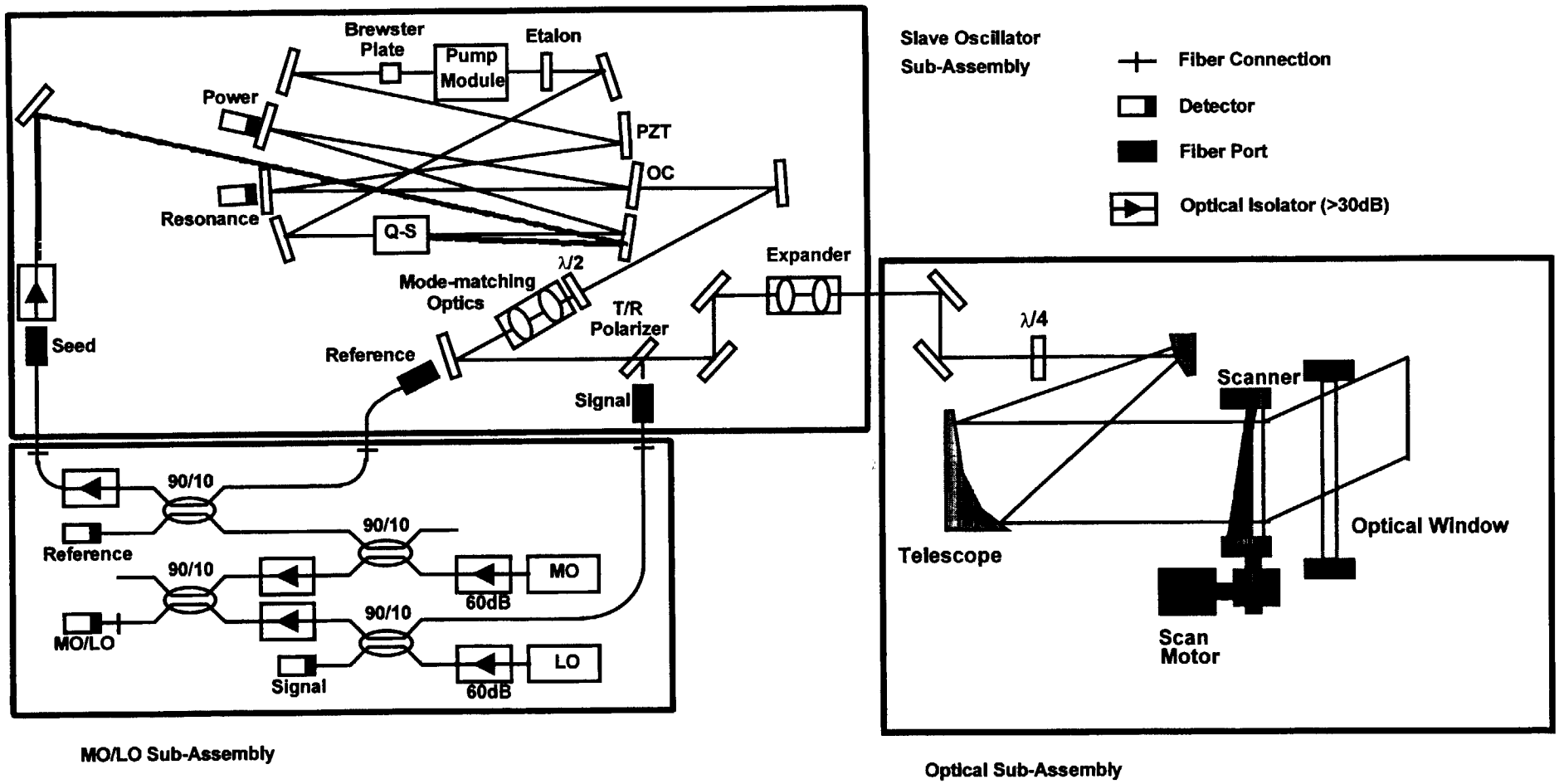

FIGURE 2 OPTICAL TRAIN COMPONENTS

SPARCLE System Block Diagram

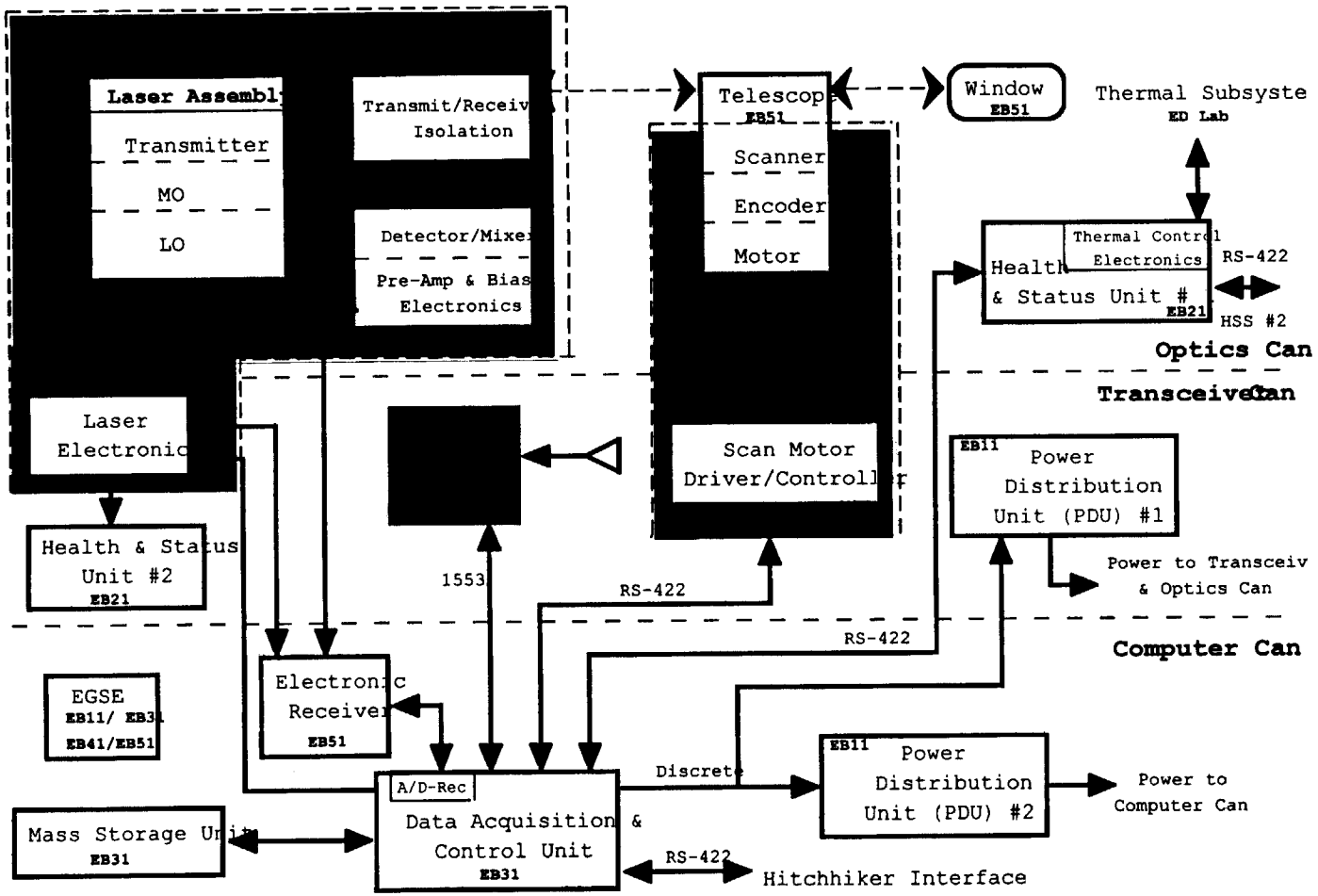

A4.7

Principle Of Instrument Operation

The lidar instrument contains the following main elements, a transceiver, a telescope, a scanner, and an electronics receiver. The transceiver consists of three lasers and an optical detector for the return signal together with ancillary detectors for monitoring performance and optics associated with beam routing. The three lasers are the master oscillator (MO), local oscillator (LO) and slave oscillator (SO) respectively. The master and local oscillator lasers are continuous wave (cw) lasers whilst the slave oscillator is a pulsed laser. All three use solid-state Tm,Ho:YLF as the lasing material.

The MO is used to control the frequency characteristics of the SO. The SO produces linearly polarized, 0.1 J, 0.15-0.2 μs long single mode pulses at a nominal wavelength of 2.051 μm and a pulse repetition frequency of 6 Hz. The beam from the laser passes through a polarizing beam splitter (T/R polarizer in Fig. 2) which acts as a transmit/receive switch to separate the outgoing beam from the incoming signal beam. The beam diameter is then expanded to match the input diameter of the telescope. The beam passes through a quarter-wave plate ($\lambda/4$ in Fig. 2) that changes the polarization to circular. It is then expanded by the telescope to a nominal 25 cm diameter collimated beam that fills the aperture of the Si wedge scanner. At this point the beam direction is towards nadir. On passing through the wedge, the beam is refracted 30 deg off of nadir, passes through the optical window and exits the Optics Canister. By rotating the wedge, the beam can be made to sweep out a cone and when this cone pattern is combined with the forward motion of the Space Transportation System (STS) then the beam pattern on the ground describes a cycloid.

As the beam is transmitted through the atmosphere, a small fraction is backscattered by aerosols, clouds, and the earth's surface. The backscattered signal is Doppler frequency shifted due to the relative velocity of the target and the spacecraft.

The backscattered signal is collected by the telescope and passes back through the telescope elements to the quarter-wave plate which changes the polarization of the beam back to a linear polarization orthogonal to that of the transmitted beam. This change in polarization causes the return signal to be reflected at the transmit/receive switch beam splitter. The signal is then coupled into a fiber optic cable, combined with the signal from the local oscillator laser and focused onto the InGaAs signal detector. The heterodyne beat signal frequency between the local oscillator and the signal beam is amplified and digitized by the receiver and A/D electronics.

This heterodyne beat signal has a frequency equivalent to the Doppler shift due to the combination of the spacecraft, earth rotation and wind velocities (~+/- 4 GHz for the SPARCLE configuration without consideration of pointing errors). To reduce the bandwidth requirements on the detector and its associated electronics, the offset frequency between the local oscillator and master oscillator is varied as a function of orbit

location, instrument attitude and scanner azimuth angle. This variation results in reducing the heterodyne beat frequency to that due solely to contributions from the wind velocity and instrument laser frequency tuning and pointing errors. The digitized signal is stored together with appropriate housekeeping and health and status data and downloaded to the ground as frequently as possible. Some of the data will also be used by the instrument to determine roll, pitch and yaw bias errors between the instrument and the GPS/INS. These bias errors will then be used to update the laser frequency-tuning algorithm. All of the data will be stored on the instrument for extraction and analysis after the instrument is recovered.

On the ground, the data are run through a velocity estimator to convert the signal frequency into a line of sight velocity vector. Velocity vectors from individual shots at different perspectives can be combined to produce a vector or vectors representative of the wind field. These wind products will be used by members of the NWP and Global Climate Change communities to assess the value of the instrument and each of its different operational modes.

Modes Of Operation

The instrument has four modes of instrument functional operation (Table 1.): TCS, Stabilization, Standby and Operational.

On power up the instrument automatically enters the TCS mode. This mode is used to bring the transceiver fluid loop to within the temperature range required for laser operation. After the PCM reservoir has been exhausted during the operational mode then the instrument also uses this mode to resolidify the PCM material. This mode can also be used for INS/GPS characterisation and data processing/downlinking opportunities.

The Stabilization mode is entered after the transceiver cooling loop has been brought to within the temperature range required for laser operation. The master and local oscillator lasers within the transceiver are powered on so that their output characteristics (frequency stability, mode quality) can stabilize. The duration of this mode is dictated by the time required to stabilize these lasers and will be at most 30 minutes in duration.

The Standby mode is entered after the transceiver cooling loop has been brought to within the temperature range required for operation. The master and local oscillator lasers within the transceiver remain powered on so that their output characteristics (frequency stability, mode quality) can remain stabilized. This mode is used to hold the instrument in a state of readiness for collecting data. This mode may also be used to 'hold' the instrument in a state of readiness between Operational mode data collecting opportunities.

In the Operational mode the Operational Science Modes (OSMs) are performed. The Operational mode consists of a nominal twelve OSMs listed in Appendix 1. These modes identified in the Appendix are labeled and identified from a science data perspective.

From an operational perspective these OSMs can be broken down into the four groups listed in Table 1. OSM 6 is used to provide fine calibration of the SPARCLE GPS/INS and is conducted at the beginning and end of every Operational mode as well as at nominal 30 minute intervals throughout the Operational mode. The maximum duration of an Operational mode is limited by the thermal requirements in the Optical Canister. The local, master and slave oscillators require a water/methanol coolant mixture at a temperature of 20.3 +/- 2 deg C and during Operational mode the transceiver dissipates more power than can be radiated from the canister. To overcome the heat rejection problem, a phase change material is used to store the excess heat which is then dissipated after completion of an Operational mode. The phase change material is sized to permit 90 minutes of uninterrupted Operational mode.

Transition from functional mode to functional mode, between OSMs and overall timing of the instrument operation is controlled by either a script that can be uploaded from the ground or by direct control from the ground.

Mode	Why?	Duration			How Entered	Attitude
		Min.	Max.	Total		
TCS	Stabilize fluid loop temperature (warm-up or PCM resolidification). Collect INS/GPS data.	Minutes	12 hrs (thermal) as much as possible (science)	As much as possible	Automatically entered on power up. Can also be entered from Stabilization or standby modes.	-ZLV desired (except during IMU updates) -ZDS desired during PCM recovery no deadband or rate requirement
Stabilization	Stabilize output characteristics of the MO and LO lasers	30 mins.	30 mins.	Depends on scheduling	From TCS	-ZLV required no deadband or rate requirement
Standby	Ready to operate waiting for science opportunity	0 mins.	As little as possible	Depends on scheduling	From stabilization or from operational mode	-ZLV required no deadband or rate requirement
OSM 1A	Science Data Collection	30 mins.	90 mins.	Minimum of 3 hrs required	From standby or from another operational mode	-ZLV, 0.1 deg deadband, <0.04 deg/sec deadband rate (total all axes) arbitrary but known VV
OSM 1B	Science Data Collection	30 mins.	90 mins.	Minimum of 1.5 hrs required	From standby or from another operational mode	30 deg roll from –ZLV, 0.1 deg deadband, <0.04 deg/sec deadband rate (total all axes) +/- XVV
OSMs 2A,2B,3A,3B, 3C,4A,4B,4C, 5	Science Data Collection	30 mins.	90 mins.	Minimum of 16.5 hrs required	From standby or from another operational mode	-ZLV, 1 deg deadband, <0.04 deg/sec deadband rate (total all axes) arbitrary but known VV
OSM 6	Fine Calibration of SPARCLE INS	2 mins.	5 mins.	Minimum of 3 – 5 hrs required	From standby or from another operational mode	-ZLV, 0.1 deg and then 1 deg deadband, < 0.04 deg/sec deadband rate (total all axes) arbitrary but known VV. Strongly desire no thruster firings in several ~20 second periods

Table 1: Instrument Functional Modes.

A4.13

2.1 MISSION OBJECTIVES

The objectives of the SPAce Readiness Coherent Lidar Experiment (SPARCLE) are:

1) to demonstrate that coherent Doppler wind lidar (CDWL) technology is feasible and scalable for providing the desired global wind measurements of future science and operational missions, 2) to validate wind measurement performance prediction models for use in assessing proposed future follow-on missions, and 3) to measure characteristics of the atmosphere, clouds, and earth surface for optimum design of future missions.

The first objective reveals that SPARCLE is primarily a technology demonstration mission, rather than a science mission. The results of SPARCLE and extrapolation of those results to future missions are expected to show that CDWL technology is the correct path for NASA, NOAA, DOD, and other agencies to obtain the wind measurements they desire. Attributes of the desired wind measurements include good horizontal and vertical resolution and coverage, low bias, horizontal "vector" measurements, and accuracies of the horizontal vectors of 1-2 m/s. Practical requirements of a space-based sensor include low mass and volume, long life, and minimal need for power and heat removal.

The second objective arises from the relatively high cost of space missions, and the need to correctly model the performance of proposed sensors so that they do what they are advertised to do. Despite 30 years of ground-based and airborne wind measurements using CDWL technology, the launch forces, space environment, large range to target, and huge Doppler shifts of a space mission argue for a technology demonstration mission to confirm performance prediction models of space-based CDWL sensors.

The third objective will allow the lidar size (sensitivity), scan pattern, calibration techniques, and data processing to be optimized for future missions. The vantage point, earth coverage, and unprecedented similarity to future operational missions will allow SPARCLE to deliver valuable atmosphere, cloud, and earth data for this optimization.

2.4 OPERATIONS SCENARIO

2.4.1 OPERATIONS DESCRIPTION

A "top level" description of SPARCLE operations will be defined in this section. More detailed information on SPARCLE operations is defined in Section 4. Details for orbiter attitudes/durations for the various modes defined in this Section are found in Table 1. Specific pointing requirements are further defined in Section 4.

Nominally, SPARCLE will be controlled via "script" commands that are stored within the instrument or sent from the ground. During the initial phase of the mission, post orbiter insertion, it is required to have power applied to SPARCLE from the Hitchhiker Avionics in order to have the survival heaters engaged.

Upon power being supplied to SPARCLE, the Power Distribution Unit (PDU) will supply power to the Command and Data Management Subsystem (CDMS) which will perform the nominal "boot-up" and self test sequences. After the initial power up sequence, the instrument will be downlinking Health and Status data from the Health and Status Subsystem (HSS) over the low rate data stream at a 1 hertz rate. Upon successful completion of the initial self tests, the instrument will proceed directly into the TCS mode during which time the fluid loop temperature will be warmed to the required value for laser operations. During this mode, the SPARCLE unique INS/GPS will be powered and data will be gathered for analysis to determine the offset between the orbiter IMU and SPARCLE INS with repsect to attitude (details in Section 4). Once the fluid loop temperature has stabilized, the instrument progresses into the Stabilization mode. During this mode, the MO and LO lasers are powered and they will require 30 minutes maximum duration to achieve frequency stability. At this time, the instrument will be ready to perform science gathering operations. Depending upon the "windows of opportunity" the instrument would either enter the Standby mode, or go directly into the Operational mode. The Standby mode would be entered if there were not sufficient targets of opportunity to obtain useful data in the near term. Once in the Standby mode, the instrument is capable of proceeding to the Operational mode upon receipt of a command to do so.

At the end of an Operational mode, the instrument would then return to Standby or TCS mode depending upon near term targets of availability, and the state of the PCM within the system. If telemetry determines that there is not sufficient PCM left to conduct any OSM's, then the instrument will be placed in TCS mode in order to recover the PCM. Even if there was sufficient PCM, the instrument could still be put into the TCS mode if it was desired due to lack of available targets of opportunity.

The SPARCLE operations will be worked closely with mission timeliners during the mission to ensure that operations are maximized over areas that provide the greatest scientific return. These areas will change during the mission due to dynamic weather conditions.

TABLE E.2
PAYLOAD ASSEMBLIES

Assembly Name	Optics Can	Computer Support Can	Transceiver Support Can
Weight	296 lb	211 lb	195 lb
Size			
(X in)	19.75 thru	19.75 thru	19.75 thru
(Y in)			
(Z in)	33.25	33.25	33.25
Mount Type	bolted	bolted	bolted
FOV (deg)	30 deg. Half angle	N/A	N/A
Operating Temp			
(min)	0 deg C	-20 deg C	-20 deg C
(max)	25 deg C	40 deg C	40 deg C
Non-Operating Temp			
(min)	-20 deg C	-40 deg C	-40 deg C
(max)	40 deg C	60 deg C	60 deg C
Storage Temp			
(min)	15 deg C	15 deg C	15 deg C
(max)	30 deg C	30 deg C	30 deg C

OPTICS CANISTER

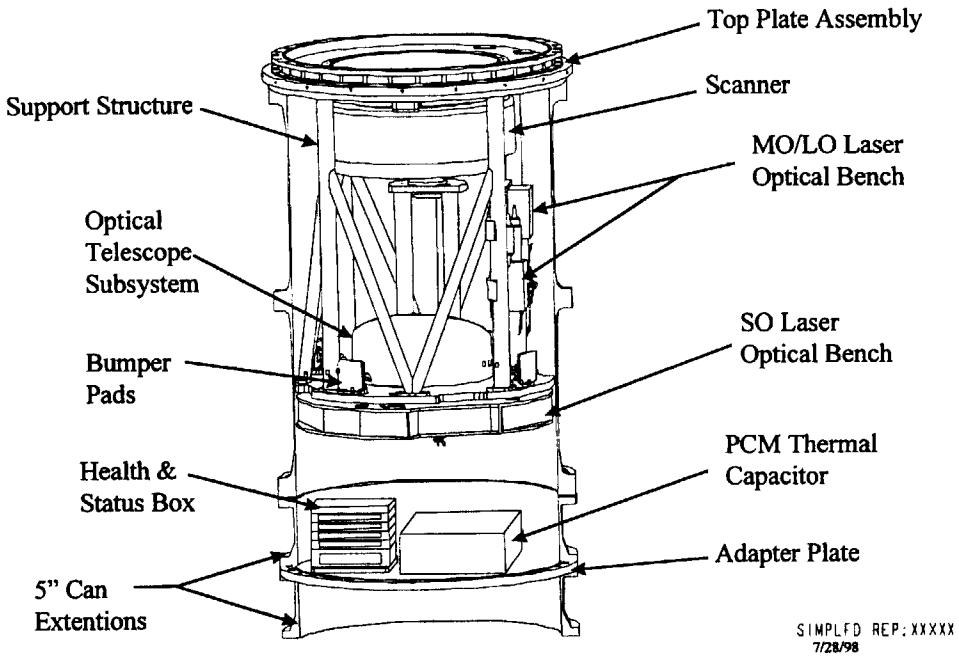

FIGURE 4 OPTICS CAN MECHANICAL LAYOUT

Computer Support Can

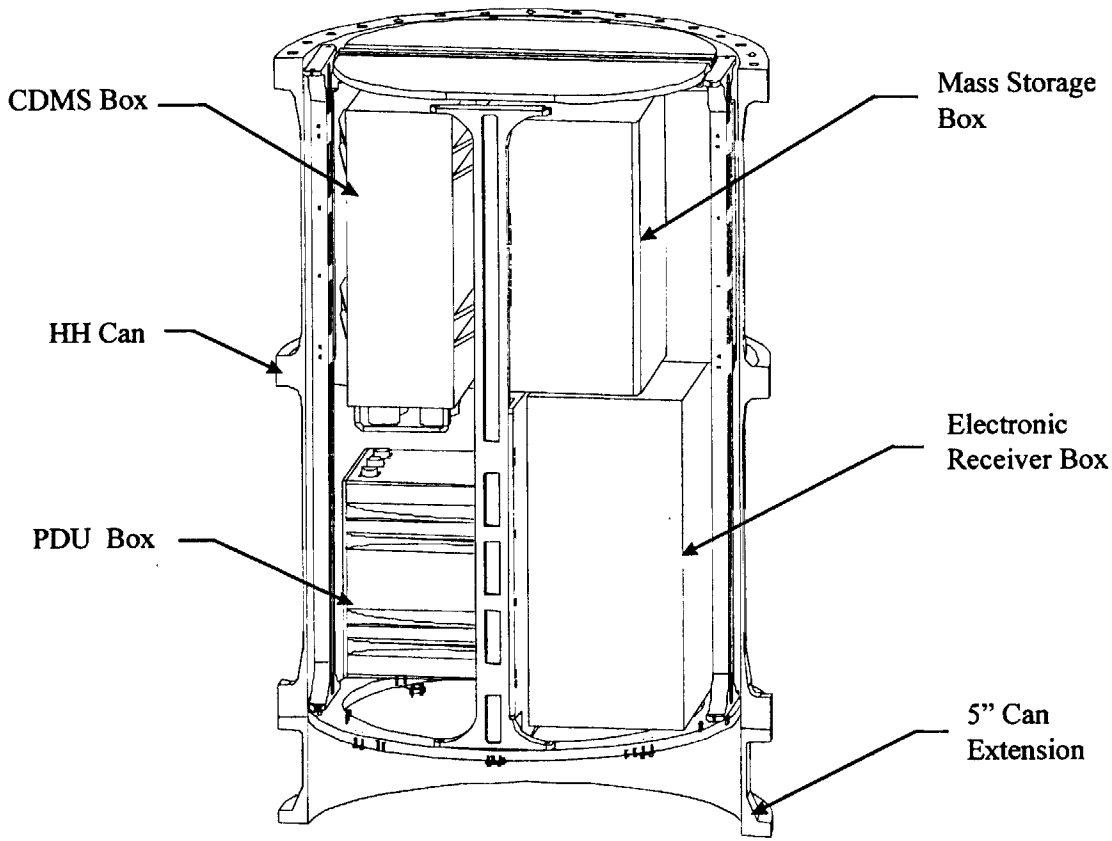

FIGURE 5 COMPUTER SUPPORT CAN MECHANICAL LAYOUT

A4 20

Transceiver Support Can

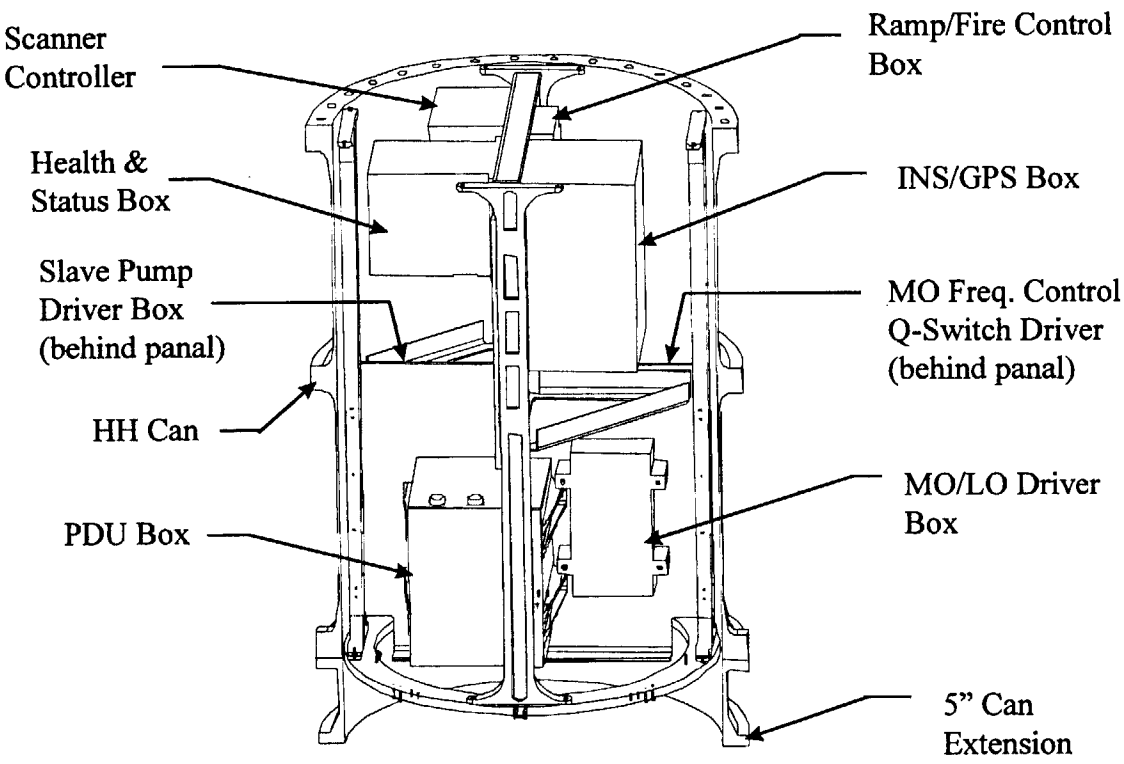

FIGURE 6 TRANSCEIVER SUPPORT CAN MECHANICAL LAYOUT

A4 21

3.0 PAYLOAD REQUIREMENTS FOR STANDARD SERVICES

3.1 Carrier to Payload Electrical Interfaces

TABLE E-3.1.1
STANDARD AVIONICS PORT REQUIREMENTS

PORT NUMBER:	Optics can
SIGNAL INTERFACE CONNECTION # OF BI-LEVEL COMMANDS:	4
NUMBER OF THERMISTORS:	3
ASYNCHRONOUS UPLINK:	none
ASYNCHRONOUS DOWNLINK:	none
MEDIUM RATE ku BAND DATA RATE:	none
ANALOG DATA:	1
IRIG-B GMT:	none
GMT MIN:	none
CREW PANEL SWITCHES:	none
ORBITER CCTV INTERFACE:	none
PORT TO PORT INCTERCONNECT REQ'D:	yes
to route undedicated wire in second standard interface port assigned to same customer!	
POWER INTERFACE CONNECTION	
POWER CIRCUIT A - AMPS MAX	10 Amps
POWER CIRCUIT B - AMPS MAX	10 Amps
POWER CIRCUIT HTR- AMPS MAX	5 Amps
TOTAL ENERGY REQUIRED	TBD KWH

The two power circuits will not be routed internal to the optics can. These circuits will be utilized to power the pump that will be located on top of the cross bay bridge.

OTHER	Hitchhiker Motorized Door Assembly**

** Please note: we would like access to a nadir viewing shuttle bay camera during modes of data collection. The exact settings of the camera will be worked as more knowledge of the mission timeline become available.

TABLE E-3.1.1-1
STANDARD AVIONICS PORT REQUIREMENTS

PORT NUMBER:	Computer Support Can
SIGNAL INTERFACE CONNECTION # OF BI-LEVEL COMMANDS:	4
NUMBER OF THERMISTORS:	3
ASYNCHRONOUS UPLINK:	max @ 1200 baud
ASYNCHRONOUS DOWNLINK:	max @ 1200 baud
MEDIUM RATE ku BAND DATA RATE:	max @ 1 MB/s
ANALOG DATA:	1
IRIG-B GMT:	yes
GMT MIN:	yes
CREW PANEL SWITCHES:	none
ORBITER CCTV INTERFACE:	none
PORT TO PORT INCTERCONNECT REQ'D:	yes
to route undedicated wire in second standard interface port assigned to same customer!	
POWER INTERFACE CONNECTION POWER CIRCUIT A - AMPS MAX POWER CIRCUIT B - AMPS MAX	 10 x 2 = 20 Amps 10 x 2 = 20 Amps

POWER CIRCUIT HTR- AMPS MAX	5 Amps
TOTAL ENERGY REQUIRED	TBD KWH
OTHER	I/F To Orbiter GPS/ INS Data, Access to Orbiter PCD Comm. Data, Access To Orbiter MAGR Data

TABLE E-3.1.1-1
STANDARD AVIONICS PORT REQUIREMENTS

PORT NUMBER:	Transceiver Support Can
SIGNAL INTERFACE CONNECTION # OF BI-LEVEL COMMANDS:	0
NUMBER OF THERMISTORS:	3
ASYNCHRONOUS UPLINK:	none
ASYNCHRONOUS DOWNLINK:	none
MEDIUM RATE ku BAND DATA RATE:	none
ANALOG DATA:	1
IRIG-B GMT:	none
GMT MIN:	none
CREW PANEL SWITCHES:	none
ORBITER CCTV INTERFACE:	none
PORT TO PORT INCTERCONNECT REQ'D:	yes

to route undedicated wire in second standard interface port assigned to same customer!

POWER INTERFACE CONNECTION

POWER CIRCUIT A - AMPS MAX	10 x 2 = 20 Amps
POWER CIRCUIT B - AMPS MAX	10 x 2 = 20 Amps
POWER CIRCUIT HTR- AMPS MAX	5 Amps
TOTAL ENERGY REQUIRED	TBD KWH
OTHER	Orbiter GPS Antenna I/F To Orbiter GPS/ INS Data, Access to Orbiter PCD Comm. Data, Access To Orbiter MAGR Data

The payload will meet the standard electrical interface requirements (including connectors, pin assignments, impedance, signals, levels, etc.), specified in the CARS with several addition interfaces required. The SPARCLE instrument requires very precise attitude and position information in order to proprely demonstrate the CDWL technology. Currently, there are several options being pursued in order to provide the information to the instrument. The only option that currently would allow SPARCLE to meet all of its requirements would mean having access to the shuttle GPS antenna. Data would be sent directly to the SPARCLE dedicated GPS in a manner similar to when the orbiter flies the Space Integrated GPS/INS System (SIGI) as a DTO. This allows near continuous position update to the SPARCLE GPS/INS which then provides a more refined attitude solution which would be utilized by the SPARCLE CDMS for pre-shot calculations. This SPARCLE unique GPS/INS unit will be located in the Transceiver Support Canister. The SPARCLE dedicated GPS/INS unit will also require access to the data from the orbiters IMU and MAGR receiveres during initialization of the SPARCLE GPS/INS. The transfer delay of the orbiter's IMU data to the SPARCLE payload needs to be minimized to maximize the performance of the SPARCLE payload and it is required not to exceed 30 seconds. Any delays greater than 30 seconds will adversley affect the capability of the instrument to perfrom. In addition to the three thermistors provided as a standard service, it is requested that payload obtain as many as possible additional thermistors (29) to be processed by the Hitchhiker thermal multiplexer. The SPARCLE payload will require two of the standard interface connections or "ports" for the carrier to payload electrical interface. For each of the ports, a copy of Table E-3.1.1 is filled in to show which of the standard electrical services will be required by the payload. Unused services will be left open circuited in the payload unless other termination is required by GSFC.

Canister to Canister Interfaces

The SPARCLE payload will require three additional signal interface connections (one per canister) along with three additional power connections (one per canister) to be utilized for routing signals and power between the optics, computer support, and transceiver support canisters. The signal interface connectors should include the capability of

interfacing to a maximum of five coax lines. The exact pin functions for these connectors will be provided as the design of the SPARCLE payload matures. One test connector for each canister is also required in order to support ground testing. These connectors could possibly be shared with hitchhiker for routing of the 29 thermistors to the hitchhiker thermal mux. Unused services will be left open circuited in the payload unless other termination is required by GSFC.

3.3 CARRIER TO PAYLOAD THERMAL INTERFACES/DESCRIPTION

The thermal control system is based around a 60/40 water/methanol fluid loop with a phase-change material (PCM) thermal capacitor/heat exchanger and external radiator. The loop will include a pump, the PCM heat exchanger, the laser subsystem, the top-plate radiator, external radiator and associated valves and fittings. A survival heater system will also be incorporated that will be thermostatically controlled and shall require power that is independent from the operational power of the experiment.

The water/methanol fluid lines are routed from the Optics canister to the pump enclosure and from the pump enclosure to the external radiator. The MPESS shall accommodate these lines with minimal thermal conductance to preclude localized hot spots or freezing.

The thermal control system for the Computer Support and Transceiver Support cans utilizes ammonia heat pipes to optimize heat rejection to the canister top plates. In addition, a survival heater system will be included that will be thermostatically controlled and shall require power that is independent from the operational power of the experiment.

All of the canisters will be uninsulated with a bottom insulating end cap.

3.4 GROUND OPERATIONS REQUIREMENTS

TABLE E.4

GROUND OPERATIONS REQUIREMENTS

a. Maximum/Minimum Allowed Storage Temperatures	30/15 deg C
b. Maximum/Minimum Allowed Relative Humidity	90/15 %

Please note that the 90% is for transportation only. The Laser needs a humidity controlled environment during timeframes during which the Laser will be operational (i.e < 50%).

c. Cleanliness Requirement For Payload	class 10K

d. Customer Supplied GSE — Sparcle C/O Unit

e. Requirements For Gases/Liquids — 60/40 H20/MeOH

Please note that dry nitrogen is required to backfill all canisters prior to launch. The water methanol mixture is required to fill the SPARCLE fluid system and may include a small portion of optishield corrosion inhibiter.

f. Requirements For Payload Servicing @GSFC — EMI Test, Integrated Thermal Vac Test, Functional Test w/ Hitchhiker ACE, Precise Alignment

f1. Requirements For Payload Servicing @ KSC — IVT*

*note: we need precision alignment of the optics can and the INS to ensure pointing knowledge

g. Requirements For Access During Orbiter Integration — alignment check

h. Requirements For Access On Launch Pad — N/A

i. Requirements For Post Landing Access — alignment check

j. Any Other Special Requirements — TBD

k. Sizes/Weights Of Items Required For Shipment To KSC — TBD

3.5 SAFETY

a. Contains Pressurized Volumes — yes

The optics can will be pressurized to 0.5 atm with dry nitrogen. The transceiver and computer support cans will be pressurized to 1.0 atm with dry nitrogen. The SPARCLE system a pressurized fluid loop with TBD MDP at this time.

b. Contains Radioactive Material — no

c. Contains Light Or RF Source — no

d. External Electric Or Magnetic Fields — no

e. External Electrically Charged Surface — no

f. External Hot Or Sharp Surface — no

g. Contains Toxic Material — no

h. Contains Outgassing Material — yes

The experiment will contain materials that outgas. The MSFC Materials and Process Laboratory will be responsible for providing materials certification for the payload per the intercenter agreements.

i. Vents Fluids Or Gasses — no

j. Contains Cryogens — no

k. Has External Moving Parts — no

l. Contains Explosive Devices — no

m. Contains/Generates Explosive/Flammable Material — maybe

The fluid loop contains a mixture of 60/40 water methanol. The hazard analysis has not yet been completed to determine the nature of the potential hazard.

n. Customer Supplied GSE Contains Radioactive/Light RF Sources Or Pressurized Volumes. — yes

The ground checkout unit will probably contain a laser that we will use as a reference during ground based testing.

o. Any Other Hazards — maybe

There is a small potential that the laser would be an eye hazard. The preliminary analysis indicates that we are approximately 100 times eyesafe but we are continuing to refine the analysis. The preliminary analysis indicates that the transmitted radiation is about 100 times less than the ANSI maximum Permissible Exposure (MPE) limit. The transmitted laser radiation intensity, inside the canister, before being expanded by the telescope is not eyesafe. Furthermore, the direct exposure to radiated energy from the diode lasers and the CW lasers are harmful to the eye. However, no harmful laser radiation can escape from the canister enclosure.

4.0 MISSION OPERATIONS

4.1 OPERATIONAL SCENARIO

SPARCLE's signal strength is inversely proportional to range squared. Thus the lower the orbit altitude the better. An orbit altitude less than or equal to 350 km is required and less than or equal to 300 km is desired. Most of the ground based opportunities (lidars, weather stations, radars, etc.) for backscatter and wind observation validation exist between 28 deg North and 58 deg North. It is therefore very desirable to be in a 51 degree or higher inclination orbit. It is the goal of the SPARCLE observation plan to make measurements around the globe with no bias towards specific areas. The exception to this is the desire to be operating while passing over specific ground or airborne validation sites.

After initial opening of the orbiter bay doors there is frequently debris floating in the payload bay. This debris can potentially contaminate the SPARCLE optical window if the Optics Canister MDA is opened too soon after bay door deployment and would result in reduced SPARCLE instrument performance. It is therefore required that a visual check for debris be performed prior to the first opening of the SPARCLE Optics Canister MDA.

Whenever the Optics Canister MDA is commanded, through the Hitchhiker ACCESS system, to open it is desired to verify that the MDA has actually opened (crew visual check or via PLB camera), The MDA will be opened either immediately before power on of the SPARCLE instrument or at some time during the TCS mode (discussed below). The MDA must be open before the instrument can transition out of TCS mode.

It is required that Hitchhiker Avionics be powered on shortly (30 minutes TBR) after orbit insertion and the payload power relay XX and heater relay XX are set early in the mission. This will enable activation of the SPARCLE survival thermal control system

soon after orbit insertion. This is required to prevent potential freezing of the SPARCLE fluid coolant system from occurring.

It is required to monitor the instrument health and status continuously (real-time) over the LR datastream. It is required to have the ability to uplink command scripts and individual commands to the instrument via the LR datalink during instrument operation.

All operational mode data collected during operation will be stored on board, however it is strongly desired to take advantage of Ku coverage whenever available to downlink collected operational mode data for analysis on the ground. The instrument is able to make optimum use of the Ku link during the non-operational mode periods. During the OSM 6 operational mode it is required to have realtime Ku coverage for downlinking data to verify the INS alignment algorithm. For the initial time this mode is conducted an extensive signal search may need to be conducted (see later) and so a 30 minute period of Ku coverage is required. For subsequent repeats of this mode 5 minutes of Ku coverage is anticipated as being sufficient. It is also strongly desired to have Ku coverage for downlinking data (5 mins periodically as coverage is available) during the other OSMs to be able to verify instrument performance. The LR datastream is insufficient for downlinking the data collected during the operational mode.

All of the SPARCLE operational modes discussed in the following operational scenario are listed, together with their attitude requirements, in Table 1.

Prior to SPARCLE activation the orbiter is placed in a -ZLV attitude and operation of the orbiter IMU is verified. The SPARCLE experiment is powered on and the system will automatically enter into TCS mode. The Optics Canister coolant loop will be brought to within the operational temperature constraints of the lasers during this mode. The period of time for this will depend on the prior orientation of the orbiter and is outlined in Table E7. It is desired to perform an orbiter IMU update in this mode immediately before transitioning to the stabilization mode and also immediately after transitioning from standby mode. This enables the alignment of the SPARCLE INS with respect to the orbiter IMU to be determined both before and after SPARCLE operations.

From TCS mode the instrument will enter a 30 minute duration stabilization mode for stabilization of the output characteristics of the local and master oscillators. During this mode the LR data stream will be sufficient for downloading instrument status.

The instrument will then enter the standby mode in which it is ready to collect science data. From standby mode the instrument will transition to operational mode. It is anticipated that the period of time spent in standby mode will be short. The duration of standby mode will be dependent on the instrument scheduling and optimization for science data collection.

When it initially enters operational mode, the SPARCLE INS/GPS calibration mode (OSM 6 in Table 1 and Appendix 1) will be performed to initialize and verify the

instrument pointing knowledge. Initialization and verification of pointing knowledge is an important aspect of SPARCLE operations and further explanation is provided in later sections of this document. Upon completion of OSM 6 the instrument will transition between the other OSMs and standby mode according to the schedule determined within the operating script (or by ground command) with periodic returns to OSM 6 for INS calibration/verification. When the PCM material is exhausted or when commanded to do so (via script or ground command) the instrument will transition to TCS mode for resolidification of the PCM material. As mentioned previously the maximum continuous operation in operational mode is limited by thermal constraints to 90 minutes. Minimum total duration in the operational mode is required to be 25 hours broken down among the OSMs as listed in Table 1 (by attitude configuration) and Appendix 1 (by OSM). It is strongly desired to obtain a total of 50 hours in the operational mode. The maximum length of useful operations is constrained by the volume of data that can be collected/stored by the SPARCLE mass storage unit..

Operation of the SPARCLE instrument in operational mode will be supplemented by real-time video camera observations of the Earth surface and atmosphere in the -ZLV direction. High-resolution color camera coverage is required at all times during daylight lidar operations, and high-resolution B&W camera coverage is required during nighttime lidar operations. ***HH needs to define camera requirements early to make sure they are manifested via the FRD (they don't always fly MLA (b/w) camera anymore).*** Video data may be recorded on board as an alternative to downlinking it real-time, provided navigation and time-tag information is available.

The time required for PCM resolidification is dependent on the orbit attitude.

When the SPARCLE instrument is first turned on, the SPARCLE INS has no knowledge of its current attitude. To overcome this we have developed a two step mechanism to obtain the required attitude knowledge. The first step requires aligning the SPARCLE INS to the orbiter IMU by providing the SPARCLE INS with attitude information obtained from the orbiter IMU. Although there is the potential for relatively large differences between the orientations of these two units, the errors will be sufficiently small that they will enable the SPARCLE attitude uncertainty to be reduced sufficiently that the SPARCLE instrument will be able to capture the signal.

The SPARCLE instrument will then be used (OSM 6) to refine the attitude knowledge by analyzing the Doppler frequency offsets from the lidar earth surface return signal as a function of azimuth. The initialization process relies on getting lidar signals from earth surface returns and so it is required that this occur over regions of the globe that are essentially cloud free. In order to assist with mission planning, the SPARCLE science team will identify the most likely locations for these in advance of each days mission. Use of the camera documented elsewhere will also be required during this initialization process. The orbiter weight and CG as a function of flight time will be required for post mission processing to assist in removing residual errors in this process.

In order to assist removing residual errors during post processing on the ground it is desirable for the SPARCLE GPS/INS to operate for extended periods on orbit so that its drift characteristics can be evaluated. It is therefore desired that as much time as possible be spent in the TCS mode (without impacting the ability to complete the operational mode requirements). To assist calibrating these drifts it is desirable that this occurs through as many orbiter IMU alignment cycles as possible and that at least two of these comparisons occur prior to SPARCLE being placed into the operations mode for the first time. This does not require opening of the MDA.

Pointing Knowledge Initialization (OSM 6) Details

Before lidar pointing calibration operations begin, and as close to operations as Shuttle priorities allow, an update of the orbiter IMU is requested.. During this update it is required that the attitude solution be provided to the SPARCLE instrument so that the SPARCLE INS can be provided a coarse initialization.

The initial phase of OSM6 requires a -ZLV orientation with an orbiter pointing deadband of 0.1 °. The SPARCLE scanner azimuth angle will be set to point the SPARCLE lidar beam orthogonal to the orbiter ground track. This will permit sample data to be captured to assess how well the INS is aligned with respect to the SPARCLE instrument. While it is intended that the instrument will be capable of analyzing this data on board, the performance of the SPARCLE cpu limits the complexity of the algorithms that can be performed and it is required that this data can be transmitted to the ground in the event that more advanced analysis is required. To facilitate this it is required that this period of SPARCLE initialization and operation have realtime Ku coverage to permit downlinking of instrument raw data for analysis purposes as the raw data is too large to be downlinked in the LR data stream. If it is determined that the instrument is not capturing any signal, then the instrument will be commanded to go into a "search" mode to find the signal. (Adjustments will be made to combinations of the azimuth angle, master oscillator laser tuning, and the receiver range of regard). After signal is verified, the instrument is commanded to enter an 8-point scan of the lidar to acquire velocity signals from the Earth's surface in order to obtain fine-resolution pointing and range data. After obtaining this data and using it to compute a more accurate pointing knowledge, the 8-point scan is subsequently repeated for verification. Upon successful completion of the second 8-pt scan, the pointing deadband shall be relaxed to 1 deg and the 8 pt scan repeated. If the pointing knowledge is verified to be within the desired specification, the instrument is commanded to enter into the desired science mode of operations for a specified period of time. The lidar receiver system will be optimized during the mission to minimize required data stored, maximize data resolution, or both, depending on the results of the pointing calibration procedure. The 8 point scan routine will be performed every 30 minutes during science data takes in order to compensate for SPARCLE INS drifts. It is also required that this 8 pt scan routine be performed immediately before and after passing over ground calibration sites. It is anticipated that it will take approximately 5 minutes for each 8-pt scan routine with the exception of the initial one thus Ku coverage is required for 5 minutes during each of these modes. During the first operation

of this mode a more prolonged search mode may be required and so Ku band coverage is requested for 30 minutes.

Wind velocity data will be verified post-mission by comparison with ground-based measurements. The SPARCLE science team anticipate that there will be a few (~5-10) ground sites at which wind measurements will be particularly valuable. Orbital predictions and weather forecasts will be utilized to determine ideal instrument operating modes to ensure data collection over those sites. While realizing that flexibility will be limited, the SPARCLE science team will appreciate assistance from Hitchhiker and Shuttle teams in obtaining possible adjustments to the mission timeline if such an opportunity arises.

4.2 EXPERIMENT POWER

Subsys	TCS		Stabilization		Operation		Standby	
	AVE	PK	AVE	PK	AVE	PK	AVE	PK
CDMS	95.1	95.1	95.1	95.1	101.5	174.3	95.1	95.1
MSU	30	52	30	52	30	52	30	52
ERS	0	0	20	20	20	20	20	20
SS	0	0	0	0	43.1	116.4	28.4	28.4
SIGI	40	70	40	70	40	70	40	70
HSS	25	27	25	27	25	27	25	27
LTS	56.5	139	80	80	185	185	80	80
TCS	240	362	240	282	220	262	240	282
PDU	124.2	158.5	135.1	144.7	168.5	185.9	142.2	151.8
TOTALS	610.8	903.6	665.2	770.8	833.1	1092.6	700.7	806.3

4.3 THERMAL OPERATIONS

TABLE E.7
THERMAL CONSTRAINTS

TCS Requirements for Orbiter Attitudes

SPARCLE Mode	Orbiter Attitude	Duration Requirements
TCS	-ZLV (Desired during warm-up)	Notes 1 & 2
	DSP/-ZLV (Desired during PCM recovery)	TBD -ZDS + TBD -ZLV (or TBD -ZLV if cannot accommodate -ZDS)
Stabilization	-ZLV (Required)	30-minutes continuous
Standby	-ZLV (Required)	As little as possible (Note3)
Operational	-ZLV (Required)	90-minutes continuous
Non-Operational	-ZLV (Desired)	Continuous (Note 4)

(1) The TCS mode includes both system warm-up following non-operation and post-operational PCM recovery. During this mode, the TCS is being conditioned (warm-up or recovery) to bring the system temperature within operational limits with PCM solidified. Bay-to-Earth (-ZLV) is desired thermally during system warm-up and post-operational PCM recovery. However, the PCM recovery duration can be reduced by orienting -ZDS for a portion of that recovery.

(2) If the TCS mode immediately follows a non-operational mode (either first activation or >12 hours since last operation), the TCS will require 3 hours (TBR) if the Orbiter has been -ZLV for previous 12 hours or as much as 12 hours (TBR) if the Orbiter has not been in prolonged -ZLV orientation prior to SPARCLE activation. Following PCM re-solidification, the TCS requires <30 minutes (TBR) for fluid loop reconfiguration and system stabilization prior to entering another Stabilization Mode.

(3) Standby is intended for very short and intermittent use since time in Standby reduces available Operational time. Time in Standby corresponds to reduction in 90-minutes of continuous Operation.

(4) To preclude freezing of external radiator fluid as well as remain conditioned for subsequent SPARCLE operation, -ZLV is desired during non-operational modes with allowance for -ZDS and -ZSI as detailed below.

Thermostatic Equipment	Duty Cycle	Power	Comments/Duration/Att
Survival Heaters	0%	TBD	Bay to Sun (hot)
Operational Heaters	TBD	TBD	Bay to Earth (nominal)
Survival Heaters	80%	TBD	Bay to Space (cold)

PAYLOAD with heaters off:

Attitude	Max Duration	Recovery Time	Effect If Violated
Bay to Sun	TBD	TBD	TBD
Bay to Earth	TBD	TBD	TBD
Bay to Space	TBD	TBD	TBD

PAYLOAD with heaters on:

Attitude	Max Duration	Recovery Time	Effect If Violated
Bay to Sun	TBD	TBD	TBD
Bay to Earth	TBD	TBD	TBD
Bay to Space	TBD	TBD	TBD

4.4 EXPERIMENT COMMANDING

The SPARCLE instrument operation is controlled by a script or by direct commands from the ground. The script can be uploaded in advance and a default script is always available in the event of communications problems while the instrument is powered on and being commanded from the ground. The script consists of simple commands to transition between operational modes and OSMs at particular UTC times. In the event of a fault during execution of one of the modes the script will be overidden. The exact action taken in the event of a fault will depend on the nature of the fault but for most faults the instrument will fall back to the TCS mode and await commands from the ground. The instrument is designed such that fault diagnostics and corrective action will be conducted by the SPARCLE team members in the POCC over the LR datastream.

The control of individual subsystems within a given mode is commanded by the onboard program for that particular mode unless overidden via ground control.

When power is applied to the instrument (by Hitchhiker through ACCESS) the SPARCLE instrument CDMS will boot, perform internal diagnostics and self checks, place the instrument into TCS mode and commence operation of a script (unless commanded to do otherwise from the ground). The script exercised will be the most recently uploaded script if the UTC timing values in the script match the current UTC otherwise the default script, which uses relative timing information, will be executed.

Realtime commands from the ground can be issued for the purposes of instrument activation/deactivation, operating mode selection, data downlinking, and data acquisition parameter updating. Data acquisition parameter updates for the SPARCLE instrument are sent as commands when the SPARCLE instrument is in any of the modes of operation. A computer reset command can also be sent in these modes. Although the instrument is designed to operate autonomously it is required that a command window be available at the start of each operations mode and desired that further windows be available during each operational mode. There are no critical commands which, if incorrectly transmitted, could damage the payload.

4.5 EXPERIMENT TELEMETRY

Experiment telemetry for the SPARCLE payload consists of low-rate (LR) and medium-rate (MR) data and is described in Tables E.9 and E.10. The data flow from SPARCLE is packet-type output. The LR data downlink is required at all times during the SPARCLE mission flight. The MR data downlink is requested to be available during mission operational times (estimated operational time of two orbits per day). The SPARCLE

payload request as much as possible KU band usage for MR downlink during mission non-operational times.

Each SPARCLE data cycle consist of approximately one orbit (90 minutes). The SPARCLE data volume computations are based on approximately 50 hours of LR and HR data during the SPARCLE mission. The SPARCLE instrument has an on-board storage capability of 80 Gbytes. The downlink data will be packetized with a fixed packet format

TABLE E.9
LOW RATE DATA STREAM CONTENTS

Commands/Telemetry	Baud	Type
Commanding to CGSE/ACCESS	1200	RS232
Async Data Unformatted	1200	N/A
Async Data Formatted	19.2 k	RS232
Analog Data	19.2 k	RS232
CGSE/ACCESS Ancillary Data	19.2 k	RS232
Shuttle Orbit/Attitude Data	19.2 k	RS232
PCM-A	19.2 k	N/A
PCM-B	19.2 k	N/A
Command Status	19.2 k	RS232
Data Link Status	19.2 k	RS232
CGSE/ACCESS AIA Data	19.2 k	RS232

TABLE E.10
MEDIUM RATE DATA CHARACTERISTICS

Experiment Name	Rate (MB/s)	Frame Sync Pattern	Frame Counter Location	Minor Frame Size (bytes)	Major Frame Size	Fill Pattern
SPARCLE	1 MB/s ***not possible (880 kbps max with current avionics)***	??	Byte 2	1024	256	FFF

4.6 CREW INVOLVEMENT

In order to minimize the risk of payload bay debris contaminating the SPARCLE optical window it is requested that the orbiter crew check for orbital debris prior to the initial opening of the MDA on the Optics Canister. Otherwise, it is not expected that the crew will be involved in day to day SPARCLE operations unless the data that SPARCLE

requires to meet attitude/position requirements is somehow sent through a PGSC in the middeck to SPARCLE for further processing.

4.7 ORBITER POINTING

Table X lists the orbiter pointing requirements required for SPARCLE operations:

Attitude	Deadband (deg)	Rate (deg/s)	Total Time (hrs)	Notes
-ZLV	n.a.	n.a.		TCS warmup, Stabilization and Standby Modes
-ZDS	n.a.	n.a.		TCS PCM resolidification
-ZLV arbitrary VV	0.1	< 0.04	minimum of 1.5 - 2.5 in ~2.5 min periods	OSM6 prefer no thruster firings
-ZLV arbitrary VV	1	< 0.04	minimum of 1.5 - 2.5 in ~2.5 min periods	OSM6 prefer no thruster firings
-ZLV arbitrary VV	0.1	< 0.04	minimum 3	OSM 1A
-ZLV arbitrary VV	1	< 0.04	minimum of 16.5	All OSMs not identified elsewhere
30 deg roll from -ZLV +/-XVV	0.1	< 0.04	minimum of 1.5	OSM 1B

Table X Pointing requirements for SPARCLE operations

It is assumed that where an arbitrary VV is specified that this value will be known. In all cases where a deadband is specified it is required that the velocity vector be held to within the same deadband requirements.

Need matrix showing cooling rates if –ZDS or equivalent is not flown.

4.8 FIELD OF VIEW

The SPARCLE instrument instantaneous receiver field-of-view is 25 cm in diameter with a half-angle of 40 microradians at a 30 deg half-cone angle to the SPARCLE telescope optical axis. This field of view is rotated about the telescope optical axis by the scan motor. The optical axis is offset from the Hitchhiker canister mechanical centerline along the longitudinal axis of the Optics Canister by 1.62 inches along the lid hinge axis toward the mounting beam. TBD in X and TBD in Y. The SPARCLE slave oscillator beam has a 30 microradian divergence, a 19.6 +/- 2.5 cm (1/e2) diameter, and is co-aligned to the

center of the SPARCLE telescope axis and the receiver optical axis. During pre-launch integration to the orbiter the alignment of the SPARCLE instrument (ie the SPARCLE telescope optical axis) is required to fall within 0.1 deg of the orbiter +Z axis. This alignment will be determined by TBD. Due to orbiter flexing and SPARCLE instrument location within the orbiter bay, deviations between the SPARCLE optical axis and the orbiter +Z axis are possible during a mission.

The TCS utilizes the hitchhiker canister top plates as thermal radiators for passive heat rejection. The TCS requires a large "view" out of the orbiter in order to meet the 90-minutes of continuous operation requirement. At a minimum, a 45° half cone angle from the top plates should remain free of blockage (e.g., module type payloads, Orbiter bulkhead, etc.). Also, blockage of the external radiator view to space should be minimized as much as possible.

4.9 CONTAMINATION CONSTRAINTS

It is requested that the MDA on the Optics Canister be closed during all shuttle operations that might induce contamination upon the Optical window. These include Flash Evaporator System (FES) Operations, Fuel Cell Purges, and Waste Water Dumps as well as other Payload Operations that might affect SPARCLE. ***How soon before operations do these activities need to be inhibited? TBD minutes?***

In order to minimize the risk of payload bay debris contaminating the SPARCLE optical window it is requested that the orbiter crew check for orbital debris prior to the initial opening of the MDA on the Optics Canister.

Need Sun and RAM avoidance constraints and associated avoidance angles.

4.10 CUSTOMER GROUND SUPPORT EQUIPMENT (CGSE)

Science Team Inputs

4.11 PAYLOAD OPERATIONS CONTROL CENTER (POCC) REQUIREMENTS

4.11.1 HITCHHIKER CUSTOMERS

8-16 people; details of experiment operations, duty cycle, and shift operations are still TBD.

Science Team (8)
Science Co-Investigator
Global Hydrology Control Center (GHCC) Program Scientist
Data Acquisition and Processing (2)
Validation (4)

Engineering Team (5-8)
Project Manager
Project Engineer
Co-Investigator
2-5 additional people

SPARCLE requires 6 customer space units (CSUs)

Does this mean that you require 6 entire consoles or enough consoles to support 6 sets of GSE? One console can support 2 sets of GSE and 2 operators.

Identify any additional requirements not listed above.
N/A

Would you like to be assigned an e-mail address in the control center for simulation/mission operations?

Will you need additional space for non-operations personnel that will be monitoring the mission?

SPARCLE requests space in the POCC for team members who are not occupying the 6 CSUs.

Appendix 1 The Operational Science Modes (OSMs)

OSM	LIDAR POINTING	ORBITER ATTITUDE	MINIMUM MODAL TIME	COMMENTS
1A	Azimuth: Fixed, selectable for all angles between 0 and 359. Dwells: variable up to 90 min. Slew: slow (~ 10 deg/sec)	-ZLV ± 0.1 degree deadband	3 hours 30 minute segments	Used for LOS data collection to support signal searching, shot accumulation, etc.
1B	Azimuth: Fixed at 90 or 270 Dwell: variable up to 90 min. Slew: N/A	30 degree roll ± .1 degree deadband	1.5 hours	Used to check pointing knowledge, vertical velocity, cloud porosity, long shot accumulation…
2A	Azimuth: 45 and 135 Dwell: 25 to 35 seconds (TBD) Slew: medium (~ 30 deg/sec)	-ZLV ± 1 deg deadband	3 hours 3 consecutive 30 minute segments	Used to obtain vector wind obs with highest number of accumulated shots.
2B	Azimuth: + 45 and –45 Dwell: up to 30 seconds Slew: medium(~30 deg/sec)	-ZLV ± 1 deg deadband	3 hours 3 consecutive 30 minute segments	Used to evaluate a scan mode proposed by ESA

3A	Azimuth: 45,-45,135,-135 in sequence. Dwell: 12-16 seconds (TBD) Slew: fast (~60 deg/sec)	-ZLV ± 1 deg deadband	1.5 hours	Used to demonstrate two profiles per scan sequence
3B	Azimuth: 30,-30, -60, +60, -120,+120,+150,-150 Dwell: 5-8 seconds (TBD) Slew: fast	-ZLV ± 1 deg deadband	3 hours 3 consecutive 30 minute segments	Most likely step-stare pattern to be used on first operational mission
3C	Azimuth: 12 points TBD Dwell: 2-4 seconds (TBD) Slew: fast	-ZLV ± 1 deg deadband	1.5 hours	Fastest matched fore and aft samples
4A	Azimuth: 0 to 359 by 10 deg Dwell: 2.5 seconds Slew: slow	-ZLV ± 1 deg deadband	optional	Used to generate optimal cycloid pattern for VAD processed vector wind
4B	Azimuth: 0 to 359 by 22.5 deg Dwell: .5 seconds Slew: fast	-ZLV ± 1 deg deadband	3 hours 3 consecutive 30 minute segments	16 points in 16 seconds to simulate a continuous conical scan
4C	Azimuth: 0 to 180 by 10 deg 181-359 by 180 deg Dwell: 2.5 seconds Slew: slow between 0-180 Fast between 180-359	-ZLV ± 1 deg deadband	1.5 hours	Same as 4A except more efficient use of time
5	Azimuth: 0-360 Dwell: N/A Slew: variable between .05 and .20 deg/sec	-ZLV ± 1 deg deadband	optional	Used to validate lag angle compensation modeling
6	Azimuth: 0,45,90,...315 Dwell: 1 second Slew: fast	-ZLV ± 1 deg deadband or ± .1 deg	3-5 hours 2-5 minute segments	Used to provide fine calibration for SPARCLE GPS/INS

REPORT DOCUMENTATION PAGE

Form Approved
OMB No. 0704-0188

1. AGENCY USE ONLY *(Leave blank)*	2. REPORT DATE	3. REPORT TYPE AND DATES COVERED
	July 1999	Final Report 8/10/97 – 8/10/98

4. TITLE AND SUBTITLE
Analysis of Lidar Remote Sensing Concepts

5. FUNDING NUMBERS
C #NAS8-97095, TA #H-28503D

6. AUTHORS
Gary D. Spiers

7. PERFORMING ORGANIZATION NAME(S) AND ADDRESS(ES)
University of Alabama in Huntsville
301 Sparkman Drive
Huntsville, AL 35899

7. PERFORMING ORGANIZATION REPORT NUMBER
N/A

8. SPONSORING/MONITORING AGENCY NAME(S) AND ADDRESS(ES)
NASA/Marshall Space Flight Center
Marshall Space Flight Center, AL 35812

8. SPONSORING/MONITORING AGENCY REPORT NUMBER
Unknown

11. SUPPLEMENTARY NOTES

12a. DISTRIBUTION/AVAILABILITY STATEMENT
Unclassified/Unlimited

12b. DISTRIBUTION CODE

13. ABSTRACT *(Maximum 200 words)*

Line of sight velocity accuracy and measurement position sensitivity analyses for an orbiting coherent Doppler lidar are developed and applied to two lidars, one with a nadir angle of 30 deg. in a 300 km altitude, 58 deg. inclination orbit and the second for a 45 deg. nadir angle instrument in a 833 km altitude , 89 deg. inclination orbit. The effect of orbit related effects on the backscatter sensitivity of a coherent Doppler lidar is also discussed.

Draft performance estimate, error budgets and payload accommodation requirements for the SPARCLE instrument were also developed and documented.

14. SUBJECT TERMS
coherent Doppler lidar, lidar, SPARCLE, laser radar

15. NUMBER OF PAGES
186

16. PRICE CODE

17. SECURITY CLASSIFICATION OF REPORT	18. SECURITY CLASSIFICATION OF THIS PAGE	19. SECURITY CLASSIFICATION OF ABSTRACT	20. LIMITATION OF ABSTRACT
Unclassified	Unclassified	Unclassified	SAR